1990

Mathematical modelling of smelting of iron oxide: carbon composites in an induction furnace

Govind Sharan Gupta
University of Wollongong

MATHEMATICAL MODELLING OF SMELTING OF IRON OXIDE - CARBON COMPOSITES IN AN INDUCTION FURNACE

A thesis submitted in fulfilment of the requirement
for the award of the degree of

DOCTOR OF PHILOSOPHY

from

THE UNIVERSITY OF WOLLONGONG

by

GOVIND SHARAN GUPTA (B.Sc., B.E., M.Tech.)

DEPARTMENT OF MATERIALS ENGINEERING

1990

Candidate's Certificate

This is to certify that the work presented in this thesis was carried out in the laboratories of the Department of Materials Engineering in the University of Wollongong and has not been submitted to any other university or institution for a higher degree.

Govind Sharan Gupta

DEDICATED

TO

T. SUNDARARAJAN

ACKNOWLEDGEMENT

I express my deep sense of gratitude to Assoc. Prof. Nick Standish of the University of Wollongong and to Assist. Prof. T. Sundararajan (Mechanical Dept. I.I.T., Kanpur, India) for their invaluable guidance, suggestions and encouragement during this research project. I am also indebted to Assist. Prof. N. Chakraborti (Met. Dept. I.I.T.K.) for his guidance and encouragement especially at the preliminary stage of the mathematical formulation and for the computer facilities made available to me to carry out this work during my stay at I.I.T.K.

I wish to express my sincere thanks to Profs. A.K. Ghosh, N.K. Batra, H.K. Worner, Assoc. Prof. F. Paoloni, Mrs. S. Nightingale and Dr. Tara Chandra for assisting me in various ways during this work.

My thanks are due to the whole Materials Eng. Dept. for its co-operation and in particular Mr. R. Kinnell, R. De Jong, G. Hamilton, G. Tillman and N. Mackie for helping me in my experimental work. Many thanks are also due to Prof. N.F. Kennon, Mrs. M. Standen and Mr. J. Jones for their help at the beginning.

My sincere thanks to Prof. Doherty for making various helpful comments on the thesis.

The co-operation and facilities for experiment provided by the staff of TAFE at Wollongong are gratefully acknowledged.

I wish to thank most sincerely The Coal Corporation of Victoria for their financial support.

Thanks are also due to all of my friends who directly and indirectly made my stay at the Univ. of Wollongong a memorable one. I gratefully acknowledge the contributions of my friends, S.K. Choudhary, Appukuttan, S. Patjoshi, Rohit Verma, G.S. Kulkarni, Sanjay, K. Shastri, Sushil, Thomas Tharian, Mohan Nagraj, A. Singhai, A. Kulahada (all from I.I.T.K.) and Nazrul Islam, Ahmed Yunus, Budi Notowidjojo, Ardha, Xiaping Lin, Pram, Shi Hua, Yuan Hui, Aibing, Qinglin, Keshav, Tarun, Subbu, Kathryn, Vinay, Lakshmi, Cathy and Ashok.

The whole credit for this task goes to my family who patiently tolerated every demand I made of them.

INDEX

NOMENCLATURE

ρ	Density
k	Thermal conductivity
C_p	Specific heat
T	Temperature
t	time
Pe	Peclet number
μ	Viscosity
α	Thermal diffusivity

LIQUID REGION (LR):

u	Velocity vector
Fb, F	Body force or Lorentz force
τ	Stress tensor
ξ	Vorticity
ω	Angular frequency
ψ	Stream function
σ	Electrical conductivity
λ	Wave length
κ	A constant defined by eqn. (2E-15)
J	Current density
B	Magnetic field
E	Electric field
H	Magnetic field intensity
r, z	Radial and axial co-ordinates
A	Vector potential
A_1, A_2	Components of general vector potential
f	Frequency
k	Wave number

R	Crucible radius
i	Complex number
μ_o, μ_t, μ_r	Free space, total and relative permeability of magnetic material
r_e	Electrical resistivity
δ	Penetration depth, defined by equation (2A-39)
$\|J_o\|$	Amplitude of surface current
Re	Real part of electrical quantity, Reynolds number
η	A constant, defined by equation (2E-4)
U_o	Characteristic velocity, defined by equation (2E-4)
β	A constant, defined by equation (2E-10)
Z_B	Bessel function, defined in equation (2E-31)
ρ_B	A constant, defined in equation (2E-31)
ϕ	Variable angle, defined in equation (2E-43)
$a,b,u_o,v_o,X_o,$ Y_o,U_1,V_1	Functions of ρ_B and ϕ as defined in equations (2E-26-29)
$\boxplus H$	Variable, defined by equation (2E-52)
Pr	Prandtl number
$\Delta R_1,\Delta R,\Delta Z$	Lattice spacing in R and Z direction

BED REGION (BR):

H	Bed height
r_p	Average radius of the pellet
N_P	Total number of pellets in bed
Vv	Void volume per cell
r_c	Cell radius
ξ_B	Vorticity
ψ_B	Stream function
θ	Angular spherical polar co-ordinate
E^2_B	Differential operator

V_θ	Tangential velocity component
V_r	Radial velocity component
$\underline{V}$	Velocity vector
FeO	Iron oxide
$\underline{C}$	Dissolve carbon in iron melt
ΔH_m	Enthalpy of reaction (2B-13)
ΔH_r	Heat of reaction (2B-13)
C_{FeO}	Concentration of iron oxide in the melt
$D_{F\text{-}S}$	Diffusivity of binary system (FeO-Slag)
R	Rate of reaction (2B-13)
r_p	Radius of pellet
U_{AV}	Average velocity of liquid iron in bed region
T_∞	Temperature remote from the pellet
G,F	Functions of vorticity, r and θ
M_{melt}	Molecular weight of melt
ω_p	Pellet void fraction
k_υ	Velocity constant in equation (B-5)
POWIND	As defined by equation (2E-125)
HEATBL	As defined by equation (2E-126)
GASHIT	As defined by equation (2E-127)
HITMEL	As defined by equation (2E-128)
HFEPRO	As defined by equation (2E-129)
BCPART	As defined by equation (2E-130)
ACUHIT	As defined by equation (2E-131)
CFEOPR	As defined by equation (2E-133)
COUTFL	As defined by equation (2E-134)
$\Delta X,\Delta Y$	Lattice spacing in X and Y direction in Fig. 15
m	Rate of melting of pellet
$\Delta R_m,\Delta\theta$	Lattice spacing in radial and angular direction

$\| \ \|$	Used for absolute value

JET REGION (JR):

$\underline{W}$	Velocity vector
P,p	Pressure
W_o	Oxygen jet velocity
Z_{max}	Distance between lance and pellet
W	Radial oxygen velocity in potential region
U	Axial velocity in potential region
W_r	Radial oxygen velocity in boundary layer region
W_z	Axial oxygen velocity in boundary layer region
A_g	Constant defined in equation (2C-4)
Φ	As defined in equation (2C-)
ν	Oxygen kinematic viscosity
Z_1	Bed - jet region interface
M_{O2}	Oxygen concentration
$D_{O2\text{-}CO}$	Diffusion coefficient for O_2-CO binary system
$M_{O2,\infty}$	Initial molar concentration of oxygen
J_{O2}	Mass flux of oxygen
Pt	Total partial pressure of gas
D	Variable height of liquid region
ΔH_1	Enthalpy for reaction (B-)
L	Latent heat of fusion for iron
M_{Fe}	Rate of production of Fe per cell
V_c	Volume of cell in equation (2D-14)
V_B	Volume of bed
ε_B	Bed void fraction

SUBSCRIPTS

R_w	Outer radius of the crucible

B	Bed region, Also used for Bessel functions
m	Melt in BR
p	Pellet
c	Cell
v	Volume
mHT	Melt heat transfer
mMT	Melt mass transfer
-	Vector quantity
s	solid
AV	Average
M.P.	Melting Point
i	Initial
mag.	Magnetic
g	Gas
max	Maximum
o	Original or initial
z	Component of field variables in Z direction
r	Component of field variables in R direction
θ	Component of field variables in θ direction
gHT	Gas heat transfer
gMT	Gas mass transfer
pres.	Prescribed value
O_2	Oxygen
ind	Induction
HT	Heat transfer
MT	Mass transfer
i , j	Variables to denote the grid points in all regions
N	Total number of grid points in R direction in LR
M	Total number of grid points in Z direction in LR

LNK	Total number of grid points in radial direction in BR
LL	Total number of grid points in angular direction in BR
rms	Root mean square quantity
Fe	Iron
FeO	Iron oxide
w	**Wall**

SUPERSCRIPTS

o	Degree
*	Nondimensional quantity
n	current time step
n+1	One step advanced time
^	Unit vector
`	General field variables
-	Complex conjugate of field variables

ACRONMYS

ISP	Induction smelting process
f/c	Furnace
M.M.	Mathematical model
LR	Liquid region
BR	Bed region
JR	Jet region
CIF	Coreless induction furnace
MHD	Magnetohydrodynamics
MGD	Magnetogasdynamics
PDE	Partial differential equation
AC	Alternating current

M.P.	Melting point
B.L.	Boundary layer
FDM	Finite difference method
FEM	Finite element method
FVM	Finite volume method
FD	Finite difference
eqn.	Equation
GDE	Governing differential equation
B.Cs.	Boundary conditions
temp.	Temperature
concn.	Concentration
SF	Stream function

SYNOPSIS

Brown coal is a widely available low rank coal which has not normally been used in Metallurgical Processes. However, because of its high Hydrogen content, it is a good reductant as well as a part of the source of heat in conjunction with top blown Oxygen/Air. To carry out an experimental evaluation of the optimum smelting conditions in an induction furnace would be expensive in money and effort. Hence, the reason for modelling.

In the Induction Smelting Process self-fluxed composite pellets (made of Iron ore + Brown Coal + Lime) are melted in a single phase induction furnace in conjunction with top blown Oxygen. Therefore, the process has three distinct regions, which are to be modelled:

A. Electromagnetic Stirred Region,

B. Liquid-Solid Interaction (Bed) Region and,

C. Gas Jet and Solid Interaction Region.

Each region involves the consideration of non-steady state energy and species balances with momentum transfer.

Region (A) has been solved using the Navier-Stokes and Energy balance equations with Maxwell's equations. To calculate the body force a numerical solution has been developed.

Region (B) has been solved using the momentum, heat and mass transfer equations. A new approach, known as the 'Cell Model', has been adopted to solve this region. All energy, species and momentum balance equations are solved for a typical particle inside a cell, which later gives the response of total system (i.e. the Bed Region) by multiplying the number of particles in the system by the single particle response.

Region (C) has been described by energy, species and momentum balance equations. To calculate the velocity in this region an analytical solution has been adopted.

All three regions have been connected by doing overall heat and mass balances for the entire process. Many complex partial differential equations have been formulated with appropriate boundary conditions to define each region. The governing equations, which are highly non-linear and complex in nature, have been solved by the Finite Difference Method using various techniques, depending on the nature of the individual differential equation. The solution of these equations gives considerable insight into the liquid iron and oxygen temperature and velocity, and FeO and Oxygen concentrations inside the furnace at different times. Also, it predicts the effects of numerous parameters on the entire process such as pellet size, gas jet velocity, preheating of pellet, energy consumption, effect of composition etc.

Computer predictions have been compared with an experiment for the temperature and composition. A velocity measurement device has also been developed to measure the liquid iron velocity at high temperature. Computed and experimental results show resonable agreement.

Although the model has been developed for a particular process, the treatment is general and could be readily extended to any other related process. Also, the solution in each region can be applied separately to define any other related process after a few minor modifications, e.g. the region (A) solution can be applied to various types of induction smelting/refining processes and, the region (B) solution can be applied to different packed-bed processes.

CHAPTER 1

INTRODUCTION

The application of electromagnetic induction in metallurgy started at the beginning of this century[1] in induction heating and melting. Usually, induction heating involves electromagnetic induction, a skin effect and heat transfer. The basic principle in induction heating or melting is that a coil current produces a pulsating magnetic field which induces voltages in the material, which acts as a short-circuited secondary, causing current to flow and heat the metal.

Induction melting has many advantages, viz. low running cost, quick melting, reduced metal loss, stirring of the melt, freedom from detrimental gases etc. In practice, two types of induction melting units are used

1) Coreless Induction Furnaces and,
2) Channel Induction Furnaces.

Among these furnaces, coreless furnaces are widely used for melting purposes operating at different frequencies, viz low (50-60Hz), medium (150-5000Hz), and high frequency. Medium frequency furnaces are commonly used for melting purposes in foundries.

Induction furnaces are generally not used for smelting purposes, which we are considering in the present study, where self fluxed pellets (made up of iron ore + brown coal + lime) are melted in a medium frequency induction furnace in conjunction with top blown oxygen/air.

This process can be categorized as one of the direct smelting reduction processes which are currently receiving special attention.

Generally, smelting reduction has two stages: (1) prereduction of iron ore i.e. smelting gasifier and (2) smelting of prereduced ore into an iron-carbon bath with the help of coal, oxygen and flux. Smelting reduction is essentially done in a vessel containing liquid iron. Raw materials- ore, coal and flux-are introduced in the vessel which may involve oxygen or air. Reduced gases are used either for the prereduction of ore or for the postcombustion in a smelting bath to transfer the combustion heat to slag and metal. The salient features of the smelting reduction are direct use of coal and fine ore, lower energy consumption, reduced air pollution and high productivity.

The smelting reduction process is associated with the development of direct reduced iron ore. Abundant literature is available on direct reduced iron ore and it is well documented[2-4]. Many smelting reduction processes like, SKF Plasmasmelt, ELRED, INRED, MIDREX Electro Thermal, Corex, Converted Blast Furnace, HISmelt etcetra, have emerged recently[5-18]. Some of these processes use electricity as part of the energy input (e.g. SKF Plasmasmelt, INRED). Some of these processes also use oxygen/air (e.g. converted

blast furnace, INRED, HISmelt). The Induction Smelting Process, considered in the present work, has some common features with the INRED process. Both processes use electricity as part of their energy input, and the oxygen injection. The latter process is fully developed while the former is in its developmental phase.

All these smelting processes lack fundamental research. In Europe[6] and America[18] attention is being given to understanding the mechanism/kinetics, modelling, and metal and slag properties in smelting reduction processes. No proper kinetics and modelling work is available for a particular smelting reduction process but high temperature iron and steel making kinetics[19-34] and modelling[35-40] may be applied to get some idea of these smelting reduction processes. An attempt has been made in the present work to develop a mathematical model for the Induction Smelting Process.

The main aim of the Induction Smelting Process is to use brown coal as a reductant. Brown coal is a widely available low rank coal which is not normally used in metallurgical processes. However, because of its high hydrogen content, it is a good reductant as well as a partial source of heat. This process, named the Induction Smelting Process, minimises the requirement for pretreatment of the ore and coal, eliminates some environmental problems, and reduces the degree of recycle in comparison to existing conventional metallurgical smelting units. The possible use of microwave heated pellets in the smelting is also examined[41].

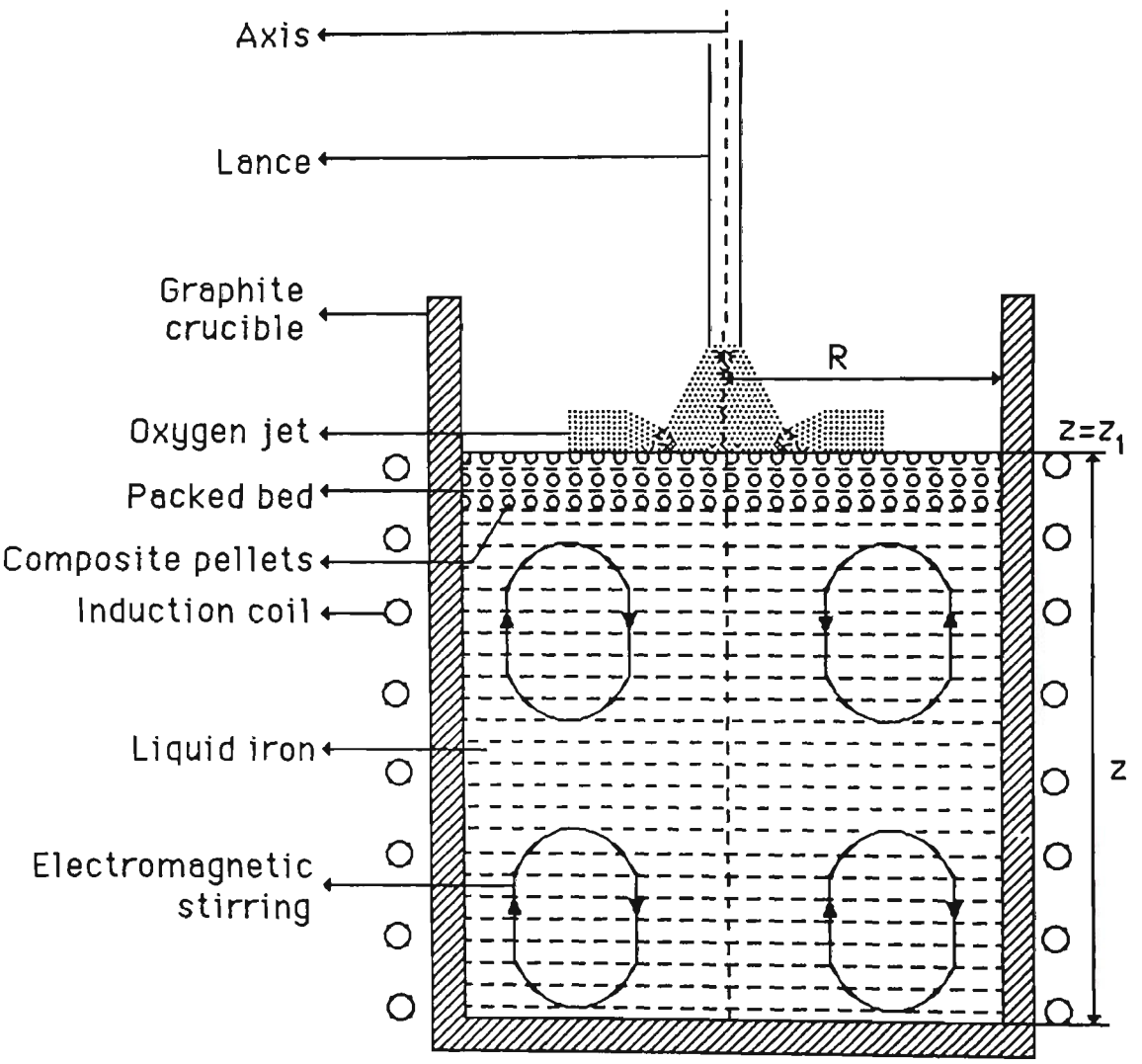

Fig. 1. A schematic diagram of the Induction Smelting Process.

Induction Smelting is a very new smelting process. Using brown coal as a reductant, high alloy Fe-Cr has been produced from iron-chromium ore[42]. Because the process is in its infancy, to carry out an experimental evaluation of the optimum smelting conditions would be expensive and time consuming. Therefore, it was thought that a mathematical model should be developed for induction smelting which can be used to optimise the process performance and to assess the optimum design.

A schematic sketch of the Induction Smelting Process is shown in Fig. 1, which depicts the essential features of the process. To start the process, heel material which is melted first, is used for convenience (normally a medium frequency furnace needs no starting plug). Then self fluxed composite pellets (either in cold condition or microwave heated) are charged into the furnace in conjunction with top blown oxygen to start the smelting. Usually, pellets are charged after some time interval till the smelting is finished. The operating temperature of the process varies from 1300 - 1500°C depending upon the requirement.

From the above description it is evident that the process is fairly complex and development of a mathematical model for this process is a formidable task. In addition, the model will require detailed material properties which may not be available for the operating regime being considered.

From Fig.1 it is obvious that the process has three distinct regions, viz a Liquid Region (LR), a thin Bed Region (BR) and a gas Jet Region (JR). Therefore, three separate models have to be

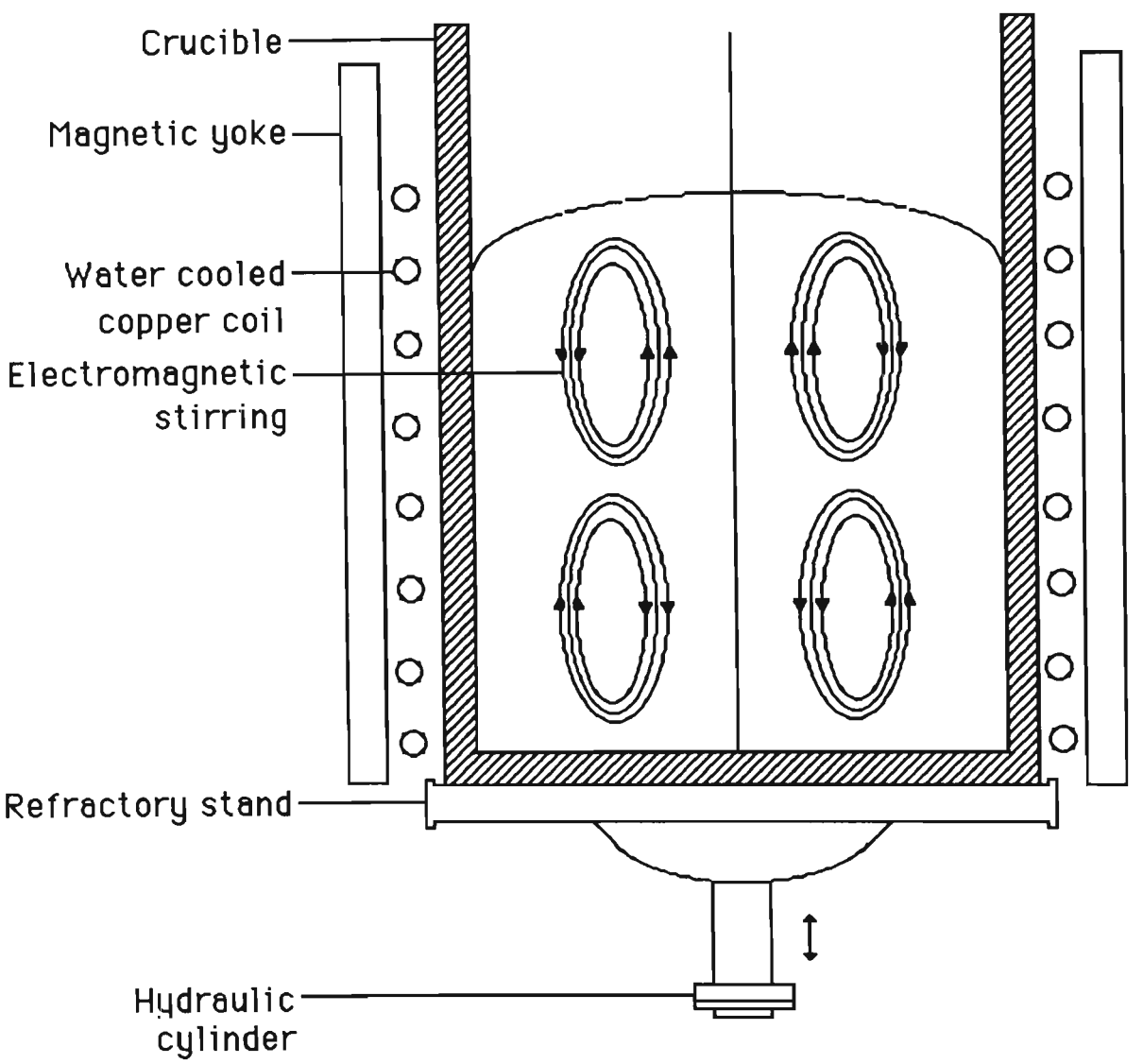

Fig. 2. A sketch of a coreless induction furnace

developed, one for each region, which can be linked to each other through appropriate boundary conditions. Since induction smelting uses a coreless induction furnace, it would be advantageous from a mathematical viewpoint to look in detail at the construction of the coreless induction furnace. The general working principle and construction of the coreless furnace is as follows:

The composite pellets are smelted inside a cylindrical graphite crucible which stands on a hydraulically operated platform. On the inside the furnace is rammed with refractory lining. A cylindrical water cooled copper coil surrounds the outside of the refractory as shown in Fig. 2. An alternating current (AC) in the coil produces a pulsating magnetic field in the vertical direction. Outside the coil, there are packets of magnetic laminations which provide return paths for the flux, improving the power factor and reducing the risk of flux linking with surrounding metal work to cause stray heating. The whole furnace is contained in a mechanically rigid structure and mounted.

Since the melt is fluid, there will be hydrodynamic forces set up by the interaction of the fluxes and currents which produce a modest stirring in medium frequency furnaces. With this mechanism, the whole bath is stirred, which makes these furnaces more suitable for high grade steel production. Stirring improves homogenization in the melt, and heat and mass transfer. On the other hand it causes rapid lining wear and tear, and entrapment of solid particles in the melt. Normally, these flows due to electromagnetic force are termed electromagnetically driven flows and fall in the magnetohydrodynamics field. These flows eg, induction melting,

induction stirred ladle metallurgy, continuous casting, electro-slag refining etc occur in many metal processing operations. In induction melting, the flow is usually turbulent, especially in low frequency induction furnaces. Turbulent recirculating fluid flow phenomena in these systems represent a very complex but interesting class of electromagnetically driven flows.

The magnetohydrodynamics field has been influenced by the electrical discipline in the past. Not much work is reported on electromagnetically driven flows that are applicable to metals processing operations in metallurgy. Recently, among metallurgists there has been a growing interest in understanding these phenomena properly, in order to improve various existing metals processing operations. Due to this impetus, it is now possible to reasonably understand momentum, heat and mass transfer in these processes. Still, much work has to be done in this direction so that one can confidently predict fluid phenomena occurring in electromagnetically driven flows. The pioneering work in this direction has been done by many researchers[43-78]. A good discussion of the MHD of fluids is given in reference 50.

In low frequency furnaces stirring is vigorous and flow is turbulent but in medium frequency furnaces, stirring is modest and therefore the flow is less turbulent. In a single phase coreless induction furnace there is a typical double toroid stirring pattern i.e. there are four circulating loops which are produced by stationary magnetic fields as shown in Fig. 2.

In order to calculate the fluid flow in single phase coreless furnaces one has to solve the Navier-Stokes equation with Maxwell's equations. And in order to include turbulent viscosity in the Navier-Stokes equation one has to obtain it by applying a suitable turbulence model. Amongst the available turbulence models the k - ε and k - W models are widely used for this purpose. The performance of these two turbulence models is quite satisfactory. Improvements in these models are in progress[51].

Only a little work has been accomplished[44,47,52-53,60] on heat transfer in the induction melting furnaces. Heat transfer problem has been solved by considering a homogeneous bath with little variation in bath temperature. But in the present Induction Smelting Process the situation is quite different. A steep temperature gradient exists inside the furnace due to the feeding of composite pellets and to various other losses, viz wall losses, radiation losses etc.

In the liquid region, in the induction smelting problem, we have assumed that only liquid iron exists as a major component, together with some slag. Due to good stirring in the liquid region the slag-metal mixture is quite homogeneous and an infinite area prevails for any minor slag - metal reaction. Therefore, no mass transfer calculation is involved in this region.

The heat transfer equation can be solved simultaneously with the fluid flow equations to obtain the thermal and flow behaviour of the fluid.

The bed region can be considered to be thin packed bed region. Initially, the solution of this region has been tried by using the vectorial form of Ergun equation proposed by Stanek and Szekely[79-81] for low Reynolds numbers, but some numerical instability in the solution resulted. Therefore, we adopted a relatively new approach known as the cell model approach, which has been used by many other researchers in chemical and mechanical disciplines. It is believed that this is the first time such an approach has been adopted in the metallurgical field. A good discussion on the cell model is available in refs. 82 and 83.

Briefly, in the cell model the assemblage is divided into a number of identical cells, one particle occupying each cell. The boundary problem is thus reduced to the behaviour of a single particle and its bounding envelope. Transport calculations for momentum, heat and mass balance are performed for one cell and multiplying by the total number of particles present in the system, giving the total response of the system. This approach has been used quite extensively on different particles of various shapes to obtain the drag coefficient, heat and mass transfer rate[82-101,122].

The flow of any fluid can be represented with the help of the Navier - Stokes equation

$$\rho \frac{DV}{Dt} = \mu \nabla^2 \underline{V} - \underline{\nabla} p + \rho \underline{g} \qquad (1.1)$$

On making it dimensionless one gets a dimensionless number known as the Reynolds number, Re, which represents the ratio of

inertial to viscous forces. This is a very important parameter. On the basis of Reynolds number, fluid motion has been divided into three groups: low Re number (Re $\leq$ 1); intermediate Re number (1 $\leq$ Re $\leq$ 500); and high Re number (Re > 500).

Different approaches are used to solve eqn. (1.1) for different Reynolds numbers, to describe the flow, thermal and mass behaviour of the fluid. Details can be found in ref. 18. Low Reynolds number flows are widely known as 'creeping flows'. In the present work, the Reynolds number is known to vary from 0.1 to 3 which indicates that the behaviour falls into the creeping flow and intermediate Reynolds number ranges.

In the bed region the mass balance equation will be solved only for FeO, which is of prime interest. The reaction of FeO and C is considered the main reaction in this region. Therefore, the above mentioned Navier-Stokes equation should be solved simultaneously with the heat and mass balance equations in order to obtain the melt thermal, mass and flow behaviour.

The remaining region is the gas jet region. In the induction smelting problem, the gas boundary layer region has been considered of interest. Therefore, all attempts to predict flow, thermal and mass behaviour of the gas have been focussed in the boundary layer region. A good discussion on boundary layer theory is available in ref. 102.

Interaction between an impinging jet and a solid surface is of interest in many engineering applications such as annealing of

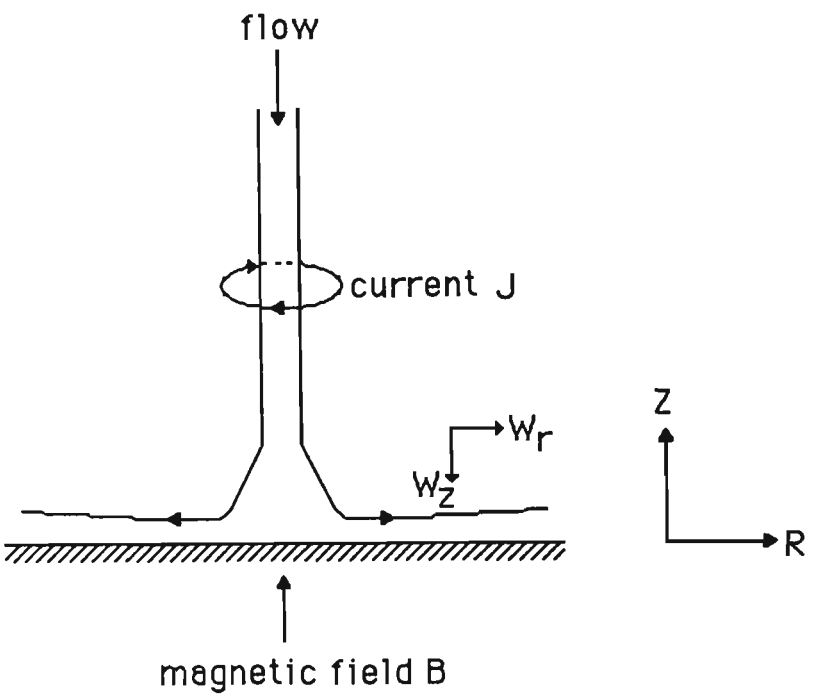

Fig. 3. Diagram of stagnation flow with an applied magnetic field.

metals, tempering of glass, drying of textiles, papers etc. In the last fifty years, many investigators[102-115] have done work on it, but still much work remains. In this area, theoretical work often lacks experimental verification.

In the jet region, the Reynolds number comes under laminar flow during operation, and therefore, laminar flow will be considered. In the present case, the gas jet also interacts with the applied axial magnetic field which acts perpendicularly to the oncoming flow as shown in Fig. 3. Interaction between the gas jet and magnetic field affects the conventional flow of fluid. This situation is quite frequent in aerodynamic flow especially in hypersonic flight. Description of this flow is given in various standard text books[116-117]. This aspect of the problem is discussed briefly in chapter 2 during the formulation of the jet region. In essence, after carefully scrutiny of the literature, the effect of the magnetic field interaction with the gas jet has been neglected in the present study. Therefore, the Navier-Stokes equation will be solved with heat and species balance equations to obtain gas flow, temperature and concentration field.

Now it is very clear how complex this process is. Numerous electrical, mechanical, chemical and physical data are involved in the whole analysis. Extremely careful attention must be paid to analysing these parameters and their effect on the whole smelting process, because these parameters are very much inter-related. Measurement of all the parameters will involve substantial experimental effort. One must also bear in mind that the process is time dependent. Therefore, at each step all the flow, heat and mass

transfer behaviours are changing. As the smelting proceeds, the liquid height gradually increases. All these factors have to be taken into account in our mathematical model.

As may be expected, the following chapters will contain numerous symbols representing quantities in various regions. Most of them have been defined in the nomenclature, but a few symbols are used more than once. To avoid ambiguity, those symbols which are recurring and have different meanings will be defined as they occur.

In general, chapter 2 is devoted to the formulation of the Induction Smelting Process which includes a liquid region, a bed region and a jet region. A new technique has been developed to calculate the electromotive force. All these regions are combined by considering overall heat and mass balance for the entire process. Chapter 3 gives an idea of the computational technique used to solve governing partial differential equations (PDEs) developed in chapter 2. Chapter 4 provides the experimental procedure to measure the various parameters to compare with the predictions. A velocity measurement device has been developed to measure the liquid iron velocity in induction furnace. Chapter 5 deals with the results and discusses the comparison between model predictions and the experimental results. The effects of various process parameters on Induction Smelting Process have also been discussed. Conclusions from the work have been described in Chapter 6. Some further details have been given in the appendices.

CHAPTER 2

DEVELOPMENT OF A MATHEMATICAL MODEL FOR THE INDUCTION SMELTING PROCESS

INTRODUCTION:

The purpose of this chapter is to develop a mathematical model for an Induction Smelting Process taking self-fluxed pellets of iron-ore as a typical example. The continuum, or macroscopic approach will be used for the mathematical treatment of the problem throughout this chapter. The structure of the model is such that it can be divided into three sections, viz:

A) Liquid (Electromagnetic stirred) region,
B) Bed (Liquid - solid interaction) region
C) Gas Jet (and solid interaction) region

Below, each section has been treated separately with its model equations. Furthermore, the non-dimensionalization of all governing equations of the model with their boundary conditions has been presented in section E. (During the development of the mathematical model it has been assumed that readers are familiar with fluid mechanics and electromagneto dynamics). In each section a few assumptions have been made in order to simplify the mathematical treatment. The justifications for the various assumptions involved in the analysis are explained wherever appropriate.

2A) ELECTROMAGNETIC STIRRED REGION:

No mass transfer is included in the induction (Liquid) region because it is assumed that in this region equilibrium prevails due to complete mixing (infinite reaction area) between the Fe and slag.

The working principle and construction of an induction furnace has already been discussed in Chapter 1. Fig. 2 shows the essential features of a single phase coreless induction furnace, as discussed in the previous chapter, which has to be modelled now. Fig. 2 also shows a typical double toroid stirring pattern which is a salient feature of a single phase coreless induction furnace, due to the creation of a stationary wave by the coils. The shape of the double toroid stirring pattern depends upon many variables, such as coil arrangement, furnace geometry, melt height etc. Before proceeding to mathematical formulation, let us see how electromagnetic stirring occurs inside the melt.

When an alternating current is applied to the furnace coil, an opposite circumferential current is induced in the z direction. Therefore, J_z is the only component of current density existing in the furnace. This induced current supplies the necessary heat to the melt and interacts with applied magnetic field B, producing two components of electromagnetic body forces. The radial (conservative or irrotational) component of the force, contributing to the magnetic pressure, only pinches the molten charge. This phenomenon is known as the 'Pinch effect' and is responsible for the distortion of the free surface of the melt (meniscus). The other axial (non conservative, rotational) component of the body

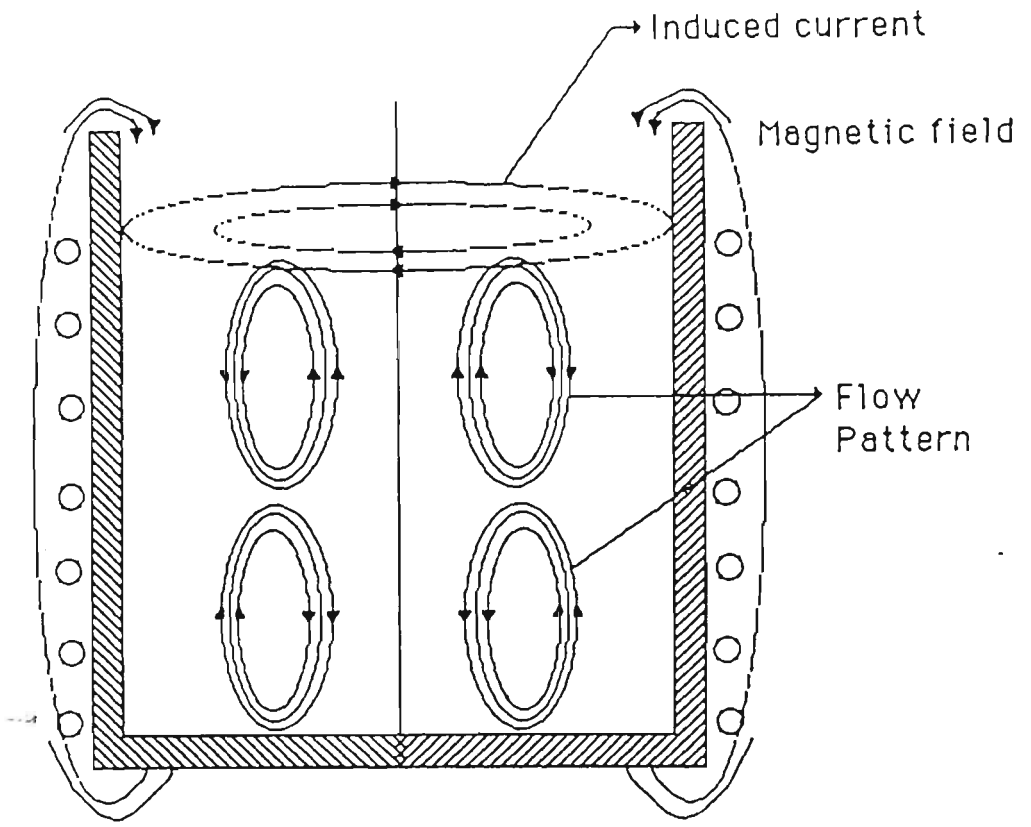

Fig. 4. Distrubution of current, magnetic and flow field.

force is responsible for the stirring in the melt. Beside this, thermal stirring may take place if the temperature gradient in the charge is considerable. The temperature is always greatest in the centre due to the less dense melt. The net radial force is zero and the average melt velocity is also zero provided nothing is being added to the melt. Fig. 4 shows the direction of current density, magnetic field, force and stirring in the melt.

The above mentioned stirring forces cause a turbulent recirculating flow in the melt. In the Induction Smelting Process considered, cold charge is being continuously added to the furnace. Therefore, a steep temperature gradient exists in the melt. In order to predict the temperature profile in the melt one has to know the exact nature of the flow and its velocity components. To know the velocity of the melt one has to solve the Navier-Stokes equation with an electromagnetic body force term and turbulent viscosity. Once the velocity is known, the temperature field can be obtained by solving the heat transfer equation with a Joulean dissipation (heat) term and turbulent diffusivity. The mathematical treatment of this section is based upon the following assumptions:

2A-1) Assumptions:

1) This region will be solved by considering an axi-symmetric problem in cylindrical co-ordinates.
2) Steady state will be assumed for flow calculations.
3) Laminar flow will be assumed in the melt.
4) Position independent physical properties of the melt will be assumed.

5) The slight curvature of the melt meniscus can be neglected.
6) The slightly helical shape of the coil has been neglected.
7) No heat releases/absorption due to chemical reactions occur.

Assumpton 3 is thought to be reasonable for the present case in which one is interested to know the overall mass, heat and momentum transfer for the smelting process which itself is a complex process. Moreover, other findings[48-49,118] show that introducing the turbulent flow, using the k-ε model, in the MHD induced flow in induction furnaces is not justifiable economically and it increases the complexity of the process for little improvement in flow calculations. Adoption of turbulent flow makes the process much more sophisticated. Nevertheless, it may be useful when it is necessary to know the exact nature of the turbulence and thus the velocity components for design purposes.

Assumption 7 seems reasonable because most of the reaction occurs in the bed region, and only a minor part of the reaction may occurs in the liquid region which has been neglected.

2A-2) MODEL FORMULATION:

LIQUID PHASE MOMENTUM BALANCE:

In the following analysis, the word *fluid* has also been used for liquid iron.

Incompressible fluid flow in the steady state can be represented by writing down the vectorial form of the equation of motion (Navier-Stokes equation) in terms of stress:

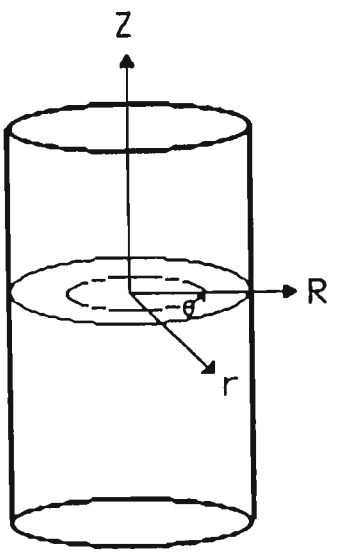

Fig. 5. Cylindrical co-ordinate system adopted for liquid region.

$$\rho_L \frac{D\underline{u}}{Dt} = -\nabla \underline{\tau} - \underline{\nabla} P + \rho_L \underline{E_b} \qquad (2A\text{-}1)$$

where the first two terms on the right side of the equation represent the stress tensor and the pressure gradient, respectively. The last term represents body forces, which may include forces such as gravitational, electromagnetic, & buoyancy, depending upon the nature of the problem. The line below the symbols indicates they are vectors. D/Dt is the substantive derivative as defined in Appendix A.

Before proceeding further, it is necessary to define the co-ordinate system adopted. Fig. 5 shows the cylindrical co-ordinate system which has been adopted throughout this section. Symmetry has been assumed in θ-direction, which makes the problem an axi-symmetrical one. In making this assumption it has been assumed that there is no substantial change of velocity, temperature etc in the θ-direction, which should be very close to reality because of good stirring in the melt. We therefore consider the two-dimensional axi-symmetric problem in the r and z directions.

Now, after taking the curl of equation (2A-1) and expanding the appropriate term with the introduction of vorticity and stream function, the equation of momentum can be written as:

$$\left[\frac{\partial}{\partial z}\left(\frac{\xi}{r}\frac{\partial \psi}{\partial r}\right) - \frac{\partial}{\partial r}\left(\frac{\xi}{r}\frac{\partial \psi}{\partial z}\right)\right] \hat{e}_\theta + \frac{\mu}{\rho_L}\left[\frac{\partial}{\partial r}\left\{\frac{1}{r}\frac{\partial}{\partial r}(r\xi)\right\} + \frac{\partial}{\partial z}\left\{\frac{1}{r}\frac{\partial}{\partial z}(r\xi)\right\}\right]$$
$$\hat{e}_\theta + \frac{1}{\rho_L}\left\{\underline{\nabla} \times (\underline{J} \times \underline{B})\right\} = 0 \qquad (A\text{-}13)$$

and the vorticity and stream function can be related by the eqn.:

$$\xi = \frac{\partial}{\partial z}\left(\frac{1}{r}\frac{\partial \psi}{\partial z}\right) + \frac{\partial}{\partial r}\left(\frac{1}{r}\frac{\partial \psi}{\partial r}\right) \qquad \text{(A-14)}$$

A full derivation of equation (A-13) has been given in Appendix A. The first two terms in equation (A-13) represent convective and diffusive transport of momentum, respectively, and the third term arises from the interaction of the induced current and the applied magnetic field i.e. electromagnetic force.

Now it is evident from (A-13) why this problem is an MHD one. In a broad sense the study of the interaction of electromagnetic field with fluid comes under the magnetohydrodynamics field. It is clear from equation (A-13) that the electromagnetic field is related to the equation of motion. The MHD field is well developed and abundant literature is available. Without going into detail we will write down Maxwell's equation under the MHD approximation in order to calculate the electromagnetic body force term. (Full discussion of these equations is available in ref. 50).

$$\Delta \times E = -\frac{\partial B}{\partial t} \qquad \text{(2A-2)}$$

$$\nabla \times H = J \qquad \text{(2A-3)}$$

$$\nabla . J = 0 \qquad \text{(2A-4)}$$

$$\nabla . B = 0 \qquad \text{(2A-5)}$$

Ohm's law, in the presence of moving fluid takes the following form:

$$J = \sigma [E + \underline{u} \times B] \qquad (2A\text{-}6)$$

Assuming that the material is magnetically linear we can state:

$$B = \mu_t H \qquad (2A\text{-}7)$$

where μ_t is permeability of the magnetic material which is:

$$\mu_t = \mu_r \mu_o \qquad (2A\text{-}8)$$

where μ_r is the relative permeability. For liquid metal it is 1. Therefore, equation (2A-7) becomes:

$$B = \mu_o H \qquad (2A\text{-}9)$$

where μ_o = the magnetic permeability of free space

In deriving Maxwell's equations, the displacement current has been neglected.

Furthermore, if we assume that the electric fields induced by the motion of the liquid metal are negligible, then equation (2A-6) reduces to

$$J = \sigma E \qquad (2A\text{-}10)$$

By writing down the current density in this form, without affecting the flow calculations appreciably, we can solve the

body force term separately from the equation of motion. Therefore, the equations do not need to be solved in a coupled manner, which renders the computational task much easier.

Now let us examine the general nature of all the electrical quantities and their inter-relationship.

All the electrical quantities E, B and J are vectors, and are functions of position and time. When an AC current is applied in the furnace coil, E, B and J all vary sinusoidally, which means they all are complex quantities and one only has to consider their real parts in the final calculations.

As already discussed, the current density J only has its azimuthal component J_θ, and the magnetic field B has radial B_r and axial B_z components, which means:

$$\underline{J} = J_\theta \hat{e}_\theta \qquad (2A\text{-}11)$$

$$\underline{B} = B_r \hat{e}_r + B_z \hat{e}_z \qquad (2A\text{-}12)$$

Then the body force, which is also called the Lorentz force or pondermotive force, becomes:

$$JXB = - J_\theta B_r \hat{e}_z + J_\theta B_z \hat{e}_r \qquad (2A\text{-}13)$$

(In Appendix E, the main vector operations have been given in order to understand the mathematical manipulation).

$$\nabla X(JXB) = \left[\frac{\partial}{\partial r}(J_\theta B_r) + \frac{\partial}{\partial z}(J_\theta B_z)\right]\hat{\theta} \qquad (2A\text{-}14)$$

The body force term can be derived in a different form with the help of equations (2A-3) and (2A-9) which gives:

$$\underline{J}X\underline{B} = \left[\underline{\nabla} X \left(\frac{\underline{B_o}}{\mu_o}\right)\right] X \underline{B}$$

$$= -\underline{\nabla}\frac{\underline{B^2}}{2\mu_o} + \frac{1}{\mu_o}\underline{B}.\underline{\nabla}\underline{B} \qquad (2A\text{-}15)$$

This is a very useful equation which gives an insight into the nature of the body force. The first term on the right side of the equation is the magnetic pressure, which is responsible for the 'pinch effect', and the second term is responsible for the stirring in the melt.

There are several other useful equations of fundamental interest which can be derived using Maxwell's equations and Ohms law which are not derived here, but can be found in ref. 50.

At this stage it is convenient to introduce the vector potential, A, in order to represent body force term in an easier form:

$$B = \nabla X A \qquad (2A\text{-}16)$$

$$E = -\frac{\partial A}{\partial t} \qquad (2A\text{-}17)$$

$$\nabla.A = 0 \qquad (2A\text{-}18)$$

Taking the curl of equation (2A-16) and using equations (2A-3), (2A-9) and (2A-10), after some manipulation, we obtain:

$$-\nabla^2 A = \mu_o \sigma E \qquad (2A\text{-}19)$$

By using equation (2A-17) we get:

$$\nabla^2 A = \mu_o \sigma \frac{\partial A}{\partial t} \qquad (2A\text{-}20)$$

or

$$\frac{\partial}{\partial r}\left[\frac{1}{r}\frac{\partial}{\partial r}(rA_\theta)\right] + \frac{\partial}{\partial z}\left[\frac{1}{r}\frac{\partial}{\partial z}(rA_\theta)\right] = \mu_o \sigma E \qquad (2A\text{-}21)$$

Equation (2A-16) also gives:

$$B_z = \frac{1}{r}\frac{\partial}{\partial r}(rA_\theta) \qquad (2A\text{-}22)$$

$$B_r = \frac{\partial A_\theta}{\partial z} \qquad (2A\text{-}23)$$

Equations (2A-17) and (2A-10) give:

$$J_\theta = -\sigma \frac{\partial A_\theta}{\partial t} \qquad (2A\text{-}24)$$

As we know, J_θ is the only component of the current density, J, which exists. Similarly it can be shown with the help of equations (2A-16, 3 & 9) that the only component of the vector potential which has to be considered is A_θ.

From equation (2A-13) we obtain two body force terms, the axial force F_z, and radial force F_r.

$$F_z = -J_\theta B_r \qquad (2A\text{-}25)$$

and

$$F_r = J_\theta B_z \qquad (2A\text{-}25)$$

The coil current for a stationary wave produced by a single phase connection may be written as :

$$J_\theta = J_o e^{i\omega t} \sin kz \qquad (2A\text{-}27)$$

where $k(=1/\lambda)$ is the wave number, λ is the wavelength, ω is the angular frequency, f is the frequency and $i = \sqrt{-1}$.

Noting the resemblance between J_θ and A_θ, the latter can also be expressed as:

$$A_\theta (r,z,t) = \acute{A}_\theta (r,t) \sin kz \qquad (2A\text{-}28)$$

Putting this value into equation (2A-21), after simplification we get:

$$\frac{1}{r}\frac{\partial}{\partial r}\left(r \frac{\partial \acute{A}_\theta}{\partial r}\right) - \left(k^2 + \frac{1}{r^2}\right)\acute{A}_\theta = \mu_o \sigma \frac{\partial \acute{A}_\theta}{\partial t} \qquad (2A\text{-}29)$$

Now let us define:

$$\acute{A}_\theta = A_1(r) + iA_2 (r) \qquad (2A\text{-}30)$$

After substitution of $\acute{A}_\theta$ in equation (2A-29) and separating the real and imaginary parts we get:

$$\frac{d^2A_1}{dr^2} + \frac{1}{r}\frac{dA_1}{dr} - \left(k^2 + \frac{1}{r^2}\right)A_1 + \mu_o\sigma\omega\, A_2 = 0 \qquad (2A\text{-}31)$$

and

$$\frac{d^2A_2}{dr^2} + \frac{1}{r}\frac{dA_2}{dr} - \left(k^2 + \frac{1}{r^2}\right)A_2 - \mu_o\sigma\omega\, A_1 = 0 \qquad (2A\text{-}32)$$

Equations (2A-31 & 32) can be solved very easily by introducing the appropriate boundary conditions. Once the vector potential solution is known, then the body force can be obtained. To obtain the body force let us express it in terms of vector potentials which are already known. Equations (2A-22-24), with the help of equation (2A-30), gives:

$$B_z = \frac{1}{r}\frac{d}{dr}(rA_1 + i\, r\, A_2)\, e^{i\omega t} \sin kz \qquad (2A\text{-}33)$$

$$B_r = -k\,(A_1 + i\, A_2)\, e^{i\omega t} \cos kz \qquad (2A\text{-}34)$$

$$J_\theta = -i\sigma\omega\,(A_1 + i\, A_2)\, e^{i\omega t} \sin kz \qquad (2A\text{-}35)$$

After substituting these values in the body force terms we get, for the axial body force:

$$J_\theta B_r = \left[\left\{-i\sigma w\,(A_1 + i\, A_2) \sin kz\right\}\left\{-k\,(A_1 + i\, A_2) \cos kz\right\}\right] e^{2i\omega t} \qquad (2A\text{-}36)$$

On time averaging and taking the real part of eqn. (2A-36) we obtain

$$\text{Re } (J_\theta B_r) = \frac{1}{2}[-\sigma\omega k A_1 A_2 \sin 2kz] \qquad (2A\text{-}37)$$

Similarly, the radial body force term can be written, after time averaging and considering its real part only:

$$\text{Re } (J_\theta B_r) = \frac{\sigma\omega}{2}\left[2\frac{A_1 A_2}{r} + A1\frac{dA_z}{dr} + A2\frac{dA_1}{dr}\right]\sin^2 kz \qquad (2A\text{-}38)$$

Now one can obtain the solution of the equation of motion after substituting the value of the force term. An alternate approach to obtaining the body force term, based on ref. 43, has been presented in Section E.

Analytical solution[1] for the magnetic field and other electrical quantities shows that the magnitudes of the fields fall exponentially inside the crucible from the surface of the crucible where they have their maximum values. From this analytical solution one obtains an extremely useful parameter δ, known as skin depth or penetration depth

$$\delta = \sqrt{\frac{2\, r_e}{\mu_t\, \omega}} = \sqrt{\frac{2}{\sigma\, \mu_t\, \omega}} \qquad (2A\text{-}39)$$

which is inversely proportional to the square root of the product of the magnetic permeability, the thermal conductivity of the material and the operating frequency.

Because electrical quantities decay exponentially away from the crucible surface, they are mostly concentrated within 2-3 skin depths inside the crucible. Thus, electromagnetic forces are most intense in this region. Therefore, proper care must be taken to evaluate the body force terms in this region which control the fluid motion inside the crucible. Also, towards the ends of the induction coils, the curl (J X B) concentrates more, so that the stirring motion is driven by two turbulent wall jets originating in these corners of the crucible, directed towards the center of the coil.

A typical melt diameter to penetration depth ratio, in the present study, is ~18 which reveals the fact that most of the electric fields and body forces are localized near the crucible wall. Special care has been taken in this region, for the current study, during the solution of the equation of motion. Sometimes this region is referred to as the electromagnetic wall layer region analogous to the fluid boundary layer in conventional fluid mechanics. It is emphasized that one should not underestimate or neglect the effect of the radial body force term, which is primarily responsible for the melt meniscus, because its gradient in the equation of motion becomes of the same order of magnitude as the gradient of the axial body force term, as shown by Moore and Hunt[46]. Therefore, one should consider the curl of JXB to be fundamental to an understanding of the flow.

Before closing this part, let us derive a few more important equations for later use.

With the help of equation (2A-24) and (2A-27) one gets:

$$A_\theta = \frac{J_\theta}{i\sigma\omega} \sin kz\ e^{i\omega t} + f(r,z) \qquad (2A\text{-}40)$$

And equations (2A-2), (2A-3), (2A-6) and (2A-9), after some manipulation give:

$$\frac{\partial \underline{B}}{\partial t} = \frac{1}{\mu_o \sigma} \nabla^2 \underline{B} + \underline{\nabla} \times (\underline{u} \times \underline{B}) \qquad (2A\text{-}41)$$

where, $1/\mu_o\sigma$ is known as magnetic diffusivity.

2A-3) LIQUID PHASE ENERGY BALANCE:

If we neglect the viscous dissipation in the fluid then the energy equation can be written

$$\rho_L C_{p.L} \frac{DT_L}{Dt} = k_L \nabla^2 T_L + \bar{J}_\theta^2 r_e \qquad (2A\text{-}42)$$

A detailed discussion on energy balance equation is given in Ref.50. The first term on the right side of the equation is the energy transfer due to molecular conduction (eddy conduction has been neglected as we are considering laminar flow). The remaining terms on the right hand side are Joulean heat dissipation (i.e. heat generation rate per unit volume due to current) where r_e is the resistivity of the fluid. In formulating this equation, pressure variations which may arise due to magnetic field and buoyancy have been neglected.

There are two distinct temperature regions in an induction furnace

1) near the crucible axis i.e. the central region in which heat dissipation is negligible, and

2) near the crucible wall i.e. the electromagnetic boundary layer region (as discussed earlier) in which heat sources are localized.

Near the wall, turbulence is decaying and a steep temperature gradient exists which may be used to define the heat transfer coefficient. In the rest of the furnace, the temperature is expected to be homogeneous, due to good stirring.

Equation 2A-42 in cylindrical co-ordinates (axi-symmetrical form) can be expressed:

$$\rho_L C_{p.L} \frac{\partial T_L}{\partial t} + \rho_L C_{p.L} u_r \frac{\partial T_L}{\partial r} + \rho_L C_{p.L} u_z \frac{\partial T_L}{\partial z} = k_L \frac{\partial^2 T_L}{\partial r^2} + \frac{k_L}{r} \frac{\partial T_L}{\partial r} + k_L \frac{\partial^2 T_L}{\partial z^2} + J_\theta^2 r_e \qquad (2A\text{-}43)$$

In equation (2A-43) the current density is represented by equation (2A-10) which facilitates the solution of energy balance equation separately and need not be coupled with the Joulean heat term.

2A-4) BOUNDARY CONDITIONS:

In this section we shall discuss all the boundary conditions required to solve the non-linear partial differential equation (PDEs) (A-13), (A-14) and (2A-11).

There are different ways to define the boundary conditions for these equations. Assuming a no slip condition at the solid wall (i.e. at the crucible wall), the velocity will be zero there. At the free surface of the fluid, shear stresses will be zero i.e. velocity gradient will be zero. Therefore the boundary conditions for the vorticity equation (A-13) and stream function equation (A-14) are:

At	$r = o$	$\xi = 0$	&	$\psi = 0$	(2A-44a,b)
	$r = R$	$\frac{\partial \psi}{\partial r} = 0$	&	$\psi = 0$	(2A-45a,b)
	$z = 0$	$\frac{\partial \psi}{\partial z} = 0$	&	$\psi = 0$	(2A-46a,b)
and	$z = z_1$	$\xi = 0$	&	$\psi = 0$	(2A-47a,b)

Boundary conditions (2A-44a,b) are due to the symmetry assumed about the center line.

For the energy balance equation (2A-43), a somewhat similar approach can be adopted, to express the boundary conditions.

At the center line radial thermal gradient will be zero, which yields:

$$\text{At} \quad r = 0 \qquad \frac{\partial T_L}{\partial r} = 0 \qquad \text{(2A-48)}$$

Thermal energy is lost through the vertical wall of the crucible by thermal conduction. Therefore, we write

$$\text{At} \quad r=R \qquad T_L = T_w \qquad \text{(2A-49a)}$$

$$-k_L \frac{\partial T_L}{\partial r} = -k_w \frac{\partial T_L}{\partial r} \qquad \text{(2A-49b)}$$

and, $$q_{w2} = - \frac{k_w (T_w - T_{ow2})}{r_w \ln (R/r_w)} \qquad \text{(2A-49c)}$$

Furthermore, at the bottom of the crucible thermal energy is lost by transient conduction.

$$\text{At} \quad z = 0 \quad q_{w1} = - \frac{k_w (T_w - T_{o,w1})}{\sqrt{\pi \alpha_\omega t}} \qquad \text{(2A-50)}$$

where the boundary conditions 2A-49a & 49b are due to the temperature and heat flux continuity at the inside wall of the crucible. The boundary condition 2A-49c arises due to the loss of heat to the side wall by thermal conduction. T_{ow1} and T_{ow2} are the outside temperature of the bottom and side walls of the crucible respectively. In the present case T_{ow1} and T_{ow2} have been assumed constant with the values 327 C and 927 C respectively. These values are realistic and have been used for simplicity, rather than attempting to include a more complicated heat loss condition, which could be incorporated in a future study. r_w is an outside radius of the crucible. q_{w1} and q_{w2} are the heat flux for the bottom and side walls of the crucible respectively.

At the free surface we can assign some value of temperature (later, this value will be obtained by considering the overall heat balance for the whole system as explained in section D).

$$\text{At} \quad z = z_1 \quad T_L = T_\infty \qquad \text{(2A-51)}$$

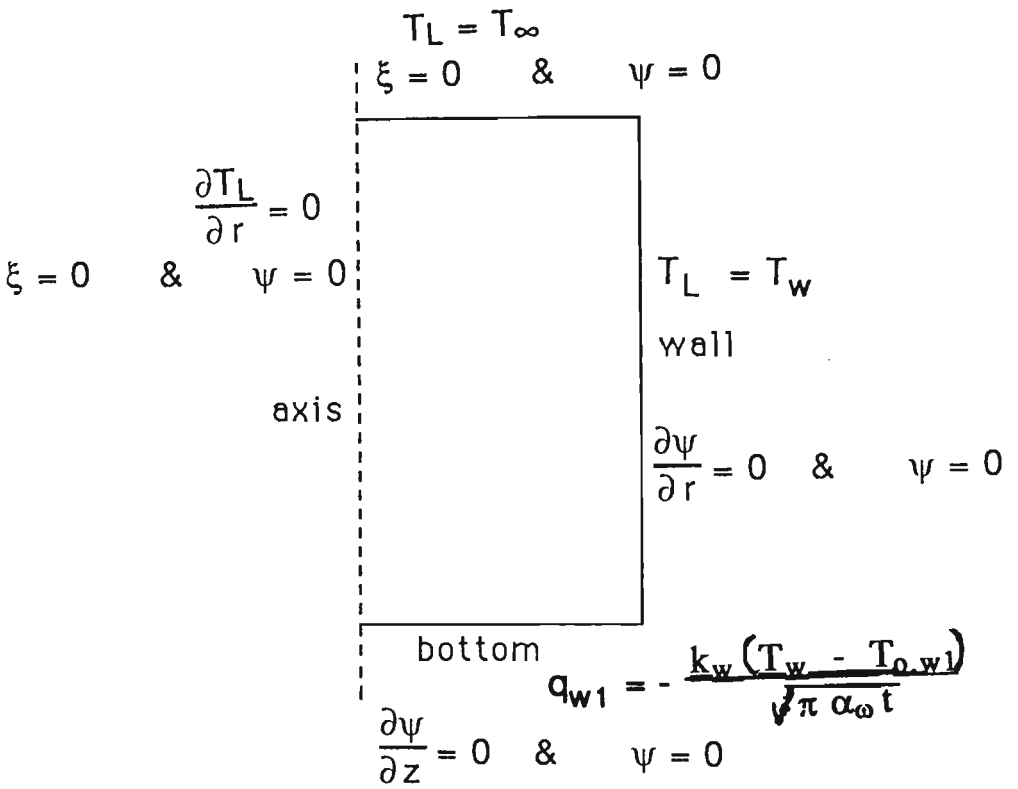

Fig.6. Boundary conditions used for liquid region

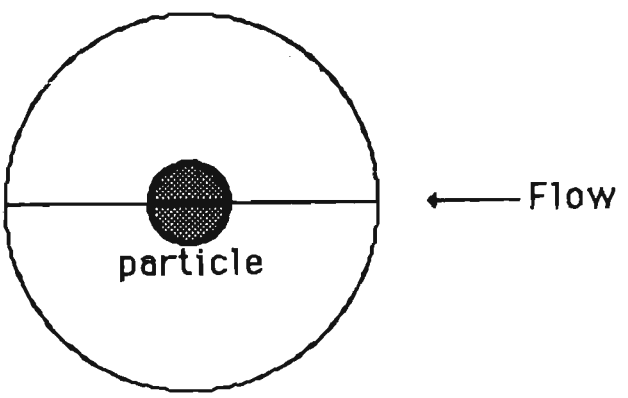

Fig. 7. Single particle and its bounding envelope.

where z_1 is the fluid/gas jet interphase height, which varies with time as melting proceeds in the z-direction.

All the boundary conditions are shown in dimensional form in fig. 6. Boundary conditions for equations (2A-31 & 32) can be expressed as follows:

At $r = 0$ A_1 and A_2 are finite

Therefore, we may write

$$\text{At} \quad r = 0 \quad \frac{dA_1}{dr} = 0 \qquad (2A\text{-}52)$$

$$r = 0 \quad \frac{dA_2}{dr} = 0 \qquad (2A\text{-}53)$$

$$r = R \quad A_1 = 1 \qquad (2A\text{-}54)$$

$$\text{and} \quad r = R \quad A2 = \frac{|J_o|}{\sigma\omega} \qquad (2A\text{-}55)$$

The last value arises from the surface value of the vector potential and is easily derivable from equation (2A-40).

SECTION B: PACKED BED REGION:

As already discussed in Chapter 1 this region will be solved by using a relatively new approach known as the Cell Approach or Cell Model. The cell can be defined as the region of influence of a single particle in the System. Depending on the void/particle size ratio, the cell dimensions can be determined. Fig.7 shows a spherical cell surrounding a particle. Normally, for a system, the assemblage may be considered to consist of a number of identical

unit cells, each of which contains a particle surrounded by a fluid envelope. Usually, a spherical cell is assumed but it is not necessary to assume a spherical shape only. It is a matter of convenience and also depends on the requirement of the particle shape, system geometry etc. A good discussion on the cell approach and its use is given in ref. 82.

The approach which will be adopted is to first study a typical particle inside a cell. In the process considered in this work, spherical self-fluxed pellets are used, so a spherical pellet will be considered within this cell. Fluid flow behaviour, heat and mass transfer will be studied within the cell by solving the Navier-Stokes equation for fluid motion, the energy balance equation for heat transfer, and the species balance equation for mass transfer. It must be noted here that the numerical solution of the equation of motion was attempted about two decades ago, first by Jenson[119] and later by Hamebeic Le Lair[83] using the finite difference techniques, and since then better numerical techniques have been developed.

Once the desired result is obtained for a single cell then one can easily extend this model to the whole system by knowing that:

Response of total system = Number of particles x Response of a single particle.

In the present process we have assumed a thin packed bed region consisting of three layers of pellets which, is the case during the operating conditions under consideration. The top layer is assumed

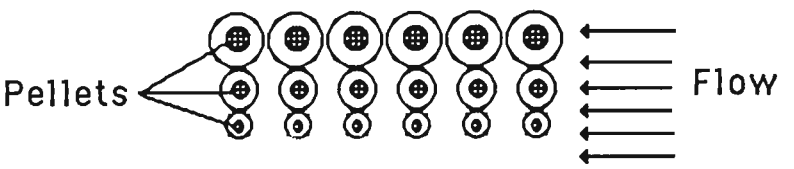

Fig. 8. A schematic diagram for cell model in bed regon.

to be newly added pellets. Change has occurred in fluid flow, heat and mass transfer and in reaction in the middle layer. An extensive change has occurred in the afore mentioned quantities in the lower layer and after that we have assumed that the lower pellets melt totally after a certain time. After that time, the middle layer becomes the lower one, the top layer becomes the middle and freshly added pellets become the top layer. Therefore the situation remains the same until the process is finished i.e. all smelting operations are completed. Fig.8 shows a typical packed bed region for this model.

It is convenient to divide the total number of cells into three categories:

$$\dot{R} \text{ system} = N_1 \dot{R}_1 + N_2 \dot{R}_2 + N_3 \dot{R}_3$$

Where $\dot{R}$ system = the rate of conversion for total system

$\dot{R}_1$ = the rate of conversion of one particle in the top layer

$\dot{R}_2$ = the rate of conversion of one particle in the middle layer

$\dot{R}_3$ = the rate of conversion of one particle in the lower layer

and N_1, N_2, N_3 are the number of particles in the top, middle and lower, layers respectively.

Now the approach for the packed bed region is quite obvious. Therefore, before writing down the PDEs for momentum, heat and mass balance, let us determine the size of the cell.

It is suggested, before going to the model formulation, that the reader refers to Appendix B which gives a discussion of the

reaction kinetics considered for this packed bed region. It also gives some other information which may be helpful in understanding the formulation for this region.

2B-1) DETERMINATION OF THE CELL SIZE:

From Fig.8

Volume of Bed = $\pi R^2 H$

Volume of particles = $\dfrac{\text{Total mass}}{\text{Density of particle}}$

Total void = $\pi R^2 H$ - Volume of particles

Number of particles within the Bed = $\dfrac{\text{Total volume of particle}}{\frac{4}{3}\pi\ \bar{r}_p^3} = Np$

Therefore void volume per particle $Vv = \dfrac{\text{Total void volume}}{Np}$

Total volume of cell = $\frac{4}{3}\pi \bar{r}_p^3 + Vv = \frac{4}{3}\pi\ r_c^3$

$$\therefore \text{ Cell Radius } r_c = \sqrt[3]{\frac{3}{4\pi}\left(\frac{4}{3}\pi\ \bar{r}_p^3 + V_v\right)} \qquad (2B\text{-}1)$$

where $\bar{r}_p$ is the average radius of the pellets and H is the bed height.

Now that the size of the cell is known, all transport calculations can be made within the cell by writing down the appropriate P.D.E.s. First, let us outline the assumptions upon which this model is based.

2B-2) ASSUMPTIONS:-

1) The equation of motion will be solved in the steady state.
2) The packed bed has three layers of pellets which makes it a thin packed bed region.
3) Fluid flow outside the cell is undisturbed.
4) The problem will be solved in two-dimensional spherical co-ordinates (r,θ) i.e. Axi-symmetry in the azimuthal direction will be assumed.
5) Incompressible fluid will be assumed with constant physical properties.
6) Wall and entry effects to the bed will be neglected.

2B-3) PACKED BED MOMENTUM BALANCE:

As we know, in a packed bed region, the fluid is already in motion under the influence of the Lorentz force, and its fluid flow behaviour is already known from Section A. Therefore there is no need to consider the Lorentz force again, because it has been assumed that fluid behaviour is governed by the particle effect inside the cell.

In the above case the equation of motion (2A-1) becomes:

$$\rho_m \frac{DV}{Dt} = \mu_m \nabla^2 \underline{V} - \underline{\nabla} p - \rho_m \underline{g} \qquad (2B\text{-}2)$$

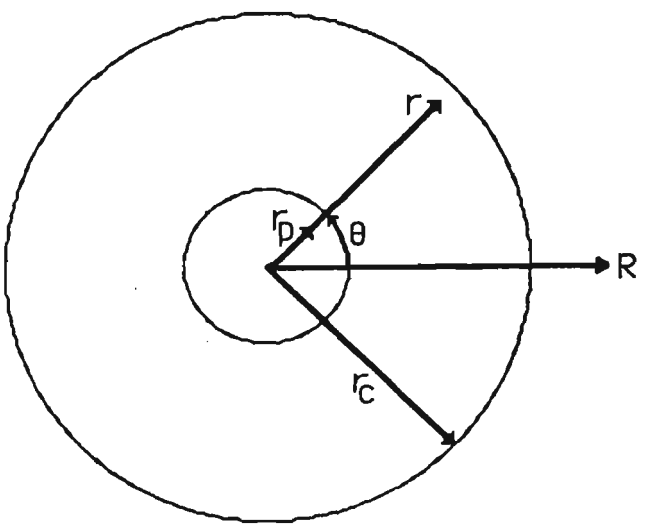

Fig. 9. Two dimensional co-ordinate system for bed region.

This time, details of how to obtain the final equation of motion from equation (2B-2) are omitted as almost all the steps are the same as described in Appendix A. The only difference is that now the equation is in polar co-ordinates which are defined in Fig. 9.

Therefore, taking the curl of equation (2B-2) and introducing the stream function (ψ_B) and vorticity (ξ_B) and following the same steps as in Appendix A, after some manipulation one obtains:

$$\frac{\rho_m}{\mu_m}\left[\frac{\partial\psi_B}{\partial r}\frac{\partial}{\partial\theta}\left(\frac{E_B^2\,\psi_B}{r^2\sin^2\theta}\right) - \frac{\partial\psi_B}{\partial\theta}\frac{\partial}{\partial r}\left(\frac{E_B^2\,\psi_B}{r^2\sin^2\theta}\right)\right]\sin\theta = E_B^4\,\psi_B \quad (2B\text{-}3)$$

where

$$E_B^2 = \frac{\partial}{\partial r^2} + \frac{\sin\theta}{r^2}\frac{\partial}{\partial\theta}\left(\frac{1}{\sin\theta}\frac{\partial}{\partial\theta}\right) \quad (2B\text{-}4)$$

$$V_\theta = \frac{1}{r\sin\theta}\frac{\partial\psi_B}{\partial r} \quad (2B\text{-}5)$$

$$V_r = -\frac{1}{r^2\sin\theta}\frac{\partial\psi_B}{\partial\theta} \quad (2B\text{-}6)$$

Equation (2B-3) is the desired Navier-Stokes equation of motion in polar co-ordinates, allowing for axial symmetry, written in terms of the stream function.

If the convective derivative in equation (2B-2) is neglected, then after some manipulation we obtain

$$E_B^4\ \psi_B = 0 \quad (2B\text{-}7)$$

which is the well known equation for 'creeping flow' motion i.e. where $Re \rightarrow o$. Study of the cell model first started for the creeping

flow region about six decades ago. Then it came to intermediate Reynolds numbers and subsequently to higher Reynolds numbers. The present problem falls in the creeping flow and intermediate Reynolds number regimes.

As we know, in all problems, the stream function and vorticity have their own physical significance. Here, the volumetric flow rate of fluid, at any point, crossing any continuous surface whose outer boundary is a circle centred on the axis of symmetry and passing through the point in question, is given by $2\pi\psi_B$. It is obvious that $\psi_B=0$ on the axis of symmetry. Stream surfaces are surfaces of constant ψ_B and are parallel to the velocity vector, $\underline{V}$ at every point.

ξ_B is given from equation (A-5). It can be shown that ξ_B is twice the angular rotation of a fluid element. When $\xi_B = 0$, the flow is irrotational. For axi-symmetrical problems, the vorticity becomes a scalar function.

Equation (2B-3) may be split into two simultaneous second order differential equations by introducing the vorticity as follows:

$$E_B^2 \Psi_B = \xi_B \; r \sin\theta \qquad (2B\text{-}8)$$

$$\frac{\rho_m}{\mu_m}\left[\frac{\partial\psi_B}{\partial r}\frac{\partial}{\partial\theta}\left(\frac{\xi_B}{r\sin\theta}\right) - \frac{\partial\psi_B}{\partial\theta}\frac{\partial}{\partial r}\left(\frac{\xi_B}{r\sin\theta}\right)\right]\sin\theta = E_B^2(\xi_B\, r\sin\theta) \qquad (2B\text{-}9)$$

Equations (2B-8) and (2B-9) describe the flow behaviour of the fluid with appropriate boundary conditions.

2B-4) THE ENERGY BALANCE EQUATION:

Application of the first law of thermodynamics to an infinitesimal element of incompressible fluid yields

$$\rho_m C_{pm} \frac{DT}{Dt} = K_m \nabla^2 T + \mu_m \Phi + \Delta H_r \qquad (2B\text{-}10)$$

where Φ is a viscous dissipation term which is not of significant importance in this case and can be neglected (it becomes appreciable in high speed and large viscosity fluids). Therefore, equation (2B-10) in axisymmetric and spherical polar co-ordinates may be expressed as

$$\frac{\partial T_m}{\partial t_{mHT}} + Vr \frac{\partial T_m}{\partial r} + \frac{V_\theta}{r} \frac{\partial T_m}{\partial \theta} = \alpha_m \left[\frac{1}{r^2} \frac{\partial}{\partial r} \left(r^2 \frac{\partial T_m}{\partial r} \right) + \frac{1}{r^2 \sin\theta} \frac{\partial}{\partial \theta} \left(\sin\theta \frac{\partial T_m}{\partial \theta} \right) \right] + \frac{\Delta Hr}{\rho_m C_{p.m}}$$

(2B-11)

The first two terms in the above equation are radial and angular diffusive transfer of heat, respectively. The third term is the heat of reaction during chemical reaction between various species. The second and third term in the left side of the equation denote radial and angular convective heat transfer due to motion of the fluid in

these directions. The first term on the left side shows the transient nature of the equation i.e. variation of temperature with respect to time. Here, the heat of reaction ΔH_r, for the main reaction between FeO_S and $\underline{C}$ may be given as

$$\Delta H_r = \frac{df}{dt} \Delta H_m \qquad (2B\text{-}12)$$

First term on the right side of the equation is the rate of reaction for

$$FeO_S + \underline{C} \rightarrow Fe + CO\uparrow \qquad (2B\text{-}13)$$

and ΔH_m is enthalpy for the above reaction, the estimation of which is given in Appendix D.

A full discussion and derivation of the chemical kinetics of the smelting process is given in Appendix B.

2B-5) SPECIES BALANCE EQUATION:

In the bed region three species are considered

1) $FeO + C$
2) Fe
3) Slag which contains Al_2O_3, SiO_2, CaO etc.

In order to evaluate the concentration of the FeO, a mass transfer equation for a typical cell is used. Because the main reaction is assumed to be between FeO_S and $\underline{C}$, which is true for

the present smelting process, the mass transfer equation is written only for FeO which controls the main reduction process. Obviously, to know the concentration of FeO is more important than to know that of other minor elements. This also shows how efficient the process is. Assuming that slag and FeO + C are the major components in the bed region, the mass transfer equation is written only for FeO.

Therefore, like the energy balance equation, the transport of mass from a pellet to a flowing fluid is given by the principle of the conservation of mass

$$\frac{DC_{FeO}}{Dt_{mMT}} = D_{F\text{-}S}\,\nabla^2 C_{FeO} + R \qquad \text{(2B-14)}$$

In polar co-ordinates for axi-symmetric flow it yields

$$\frac{\partial C_{Feo}}{\partial t_{mMT}} + V_r \frac{\partial C_{FeO}}{\partial r} + \frac{V\theta}{r}\frac{\partial C_{FeO}}{\partial \theta} = D_{F\text{-}S}$$

$$\left[\frac{1}{r^2}\frac{\partial}{\partial r}\left(r^2\frac{\partial C_{FeO}}{\partial \theta}\right) + \frac{1}{r^2\,\mathbf{S}in\theta}\frac{\partial}{\partial \theta}\left(\sin\theta\frac{\partial C_{FeO}}{\partial \theta}\right)\right] + \Delta R \qquad \text{(2B-15)}$$

where $D_{F\text{-}S}$ is the diffusivity of the binary system (Feo-slag). The driving force for diffusion is provided by the molar concentration gradients of FeO. Once again, like the energy balance equation, the first two terms on right side of the equation are radial and angular diffusive transfer of mass and the last two terms on left side are the convective mass transfer due to the motion of fluid in radial and angular directions. The first term on left side is the pure time

derivative molar concentration of FeO and ΔR is the rate of reaction for the reaction under consideration (i.e. equation (2B-13)), and can be written as:

$$\Delta R = \dot{R} = \frac{df}{dt} \qquad (2B\text{-}16)$$

Full details of reaction kinetics are given in Appendix B

Now the remaining task is to specify the proper boundary conditions for the PDEs discussed in section (2B-3-5).

2B-6) BOUNDARY CONDITIONS:

a) FOR THE EQUATION OF MOTION

As already discussed in section (2B-3) the stream function will be zero on the axis of symmetry, therefore,

$$\text{at } \theta = 0^{o} \qquad \psi_B = 0 \qquad (2B\text{-}17)$$

$$\text{at } \theta = \pi \qquad \psi_B = 0 \qquad (2B\text{-}18)$$

The third boundary condition arises from no flow across the pellet/fluid interface and this yields

$$\text{at } r = r_p \qquad \psi_B = 0 \qquad (2B\text{-}19)$$

The fourth boundary condition comes by considering the undisturbed stream flow outside the cell radius i.e.

$$\text{at } r = r_c \qquad \psi_B = \frac{1}{2} U_{Av} r^2 \sin^2\theta \tag{2B-20}$$

Besides these we also get

$$\text{at } r = r_p \qquad \frac{\partial \psi_B}{\partial r} = 0 \tag{2B-21}$$

and

$$\frac{\partial \psi_B}{\partial \theta} = \frac{\partial^2 \psi_B}{\partial \theta^2} = 0 \tag{2B-22}$$

Similarly, for vorticity, along the axis of symmetry we have

$$\text{at } \theta = 0 \qquad \xi_B = 0 \tag{2B-23}$$

$$\theta = \pi \qquad \xi_B = 0 \tag{2B-24}$$

On the surface of the pellet, from equation (2B-8)

$$r = r_p \qquad \xi_B = \frac{E_B^2 \psi_B}{r_p \sin\theta} \tag{2B-25}$$

And outside the cell radius, the flow is undisturbed, which gives

$$\text{at } r = r_c \qquad \xi_B = 0 \tag{2B-26}$$

where U_{av} is the average fluid velocity in the packed bed region as defined in section D.

Equation (2B-3) must be solved with the boundary conditions (2B-17-22). If equation (2B-8&9) is to be used then one must use

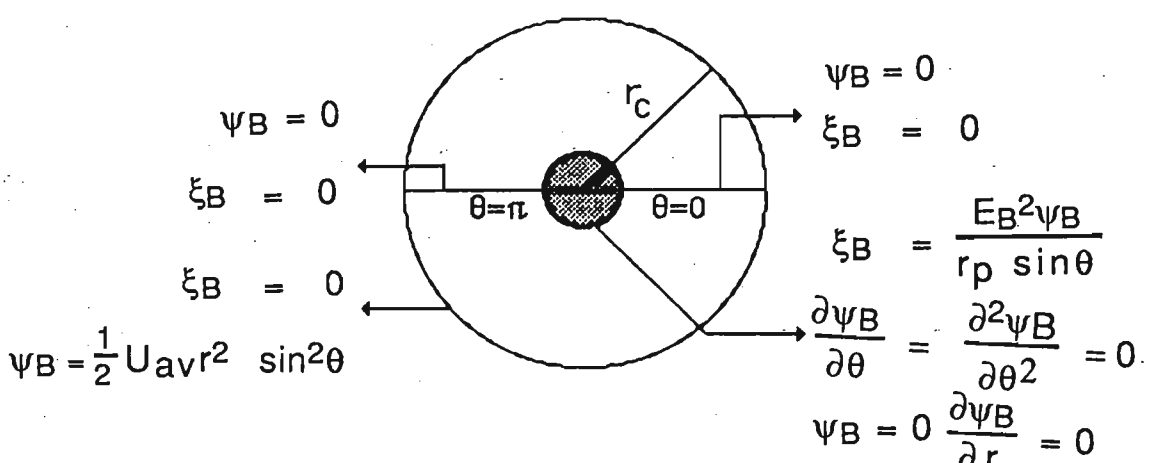

Fig. 10. Boundary conditions for equation of motion in bed region.

vorticity and stream function boundary conditions. Fig. 10 shows all the boundary conditions for the equation of motion.

b) FOR THE ENERGY BALANCE EQUATION:

For the Heat Transfer equation, a uniform temperature on the surface of the pellet is considered, which may be taken to be the melting point temperature of the pellet. The reason behind this is the knowledge that in induction smelting the overall furnace temperature is quite high, between (1300-1500°C) depending upon situations. Therefore, it has been assumed that as soon as pellets are charged into the furnace their surface temperature reaches melting point instantaneously. The small time lag has been neglected. In the actual situation, it is a reasonable assumption because as soon as pellets are charged they are also exposed to the O_2 - jet which also creates a high temperature at the top of the furnace. Absorption of heat by pellets has been taken into account by performing overall heat transfer for the smelting process, as discussed in section D. Therefore, we can write

at $r = r_p$ $\quad Tm = T_{M.P.}$ of the pellet (2B-27)

A uniform temperature (T_∞) has been assumed in the continuous phase remote from the pellet i.e. outside the cell region. This temperature has been calculated by performing an overall energy balance for the packed bed regions. This temperature changes with time as is described in more detail in section D. From the above reasoning we have

at $r = r_c$ $T_m = T_\infty$ (2B-28)

The other two boundaries are simple. On the axis of symmetry the angular derivative of temperature will vanish which yields

$$\text{at} \quad \theta = 0 \qquad \frac{\partial T_m}{\partial \theta} = 0 \tag{2B-29}$$

$$\text{at} \quad \theta = \pi \qquad \frac{\partial T_m}{\partial \theta} = 0 \tag{2B-30}$$

c) FOR THE SPECIES BALANCE EQUATIONS:

At the surface of the pellet, the concentration of FeO has been prescribed. This has been done by knowing the composition of the pellet. One can easily assess the initial concentration of FeO(FeO,i) present in the pellet. Hence

$$\text{at} \quad r = r_p \qquad C_{FeO} = C_{FeO,i} \tag{2B-31}$$

where subscript i denotes initial.

Remote from the surface (i.e. outside the cell region) the concentration has been calculated by performing an overall mass balance for the whole smelting process. This concentration also changes with time, like temperature, as detailed in section D. Therefore,

$$\text{at} \quad r = r_c \qquad C_{FeO} = C_{FeO,\infty} \tag{2B-32}$$

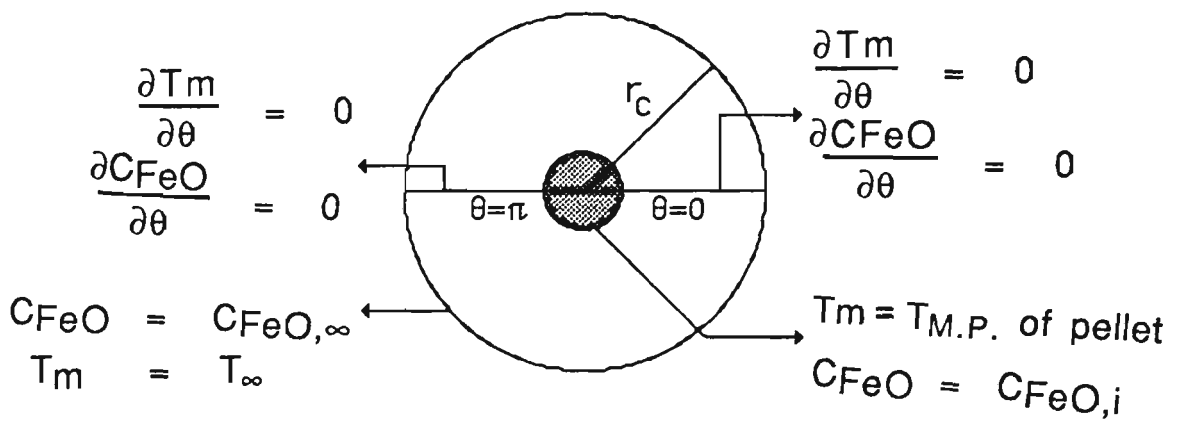

Fig.11. Boundary conditions used for heat and mass transfer calculations in bed region.

The remaining two boundary conditions can be obtained in the same way as for the heat transfer equation above, which gives (on the axis of symmetry)

$$\text{at } \theta = 0 \qquad \frac{\partial C_{FeO}}{\partial \theta} = 0 \qquad \text{(2B-33)}$$

$$\theta = \pi \qquad \frac{\partial C_{FeO}}{\partial \theta} = 0 \qquad \text{(2B-34)}$$

Fig. 11. shows all the essential heat and mass transfer boundary conditions.

SECTION C: GAS JET REGION

In this region, heat, mass and momentum transfer equations will be solved only in the boundary layer region, as was discussed in Chapter 1. Boundary layer theory will be applied extensively to solve this region.

In fact, this region comes under the special branch of MHD known as Magnetogasdynamics or Magnetoaerodynamics (MGD). As The terminology suggests this is the study of the interaction of gasdynamics and electromagnetodynamics. MGD has been applied in many areas such as the hypersonic flow around a missile, the flow of 'solar wind', re-entry of vehicles into the atmosphere etc. A good discussion on MGD is given in ref. 116-117. Ref. 50 also gives a brief but comprehensive discussion of MGD.

A comprehensive discussion of MGD has been omitted here, but as there is resemblence to the present problem, some aspects of MGD will be discussed. Fig 3. shows a magnetic field applied so that it acts perpendicularly to the oncoming flow. The pondermotive force acts in a direction to decelerate the tangential velocity W_r, since the current J flows in loops. It means that magnetic interaction will cause mainly

1) the pressure at the stagnation point 'O' which is determined principally by the normal velocity, to change little.
2) the coefficient of heat transfer and skin friction to decrease, due to a decrease in velocity.

Here the pressure at stagnation point changes due to the magnetic pressure term. In our case, the applied magnetic field is not very strong and moreover, the velocity of the gas jet (0_2-jet) is very low, which makes the magnetic Reynolds number very low ($Re_{mag}<<1$). As suggested[116-117,50], in these conditions the effect of electro magnetic interaction with gas dynamics can be neglected in the heat, mass and momentum balance equations. Gas dissociation and ionization phenomena play an important role in MGD, which are neglected here. This assumption is quite reasonable and should not affect the results appreciably. This flow can be treated as a classical potential flow. In the case considered here we have circular free 0_2 jet impinging on a solid surface (pellets surface). Due to the low velocity of the 0_2-jet (low Reynolds number), the flow is laminar.

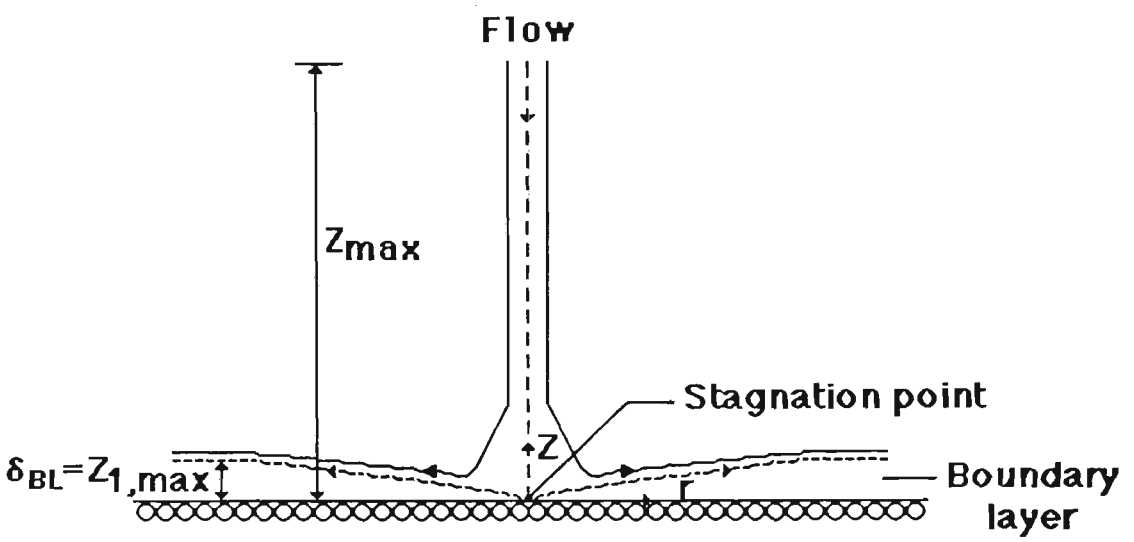

Fig. 12. A schematic diagram of jet region.

Now the problem is well defined so we can start formulation for this region. First the assumptions upon which the modelling of this region is based are identified:

2C-1) ASSUMPTIONS:

1) There is no interaction of the electromagnetic field with the O_2-jet.
2) Symmetry will be assumed along the axis in cylindrical coordinates.
3) The heat, mass and momentum transfer equations will be solved only in the boundary layer regions.
4) The buoyancy effect has been neglected.
5) No liquid layer exists above the top layer of pellets.
6) The solid surface of pellets is considered to be a flat surface.
7) No reaction occurs between the different gaseous species in the boundary layer region except at the pellet surface.

2C-2) THE MOMENTUM BALANCE EQUATION:

Fig.12 shows a stream impinging on the pellet surface at right angles to it and flowing away radially in all directions. The flow is in the direction of the negative z-axis. The flow field can be divided into two regions - a potential and viscous region. Only the viscous region will be treated here, as discussed earlier. In this case, the Navier-Stokes equations for rotational symmetry, in cylindrical coordinates, can be written as:

$$\rho_g \frac{D\underline{w}}{Dt} = \mu_g \nabla^2 \underline{W} - \underline{\nabla} p - \sigma B_o^2 W \qquad (2C\text{-}1)$$

where W is the velocity vector in the gas-jet region, and the last term on the right is due to the magnetic field interaction with the gas. If we neglect this term then we obtain

$$\rho_g [\underline{W} . \underline{\nabla} \underline{W}] = \mu_g \nabla^2 \underline{W} - \underline{\nabla} P \qquad (2C\text{-}2)$$

and the equation of continuity gives

$$\underline{\nabla} . \underline{W} = 0 \qquad (2C\text{-}3)$$

Equation (2C-2) gives the desired flow field behaviour in the potential and viscous (boundary layer) regions when it is solved with appropriate boundary conditions. Fortunately, for these two regions, exact solutions of equations (2C-2) and (2C-3) are available[102]. Therefore, no dimensionless form and no boundary conditions will be presented here. However, some manipulation has been done in order to get the velocity components in the viscous region in calculable form and these are given below.

If U and W are the radial and axial components of velocity in the potential region, while those in the viscous region are $Wr^{(r,z)}$ and $W_z^{(r,z)}$ then one can write, from Fig. 12

$$W_z/\text{at } Z \text{ max} = - W_o = -2 \text{ Ag } Z \text{ max}$$

$$\text{or,} \qquad Ag = \frac{W_o}{2Z_{max}} \qquad \text{(2C-4)}$$

where, Ag is a constant

and W and U can be written as [28]:

$$W = -\,2Ag\,Z$$

$$\text{or} \qquad W = -\,\frac{W_o\,Z}{Z_{max}} \quad \text{(from the equation (2C-4))} \qquad \text{(2C-5)}$$

$$\text{and} \qquad U = Ag\,r$$

This gives, after substituting the value of Ag,

$$U = \frac{W_o}{2\,Z_{max}}\,r \qquad \text{(2C-6)}$$

Similarly, Wr and Wz can be expressed as[28]:

$$\frac{Wr}{U} = \frac{d\dot{\Phi}}{d\xi} \quad \text{which gives}$$

$$Wr = \frac{W_o}{2Z_{max}}\,r\,\frac{d\dot{\Phi}}{d\xi} \qquad \text{(2C-7)}$$

$$\text{and} \qquad W_z = -\,2\sqrt{Ag\,\upsilon}\;\dot{\Phi}\,(\zeta)$$

$$\text{or} \qquad W_z = -\sqrt{\frac{2Wo\,\upsilon}{Zmax}}\;\dot{\Phi} \qquad \text{(2C-8)}$$

TABLE IA[102]

FUNCTIONS OCCURRING IN THE SOLUTION OF AXIALLY SYMMETRICAL FLOW WITH STAGNATION POINT

axially symmetrical			
$\sqrt{2}\cdot\zeta=\sqrt{\frac{2a}{\nu}}z$	ϕ	$\frac{d\phi}{d\zeta}=\frac{u}{U}$	$\frac{d^2\phi}{d\zeta^2}$
0	0	0	1·3120
0·2	0·0127	0·1755	1·1705
0·4	0·0487	0·3311	1·0298
0·6	0·1054	0·4669	0·8910
0·8	0·1799	0·5833	0·7563
1·0	0·2695	0·6811	0·6283
1·2	0·3717	0·7614	0·5097
1·4	0·4841	0·8258	0·4031
1·6	0·6046	0·8761	0·3100
1·8	0·7313	0·9142	0·2315
2·0	0·8627	0·9422	0·1676
2·2	0·9974	0·9622	0·1175
2·4	1·1346	0·9760	0·0798
2·6	1·2733	0·9853	0·0523
2·8	1·4131	0·9912	0·0331
3·0	1·5536	0·9949	0·0202
3·2	1·6944	0·9972	0·0120
3·4	1·8356	0·9985	0·0068
3·6	1·9769	0·9992	0·0037
3·8	2·1182	0·9996	0·0020
4·0	2·2596	0·9998	0·0010
4·2	2·4010	0·9999	0·0006
4·4	2·5423	0·9999	0·0003
4·6	2·6837	1·0000	0·0001

The following equation shows the relationship between axial distance and ζ

$$\sqrt{2}\ \zeta = \sqrt{\frac{2A_g}{\upsilon}}\ Z_1 \qquad (2C\text{-}8)$$

The value of $\sqrt{2}\ \zeta$ changes with axial distance z_1, and in the present case varies from 0 to 10.0036. Values of Φ, $\sqrt{2}\ \zeta$, and $d\Phi/d\zeta$ are given in ref. 28 and reproduced in Table IA. Values of Φ and $d\Phi/d\zeta$ for $\sqrt{2}\ \zeta > 4.6$ have been calculated. Many correlations have been established between these values which are given in Appendix D, so that one may obtain value of U, W, Wr and Wz at any point.

2C-3) THE HEAT TRANSFER EQUATION:

The energy balance equation under the boundary layer approximations & disregarding the viscous and magnetic interaction terms, in cylindrical coordinates for the axisymmetrical case, may be written as follows:

$$\rho_g\ Cp.g.\ \left[\frac{\partial Tg}{\partial tg_{HT}} + W_r\ \frac{\partial T\,g}{\partial r} + W_z\ \frac{\partial T_g}{\partial z_1}\right] = k_g\ \frac{\partial^2 T_g}{\partial z_1^2} \qquad (2C\text{-}9)$$

Here, each term has the same meaning as described in Sections 2A-3 and 2B-4, except that there is no source term due to neglecting any chemical reaction between gaseous species in the boundary layer region.

2C-4) THE MASS TRANSFER EQUATION:

The species balance equation can be written in the form of molar concentrations of oxygen, under the same assumptions in which energy balance equation has been derived in the previous section, as:

$$\frac{\partial M_{O2}}{\partial tg_{MT}} + Wr\,\frac{\partial M_{O2}}{\partial r} + Wz\,\frac{\partial M_{O2}}{\partial z_1} = D_{O2\text{-}cc}\,\frac{\partial^2 M_{O2}}{\partial z_1^2} \qquad (2C\text{-}10)$$

Again, the meaning of each term in equation (2C-10) is the same as described in Section (2B-5)

2C-5) THE BOUNDARY CONDITIONS:

No boundary conditions will be presented for the momentum balance equation (2C-2) for reasons already given in Section 2C-2.

For the energy balance equation (2C-9), on the axis of symmetry the radial derivative of the temperature will be zero i.e.

On the axis $r = 0$ $\qquad \frac{\partial Tg}{\partial r} = 0 \qquad (2C\text{-}11)$

Outside the boundary layer, the temperature has been prescribed, therefore,

at $z = z_{1\ max/B.L.}$ $\qquad Tg = T_{pres.} \qquad (2C\text{-}12)$

And the third temperature boundary comes at the pellet surface, which gives

$$\text{at } z = z_1 \qquad Tg = T_\infty \tag{2C-13}$$

where T_∞ has been calculated in section 2D.

We need only three boundary conditions for eqn. (2C-9), two in the Z direction due to the second derivative of Tg in Z, and one in the r direction which is due to single radial derivative of temperature present in the energy equation.

In Sections 2A, 2B and 2C one will find a close analogy between the heat and mass transfer equations. Therefore, the boundary conditions for the species equation can be written in the same form as for the energy equation. i.e.

$$\text{On the axis } r = 0 \qquad \frac{\partial M_{O2}}{\partial r} = 0 \tag{2C-14}$$

$$\text{At } z = z_{1\ max/B.L.} \quad M_{O2} = Mo_{2,\infty} \tag{2C-15}$$

the value of $Mo_{2,\infty}$ is the molar concentration of O_2 as given in Appendix D.

$$\text{At the surface } z = z_1 \qquad -D_{O2\text{-}CO} \frac{\partial M_{O2}}{\partial z_1} = Jo_2 = \dot{R}o_2 \tag{2C-16}$$

The boundary condition (2C-16) describes the reaction between the pellet and oxygen at the surface. R_{02} is rate of consumption of oxygen, and Jo_2 is mass flux of oxygen. The following reaction has been considered between the pellet and O_2 at the surface:

$$2C + O_2 \rightarrow 2CO \qquad (2C\text{-}17)$$

R_{O_2} is the rate of reaction for reaction (2C-17) which can be given by [160]

$$R_{O2} = (1.- \omega_p)\ (0.132)\ Exp\ (-16{,}400/T_\infty)\ P_{O2} \qquad (2C\text{-}18)$$

From the gas law one can write the partial pressure of any gas, i.e.

$$P_{02} = M^*_{02} \quad Pt \qquad (2C\text{-}19)$$

where $M_{O_2}^*$ is the molar fraction of O_2 in the gas, and P_{O_2} is the partial pressure of the gas. In the current study $M^{*o}_2 = 1$, pure O_2 gas is used in the experiment.

$$\therefore \quad P_{O_2} = Pt \qquad (2C\text{-}20)$$

2D) THE INTERACTION OF SECTIONS WITH EACH OTHER: FINAL BOUNDARY CONDITIONS:

In this section connection will be provided between the Liquid, Bed and gas Jet regions by considering the overall heat and mass balance of the process.

The heat and mass transfer and melting of pellets depends on the following factors:

i) Induction flow (average induction velocity U_{AV}) through the bed.

ii) The average bed temperature, T_∞;

iii) Average Feo Concentration $C_{FeO,\infty}$

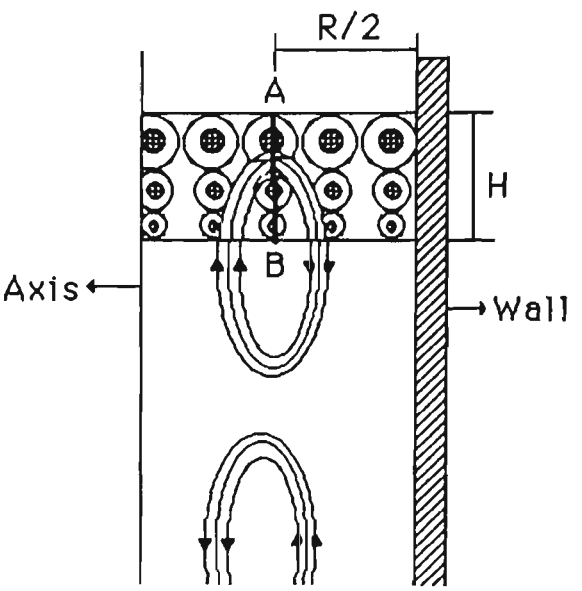

Fig.13. Diagram used for overall heat and mass balance in smelting process.

These, in turn, depend on the induction liquid flow, the liquid temperature (from the induction region), the induction heating near the side walls, the gas boundary layer, heating at the top of the bed and the heat absorbed by the pellets and the reaction (2B-13).

Coupling is done as follows:

a) Determine the U_{AV} in the bed region which provides a link between the induction (liquid) and bed regions.

b) Determine T_∞ at the gas jet and solid-liquid interface which provides a link between the liquid, bed and gas jet regions.

c) Calculate $C_{FeO,\infty}$ in the bed which provides a link between the liquid and bed regions.

The bed region is divided into a number of cells. Therefore, one has to specify U_{AV},T_∞ and $C_{FeO.\infty}$ at the edge of the cell boundary. These values will now be calculated one by one. Fig. 13 shows all essential features involved. Overall heat and mass transfer for the Induction Smelting Process have been considered across the mid plane of the crucible radius in BR i.e. across the line AB as shown in Fig. 13.

2D-1) THE AVERAGE FLOW VELOCITY U_{AV}:-

As we have discussed in the equation (2B-20), the U_{AV} is the undisturbed liquid velocity outside the cell. Within the packed bed region and outside the cell this velocity varies point to point. For the sake of mathematical simplicity this velocity has been

averaged over the cross section at r = R/2 in the bed height H as shown in Fig. 13. To obtain good average properties of the melt, it has been assumed that most of the fluid passes the plane AB (Fig. 13.), which is located at r=R/2. The value of r may be changed.

Here U_{AV} is the average velocity of the melt due to induction or liquid region flow in the bed region in the absence of pellets. Therefore, the volume flux across A B in Fig. 13. is

$$\text{volume flux} = \int \underline{V} \cdot d\,\underline{A} \qquad \text{(2D-1)}$$

or $$\pi R H U_{AV} = \int_0^H u_r \pi R\, dh$$

or $$U_{AV} = \frac{1}{H}\int_0^H u_r\, dh \qquad \text{(2D-2)}$$

It can be integrated across AB.

2D-2) CALCULATION OF T_∞:

In brief, heat balance for the bed can be done by considering the following factors:

Energy in (from the induction region) + heat due to induction heating + heating by gas B.L. = Heat consumed for pellet melting + heat absorbed by endothermic reaction + heat going to the induction region + storage of heat in the bed region

(2D-3)

We will consider these factors in turn

A) Energy in: $\rho_L U_{AV} 2\pi \frac{R}{2} H C_{p,L} \bar{T}_L$ (2D-4)

where $\frac{1}{H} \int^H u_r T_i \, d h = U_{AV} \bar{T}_L$

and $\bar{T}_L$ is the average liquid temperature in bed region.

It is worthwhile to write down the following for completeness

Volume flow rate = $U_\infty 2\pi \frac{R}{2} H$ (2D-5)

Mass flow rate = ρ_L x volume flow rate (2D-6)

Enthalpy or Energy = $C_{p,L} T_{ind}$ x mass flow rate (2D-7)

B) Energy out = $\rho_L U_{AV} \pi RH C_{p,L} T_\infty$ (2D-8)

C) Heat due to induction heating = $P_{ind.} \frac{H}{D}$ (2D-9)

D) Net heat generation due to the gas boundary layer

$$= \int_0^r \left[Ro_2 . \Delta H_1 - kg \frac{\partial Tg}{\partial Z} \right] 2\pi r \, dr \qquad (2D\text{-}10)$$

where $- kg \frac{\partial Tg}{\partial Z}$ is the heat loss to the gas and

ΔH_1 is the heat of reaction for reaction (B-6) and calculated in Appendix D.

E) Heat given to the pellet for melting = $N . L_1 . \dot{m}$ (2D-11)

where L_1 is the latent heat absorbed by the pellet to increase its temperature from room temperature to its melting point. The melting rate, m, of pellet can be given by the temperature derivative at the pellet surface divided by the latent heat of fusion, L, i.e.

$$\dot{m} = \left\{-k_p \frac{\partial T_p}{\partial r}\Big|_{r=r_p}\right\}/L \quad . \qquad (2D\text{-}12)$$

F) Heat given to iron (Fe) production = $\dot{M}_{Fe}\ \Delta H\ N$ (2D-13)

where $\dot{M}_{Fe}$ is the rate of production of Fe per cell i.e.

$$\dot{M}_{Fe} = \frac{df}{dt}|_{FeO} \cdot C_{FeO,i}\ Vc \qquad (2D\text{-}14)$$

G) Rate of heat accumulation in the bed region

$$= \rho_L\ C_{p,L}\ V_B\ \frac{\partial T\infty}{\partial t} \qquad (2D\text{-}15)$$

By combining Equations (2D-4) and (2D-8) to (2D-15), the overall heat balance equation can be obtained :

$$\pi \rho_L\ C_{p,L}\ U_{AV}\ RH\ \overline{T}_L + \frac{H}{D}\ P_{ind.} + \int_o^r \left\{\frac{df}{dt}|_{co} \cdot \Delta H_1|_{co} - K_g \frac{\partial T_g}{\partial Z_1}\right\} 2\pi\ r\ dr =$$

$$\pi \rho_L\ C_{p,L}\ U_{AV}\ RH\ T_\infty + N.\ L_1$$

$$\left[\left\{-k\ \frac{\partial T_p}{\partial r}|_{r=r_p/L}\right\} .\ 4\pi r_p^2\ (t)\right] + \left[\frac{df}{dt}|_{Feo}\ C_{Feo.init} - V_c\right] .\ \Delta H\ .\ N +$$

$$\pi R^2\ H\ \rho_L\ C_{P.L}\ \frac{\partial T\infty}{\partial t} \qquad (2D\text{-}16)$$

Equation (2D-16) is the desired equation for overall heat balance in the bed region, which provides the temperature T_∞.

2D-3) CALCULATION OF $C_{FeO,\infty}$:

The overall concentration balance can be done in the same way as for heat balance i.e.

Rate of accumulation of FeO = Rate of production of FeO + Rate of outflow of FeO + Rate of reaction of FeO + Rate of inflow of FeO

(2D-17)

Each of the above mentioned terms can be justified as follows.

It has been assumed that almost all of the FeO is converted into Fe before it enters the bed region, through the induction region, due to recirculation motion. Since a negligible amount of FeO is present in the inflow stream when it enters the bed region it means that

rate of inflow of FeO = 0 (2D-18)

Rate of outflow of FeO from the bed region = π R H U_{AV} $C_{FeO.\infty}$

(2D-19)

$$\text{Production of FeO (mole/s)} = \frac{\dot{m}\, X_{FeO} N}{M_{FeO}} \qquad (2D\text{-}20)$$

where, M_{FeO} is the molecular weight of FeO and X_{FeO} is the weight fraction of FeO in pellet.

Rate of reaction of FeO can be given as

$$\frac{df}{dt}\,|_{FeO}\,C_{FeO.i}\;\varepsilon_B\,\pi R^2H \qquad (2D\text{-}21)$$

and finally the rate of accumulation of FeO in the bed region is

$$\frac{dC_{FeO.\infty}}{dt}\qquad \varepsilon_B\,\pi R^2H \qquad (2D\text{-}22)$$

By combining all these equations as indicated in equation (2D-17) we obtain the overall mass balance.

$$\varepsilon_B\,\pi R^2H\;\;\frac{d\,C_{FeO.\infty}}{dt} = \frac{\dot{m}\,X_{FeO}\,N}{M_{FeO}} - \pi R\,H\,U_{AV}.C_{FeO.\infty} +$$

$$\frac{df}{dt}\,|_{FeO}\,C_{FeO,i}\;\varepsilon_B\,\pi R^2H + O \qquad (2D\text{-}23)$$

2E) NON-DIMENSIONALIZATION

When a parametric study is to be made, the most logical and efficient analysis requires that the mathematical model be put in dimensionless form. This has many advantages over dimensional form, principally a significant reduction in the number of independent variables. The non-dimensionalization also appreciably decreases the required number of experiments to be performed for comparison purposes. Furthermore, the normalized (dimensionless) solution can often be used for similar problems with very different linear dimensions, thermal conductivities, temperatures and so forth.

Let us first identify the non-dimensional numbers to make the previously mentioned equations, in section 2A, 2B and 2C, dimensionless.

$$r = RR^*, \quad Z = RZ^*, \quad \rho_L = \rho_{L,o}\,\rho_L^* \qquad \text{(2E-1a-c)}$$

$$C_{p.L} = C_{p.L.o}\,C_{p.L}^*, \quad k_L = k_{L.o}\,k_L^*, \quad T_L = T_i\,T_L^* \qquad \text{(2E-1d-f)}$$

$$\psi = R^2 U_o\,\psi^*, \quad \xi = \frac{U_o}{R}\,\xi^*, \quad t = t^*/\omega \qquad \text{(2E-1g-i)}$$

$$B_z = \mu_o H_{z.o}\,B_z^*, \quad B_r = \mu_o H_{z.o}\,B_r^*, \quad J = \frac{H_{z.o}}{R}\,J^* \qquad \text{(2E-1j-l)}$$

$$A = H_{z.o}\,\mu_o\,R\,A^*, \quad u_r = U_o\,u_r^*, \quad u_z = U_o\,u_z^* \qquad \text{(2E-1m-0)}$$

$$t_L = \frac{R^2}{\alpha_{L.o}}\,t_o^*, \quad Z_1 = RZ_1^*, \quad V_r = U_{AV}\,V_r^* \qquad \text{(2E-1p-r)}$$

$$V_\theta = U_{AV}\,V_\theta^*, \quad r = r_p\,R_m^*, \quad \Psi_B = U_{AV}\,r_p^2\,\Psi_B^* \qquad \text{(2E-1s-u)}$$

$$\xi_B = \frac{U_{AV}}{r_p}\,\xi_B^*, \quad E_B = E_B^*/r_p, \quad U_{AV} = U_o U_{Av}^* \qquad \text{(2E-1v-x)}$$

$$T_m = T_i\,T_m^*, \quad t_{MHT} = \frac{r_p^2}{\alpha_{m.o}}\,t_{mHT}^*, \quad \alpha_m = \alpha_{m.o}\,\alpha_m^* \qquad \text{(2E-2a-c)}$$

$$\rho_m = \rho_{m,o}\,\rho_m^*, \quad C_{p.m} = C_{p.m.o}\,C_{p.m}^*, \quad k_m = k_{m.o}\,k_m^* \qquad \text{(2E-2d-f)}$$

$$C_{Feo} = C_{Feo.i}\,C_{Feo}^*, \quad D_{Fe\text{-}c} = D_{Fe\text{-}c.o}\,D_{Fe\text{-}c}^*, \quad t_{MMT} = \frac{r_p^2}{D_{Fe\text{-}c.o}}\,t_{MMT}^* \qquad \text{(2E-2g-i)}$$

$$Rc = r_p R_M^*, \quad W_r = W_o\,W_r^*, \quad W_z = W_o\,W_z^* \qquad \text{(2E-2j-l)}$$

$$\rho_g = \rho_{g,o}\,\rho_g^*,\quad C_{p.g} = C_{p.g.o}\,C_{p.g}^*,\quad k_g = k_{g.o}\,k_g^* \qquad \text{(2E-2m-o)}$$

$$T_g = T_i\,T_g^*,\quad t_{gHT} = \frac{R^2}{\alpha_g}\,t_{gHT}^*,\quad t_{gMT} = \frac{R^2}{D_{o\text{-}co.i}}\,t_{gMT}^* \qquad \text{(2E-2p-r)}$$

$$M_{o2} = M_{o2.\infty}\,M_{o2}^*,\quad D_{o2\text{-}co} = D_{o2\text{-}co.i}\,D_{o2\text{-}co}^* \qquad \text{(2E-2s-t)}$$

where the starred quantities are non-dimensional.

Those parameters which have more than one component above, like the vector potential A(A_θ, $\acute{A}_\theta$, A_1, A_2 etc), and the magnetic field (B_r, B_z) have been expressed by a single dimensionless parameter, which is applicable to all components belonging to that parameter to make them dimensionless.

I) THE ELECTROMAGNETIC STIRRED REGION:

First let us consider the vorticity equation (A-13) which can be expressed in a non-dimensional form with the help of the above dimensionless parameters and equation (2A-14). After some simplification we get:

$$\frac{\partial}{\partial z^*}\left\{\frac{\xi^*}{R^*}\left(\frac{\partial \psi^*}{\partial R^*}\right)\right\} -$$

$$\frac{\partial}{\partial R^*}\left\{\frac{\xi^*}{R^*}\left(\frac{\partial \psi^*}{\partial z^*}\right)\right\} + \frac{1}{\eta}\left[\frac{\partial}{\partial R^*}\left\{\frac{1}{R^*}\frac{\partial}{\partial R^*}\right\}(\xi^* R^*) + \frac{\partial}{\partial z^*}\left\{\frac{1}{R^*}\frac{\partial}{\partial z^*}(R^*\xi^*)\right\}\right]$$

$$+\left\{\frac{\partial}{\partial z^*}(J_\theta^* B_z^*) + \frac{\partial}{\partial R^*}(J_\theta^* B_r^*)\right\} = 0 \qquad \text{(2E-3)}$$

Where, $\eta = \dfrac{RH_{z.o}\sqrt{\mu o \rho L}}{\mu}$, is a dimensionless constant (2E-4)

and $U_o = H_{z.o}\sqrt{\frac{\mu_o}{\rho_L}}$ is the characteristic velocity of the fluid(2E-5)

The dimensionless form of the stream function, equation (A-14), is:

$$\frac{\partial}{\partial z^*}\left\{\frac{1}{R^*}\left(\frac{\partial \psi^*}{\partial z^*}\right)\right\} + \frac{\partial}{\partial R^*}\left\{\frac{1}{R^*}\left(\frac{\partial \psi^*}{\partial R^*}\right)\right\} - \xi^* = 0 \qquad (2E\text{-}6)$$

Also, the dimensionless form of equations (A-29, 37-38) will be :

$$\frac{d^2\acute{A}_\theta^*}{dR^{*2}} + \frac{1}{R^*}\frac{d\acute{A}_\theta^*}{dR^*} - \left(\beta^2 + \frac{1}{R^{*2}}\right)\acute{A}_\theta^* = 0 \qquad (2E\text{-}7)$$

$$R_e\,(J_\theta^*\, B_r^*) = -\frac{\sigma\omega k\mu_o R^3}{2} A_1^*\, A_2^*\, \sin 2\kappa z^* \qquad (2E\text{-}8)$$

and

$$R_e\,(J_\theta^*\, B_z^*) = \frac{\sigma\omega k\mu_o R^2}{2}\left(2A_1^*\, A_2^* + A_1^*\frac{dA_2^*}{dR^*} + A_2^*\frac{dA_1^*}{dR^*}\right)\sin 2\kappa z^* \qquad (2E\text{-}9)$$

where $\beta = R(k^2 + i\omega\mu_o\sigma)^{1/2}$ (2E-10)

Here, as mentioned earlier, we will adopt another approach to obtain the body force term; details may be obtained in ref.43 upon which this approach is based.

Equation (2E-7) is a modified Bessel equation of the first order, the general solution of which is:

$$\acute{A}_\theta^* (R^*) = C_1 I_1 (\beta R^*) + C_2 K_1 (\beta R^*) \qquad (2E\text{-}11)$$

Where I_1 and K_1 are modified Bessel functions of first order with complex argument. C_1 and C_2 are the integration constants. The solution of equation (2E-11) in terms of vector potential is:

$$\acute{A}_\theta^* (R^*) = \frac{I_1(\beta R^*)}{\beta\, I_o(\beta)} \qquad (2E\text{-}12)$$

The dimensionless form of equation (2A-22-24) can be written as:

$$B_z^* = \frac{1}{R^*} \frac{d}{d R^*} (\acute{A}_\theta^* R^*) \sin \kappa z^* \qquad (2E\text{-}13)$$

and

$$B_r^* = \kappa A_\theta^* \cos \kappa z^* \qquad (2E\text{-}14)$$

where $\kappa = kR$ (2E-15)

$$J_\theta^* = i\sigma\omega\mu_o R^2 A_\theta^* \sin \kappa z^* \qquad (2E\text{-}16)$$

Therefore, with the help of equation (2E-12) we obtain the magnetic field:

$$B_z^* = \frac{I_o(\beta R^*)}{I_o(\beta)} \sin \kappa z^* \qquad (2E\text{-}17)$$

$$B_r^* = - \kappa \frac{I_1(\beta R^*)}{\beta I_o(\beta)} \cos \kappa z^* \qquad (2E\text{-}18)$$

and the induced current density is:

$$J_\theta^* = - i\omega\mu_o\sigma R^2 \frac{I_1(\beta R^*)}{\beta I_o(\beta)} \sin \kappa z^* \qquad (2E\text{-}19)$$

It is well known[39] that the general solution of the modified Bessel equation of zero order can be written as:

$$I_o (Z_B) = \sum_{n=0}^{\infty} \frac{(Z_B)^{2n}}{2^{2n}(n!)^2} \qquad (2E\text{-}20)$$

In our case $Z_B = \beta = \rho_B e^{i\phi} = \rho_B \cos \phi + i \rho_B \sin \phi$, (2E-21)

so that equation (2E-19) becomes:

$$I_o (Z_B) = \sum_{n=0}^{\infty} \frac{\rho_B{}^{2n} \cos^{2n}\phi}{2^{2n}(n!)^2} + i \sum_{n=0}^{\infty} \frac{\rho_B{}^{2n} \sin^{2n}\phi}{2^{2n}(n!)^2} \qquad (2E\text{-}22)$$

Similarly, the modified Bessel function of first order can be written

$$I_1 (Z_B) = \sum_{n=0}^{\infty} \frac{Z_B{}^{2n+1}}{2^{2n+1}(n!)(n+1)!} \qquad (2E\text{-}23)$$

for which, with the help of equation (2E-20) we get:

$$\text{or, } I_1 (Z_B) = \sum_{n=0}^{\infty} \frac{P_B{}^{2n+1}\cos(2n+1)\phi}{2^{2n+1}n!\,(n+1)!} + i \sum_{n=0}^{\infty} \frac{P_B{}^{2n+1}\sin(2n+1)\phi}{2^{2n+1}n!\,(n+1)!} \qquad (2E\text{-}24)$$

I_o and I_1 are the functions of Z_B which are defined in equation (2E-21), and ϕ is a variable angle in cylindrical co-ordinates. In our case $\phi = \theta$. Subscripts o and 1 in the equation show the order of

Bessel function. Subscript B denotes the Bessel quantity which has been adopted to avoid confusion between so many Z's.

Let $$I_o(\beta) = u_o + i\,v_o \qquad (2E\text{-}26)$$

$$I_o(\beta R^*) = X_o + iY_o \qquad (2E\text{-}27)$$

$$I_o(\beta R^*) = U_1 + iV_1 \qquad (2E\text{-}28)$$

$$\beta = a + i\,b, \qquad a \,\&\, b > 0 \qquad (2E\text{-}29)$$

where $u_o, v_o, X_o, Y_o, U_1, V_1$, a and b are real function of ρ_B and ϕ.

It is known that the modified Bessel function with complex arguments (J) can be obtained from the modified Bessel function (I) of particular order[121], using the relation:

$$J_1(\rho, \pi/2) = i\,I_1(\rho) \qquad (2E\text{-}30)$$

where $I_1(\rho)$ is real and positive.Therefore, B_z^*, B_r^* and J_θ^* can be obtained in terms of $I_o(\beta)$, $J_o(\beta R^*)$, $I_1(\beta R^*)$ and β, which are defined above, as follows:

$$B_z^* = \sin \kappa z^* \frac{(X_o + i\,Y_o)\,(u_o + i\,v_o)}{(u_o^2 + v_o^2)} \qquad (2E\text{-}31)$$

$$B_r^* = -\kappa \cos \kappa z^* \frac{\left[\{U_1(a\,u_o - b\,v_o) - V_1(b\,u_o + a\,v_o)\} + i\{V_1(a\,u_o - b\,v_o) - U_1(b\,u_o + a\,v_o)\}\right]}{(a^2+b^2)\,(u_o^2 + v_o^2)} \qquad (2E\text{-}32)$$

$$J_\theta^* = - w\mu o\sigma R^2$$

$$\frac{\left[\left\{ V_1 (a u_o - b v_o) - U_1 (b u_o + a v_o) \right\} + i\left\{ V_1 (b u_o - a v_o) - U_1 (a u_o + b v_o) \right\}\right] \sin \kappa z^*}{(a^2+b^2)\ (u_o^2 + v_o^2)}$$

(2E-33)

Therefore, complex conjugates of B_r^* and B_z^* will be :

$$\bar{B}z^* = \sin \kappa z^* \frac{X_o u_o + Y_o v_o + i(X_o v_o - u_o Y_o)}{(u_o^2 + v_o^2)} \qquad \text{(2E-34)}$$

$$\bar{B}r^* = \kappa \cos \kappa z^*$$

$$\frac{\left[\left\{ U_1 (a u_o - b v_o) + V_1 (b u_o + a v_o) \right\} + i\left\{ U_1 (b u_o + a v_o) - V_1 (a u_o - b v_o) \right\}\right]}{(a^2+b^2)\ (u_o^2 + v_o^2)} \qquad \text{(2E-35)}$$

The bars on the B_z^* and B_r^* denotes their complex conjugates.

Now we can evaluate the force terms.

$$\frac{1}{2} R_e (J_\theta^* \bar{B}r^*) = R_e \left[-iw\mu_o \sigma R^2 \kappa \frac{U_1^2 + V_1^2}{4(a^2+b^2)\ (u_o^2 + v_o^2)} \sin^2 \kappa z^* \right] \qquad \text{(2E-36)}$$

and

$$\frac{1}{2} R_e\ (J_\theta^* \bar{B}z^*) = \omega\mu o\sigma\ R^2$$

$$R_e \left[\frac{(V_1 a X_o - V_1 b Y_o - U_1 b X_o - U_1 a Y_o) - i(V_1 b X_o + V_1 a Y_o + U_1 a X_o - V_1 b X_o)}{2(a^2+b^2)\ (u_o^2 + v_o^2)} \right] x \sin^2 \kappa z^*$$

(2E-37)

Or,

$$1/2\ R_e\ (J_\theta^* \bar{B}z^*) = \omega\mu o\sigma\ R^2 \frac{V_1 a X_o - V_1 b Y_o - U_1 b X_o - U_1 a Y_o}{2(a^2+b^2)(u_o^2 + v_o^2)} \sin^2 \kappa z^*$$

(2E-38)

To obtain the solution of equations (2E-26-29) with the help of equations (2E-22&24) we begin with the equation (2E-21)

$$Z_B = \beta = a+ib = \rho_B e^{i\phi} \qquad (2E\text{-}39)$$

yielding

$$a^2+b^2 = k^2R^2 \qquad (2E\text{-}40)$$

and

$$2ab = \omega\mu_o\sigma R^2 \qquad (2E\text{-}41)$$

with the help of equation (2E-10).

Therefore:

$$\rho_B = \sqrt{a^2+b^2} \qquad (2E\text{-}42)$$

and

$$\phi = \tan^{-1}\frac{b}{a} \qquad (2E\text{-}43)$$

This solution is applicable for $I_o(\beta)$.

For $I_1(\beta R^*)$ we have:

$$\beta^2R^{*2} = U_1^2-V_1^2 + i\,2U_1V_1 \qquad (2E\text{-}44)$$

which gives:

$$\rho_B = \sqrt{U_1^2+V_1^2}\ R^* \qquad (2E\text{-}45)$$

and

$$\phi = \tan^{-1} \frac{V_1}{U_1} \tag{2E-46}$$

Similarly, for $I_o(\beta R^*)$ we obtain:

$$\rho_B = \sqrt{X_o^2+Y_o^2}\, R^* \tag{2E-47}$$

and

$$\phi = \tan^{-1} \frac{Y_o}{X_o} \tag{2E-48}$$

Now, the equation of motion can be written in two forms - one with the help of equations (2E-3), (2E-8) and (2E-9) i.e.:

$$\frac{1}{R^*}\frac{\partial\xi^*}{\partial z^*}\frac{\partial\psi^*}{\partial R^*} - \frac{1}{R^*}\frac{\partial\xi^*}{\partial R^*}\frac{\partial\psi^*}{\partial z^*} + \frac{\xi^*}{R^{*2}}\frac{\partial\psi^*}{\partial z^*} + \frac{1}{\pi}\left[\frac{\partial^2\xi^*}{\partial R^{*2}} + \frac{1}{R^*}\frac{\partial\xi^*}{\partial R^*} - \frac{\xi^*}{R^{*2}} + \frac{\partial 2\xi^*}{\partial R^{*2}}\right] + \frac{\sigma\omega k\mu_o R^3}{2} \sin 2\kappa z \left[2.\frac{A_1^* A_2^*}{R^*}\right] = 0 \tag{2E-49}$$

and in the second form with the help of equations (2E-3), (2E-36) and (2E-38) i.e.:

$$\frac{1}{R^*}\frac{\partial\xi^*}{\partial z^*}\frac{\partial\psi^*}{\partial R^*} - \frac{1}{R^*}\frac{\partial\xi^*}{\partial R^*}\frac{\partial\psi^*}{\partial z^*} + \frac{\xi^*}{R^{*2}}\frac{\partial\psi^*}{\partial z^*} + \frac{1}{\pi}\left[\frac{\partial^2\xi^*}{\partial R^{*2}} + \frac{1}{R^*}\frac{\partial\xi^*}{\partial R^*} - \frac{\xi^*}{R^{*2}} + \frac{\partial 2\xi^*}{\partial R^{*2}}\right] + \omega\kappa\mu_o\sigma R^2 \frac{V_1 aX_o - V_1 bY_o - U_1 bX_o - U_1 aY_o}{2(a^2+b^2)(u_o^2+v_o^2)} \sin 2\kappa z^* = 0 \tag{2E-50}$$

The non-dimensional form of equation (2A-43) is given by:

$$\rho_L^* C_{p.L}^* \frac{\partial T_L^*}{\partial t^*} + Pe_L U_r^* \rho_L^* C_{p.L}^* \frac{\partial T_L^*}{\partial R^*} + Pe_L U_z^* \rho_L^* \frac{\partial T_L^*}{\partial z^*} = k_L^* \frac{\partial^2 T_L^*}{\partial R^{*2}} + \frac{k_L^*}{R^*} \frac{\partial T_L^*}{\partial R^*} + k_L^* \frac{\partial^2 T_L^*}{\partial z^{*2}} + EH \quad (2E\text{-}51)$$

where

$$EH = J_\theta^2 r_e \frac{R^2}{T_i k_{L,o}} = \frac{H_z^2{}_{,o} r_e}{k_{L,o} T_i} Re\,(J_\theta^{*2}) \quad (2E\text{-}52)$$

is a dimensionless electric heat generation term.

and

$$Pe_L = \frac{RU_o}{\alpha_{L\cdot o}} = \frac{RU_o P_{L.o} C_{p.L,o}}{k_{L.o}}, \quad (2E\text{-}53)$$

is the liquid Peclet number.

This Peclet number may be referred as the magnetic Peclet number and satisfies the following relationship

$$Pe_{mag.} = Re_{mag.} \cdot Pr_{mag.} \quad (2E\text{-}54)$$

where the magnetic Reynolds number and the modified magnetic Prandtl numbers are given as

$$Re_{mag.} = U_o R \mu_o \sigma = \frac{\text{Magnetic convection}}{\text{Magnetic diffusivity}} \quad (2E\text{-}55)$$

and,

$$Pr_{mag.} = \frac{C_{P\cdot L}\, \rho_L}{\mu_o \sigma k_L} = \frac{\text{Magnetic diffusivity}}{\text{Thermal diffusivity}} \quad (2E\text{-}56)$$

The modified magnetic Prandtl numbers in the present case refer to the heat transfer in the MHD fluid flows.

From equation (2A-35), after making it dimensionless and taking its real part, we get:

$$\text{Re}\,(J_\theta^{*2}) = -\frac{\sigma^2\omega^2\mu_o^2R^4}{2}\,(A_1^{*2} - A_2^{*2})\sin^2\kappa z^* \qquad \text{(2E-57)}$$

Also, with the help of equation (2E-33) we obtain

$$\text{Re}\,(J_\theta^{*2}) = -\frac{\sigma^2\omega^2\mu_o^2R^4}{2}\sin^2\kappa z^* \left[\frac{4U_1V_1\,u_ov_o\,(a^2-b^2)+4U_1V_1ab\,(u_o^2+v_o^2)}{(a^2+b^2)^2\,(u_o^2+v_o^2)^2} - \frac{4\,u_ov_o\,ab(V_1^2-V_1^2)+(a^2-b^2)(U_1^2-V_1^2)\,(u_o^2+v_o^2)}{(a^2+b^2)^2\,(u_o^2+v_o^2)^2}\right] \qquad \text{(2E-58)}$$

Either of these equations can be used to evaluate equation (2E-52). As discussed previously, there are two procedures to calculate vector potential and hence other electrical parameters.

THE BOUNDARY CONDITIONS:

The boundary conditions (2A-44-47) for equation (2E-6) and (2E-3) can be written in dimensionless form as

At $R^* = 0$ $\xi^* = 0$ & $\psi^* = 0$ (2E-59a,b)

$R^* = 1$ $\dfrac{\partial\psi^*}{\partial R^*} = 0$ & $\psi^* = 0$ (2E-60a,b)

$z^* = 0$ $\dfrac{\partial\psi^*}{\partial z^*} = 0$ & $\psi^* = 0$ (2E-61a,b)

and $z^* = z_{1/R}$ $\xi^* = 0$ & $\psi^* = 0$ (2E-62,63)

The boundary conditions (2A-48-51) for the energy equation (2E-51) become

At $R^* = 0$ $\dfrac{\partial T_L^*}{\partial R^*} = 0$ (2E-64)

$R^* = 1$ $T_L = T_w$ (2E-65a)

$$k_L^* \frac{\partial T_L^*}{\partial R^*} = - \frac{k_{w,o}}{k_{L,o}} k_w^* \frac{\partial T_w^*}{\partial R^*} \qquad \text{(2E-65b)}$$

$$q_{rwz}^* = - \frac{k_{w,o} \cdot k_w^* \cdot (T_w^* - T_{o\,w2}^*)}{k_{L,o} \; R_w^* \; \ln (R^*/r_w^*)} \qquad \text{(2E-65c)}$$

$$z^* = 0 \quad k_L^* \frac{\partial T_L^*}{\partial z^*} = - \frac{k_{w,o}}{\alpha_{\omega,o} / \alpha_{L,o}} \cdot k_w^* \frac{(T_w^* - T_{o\,w1}^*)}{\sqrt{\frac{\alpha_\omega^* t^*}{\alpha_L^*}}} \qquad \text{(2E-66)}$$

$$z^* = z_{1/R} \quad T_L^* = T_\infty / T_i \qquad \text{(2E-67)}$$

II) Packed Bed Region:

The dimensionless form of the Navier-Stokes equation (2B-3) with the help of equation (2E-1&2) can be written as

$$\frac{N_{Re}}{2} \left[\frac{\partial \psi^*_m}{\partial R^*_B} \frac{\partial}{\partial \theta} \left(\frac{E^{*2}_B \psi^*_B}{R^{*2}_m \sin^2\theta} \right) - \frac{\partial \psi^*_B}{\partial \theta} \frac{\partial}{\partial R^*_m} \left(\frac{E^{*2}_B \psi^*_B}{R^{*2}_m \sin^2\theta} \right) \right] \sin\theta =$$

$$E_B^{*4} \; \psi^*_B \qquad \text{(2E-68)}$$

The non-dimensional equation corresponding to equations (2B-4-6) can be expressed as

$$E_B^{*2} = \frac{\partial}{\partial R^* m^2} + \frac{\sin\theta}{R^* m^2} \frac{\partial}{\partial \theta} \left(\frac{1}{\sin\theta} \frac{\partial}{\partial \theta} \right) \qquad \text{(2E-69)}$$

$$V_\theta^* = \frac{1}{R_m^* \sin\theta} \frac{\partial \psi_B^*}{\partial R_m^*} \qquad \text{(2E-70)}$$

$$V_R^* = - \frac{1}{R_m^{*2} \sin\theta} \frac{\partial \psi_B^*}{\partial \theta} \qquad \text{(2E-71)}$$

where $N_{Re} = \frac{2U_{AV}\, r_p\, \rho_m}{\mu_m}$ is Reynold number (2E-72)

Similarly, equation (2B-8 &9) in dimensionless form becomes:

$$\frac{N_{Re}}{2}\left[\frac{\partial \psi_B^*}{\partial R_m^*}\ \frac{\partial}{\partial \theta}\ \left(\frac{\xi^*_B}{R^*_m \sin\theta}\right) - \frac{\partial \psi_B^*}{\partial \theta}\ \frac{\partial}{\partial R^*_m}\ \left(\frac{\xi^*_B\, R^*_m}{\sin\theta}\right)\right] \sin\theta =$$

$$E^*_B{}^2\ (\xi^*_B\, R^*_m \sin\theta) \qquad (2E\text{-}73)$$

and $$E_B{}^{*2}\ \psi_B^*\ =\ \xi_B^*\ R_m^*\ \sin\theta \qquad (2E\text{-}74)$$

To represent equation (2E-73 & 72) in more executable form let

$$F = \frac{\xi_B^*}{R_m^*\ \sin\theta} \qquad (2E\text{-}75)$$

$$G = \xi_B^*\ R_m^*\ \sin\theta \qquad (2E\text{-}76)$$

Then equation (2E-74) becomes

$$\frac{\partial^2 \psi_B^*}{\partial R_m^{*2}} + \frac{1}{R_m^{*2}}\ \frac{\partial^2 \psi_B^*}{\partial \theta^2} - \frac{\cot\theta}{R_m^{*2}}\ \frac{\partial \psi_B^*}{\partial \theta} = G \qquad (2E\text{-}77)$$

and equation (2E-73) can be represented as

$$\frac{N_{Re}}{2}\sin\theta\left[\frac{\partial \psi_B^*}{\partial R_m^*}\frac{\partial F}{\partial \theta} - \frac{\partial \psi_B^*}{\partial \theta}\frac{\partial F}{\partial R_m^*}\right] = \frac{\partial^2 G}{\partial R_m^{*2}} + \frac{1}{R_m^{*2}}\frac{\partial^2 G}{\partial \theta^2} - \frac{\cot\theta}{R_m^{*2}}\frac{\partial G}{\partial \theta} \qquad (2E\text{-}78)$$

Also we have

$$F = \frac{G}{R_m^{*2} \sin^2\theta} \qquad \text{(2E-79)}$$

In the same way after introducing dimensionless parameters in energy balance equation (2B-11) we have

$$\frac{\partial T_m^*}{\partial t^* m M\cdot T} - \frac{Pe_{HT}}{R_m^{*2} \sin\theta} \frac{\partial \psi_B^*}{\partial \theta} \frac{\partial T_m^*}{\partial R_m^*} + \frac{Pe_{HT}}{R_m^{*2} \sin\theta} \frac{\partial \psi_B^*}{\partial R_m^*} \frac{\partial T_m^*}{\partial \theta} =$$

$$\rho_m^* \left[\frac{\partial^2 T_m^*}{\partial R_m^{*2}} + \frac{2}{R_m^*} \frac{\partial T_m^*}{\partial R_m^*} + \frac{1}{R_m^{*2}} \frac{\partial^2 T_m^*}{\partial \theta^2} + \frac{\cot\theta}{R_m^{*2}} \frac{\partial T_m^*}{\partial \theta}\right] +$$

$$\frac{\Delta H^*}{\alpha_m^* C_p^* m} \qquad \text{(2E-80)}$$

where, $Pe_{HT} = \frac{U_{AV} r_p}{\alpha_{m\cdot o}} = \frac{U_{AV}^* r_p \rho_{m\cdot o} C_{p\cdot m\cdot o}}{k_{m\cdot o}}$ (2E-81)

is the Peclet number for heat transfer in bed region.

and $\Delta H^* = \frac{df}{dt} \Delta H_m \rho_m \frac{r_p^2}{T_i k_{m.o.}} \frac{1000.o}{M_{mixt}} (1 - \omega_p)$ (2E-82)

is the dimensionless heat release/absorption term (not a constant, but a function of time and temperature).

M_{mixt}= the molecular weight of the melt, g/mole.

ω_p= the void fraction of the pellet

In dimensionless form the species balance equation (2B-15) can be written as:

$$\frac{\partial C^*_{Feo}}{\partial t^* m_{MT}} - \frac{Pe_{MT}}{R_m^{*2}\sin\theta}\frac{\partial \psi^*_B}{\partial \theta}\frac{\partial C_F^*{}_{Feo}}{\partial R^*_m} + \frac{PemT}{R_m^{*2}\sin\theta}\frac{\partial \psi^*_B}{\partial R^*_m}\frac{\partial C^*_{Feo}}{\partial \theta} =$$

$$D^*_{F\text{-}S}\left[\frac{\partial^2 C^*_{Feo}}{\partial R_m^{*2}} + \frac{2}{R_m^*}\frac{\partial C^*_{Feo}}{\partial R_m^*} + \frac{1}{R_m^{*2}}\frac{\partial^2 C^*_{Feo}}{\partial \theta^2} + \frac{\cot\theta}{R_m^{*2}}\frac{\partial C^*_{Feo}}{\partial \theta}\right]$$

$$+ \Delta R^* \qquad \text{(2E-83)}$$

In the above non-dimensional equation,

$$Pe_{MT} = \frac{U_{AV}\, r_p}{D_{F-S}} \qquad \text{(2E-84)}$$

is the Peclet number of mass transfer in bed region.

and $$\Delta R^* = R^{\cdot}\frac{r_p^2}{D_{F-S}\, C_{FeO.i}}\frac{1000.0\,\rho_{Feo}}{M_{Feo}} \qquad \text{(2E-85)}$$

is the dimensionless rate of reaction for reaction equation (2B-13). It is a function of time.

$$R^{\cdot} = \frac{df}{dt} = k_\upsilon\, e^{-k_\upsilon t}, \text{ rate of reaction equation} \qquad \text{(2E-86)}$$

M_{FeO} = Molecular weight of FeO , g/mole.

THE BOUNDARY CONDITIONS:

Equation (2E-78&79) together with equation (2E-77) gives a complete set of equations of motion with appropriate boundary conditions. Therefore, we will concentrate on obtaining

dimensionless forms of the boundary conditions for these equations only.

The boundary conditions for the stream function equation (2E-77) can be written as follows (in dimensionless form). The procedure to get the boundary conditions is the same as was adopted in the dimensional section for the equation of motion.

Along the axis of symmetry

$$\theta = 0 \qquad \psi_B^* = 0 \tag{2E-87}$$

$$\theta = \pi \qquad \psi_B^* = 0 \tag{2E-88}$$

$$\text{at} \quad R_m^* = 1 \qquad \psi_B^* = 0 ; \quad \frac{\partial \psi_B^*}{\partial R_m^*} = 0 \tag{2E-89}$$

$$R_m^* = \frac{r_c}{r_p} \qquad \psi_B^* = \frac{1}{2} R_m^{*2} \sin^2\theta \tag{2E-90}$$

The boundary conditions for the equation (2E-78) are obtained with the help of the equation (2E-76) for which the vorticity conditions are known. These are the same as we have for equation (2B-9) i.e. boundary conditions (2B-23-26).

Therefore, the boundary conditions for the equation (2E-78) are

$$\text{at} \quad \theta = 0 \qquad \xi_B^* = 0 ; \qquad G = 0 \tag{2E-91\&92}$$

$$\theta = \pi \qquad \xi_B^* = 0 ; \qquad G = 0 \tag{2E-93\&94}$$

at $R_m^* = \frac{r_c}{r_p}$ $\xi_B^* = 0$; $G = 0$ (2E-95&96)

and $R_m^* = 1$ $\xi_B^* = \frac{E_B^{*2}\,\psi_B^*}{\sin\theta}$; $G = E_B^{*2}\psi_B^*$ (2E-97&99)

The boundary conditions for equation (2E-79) can be written:

At $R_m^* = \frac{r_c}{r_p}$ $F = 0$ (2E-99)

$R_m^* = 1$ $F = \frac{G}{\sin^2\theta}$ (2E-100)

At $\theta = 0$ and $\theta = \pi$, equation (2E-79) gives a limiting case because as $\theta \to 0$ $\sin\theta \to 0$ therefore, $G \to 0$

i.e. $F = \lim_{\theta \to 0} \frac{G}{R_m^{*2} \sin\theta}$ $G \to 0$; $\sin\theta \to 0$

On simplification, this yields:

At $\theta = 0$ $F = \frac{1}{2R_m^{*2}\theta^2} \frac{\partial^2 G}{\partial \theta^2}$; $\frac{\partial G}{\partial \theta} = 0$ (2E-101)

$\theta = \pi$ $F = \frac{\partial^2 G}{2R_m^{*2}\,\partial\theta^2}$; $\frac{\partial G}{\partial \theta} = 0$ (2E-102)

Boundary conditions for the energy balance equations, (2B-27) and (2B-28) in dimensionless form are:

at $R_m^* = 1.0$ $T_m^* = \frac{T_{m.p.\ of\ pellet}}{T_i}$ (2E-103)

and $R_m^* = \frac{r_c}{r_p}$ $T_m^* = \frac{T_\infty}{T_i}$ (2E-104)

The two remaining boundary conditions (2B-29 and 30) become

At $\theta = 0$ $\frac{\partial T_m^*}{\partial \theta} = 0$ (2E-105)

$\theta = \pi$ $\frac{\partial T_m^*}{\partial \theta} = 0$ (2E-106)

The appropriate boundary conditions for $\theta = 0$ and $\theta = \pi$ are obtained by putting these values in the heat transfer equation (2E-80), which gives two limiting cases:

1. The second term of the left side of equation (2E-80) becomes infinite because
   when $\theta \rightarrow 0$ $\sin\theta \rightarrow 0$

2. The fourth term on right side of the energy equation also becomes infinite
   when $\theta \rightarrow 0$ $\cot\theta \rightarrow \infty$

The same conditions occur when $\theta = \pi$

Therefore the solution to this problem can be obtained by applying L' Hospital's rule for these terms which gives the final boundary condition for $\theta = 0$ and for $\theta = \pi$.

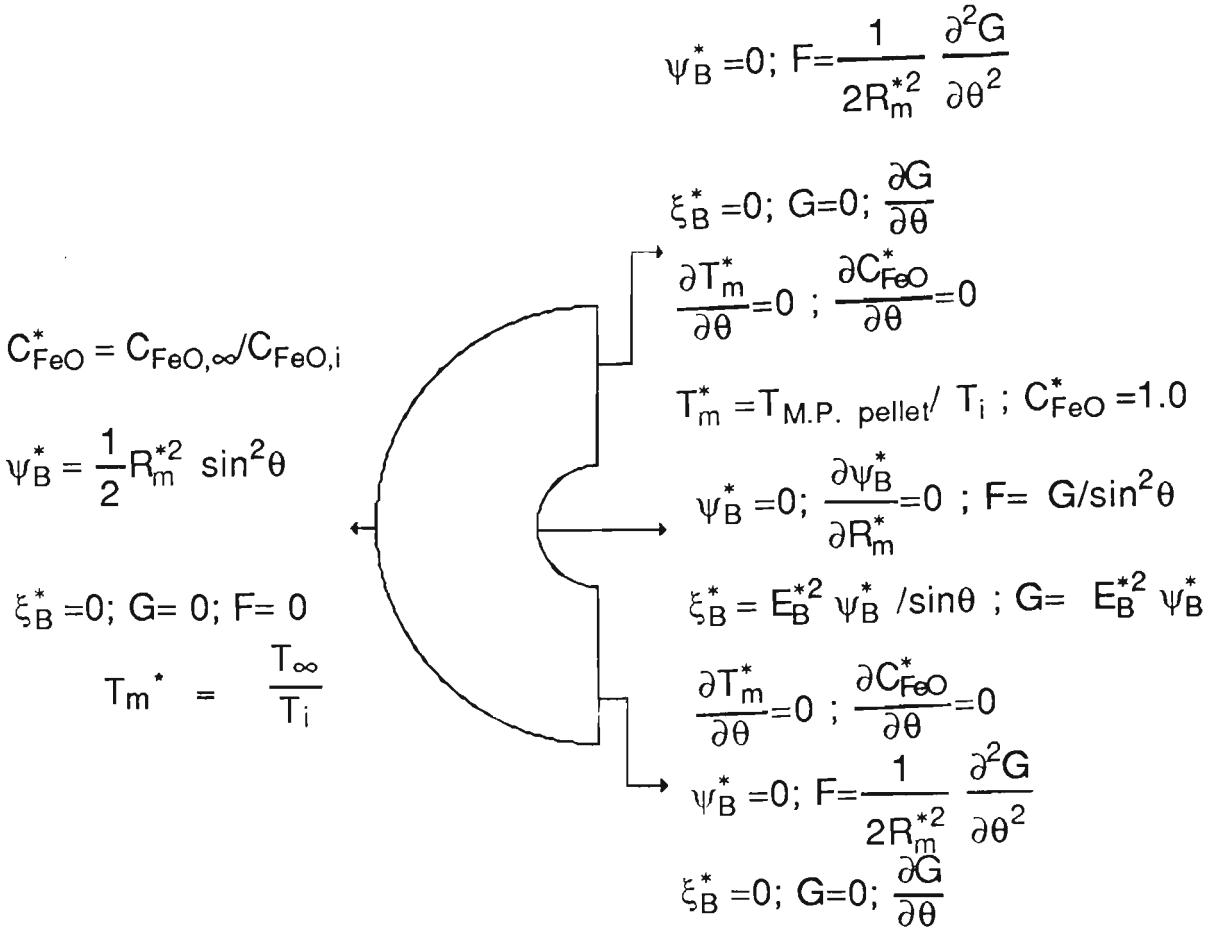

Fig. 14. Non-dimensional boundary conditions used in bed region.

$$\frac{\partial T_m^*}{2t^*_{mHT}} - \frac{Pe_{HT}}{Rm^* cos\theta} \frac{\partial^2 \psi_B^*}{\partial \theta^2} \frac{\partial Tm^*}{\partial Rm^*}$$

$$= \rho_m^* \left[\frac{\partial^2 Tm^*}{\partial R_m^{*2}} + \frac{2}{R_m^*} \frac{\partial T_m^*}{\partial R_m^*} + \frac{1}{R_m^{*2}} \frac{\partial^2 T_m^*}{\partial \theta^2} + \frac{cos^2\theta}{R_m^{*2}} \frac{\partial^2 T_m^*}{\partial \theta^2} \right]$$

$$+ \frac{\Delta H^*}{\rho_m^* C_{p.m.}^*} \qquad \text{(2E-107\&108)}$$

Similarly the boundary conditions, for the species balance equation become

$$\text{at} \qquad R_m^* = 1.0 \qquad C^*_{FeO} = 1.0 \qquad \text{(2E-109)}$$

$$R_m^* = \frac{r_c}{r_p} \qquad C^*_{FeO} = \frac{C_{Feo.\infty}}{C_{Feo.i}} \qquad \text{(2E-110)}$$

and for $\theta = 0$ and $\theta = \pi$ we have same conditions. The procedure needed to obtain these boundary conditions are the same as those described for the heat transfer case. We obtain

$$\frac{\partial C^*_{Feo}}{\partial t^*_{mMT}} - \frac{Pe_{MT}}{R_m^{*2} cos\theta} \frac{\partial^2 \psi_B^*}{\partial \theta^2} \frac{\partial C^*_{Feo}}{\partial R_m^*} = D^*_{Fe\text{-}c} \left[\frac{\partial^2 C^*_{Feo}}{\partial R^{*2}_m} + \right.$$

$$\left. \frac{2}{R^*_m} \frac{\partial C^*_{Feo}}{\partial R_m^*} + \frac{1}{R_m^{*2}} \frac{\partial^2 C^*_{Feo}}{\partial \theta^2} + \frac{cos^2\theta}{R_m^{*2}} \frac{\partial^2 C^*_{Feo}}{\partial \theta^2} \right] + \Delta R^*$$

(2E-111\&112)

Fig. 14 shows all the essential boundary conditions for equation of motion, energy and species balance.

III) THE GAS JET REGION:

The non-dimensional form of the energy and species balance equations (2C-9 and10) can be obtained by substituting dimensionless parameters which are defined in equations (2E-1&2), yielding

$$\frac{\partial}{\partial t^*_{gHT}}\left[\rho^*_g C_{p.^*g} T_g^*\right] + Pe_{gHT}\frac{\partial}{\partial R^*}\left[\rho^*_g C^*_{p.g} W^*_r T_g^*\right] + Pe_{gHT}\frac{\partial}{\partial z_1^*}\left[\rho^*_g C^*_{p.g} W^*_z T_g^*\right] = \frac{\partial}{\partial z_1^*}\left[kg^* \frac{\partial T_g^*}{\partial z_1^*}\right] \quad \text{(2E-113)}$$

$$\text{where,}\quad Pe_{gHT} = \frac{WoR}{\alpha_{g.o}} = \frac{WoR\ \rho_{g.o}\ C_{p.g.o}}{kg_{.o}} \quad \text{(2E-114)}$$

is the gas Peclet number for heat transfer.

$$\text{and}\quad \frac{\partial Mo^*_2}{\partial t_{gMT}} + Pe_{gMT}\frac{\partial}{\partial R^*}\left[W^*_r M^*_{o2}\right] + Pe_{gMT}\frac{\partial}{\partial z_1^*}\left[W^*_z Mo^*_2\right] = \frac{\partial}{\partial z_1^*}\left[D^*_{o2\text{-}co}\frac{\partial M^*_{O2}}{\partial z_1^*}\right] \quad \text{(2E-115)}$$

$$\text{where}\quad Pe_{gMT} = \frac{WoR}{Do_{2\text{-}co.i}} \quad \text{(2E-116)}$$

is the gas Peclet number for mass transfer.

The boundary conditions corresponding to these equations can be written:

on the axis $R^* = 0$ $\frac{\partial Tg^*}{\partial R^*} = 0$ (2E-117)

and $\frac{\partial Mo^*_2}{\partial R^*} = 0$ (2E-118)

At $z^* = \frac{z_{1\ max}}{R}$ /At B.L. $Mo^*_2 = 1.0$ (2E-119)

and s $Tg^* = \frac{Tpres}{T_i}$ (2E-120)

Finally, at the surface, the dimensionless conditions can be written as:

At $z^* = z_{1/R}$ $Tg^* = \frac{T\infty}{Ti}$ (2E-121)

and $-Do^*_{2\text{-}co}$ $\frac{\partial Mo^*_2}{\partial Z^*_1} = R^*_2$ (2E-122)

where $R^*_{O2} = R_{02} \frac{R \times 1000.0}{Pt \times Mo_{2.00}.\ Do_{2\text{-}co.i} \times M_{m.w.o2}}$ (2E-123)

is a dimensionless rate of reaction term which depends upon temperature and gas pressure and Ro_2 is given by equation (2C-18)

DIMENSIONLESS FORM OF SECTION D:

The dimensionless form of the overall heat balance equation (2D-16) in the bed region can be written as:

$$\rho_L^* C_{P.L.}^* R^* H^* T_L^* U_{AV}^* + POWIND.\ P^* \frac{H^*}{D^*} + HEATBL.\ GASHIT =$$

$$\rho_L^* R^* C_{P.L.}^* H^* T_\infty^* U_{AV}^* + HITMEL \left[\left\{-K_p^* \frac{\partial T_p^*}{\partial R_m^*} r^{*2}{}_{pi}\right\} / L_m\right] +$$

$$HFEPRO.\ BCPART + ACUHIT.\ R^{*2} H^* \rho_L^* C_{P.L.}^* \frac{\partial T_\infty^*}{\partial t^*} \qquad (2E\text{-}124)$$

$$\text{where } POWIND = \frac{P_{init}}{\rho_{L.o}\, U_o\, \pi\, R^2\, C_{P.L.o}\, T_{L.o}} \qquad (2E\text{-}125)$$

is a dimensionless induced power term

$$HEATBL = \frac{1}{2 C_{P.L.o}\ \rho_{L.o.}\ T_{i.}\ U_o}\ ,\ \frac{m^2\text{-}s}{cal} \qquad (2E\text{-}126)$$

is a dimensional heat release term in unit area of gas boundary layer

$$GASHIT = \int_o^{R^*} \{4.17965 \times 10^2\ (1 - w_p)\ EXP\ (-54.667/T_\infty^*)$$

$$\left\{-22251.5 - 8.57 \times 300.\ T_\infty^* - 1.03 \times 10^3 \times (300.x\ t_\infty^*)^2 -\right.$$

$$\left. 4.49 \times 10^5/(300.\ T_\infty^*)\right\} - 19.10637\ K_g^* \frac{\partial T_g^*}{\partial Z^*}\Big] R_i dR^* \frac{cal}{m^2\text{-}s} \qquad (2E\text{-}127)$$

$$HITMEL = \frac{4.\ NL_1\ kp.o\ r_p}{R^2 C_{p.l.o.}\ \rho_{L\cdot o}\ U_o} \qquad (2E\text{-}128)$$

is a dimensionless heat absorbtion term during melting of pellets

$$HFEPRO = \frac{4\ D_{F\text{-}S}\ C_{FeO.i}\ N\ r_p}{3\ R^2\ C_{P.L.o}\ \rho_{L.o.}\ T_i\ U_o} \qquad (2E\text{-}129)$$

is a dimensionless heat absorbtion term for iron production.

$$BCPART = \left[\left\{\frac{df}{dt^*}\Big|_{FeO}\ (R_c^{*3} - R_p^{*3})\right\}\{(\ 31712\cdot + 2\cdot89\ (\bar{T}_m^* \times 300\cdot) - 0\cdot53 \times 10^{-3}\ (300\cdot \times \bar{T}_m^*)^2 - 4\cdot09 \times 10^5/\ (300\cdot \times\ \bar{T}_m^*)\}\right] \qquad (2E\text{-}130)$$

$$ACUHIT = \frac{k_{L.o}}{\rho_{L.o}\ Cp\cdot L.o\ R\ U_o} \qquad (2E\text{-}131)$$

is a dimensionless heat storage term.

The overall mass balance equation (2D-23), in its dimensionless form becomes:

$$\frac{dC^*_{FcO\cdot\infty}}{dt^*} = CFEOPR.\ \frac{r_{p.i}}{R^{*2}\ H^*\ \varepsilon_B}\left\{-k_p^*\ \frac{\partial T_p^*}{\partial R_m^*}\ \ r_{p\cdot i}^{*2}\right\}_{r_F^* = 1} - COUTFL.$$

$$\frac{U\infty^*\ C^*_{FcO\cdot\infty}}{R^*\ \varepsilon_B} + 5{,}85714 \times 10^7\ r_{p,i}\ EXP\ (-5.85714 \times 10^7.\ r^2_{p.i.}\ t^*) \qquad (2E\text{-}132)$$

where $$CFEOPR = \frac{M_p \cdot r_{p.i}\, k_{p.i}\, T_{p.i}\, X_{Fe0}\, N\, 4}{L_M\, M_{Fe0}\, R\, C_{Feo.init}\, D_{F-S}} \qquad (2E\text{-}133)$$

$$COUTFL = \frac{R\, U_0}{D_{F-S}} \qquad (2E\text{-}134)$$

is a dimensionless constant

CHAPTER 3
COMPUTATIONAL TECHNIQUE

3.0) INTRODUCTION[123]:

From the variety of numerical techniques available such as the Finite Difference Method (FDM), the Finite Element Method (FEM) and the Finite Volume Method (FVM), a suitable technique must be selected that satisfies the computational requirements of the problem at hand. For instance, inexpensiveness of computation may be emphasized in one case, while high accuracy may be the first priority in another. Here, in order to simplify the numerical formulation of the otherwise physically complete induction smelting process problem, a finite difference approach has been selected.

The fundamental approximation in the method of finite differences is the replacement of each derivative in the partial differential equation (PDE) by an algebraic difference, at each discrete point in the region. These FD approximations can be of varying degrees of accuracy and can be derived in several different ways. For instance the FD expressions may be obtained by applying the balance law (say of energy momentum or mass conservation) to a differential element, or by fitting polynomials through the values of the unknown (say, temperature) between the neighbouring mesh points and differentiating, or by the use of Taylor series expansions[42]. This latter method is brief, simple and gives an indication of the accuracy of the approximation It is described in detail in reference 125.

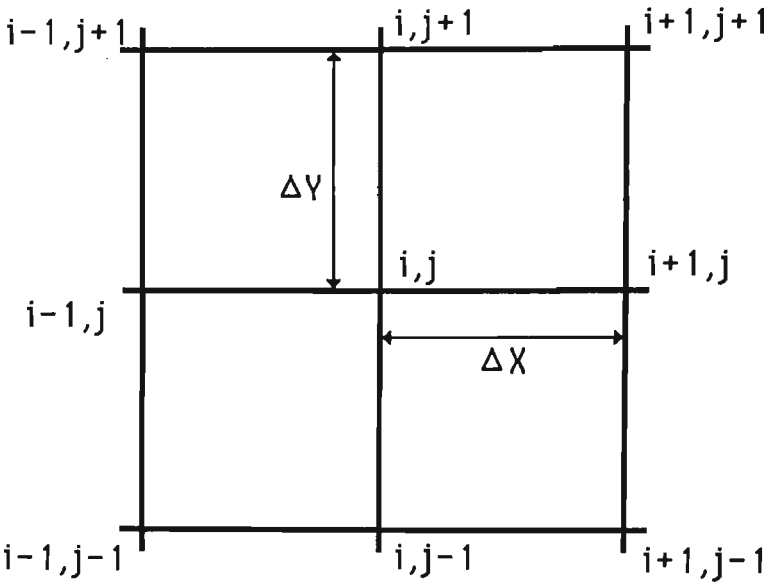

Fig. 15. Arrangement of grid points.

Using Taylor series and after some manipulation one can obtain the following finite difference formulae for the first and second derivative of θ at (i,j)[126], where θ, a variable, is given by $\theta = \theta(x,y)$.

Derivative	Difference Approximation	Order of accuracy
$\frac{\partial\theta}{\partial x} =$	$\frac{\theta_{i+1,j} - \theta_{i,j}}{\Delta x}$ (Forward)	R(x) (3.1a)
	$\frac{\theta_{i,j} - \theta_{i-1,j}}{\Delta x}$ (Backward)	R(x) (3.1b)
	$\frac{\theta_{i+1,j} - \theta_{i-1,j}}{2\Delta x}$ (Central)	$R(x^2)$ (3.1c)
$\frac{\partial^2\theta}{\partial x^2} =$	$\frac{\theta_{i-1,j} - 2\theta_{i,j} + \theta_{i+1,j}}{(\Delta x)^2}$	$R(x^2)$ (3.1d)

where i,j are variables to denote the grid points as shown in Fig 15. Similar forms exist for $\partial\theta/\partial y$ and $\partial^2\theta/\partial y^2$.

Using suitable difference expressions (forward, backward or central) for first and second derivatives as shown in equations (3.1 a-d), it is now possible to write difference equations for the momentum, energy and species balances for the fluid, mixture (fluid and solid) and gas phases at every node in the solution domain. Certain precautions, however, need to be employed in order to ensure numerical stability and convergence. It is required to handle each term in the governing PDEs differently. For this

purpose, we shall illustrate this point by obtaining the FD expressions for the one dimensional convective diffusive energy equation with heat generation. The dimensionless energy equation for this situation may be written in the form

$$Pe \frac{d\theta}{dx} = \frac{d^2\theta}{dx^2} + Q(\theta) \qquad (3.2)$$

where, the term on the LHS represents heat convection, the first term on the RHS represents diffusion and $Q(\theta)$ denotes the dimensionless rate of heat generation which may be a function of the dimensionless temperature. A good discussion on this problem is given in ref 127. Some salient features of the discussion are reproduced here.

Let us first describe the finite differencing of the convective term, $Pe \frac{d\theta}{dx}$. The derivative $d\theta/dx$ may be represented by a forward difference expression, a central difference expression or a backward difference expression as given by equations (3.1 a-c). When the Peclet number, Pe is positive (implying that the velocity is in the positive x-direction), expression (3.1b) is numerically the most stable representation of $d\theta/dx$ for all step sizes. For expressions (3.1a) and (3.1c) the step size Δx is restricted for numerical stability. If larger step sizes are used, physically meaningless results would be obtained. Similarly, when $Pe < 0$ (corresponding to velocity < 0), expression (3.1a) is the most stable difference scheme for $d\theta/dx$ and (3.1b) and (3.1c) would give converged results only if Δx is less than a critical value. Of course, the central difference scheme given by equation (3.1c) is

more accurate than the other two expressions (with an accuracy of the order of Δx^2) if the step size is chosen to be smaller than the critical value.

The diffusion term given by $d^2\theta/dx^2$, does not pose any restrictions for the sake of numerical stability. Therefore, one could use the 3-point central difference formula given by equation (3.1d). Special consideration for handling the source term $Q(\theta)$ will be discussed later. The difference expression for the transport equation (3-2) may now be written as:

$$Pe \frac{C_{i+1}\,\theta_{i+1} + C_i\,\theta_i - C_{i-1}\,\theta_{i-1}}{2\Delta x} = \frac{\theta_{i+1} + \theta_{i-1} - 2\theta_i}{\Delta x^2} + Q(\theta_i) \qquad (3.3)$$

Here, $C_{i+1} = 2$, $C_i = -2$, $C_{i-1} = 0$ for forward difference

$C_{i+1} = 1$, $C_i = 0$, $C_{i-1} = -1$ for central difference

and $C_{i+1} = 0$, $C_i = 2$, $C_{i=1} = -2$ for backward difference

Rewriting equation (3.3)

$$\theta_i\left\{2 + \frac{Pe\Delta x}{2} C_i\right\} = \theta_{i+1}\left\{1 - \frac{Pe\ \Delta x}{2} C_{i+1}\right\} + \theta_{i-1}\left\{1 - \frac{Pe\Delta x}{2}\right\} +$$

$$Q(\theta_i) \qquad (3.4)$$

The criterion for numerical stability is that each of the terms enclosed by the curly brackets should be positive. Thus, if the convective derivative $d\theta/dx$ is forward or central differenced, $Pe\ \Delta x \leq 2$ for $Pe > 0$. If $Pe < 0$, $|Pe|\Delta x \leq 2$ for backward or central difference expressions. Such criteria for any general flow problem can be established by writing down the difference expressions for the convection and diffusion terms and demanding that all the coefficients multiplying the nodal temperatures (θ, θ_{i+1} and θ_{i-1} in present case) be of the same sign.

The source term $Q(\theta)$ needs some special attention. Very often, the heat generation may depend non-linearly on the temperature and in such a case, one can not apply any direct matrix inversion procedure to obtain the nodal temperature values. Iterative methods are used to solve such non-linear problems. Starting with an initial guess for all the nodal temperatures, the solution is improved after each iteration by the use of stable numerical procedures, until sufficiently converged results are obtained. The change in the solution after each iteration is used as a measure for judging the extent of convergence.

Now the procedure to obtain a stable numerical representation in the presence of a non-linear heat generation term will be discussed. Observing that the convective and diffusive terms are linear in te mperature, one may conclude that a quasilinearization of the source term would improve stability. Such a linearization would ensure that all the terms in the governing equation are modified at approximately the same rate with each iteration. Therefore, the source term $Q(\theta)$ will be represented in a form

$[f_1(\theta_1{}^{k-1})]\ \{\theta_i{}^k\} + f_2\ (\theta_i{}^{k-1})$ where the superscripts k and k-1 denote the values corresponding to the k^{th} and $k\text{-}1^{th}$ iterations, respectively. The functions f_1 and f_2 ,which are the slope and the intercept for the linear representation in $\theta_i{}^k$, can be obtained in several ways. For numerical stability it is required that the slope be negative. Or, one needs an expression of the form:

$$Q\ (\theta) = -f_1\ \{\theta_k{}^k\} + f_2 \qquad (3.5)$$

where, f_1 and f_2 are only functions of $\theta_i{}^{k-1}$ and are positive.

Consider, for example, $Q(\theta) = 4 - 5\theta^3$. Using a Taylor series expansion about $\theta_i{}^{k-1}$, we get

$$Q\ (\theta_i{}^k) = Q\ (\theta_i{}^{k-1}) + \frac{d\theta}{d\theta}\Big|_{k-1}\ (\theta_i{}^k - \theta_i{}^{k-1}) + ...$$

$$= 4 + 10\ \{\theta_i{}^{k-1}\}^3 - 15\ \{\theta_i{}^{k-1}\}^2\ \theta_i{}^k$$

In the above example, $f_1 = 15\ \{\theta_i{}^{k-1}\}^2$ and $f_2 = 4 + 10\ \{\theta_i{}^{k-1}\}^3$. Suppose that $Q(\theta)$ was given as equal to $4 + 5\theta^3$. Following the same procedure as above, one would get a positive slope which is inadmissible from the point of view of stability. Under such circumstances, the recommended procedure is to take f_1 to be zero and $f_2 = 4 + 5\ \{\theta_i{}^{k-1}\}^3$. The differencing scheme that has been described above has been used in obtaining the finite differences expressions for the governing PDEs of the induction smelting problem. These expressions for the main governing PDEs with their boundary conditions are included in Appendix C.

3.1) DIFFERENT NUMERICAL METHODS USED IN SOLVING THE MODEL PROBLEM:

From our previous experiences regarding instability in numerical solution due to the source term and differencing scheme 41,46, every precaution has been taken to adopt the proper procedure to deal with each and every term in the mass, energy, momentum and species balance equations, in order to get a numerically stable and converged solution. Here, in brief, we will discuss only those methods which have been used to solve the all governing PDEs in the present problem. Details of these procedures are described elsewhere[125,129-131].

It should be noted that, while representing the governing equations in discretized form, one obtained a set of simultaneous non linear algebraic equations. These equations may be put in the matrix form which can be solved by using some proper numerical method. To illustrate this point let us consider the finite difference form of the equation of motion (C -1) which can be written for any node in a general form[46]:

$$C_1\ (i,j)\ \xi(i-1,j) + C_2\ (i,j)\ \xi_{i,j} + C_3\ i,j\ \xi_{i+1,j} + C_4\ i,j\ \xi_{i,j-1} + C_5\ i,j\ \xi_{i,j+1} = R_{i,j} \qquad (3.6)$$

where the right hand side term $R_{i,j}$, contains any source term that may be present and also terms with nodal variables other than ξ. C_1 - C_5 are known coefficients of variable ξ in equation (3.6) which can be easily interpreted from equation (C-1). Equation (3.6) can

be written in the pseudo-one-dimensional form for the i-direction as:

$$C_{1\,i,j}\ \xi_{i-1,j} + C_{2\,i,j}\ \xi_{i,j} + C_{3\,i,j}\ \xi_{i+1,j} = R_i \qquad (3.7)$$

$$\text{where } R_i' = R_{i,j} - C_{4i,j}\ \xi_{i,j-1} - C_{5i,j}\ \xi_{i,j+1} \qquad (3.8)$$

It is now possible to rewrite equations (3.7) and (3.8) for all i at a fixed j (say j = J) in a tridiagonal matrix form as:

$$\begin{bmatrix} C_{2\,1,J} & C_{3\,1,J} & & & & \\ C_{1\,2,J} & C_{2\,2,J} & C_{3\,2,J} & & & \\ & C_{1\,3,J} & C_{2\,3,J} & C_{3\,3,J} & & \\ & & \cdots\cdots & & & \\ & & & & C_{1\,n,J} & C_{2\,n,J} \end{bmatrix} \begin{bmatrix} \xi_{1,J} \\ \xi_{2,J} \\ \xi_{3,J} \\ \cdots\cdots \\ \xi_{n,J} \end{bmatrix} = \begin{bmatrix} R'_{1,J} \\ R'_{2,J} \\ R'_{3,J} \\ \cdots\cdots \\ R'_{n,J} \end{bmatrix} \qquad (3.9)$$

Where n denotes the total number of nodal points for a set value of J.

This system of matrix equations is known as a Tridiagonal matrix system, and a computationally very efficient tridiagonal matrix solver (TRIDAG)[125] can be used for solving this system. It is possible to directly use this subroutine for solving the one-dimensional equations. To solve the two or three-dimensional equations, such as the heat, mas and momentum transfer equations in the present case, it is possible to employ the efficient TRIDAG

algorithm in conjunction with the so called line-by-line method. Now the set of equations (3.9) can be solved by Gaussian Elimination method, on which TRIDAG subroutine is based, which can be summarised as follows:

3.1.1) GAUSSIAN ELIMINATION METHOD:

System of equations such as equation scheme (3.9) are most efficiently solved by systematically eliminating the unknowns. This is particularly simple in tridiagonal matrix case since no more than three unknowns appear in one equation. In fact, the first and last equation in (3.9) have only two unknowns, therefore, one can find the value $\xi_{n,j}$ in terms of known quantity after some manipulation which can be back substituted in the previous equation in order to find out $\xi_{n-1,j}$ and the back substitution process repeated like this until one obtains all the unknown values. This method has been used for all PDEs in the induction smelting problem except for the equation of motion in the bed region for which the following method is found more suitable.

3.1.2) GAUSS-SEIDEL ITERATIVE METHOD:

Basically, this method involved transferring all the off-diagonal terms of equations (3.9) to the right hand side, so that the i^{th} or diagonal equation becomes (in present case)

$$\xi_{1,J} = \frac{R'_{1.J} - C_{3\ 1.J}\ \xi_{2.J}}{C_{2\ 1.J}} \qquad (3.10)$$

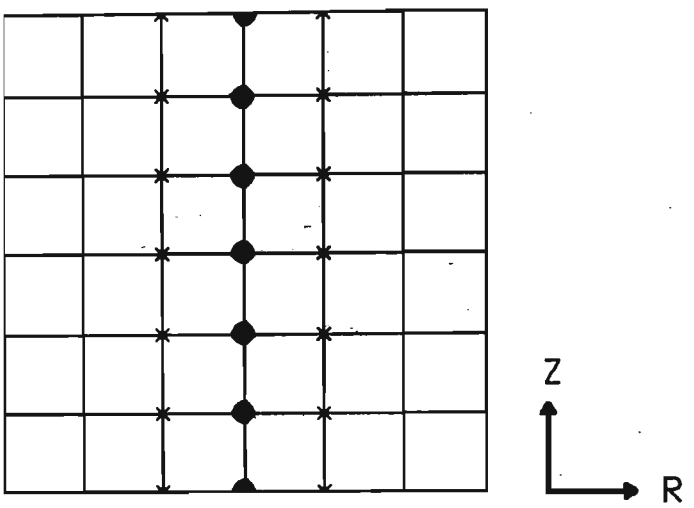

Fig.16. A schematic diagram to describe Line-By-Line Method.

In the same way all diagonal equations can be expressed. The computational procedure begins with initial guesses of $\xi_{i,J}$ for all the unknowns. An improved value for each of the unknowns is then computed and this most recently improved value is used in the right hand side in other equations. This procedure is repeated until the computed values show little further change. Details of these procedures are described elsewhere[125,132].

In the present case the line-by-line method was used to solve the equation of motion in the bed region, but unfortunately it was not possible to obtain a converged and stable solution by this method. Therefore,the Gauss-Seidel Iterative method (known as the point bypoint method also) was employed which gives a converged result.

Considering all the aspects such as faster convergence, accurate results, less computation time etc, the line-by-line method has been adopted here to solve all the governing PDEs except the equation of motion in the bed region.

3.1.3) LINE-BY-LINE METHOD[130]:

The line-by-line method can be visualized with reference to Fig. 16. The discretization equations for the grid points along a chosen line are considered. They contain the temperature (concentration, vorticity, stream function, whichever may be the case) at the grid points (shown by dots) along with the two neighbouring lines (shown by crosses). If the latter are substituted with their latest values, the equations for the grid points (shown by dots) along the chosen line would look like a pseudo-one-dimensional equation and

could be solved by calling the subroutine TRIDAG. This procedure is carried out for all the lines in the Z direction and may be followed by a similar treatment for the R-direction.

3.1.4) FULLY IMPLICIT METHOD:

In a fully implicit numerical method the solution of PDEs will be more stable than either the explicit or Crank-Nicolson method if very large time steps are being used, as in the case of present study, which implicitly reduce computational time very much. In this case derivative of temperature, concentration etc. is evaluated at the advanced time step t_{n+1} instead of the t_n. In brief, if one considered following differential equation

$$\frac{\partial u}{\partial t} = \frac{\partial^2 u}{\partial x^2} \tag{3.11}$$

then in implicit finite difference form it can be written as

$$\frac{U_i^{n+1} - U_i^n}{\Delta t} = \frac{U_{i-1}^{n+1} - 2U_i^{n+1} + U_{i+1}^{n+1}}{\Delta x^2} \tag{3.12}$$

Superscripts show time difference and subscripts show space difference at the grid points. In the space time grid it is clear from the above equation that the finite difference form is evaluated at the advanced point of time t_{n+1} instead of t_n. Equation (3.12) gives an implicit set of equations to solve for the new velocity (u) at each step in time. This scheme has been used for all transient PDEs in the present study as shown in appendix C.

3.1.5) UPWIND SCHEME:

This scheme has already been discussed implicitly in Section 3.0 in the analysis of the streamwise - diffusion equation (3.3), which suggests that $\theta_{i+1} - \theta_i$ and $\theta_i - \theta_{i-1}$ will have the same sign. Therefore, it will not be discussed here. For numerical stability and comparison of different schemes, a good discussion is available in refs. 125-126,134. In all convection-diffusion equations upwind finite difference, in the case of the steady state, and fully implicit upwind finite difference scheme, in the case of the transient equation, have been used as shown in Appendix C. Here, the implicit scheme has the advantage of unconditional stability as discussed in Section 3.1.4. Both the fully implicit scheme and upwinding sacrifice accuracy for stability.

3.1.6) OVER-RELAXATION AND UNDER-RELAXATION METHOD:

In the iterative solution of the non-linear algebraic equation, it is often desirable to speed up or to slow down the changes, from iteration to iteration, in the values of the dependent variable. This procedure is called over-relaxation or under-relaxation depending on whether the variable changes are accelerated or slowed down. Under-relaxation and over-relaxation are very useful devices for solving non-linear problems. The procedure of slowing down with the help of under-relaxation is very helpful for increasing the numerical stability while iteratively solving strongly non-linear equations. In general it can be written (say, for temperature)

$$T_{current} = w.\ T_{calculated} + (1-w)\ T_{previous} \qquad (3.13)$$

where, if $w > 1$ then the procedure is known as over-relaxation

and if $w < 1$ then the procedure is known as under-relaxation

In the computer programme for the Induction Smelting Process, only under-relaxation has been used. In the liquid region the values of the under-relaxation parameters are 0.5 and 0.8 for the stream function and vorticity respectively. In the bed region the values are 0.4, 0.5, and 0.7 for the stream function, vorticity, and FeO concentration respectively.

3.2) MESH ARRANGEMENT FOR ISP MODEL:

In the induction smelting problem, rapid changes of the field variables occur near the furnace wall. Therefore, a uniform grid may not be capable of sufficient resolution in that region. Therefore, when rapid change of the field variable (especially the Lorentz force in the present case) exists near the furnace wall (which is close to the induction coils) adoption of a uniform grid may not be suitable because, for adequate resolution, several mesh points are required. In this case a non-uniform mesh that is fine near the furnace wall and coarse elsewhere will provide more accurate results while keeping the computation inexpensive. The grid point distribution in the Induction Smelting Process for the induction region is shown in Fig. 17 in the R and Z directions. From this figure it is clear that in the Z direction mesh size is uniform because one may expect sufficient resolution in field variables by

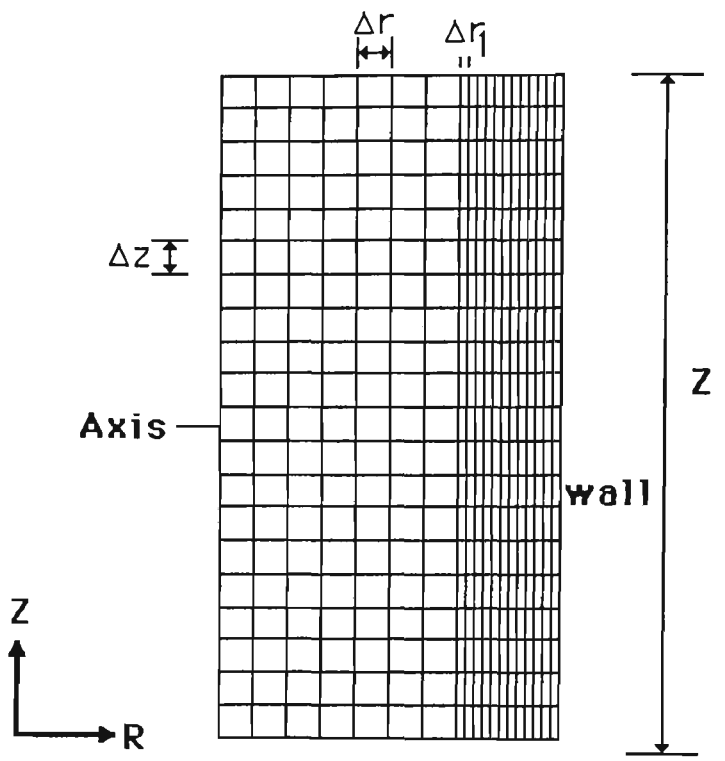

Fig.17. A mesh system for liquid region.

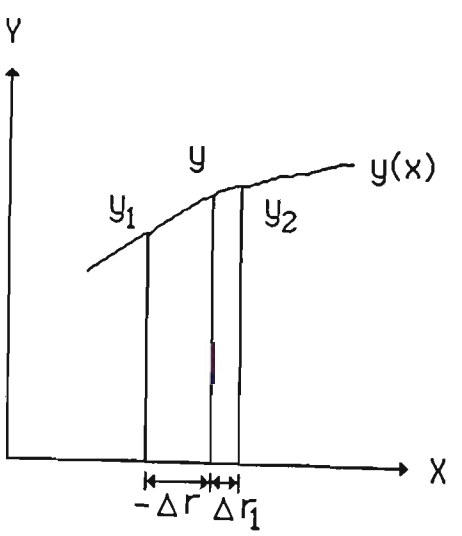

Fig.18. Curve used to calculate differential derivatives for uneven grid spacing.

adopting this mesh size. 21 grid points have been considered in the Z-direction with uniform spacing ΔZ. 20 grid points are chosen in the R-direction, of which first 8 points have uniform spacing Δr and the rest have uniform spacing $\Delta r1$ as shown in Fig. 17.

Now one has to take proper care when discretizing the governing PDEs at point 8 in R-direction because it lies in a transition position in which it has ΔR spacing on its left side and $\Delta R1$ on its right side. The finite difference approximation of the first and second derivative of any variable at this transition point (8) can be found by considering Fig. 18.

The curve in Fig. 18 can be approximated by a quadratic

$$y = ax^2 + bx + c \qquad (3.14)$$

where a,b and c are constants

with condition that at $x = 0 \qquad y = y_2$ (3.15a)

$$x = -\Delta r \qquad y = y_1 \qquad (3.15b)$$

and $x = \Delta r_1 \qquad y = y_3$ (3.15c)

with the help of equations (3.14) and (3.15) one can show, after some manipulation, that

$$\frac{d^2y}{dx^2} = 2a = \frac{2}{(\Delta r+\Delta r_1)} \left\{ \frac{y_1 - y_2}{\Delta r} + \frac{(y_3 - y_2)}{\Delta r_1} \right\} \qquad (3.16)$$

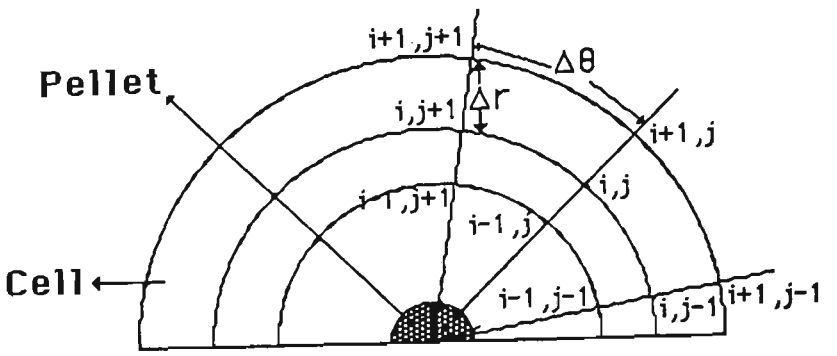

Fig. 19. Circular mesh system for bed region.

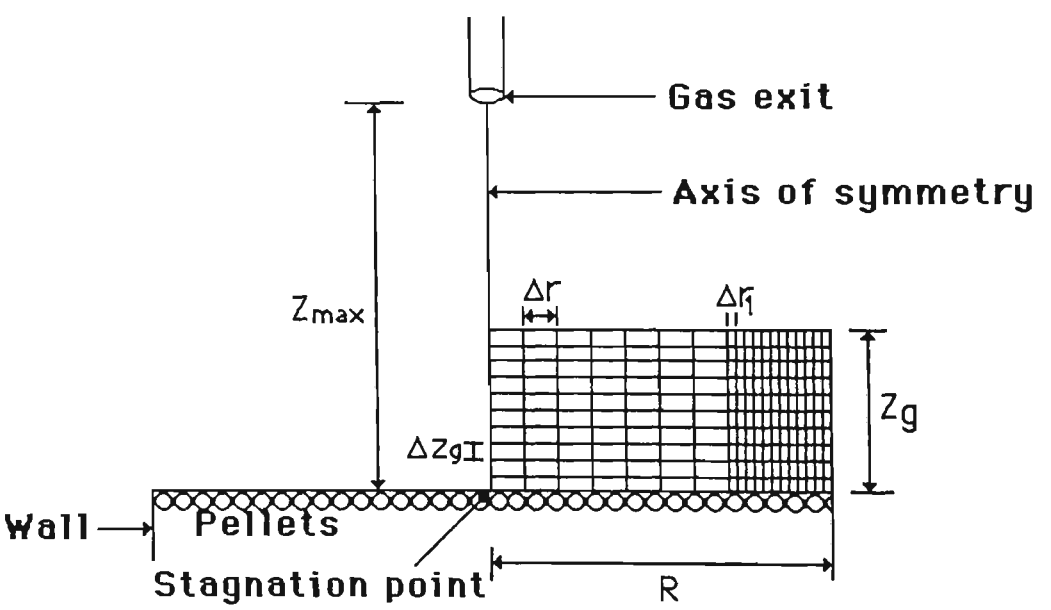

Fig. 20. Mesh system for gas jet region.

$$\text{and } \frac{dy}{dx} = b = \frac{1}{(\Delta r+\Delta r_1)} \left\{(y_3-y_2)\frac{\Delta r}{\Delta r_1} - (y_1-y_2)\frac{\Delta r_1}{\Delta r}\right\} \qquad (3.17)$$

Equations (3.16) and (3.17) can be applied during the discretization of all the differential equations in the liquid region at point 8. Appendix C shows the discretization form of the PDEs with respect to point 8.

The grid point distribution for the bed region, in which a cell model is considered, is shown in Fig. 19. A uniform grid spacing has been adopted in this region for both r and θ directions. In the r-direction 11 points are used with uniform spacing Δr and 21 points are used in θ-direction with uniform spacing Δθ as shown in Fig 19.

For the jet region, the grid point distribution in the boundary layers is shown in Fig. 20. The thickness of different boundary layers (thermal, velocity and concentration) can be estimated from the standard formulae[102] , which correlate boundary layer thickness with Reynolds number in the laminar region. To be on the safe side we have taken this thickness to be 1.0 cm in the Z-direction for the cylindrical axi-symmetric problem. The discretization of the equations in the jet region in the R direction can be represented in the same way as in liquid region i.e. the first 8 points in the R-direction have Δr uniform spacing and the rest have Δr1 uniform spacing. In the Z-direction 11 points with uniform spacing ΔZ_g have been used as shown in Fig 20.

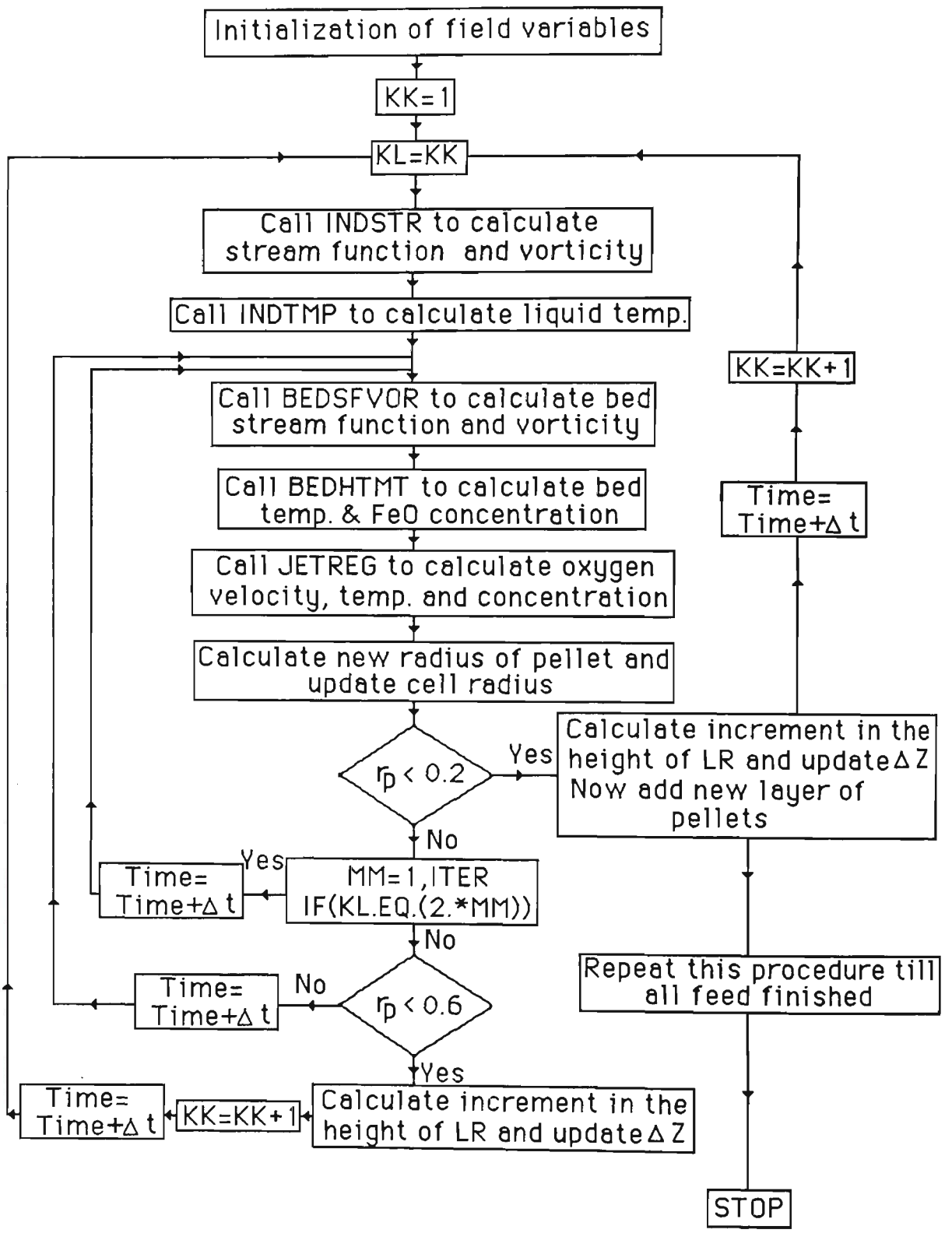

Fig. 21. Flow chart of the computer code

3.3) COMPUTATIONAL PROCEDURE FOR THE INDUCTION SMELTING MODEL:

An overall view of the computational procedure which has been adopted will be presented here. A computer code has been developed in standard FORTRAN-77 language to solve all three regions simultaneously. The structure of the computer code, in a broad sense, is as follows.

A rough flow chart of the whole process is given in Fig. 21. First all the field variables are initialized by assigning some guessed values. The actual execution starts by calling subroutine INDSTR, which solves the liquid region stream function and vorticity iteratively till these values become converged. After that the induction temperature is calculated by calling the INDTMP subroutine. Then the stream function and vorticity are calculated iteratively in the bed region by calling BEDSFVOR. The values obtained from subroutine BEDSFVOR are used to calculate the bed temperature and FeO concentration by calling subroutine BEDHTMT. Then the JETREG subroutine is called to calculate the gas velocity, temperature and concentration within the boundary layers. After this, the value of the new pellet radius is calculated in the following way. The rate of melting per cell ($\dot{m}$) can be expressed as:

$\dot{m}$ = density of pellet x rate of change of volume of the pellet

$$= \rho_p \; 4\pi \; r_p^2 \; \frac{dr_p}{dt}$$

or $$\frac{drp}{dt} = - \frac{\dot{m}}{\rho_p \, 4\pi \, r_p^2} \qquad (3.18)$$

m can be substituted from equation (2D-12) into equation (3.18), and radius of pellet (r_p) can be evaluated for each time step.

$$r_p^{n+1} = r_p^n - \frac{\dot{m}}{\rho_p \, 4\pi \, (r_p^n)^2} \, \Delta t \qquad (3.19)$$

Equation (3.9) gives the new value of the pellet radius for time step n+1.

After obtaining the new pellet radius, the void fraction and the cell dimension can be updated, as discussed in Section (2B-1).

If the calculated pellet radius is greater than the specified value (in the present case 0.6) then the computer program once again calls BEDSFVOR, BEDHTMT and JETREG for the new time step and calculates new values of velocity, temperature and concentration in bed and gas regions. This procedure is repeated until the new pellet radius becomes less than 0.6 but greater than 0.2. (The values 0.6 and 0.2 are the non-dimensional values which have taken as intermediate values of the pellet radius during calculations for keeping the computational time and cost as low as possible without losing much accuracy in the results. If we do not specify these values, then the program has to calculate the stream function, vorticity and temperature of the liquid region at each time step for a little increment in the liquid volume). With this

condition the computer calculates the increment in liquid region height as follows:

Liquid volume increment caused by pellet melting can be written

increment in volume = (rate of pellet melting x total time elapsed in obtaining this new radius x total number of pellets)/ density of melt

$$\text{or} \quad V_{incre} = \frac{\dot{m} \times t_{total} \times N}{\rho_{mix}} \tag{3.20}$$

Therefore, the increment in liquid height

$$H_{incre} = \frac{V_{incre}}{Area} = \frac{\dot{m} \times t_{total} \times N}{\rho_{mix}\, \pi R^2} \tag{3.21}$$

Once the increment in liquid height is known then the grid spacing in the Z-direction (ΔZ) for the liquid region can be updated.

The first time that the value of the pellet radius comes below 0.6 the program calculates the increment in liquid height as described above and then calls again all the subroutines in sequence i.e. INDSTR, INDTMP, BEDSFVOR, BVEDHTMT and JETREG. After calling JETREG, if the value of r_p (pellet radius) is not less than 0.2 it goes down and satisfies the condition i.e. KL = 2.*MM (because the new value of KL=2 due to increment in the value of KK in the last step, see flow chart) therefore, it goes back to call BEDSFVOR, BEDHTMT and JETREG then calculates a new r_p and cell radius till

r_p reaches below 0.2. Once r_p reaches below 0.2 it again calculates the increment in liquid height (this time it has been assumed that all pellets become melted which have r_p less than 0.2. Therefore, increment of liquid volume also takes care of unmelted (r_p < 0.2) pellet) and subsequently updates the grid spacing ΔZ. A small time difference may occur between computational and real (experimental) time due to the unmelted pellet (r_p < 0.2). However, it is believed that this small time difference will not affect the total computational time appreciably because of the very large temperature gradient which exists at the surface of the unmelted pellet (r_p < 0.2) which indicates that the pellets with radius less than 0.2 can be melted in negligible time.

Once all the pellets become melted, then new layers of the pellets are added and the above mentioned procedure is repeated again.

This whole procedure is repeated until all the feed has been fed into the furnace. Here, instead of adding new layers of pellet, after completing previous pellets melting, one could adopt a continuous feed rate.

Numerous parameters and values have been used during computation. A detailed analysis of the estimation of parameters for the ISP model problem is included in Appendix D.

The set of non dimensional differential equations with their boundary conditions have been solved in a Sequent S27 UNIX machine, using a computer program written in standard FORTRAN-

TABLE II

BASIC PARAMETERS USED IN CALCULATIONS

Parameters	Liquid Region	Bed Region	Jet Region
Crucible diameter, m	0.2	0.2	0.2
Crucible length, m	0.4	0.4	0.4
Step size in R dirn.	0.1 & 0.025	0.027	0.1 & 0.025
Step size Z & θ dirn.	0.1	0.1570796	0.01
Characteristic vel,m/s	0.3803978	0.3803978	20.0
Viscosity, kg/m-s	$6.0 \cdot 10^{-3}$	1.6	$2.06 \cdot 10^{-5}$
Following values of the parameters are given at room temperature			
Ther. cond.,cal/m-s-°K	18.0	2.0	$6.4 \cdot 10^{-3}$
Specific heat,cal/kg-°K	107.8	158.0	219.8
Density, kg/m^3	7600.0	3875.0(powder) 2230.0(bulk)	1.30
Following values are given at the melting point of pellet(1150-1190°C)			
Ther. cond.,cal/m-s-°K	8.0	0.8 (~1.0)	27.0
Specific heat,cal/kg-°K	168.52	240.0	268.47
Density, kg/m^3	6900.0	4500.0	0.2599
Initial Temperature,°K	300.0	300.0	300.0

26.	Molar concentration of FeO mol/m^3	$6.867 \cdot 10^3$
27.	Molar concentration of O mol/m^3	40.62023
28.	Diffusion Coeff. of O-CO gas m^2/s	$9.52 \cdot 10^{-10}\ Tg^{1.75}$
29.	Gas velocity m/s	20.0
30.	Void fraction of pellet	0.423
31.	Void fraction of bed	0.511
32.	Radius of pellet m	0.01
33.	Bed height m	0.045
34.	Oxygen density	$(391.87 \cdot Tg^{-1.0007})/1.301$
35.	Oxygen specific heat	$(7.16+1.0.10^{-3}Tg-.4.10^{-5}Tg^{-2})/7.0$
36.	Oxygen viscosity	$(0.68+4.82.10^{-3}Tg-7.32.10^{-7}Tg^{-2})$ 10^{-5}
37.	Oxygen thermal conductivity	$(0.92+1.816.10^{-2}Tg)/6.38.10^{-3}$
38.	Density of liquid Fe+C	$(8102.2-0.717\ T_L)/7620.6$
39.	PEHT in bed region	$4.01 \cdot 10^4\ r_p\ U_{AV}^*$
40.	PEMT in bed region	$3.9039 \cdot 10^9\ r_p\ U_{AV}^*$
41.	PEGHT in jet region	$8.957 \cdot 10^4$
42.	PEGMT in jet region	$9.71 \cdot 10^4$

TABLE I

VALUE OF PARAMETERS USED IN COMPUTER CODE

1.	Dimensionless induction power	1.0
2.	Wave number 1/m	16.667
3.	Permeability of free space H/m	$1.257 \cdot 10^{-6}$
4.	Magnetic field Wb/m^2	0.0354
5.	Magnetic field intensity A/m	$2.81835 \cdot 10^{4}$
6.	Furnace frequency Hz	2450.0
7.	η defined in eqn. (2E-3)	$4.37 \cdot 10^{4}$
8.	Spacing betwn. f/c coils m	0.03
9.	Viscosity of liquid iron	$6.0 \cdot 10^{-3}$
10.	Electrical conductivity of liquid iron mho/m	$7.968 \cdot 10^{5}$
11.	Electrical resistivity of liquid iron ohm-m	$1.255 \cdot 10^{-6}$
12.	CONSEH	$2.194208 \cdot 10^{3}$
13.	VSTRCO	$1.2850976 \cdot 10^{2}$
14.	PEL	$1.71899 \cdot 10^{3}$
15.	$D_{F\text{-}S}$, diffusion coefficient, m^2/s	$1.0 \cdot 10^{-10}$
16.	a	8.8573147
17.	b	8.6990248
18.	HEATBL m^2-s/cal	$5.3471 \cdot 10^{-9}$
19.	HITMEL	$7.90103 \cdot 10^{2}\ r_p$
20.	HFEPRO	$1.61361 \cdot 10^{-10}$
21.	ACUHIT	$6.416526 \cdot 10^{-5}$
22.	CFEOPR	$2.3288 \cdot 10^{7}$
24.	COUTFL	$3.81 \cdot 10^{8}$
25.	RYN (eqn.)	$1.85 \cdot 10^{3}\ r_p\ U_{AV}^{*}$

77 language. This program is listed in Appendix G and described in Appendix F. The CPU time to run this program on the Sequent which is Intel 386/387 based, for 21 layers of pellets (as is the case in the experiment) is ~31 minutes.

Values of density, thermal conductivity etc for liquid, pellet, mixture etc are given in Tables I and II.

CHAPTER 4

EXPERIMENTAL PROCEDURE FOR MEASURING PHYSICAL PARAMETERS

4.0) INTRODUCTION:

We have developed a mathematical model for the Induction Smelting Process. Before assessing the prediction of the model in practice one should, if at all possible, validate the model predictions by experiment, to measure the various field variables such as temperature, concentration, velocity etc. Once the field variables are known experimentally, these can be compared with predicted field variables, and so indicate the extent of the validity of the mathematical model and the assumptions upon which it is based.

Therefore, it was planned to measure a few important field variables experimentally, viz temperatures, composition of the melt, (slag and liquid iron) and velocity of the melt. These three variables are considered critical for the present smelting process upon which heat, mass and momentum transfer are based. It would be desirable to measure the other parameters, eg magnetic field, density of pellet, coil current etc. in order to supply reliable data for the computer calculations. For convenience the measurement techniques are presented in this chapter and the actual experimental results are discussed in Section 4.7.

4.1) TEMPERATURE MEASUREMENT:

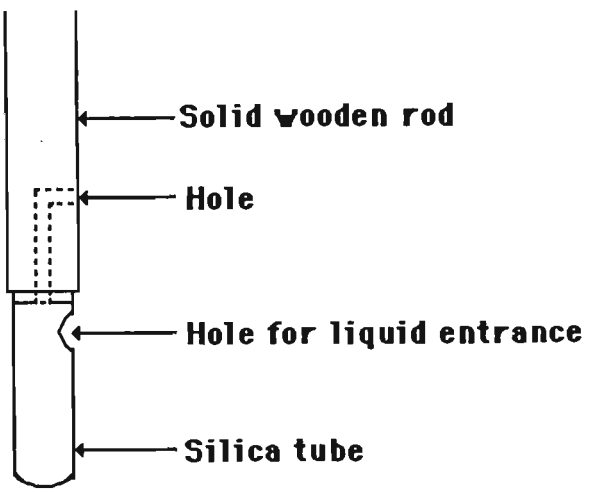

Fig. 22. Diagram for composition measurement apparatus.

High temperature measurement is a well known field and numerous temperature measurement devices are available eg, optical pyrometer, various type of thermocouples etc. Depending upon the requirement of the experiment one can select the proper measuring device. Regrettably, no temperature measurement device exists which can last long inside the melt at such a high temperature (1600°C) for the few minutes which is required in the present study in order to measure a few temperatures continuously.

In the present study, the need was to measure the temperature inside the liquid melt. Therefore, a Pt - 13% Rh thermocouple was chosen which can measure temperature up to 1700^{o}C with ±10^{o}C accuracy.

4.2) COMPOSITION MEASUREMENT:

It was initially planned that the composition would be analysed by taking samples of liquid iron and slag from various points at different time intervals during the smelting process. Therefore, a few small pure silica tubes with a side hole in each tube were made to collect the samples from different points at different time intervals. The top of the silica tube was covered with a solid wooden rod and a small hole was made in the wooden rod to facilitate escape of gas/air from the tube during the time of sample collection, as shown in Figure 22.

Unfortunately, the system did not work satisfactorily during the collection of samples in the smelting process. This is believed to

TABLE III

SLAG COMPOSITION

Fe as FeO	SiO_2	Al_2O_3	CaO	MnO	MgO
7.5	48.7	7.7	28.1	4.1	3.6

have been due to not having sufficient free passage for gases to escape from the tube, because during collection of samples the wooden hole was also covered with liquid melt, thus preventing liquid entering in the hole. However, the samples of final liquid iron and slag have been collected. The composition of the slag is shown in Table III.

4.3) VELOCITY MEASUREMENT:

This was the more crucial experiment. There are many fluid velocity measurement devices but almost all fail at very high temperature (~1600^{o}C).

Many authors[49,135-137] have tried to measure the liquid velocity by developing new measurement techniques. Most of them work below 800^{o}C. As far as is known, nobody has yet developed a satisfactory device to measure the velocity inside the liquid at high temperatures (~1600^{o}C). However, Hsiao[137] has reported a device reliably measuring the surface velocity at high temperature. Surface velocity measurement has also been tried by Lillicrap[138].

Here, we have tried to develop a velocity probe which is inexpensive and simple in construction in comparison to other existing devices while still trying to retain its sensitivity. Under these circumstances, some compromise with the versatility of the probe was inevitable. However, one can easily deduce from the probe design (Fig. 23) that by paying a little more attention to some parts of the probe, its versatility could be improved.

4.3.1) THEORY:

The velocity of the fluid can be deduced by measuring the drag force on a body immersed in the fluid. Drag (D) on a body, of area A, in the moving fluid, of density ρ , may be correlated with drag coefficient(C_D) as[102]

$$C_D = \frac{D}{\frac{1}{2}\rho U^2 A} \qquad (4.1)$$

where U is the mean fluid velocity away from the immediate vicinity of the body. C_D is a function of Reynolds number ,Re, for an incompressible fluid. A standard drag curve is available[82,102] between C_D and Re for spheres. From the drag curve it is interesting to note that C_D does not change with Reynolds number in the range 2.10^3 to 2.10^5. Also if the density of the fluid does not change appreciably with small temperature gradient then the drag force can be assumed to be independent of fluid density. One knows that in a coreless induction furnace the velocity of liquid iron normally ranges between 0.1 to 0.6 m/s. Therefore, one can select the diameter of the sphere in such a way that it gives a value of the Reynolds number higher than 2.10^3 but less than 2.10^5 . In this way, the measured drag force will be proportional to U^2.

4.3.2.) DESIGN OF APPARATUS:

A solid graphite sphere of 20.0 mm diameter was made by machining a block of pure (99.9%) graphite. We did not try to make a porous graphite sphere to eliminate the eddies shedding and thus the fluctuation in drag force readings as reported by Moore and

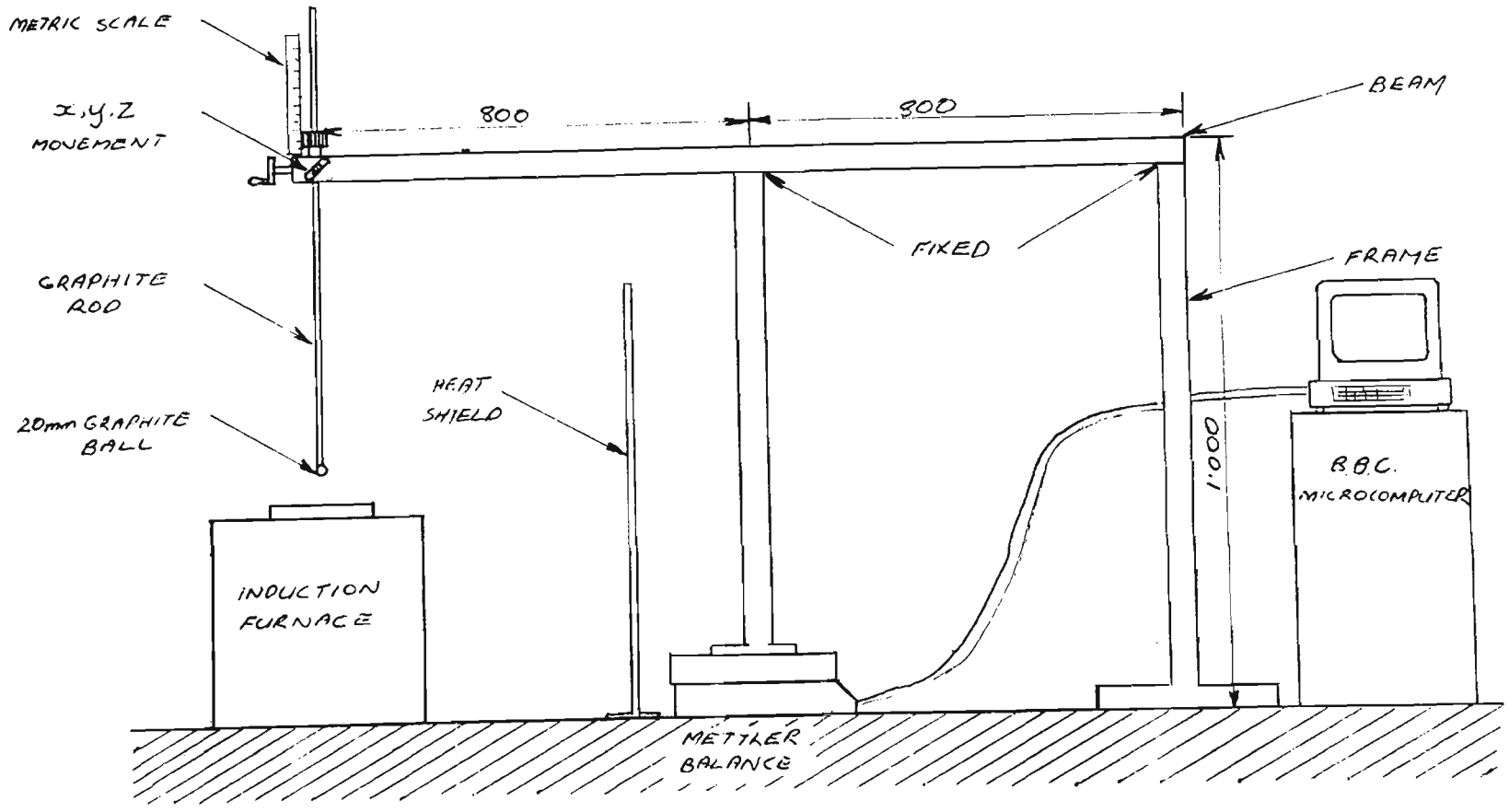

Fig. 23. Velocity measurement apparatus.

Hunt[139]. This solid sphere was attached to the end of a 1000.0 mm long and 10.0 mm diameter threaded graphite rod. Threads were made at the end of the graphite rod then screwed in the graphite sphere which was already threaded from inside. Graphite was selected due to its low cost, high melting point, and good machining properties. This graphite rod was attached to a carriage which was mounted on a long iron bar. The whole assembly was supported by a solid iron stand as shown in Fig. 23. The carriage had the capability to move the graphite rod to and fro as well as up and down with the attached side scales in both directions to facilitate taking of the readings.

The whole assembly was placed on a Mettler balance with a sensitivity of ±0.1g . The length of the bar from the fixed point of the stand was such that it measured twice the actual weight if a force exerts on the rod, which increased the sensitivity of the apparatus. The point at which the bar was clamped to the stand is a rigid point; therefore, reaction at this point will be zero and no force will be transmitted beyond this point. The point where bar and stand were clamped lies on the balance. Therefore the balance measured the actual drag force exerted on the sphere. Drag force data were recorded by attaching the Mettler balance to a BBC Personal Computer with a temperature interface via RS 232 port. The BBC Personal computer can memorize 6 data per second. Direct graphical representation of the data was obtained by using CUSTOM software developed by G. Hamilton, Senior Technical Officer of the University of Wollongong.

TABLE IV

COMPOSITION OF RAW MATERIALS

Constituents	Iron ore dry basis(db)	Marulan limestone	Brown coal slurry %	Brown coal char (db)
Fe (Total)	57.3			
SiO_2	5.28	1.8		
Al_2O_3	2.73			
Mn	0.11			
TiO_2	0.22			
S + P	0.058			0.24
LOI	9.53	42.8		
Others	0.207			
CaO		53.6		
MgO		0.6		
$Na_2O + K_2O$		0.11		
Fe_2O_3		0.4		
Al_2O_3		0.6		
Free Moist.		1.1	62.80	
Ash			1.40	2.3
Volatile			49.80(db)	0.5
Fixed Carbon			48.80(db)	97.2
Mine. & Inor.			1.00(db)	1.26
C			68.50(dmif)	94.4
H_2			4.80(dmif)	0.9
N_2			0.59(dmif)	0.42
Organic S			0.35(dmif)	
O_2			25.80(dmif)	2.8

This assembly was tested by blowing a known velocity gas on the sphere, which exerts a drag force on the sphere and was recorded by the balance. Calculation of the velocity from the drag force showed a deviation of ± 5% with the actual fluid velocity.

4.4) PREPARATION OF PELLETS:

In the present model, self fluxed composite pellets have been used as a smelting material because it is a common feed in most of the industrial smelting processes. The composite pellets used contain the iron ore and brown coal as a reductant, and burnt lime as a flux.

4.4.1) RAW MATERIALS AND PELLETS MAKING:

Lump iron ore and burnt lime were obtained from BHP Steel International Ltd., Port Kembla and materials were made of -500 mesh size. All materials were dried at 100°C to remove moisture. Brown coal was obtained from the Coal Corporation of Victoria in slurry form. The composition of iron ore, burnt lime and brown coal slurry as obtained from plants is given in Table IV.

The weights of the iron ore, lime and brown coal slurry were calculated on a stochiometry basis. Brown coal addition was 50% in excess of that required stochiometrically. The reaction which was assumed between Fe_2O_3 and C is

$$Fe_2O_3 + C = 2\,Fe + 3\,CO \qquad (4.2)$$

Because the brown coal slurry contained more than 60% water, some brown coal char(-500#) was added in order to make the

TABLE V

PROPORTION OF RAW MATERIALS

Constituents	Weight , kg	Equivalent ore,kg	Weight fraction
FeO	8.07	10.0	0.5671
CaO	0.4928	0.9194	0.0346
C	2.324	2.491(BC Char) &	0.1914
		1.424 (BC slurry)	
Others			0.2066
Total	11.29	14.23	~ 1.000

TABLE VI

CORELESS INDUCTION FURNACE SPECIFICATIONS

Inner diameter of the f/c	~301mm	
Outer diameter of the f/c	~338mm	
Spacing between the coils	~30mm	
Diameter of coil	~26mm	
Number of coil turns	13	
Coil stack height	~335mm	
f/c operating voltage, max	1500V	(290)
f/c operating frequency, max	4000Hz	(2450)
f/c operating power, max	300KW	(50)
f/c operating current, max	2900A	(~800)

Values enclosed in the bracket are the actual experimental values used in smelting operation.

composite mixture thick enough so that pellets could be made. The composition of brown coal char is also given in Table IV.

The iron ore (10.0 Kg), burnt lime (0.9194 Kg) and brown coal slurry (1.424 Kg) were mixed together with 2.491 Kg brown coal char in a mixer. Then by using a 60.0 cm diameter disc pelletiser, pellets were made in the range of +18.0mm and -22.5mm. Bags of dried pellets were made, each of them containing ~535g pellets (approximately 55 pellets per bag).

4.4.2) MEASUREMENT OF PELLET DENSITY:

The density of the powder (Fe O + C + CaO) was measured with the help of a density bottle and was found to be 3875kg/m^3. The bulk density of pellet was found by dividing its mass by its volume to be 2230kg/m^3. The void fraction of the pellet was 0.423.

4.5) MAGNETIC FIELD MEASUREMENT:

Magnetic field measurement was made for a single phase coreless induction furnace. All dimensions and specifications of the furnace are given in Table VI. The principle of magnetic field measurement is based on Faraday's law, according to which when a coil is placed in a time-varying magnetic field, then an induced voltage is developed in the coil which can be expressed as

$$e = - N \frac{d\Phi}{dt} \qquad (4.3)$$

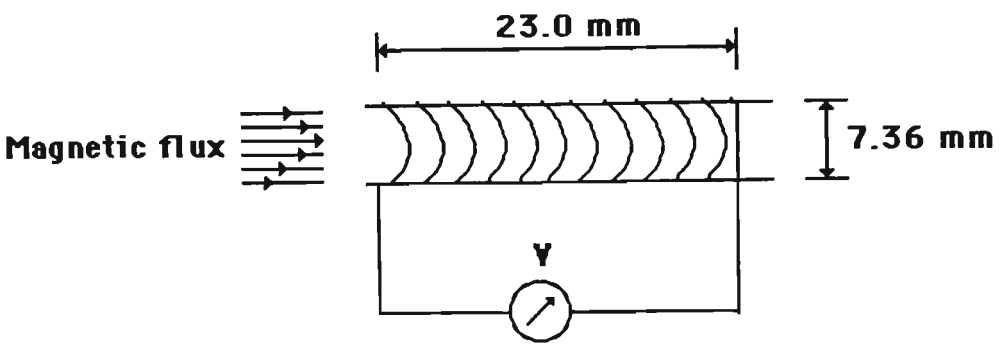

Fig. 24. Diagram for magnetic field measurement.

where e is induced voltage, Φ is magnetic flux, and N is number of coil turns.

For this purpose a coil was made by wrapping enamelled copper wire around a Perspex tube. The coil had the following dimensions

Number of copper wire turns	=	256
Length of the coil	=	23mm
Internal diameter of the coil	=	7.36mm
Diameter of enamelled Cu wire	=	0.2mm

With the help of this coil, its induced voltage was measured in the induction furnace by attaching a digital multimeter to the coil as shown in Fig. 24. During the induced voltage measurement, which was in r.m.s., furnace frequency was 2300Hz. The induced r.m.s. voltage was found to be of the order of 2.3 to 6.7 volts, due to the sinusoidal nature of the magnetic field. The calculation of the magnetic field based on these data is given in Appendix D.

4.6) MEASUREMENT OF FURNACE COIL CURRENT:

Due to the unavailability of a tong meter which can measure a high current, a current measurement device was prepared which can measure large current value without being affected by high frequency supply. The device is based on Ampere's circuital law which relates the magnetic potential induced in a loop to the current passing through the area formed by the loop.

For this purpose a 430 turn enameled copper wire loop was made in which enameled Cu wire of 0.5mm diameter was wrapped around a co-axial cable, of diameter 8.86mm, which was connected to a

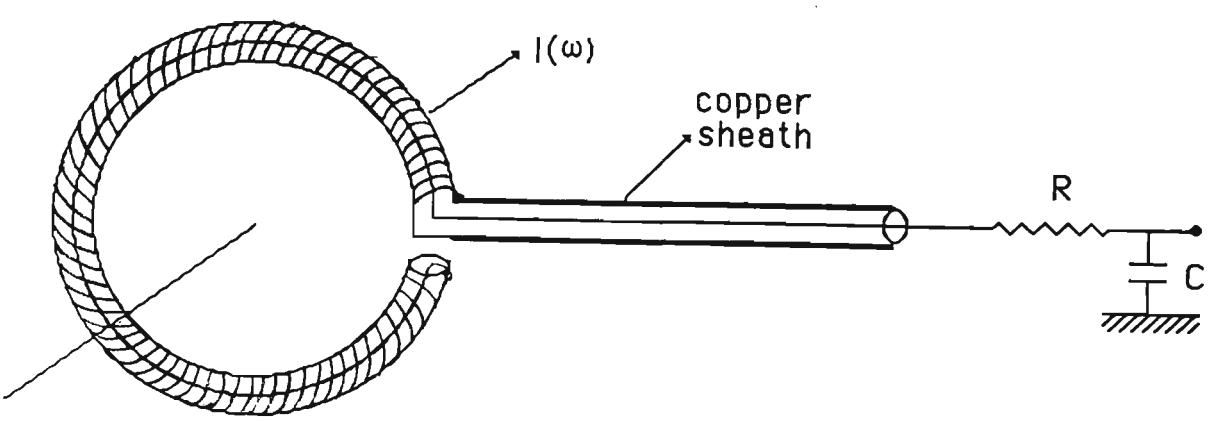

Fig. 25. Diagram of the current measurement apparatus.

resistor in series, and to a capacitor in parallel, as shown in Fig. 25. Values of the capacitor and resistor were chosen in such a way that in actual conditions it must satisfy the following condition

$$f >> 1/RC \qquad (4.4)$$

where, C is capacitor of value = 10. μF and,

R is resistor of value = 20. $K\Omega$

Different readings of output voltage were taken at known values of low currents. Analysis showed a non-linear relationship between output voltage and current. In the induction smelting experiment a furnace coil was enclosed in this loop and the output voltage was recorded at the actual operating conditions across the capacitor. The accuracy of the furnace current obtained in this way is questionable, because the non-linear relationship was established at low current value but was used to get the high current value. In the present study, the value of the furnace current obtained through this relation was 800.0 Ampere.

Because the value of the furnace current was uncertain, we did not use the numerical solution for the Bessel equation (2A-29) in our final calculations because the boundary condition (2A-55) for the equation (2A-29) needs the correct value of the furnace current. Moreover, we were not able to check the accuracy of the values obtained by the numerical solution. Therefore, the Bessel equation has been solved by adopting the second approach described in Section 2E-I. Solutions obtained by this method for the values a,b, u_o, v_o, X_o, Y_o, U_1 & V_1 have been checked by using ref.121 and were found accurate.

4.7) EXPERIMENTAL PROCEDURE AND MEASUREMENT OF VARIABLES:

All smelting operations were done in a 200mm diameter and 400mm long cylindrical graphite crucible which was made to order by the Carbon Mechanical Product Company, Sydney. The run began by melting 3.636kg pig iron as a heel. After that the actual smelting process was started by feeding each bag of pellets intermittently in conjunction with top blown oxygen through a lance. After a fixed time interval the next pellet bag was added. During the smelting operation, at various time intervals temperatures were measured, with the help of the Pt-13% Rh thermocouple attached to an Electro-Nite lance, at different locations in the melt. Data were stored in the computer by connecting the Electro-Nite lance with the computer. During the measurement of temperature all axial and radial distances of the measured point were recorded with an accuracy of $\pm$5.0mm. Also attempts were made to collect a few samples for chemical composition during the process, unsuccessfully, as explained in Section 4.2. During the temperature measurement the furnace power was switched off so that induced field should not affect temperature readings. After measuring the temperature, the furnace was set to its previous values of voltage, frequency and power. These furnace parameters were kept constant throughout the smelting operation. All measured data have been compared with model predictions in Chapter 5.

After finishing the smelting, slag was removed from the top of the liquid iron surface to measure the velocity. Unfortunately just when everything was made ready to start measuring velocity, the

crucible broke and the whole liquid melt spilled out from the furnace. Lack of time prevented repeating this (rather expensive) experiment. Therefore, we were not able to measure the velocity of the fluid under actual experimental conditions. This was the most unfortunate part of the experiment. The failure of the crucible was due to oxidation of graphite by air which was rushing up from the bottom of the crucible through the gap between the furnace and the crucible wall. This circulation was due to the large temperature difference between the top and bottom of the furnace, and its consequent density difference. It should be noted that during the preparation of the velocity probe, one trial run had been made in liquid iron to measure the velocity and our rough calculations showed the velocity of liquid iron as between 0.1 to 0.4 m/s. Unfortunately we did not keep the record of this trial run but it indicates that the velocity probe is quite capable of measuring velocity inside the melt at high temperature. During the trial run, fluctuation in the velocity was noticed which was due to the turbulent nature of the fluid flow.

During the smelting operation, various other parameters were also recorded viz, starting and finishing time of the smelting, feeding time of pellets, melt height at various time intervals etc.

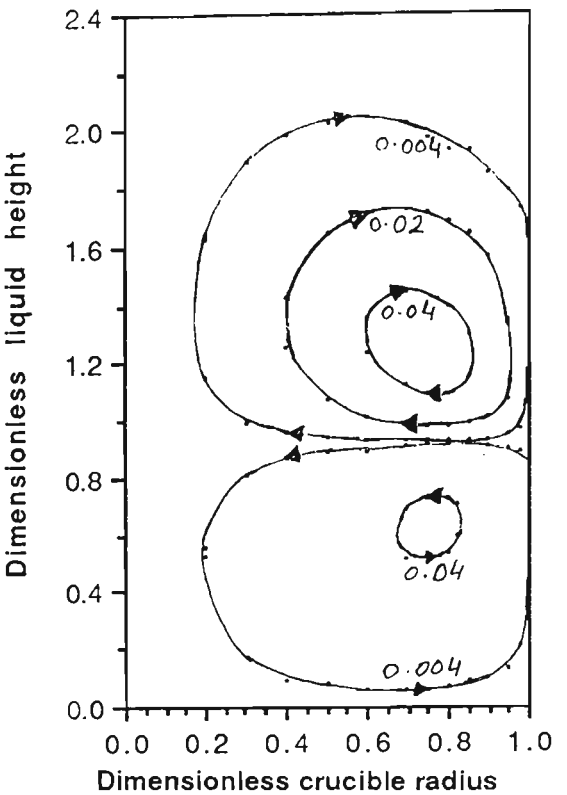

Fig. 5.3. Distribution of streamlines inside the liquid at dimensionless time=1.279.

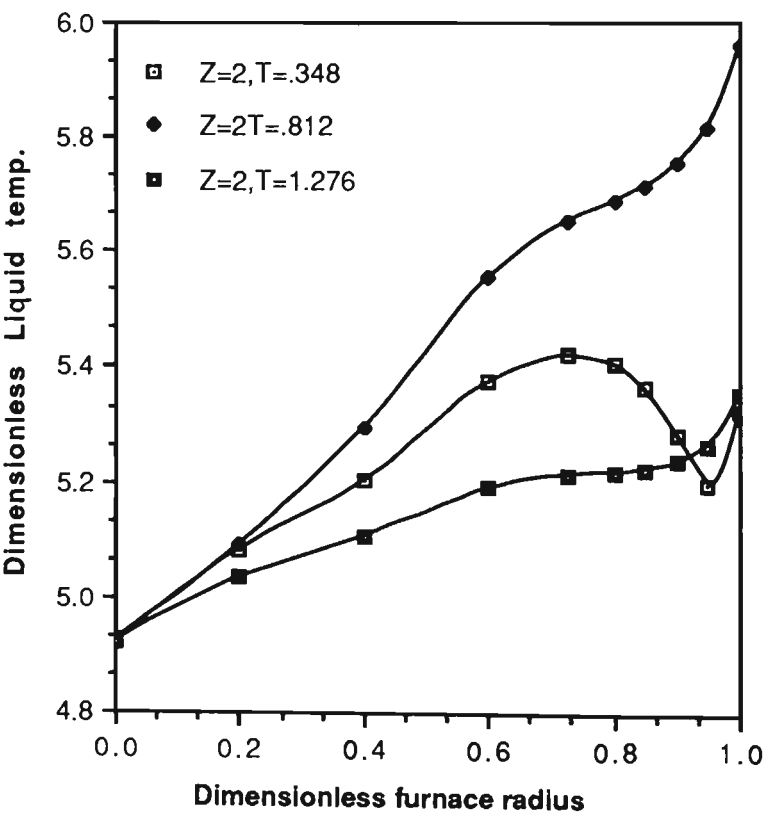

Fig. 5.4. Variation of liquid temperature in R-direction.

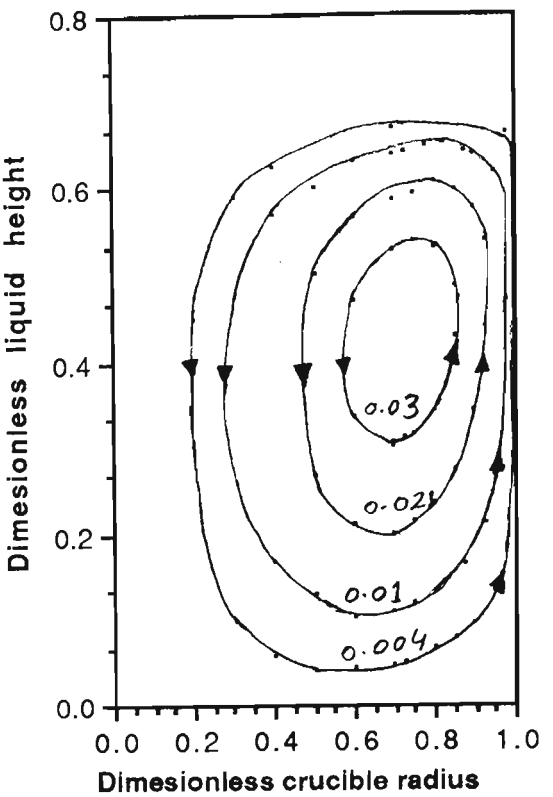

Fig. 5.1. Distribution of streamlines inside the liquid at dimensionless time=0.348.

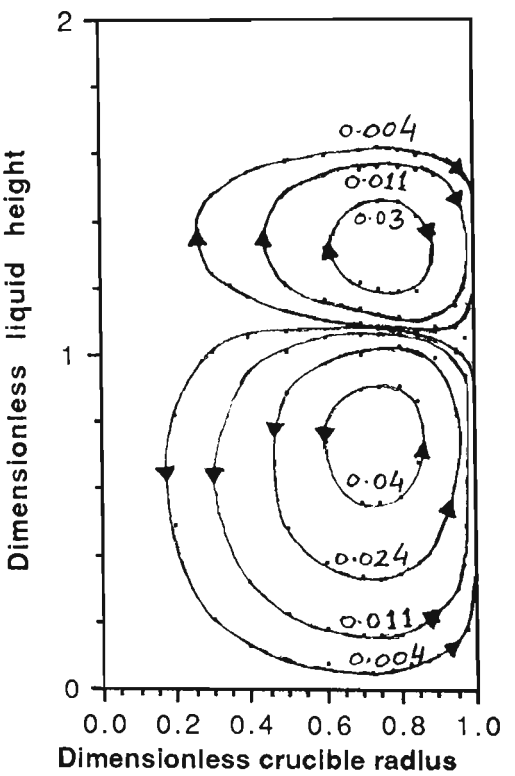

Fig. 5.2. Distribution of streamlines inside the liquid at dimensionless time=0.928

CHAPTER 5

RESULTS AND DISCUSSION

Numerical solution of the model equations, presented earlier, provides the values of various dimensionless field variables viz, liquid, mixture, and gas temperatures, velocities and concentrations as a function of different parameters involved in the equations. In view of the very large number of parameters involved in the characterization of the Induction Smelting Process, results have been presented here only for a few selected parameters.

Results in this Chapter have been presented in R and Z directions for the liquid and jet regions and in the r and θ directions for the bed region. All results have been presented with respect to the particular grid point. Therefore, we would suugest before going through this chapter one should refer to Figs. 17, 19 and 20 to get a clear idea of the grid point arrangement in all three regions. Results have been plotted at dimensionless time 0.348, 0812 and 1.276 for the liquid region which corresponds to the time required for complete melting of the first three layers of pellets, nine layers of pellets and fifteen layers of pellets respectively.

The results obtained in the present study, when plotted for various parameters, reveal some interesting trends. A typical set of streamline profiles in the liquid region is shown in Figs. 5.1 to 5.3.

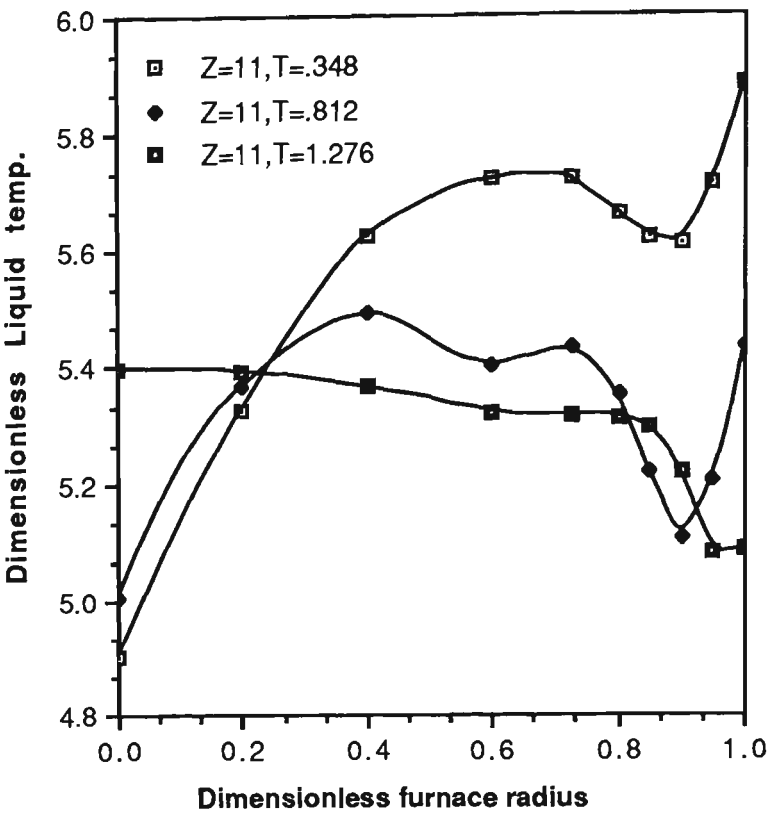

Fig. 5.5. Variation of liquid temperature in R-direction.

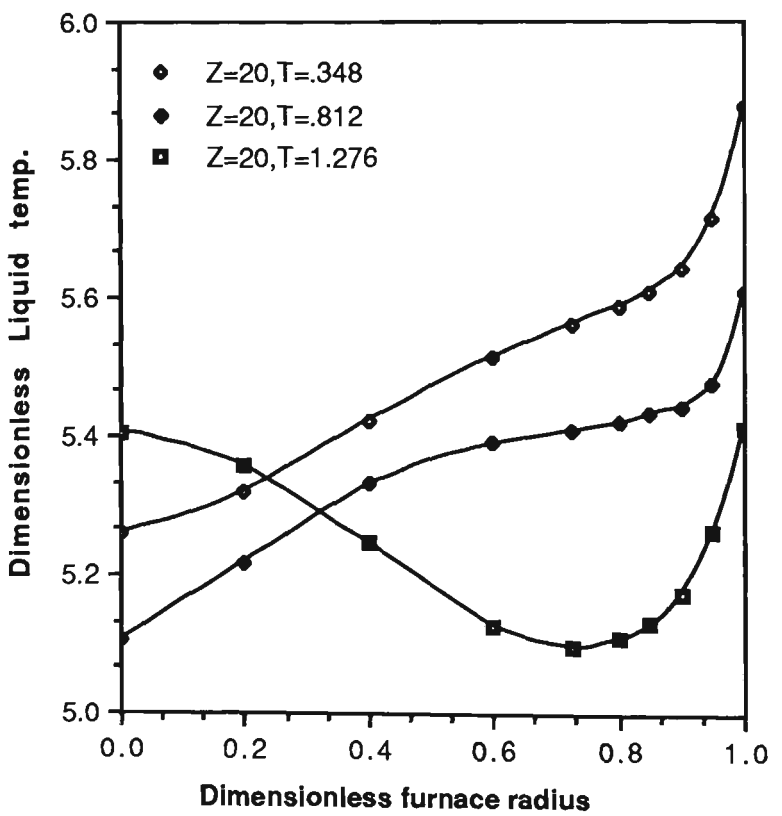

Fig. 5.6. Variation of liquid temperature in R-direction.

Streamline results have been plotted as dimensionless radial distance versus dimensionless liquid height at different dimensionless times. The value within each circulation loop shows the value of stream function for that loop. It is interesting to note how the second circulation loop of streamlines develpoed with time and liquid height. In these results maximum axial velocity has been obtained away from the axis of the furnace i.e. near the wall due to localized body forces in this region, which is in accord with the results of other investigators[42,46,47,49]. A very small recirculation loop of streamlines has also been obtained very near the crucible wall, when the height of liquid is more than 2.4, as found and explained in ref. 46. A close inspection of Fig. 5.3 reveals that the circulation velocities are higher in upper loop which is due to the lesser drag forces in the upper half of the liquid.

When only heel is present in the furnace i.e. where liquid height is very low, then only one loop has been obtained with the maximum axial velocity of 0.8m/s in the whole smelting operation. As the liquid height increases, velocity decreases and after 10.0cm of liquid height the maximum axial velocity is fairly constant throughout the smelting operation which is ~0.3m/s. Velocity values obtained in the present study are in accord with experiments carried out by other researchers[135,136,138].

Figures 5.4 to 5.6 show the radial variation of liquid temperature at different time and liquid height. These figures have been plotted at a particular nodal point in Z direction but at different time as indicated in the figures. As expected, during the smelting operation in a medium frequency furnaces, there is a significant variation in

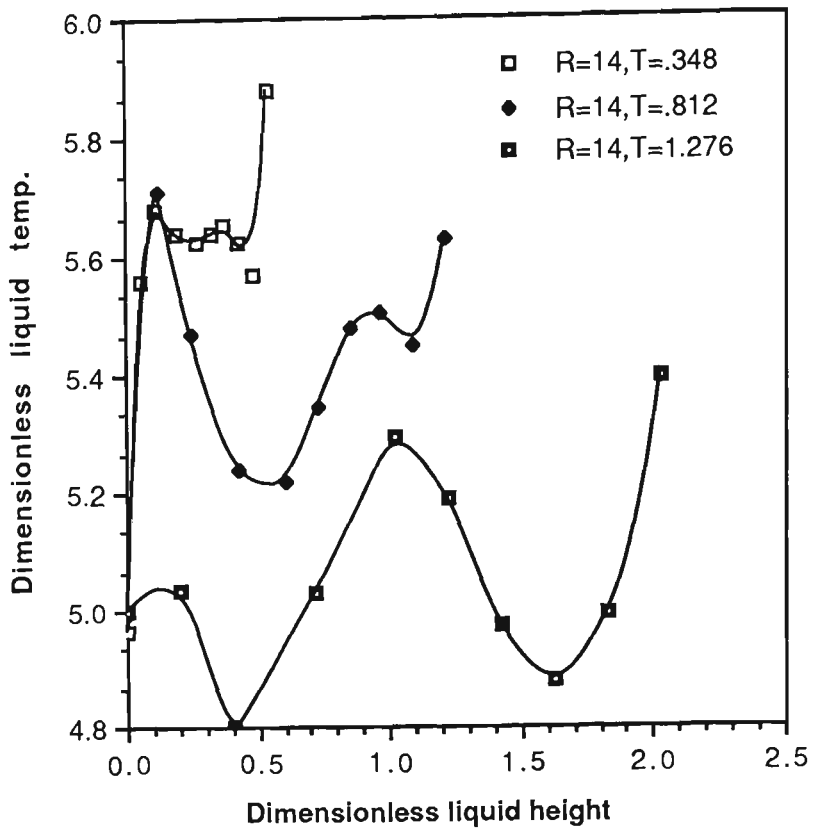

Fig. 5.9. Variation of liquid temperature in Z-direction.

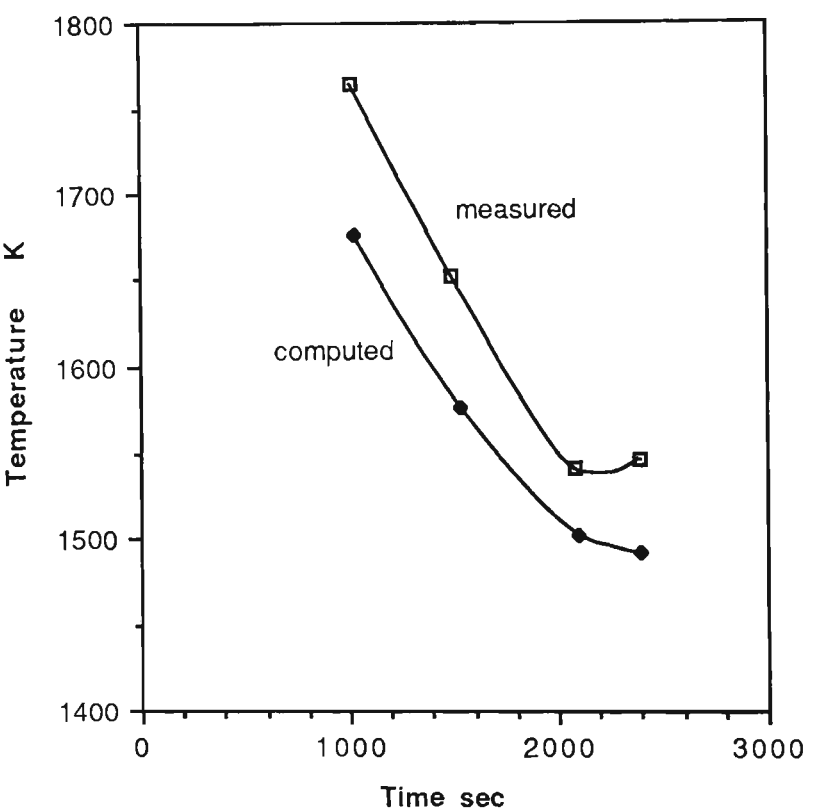

Fig. 5.10. Comparison between measured and computed temperature.

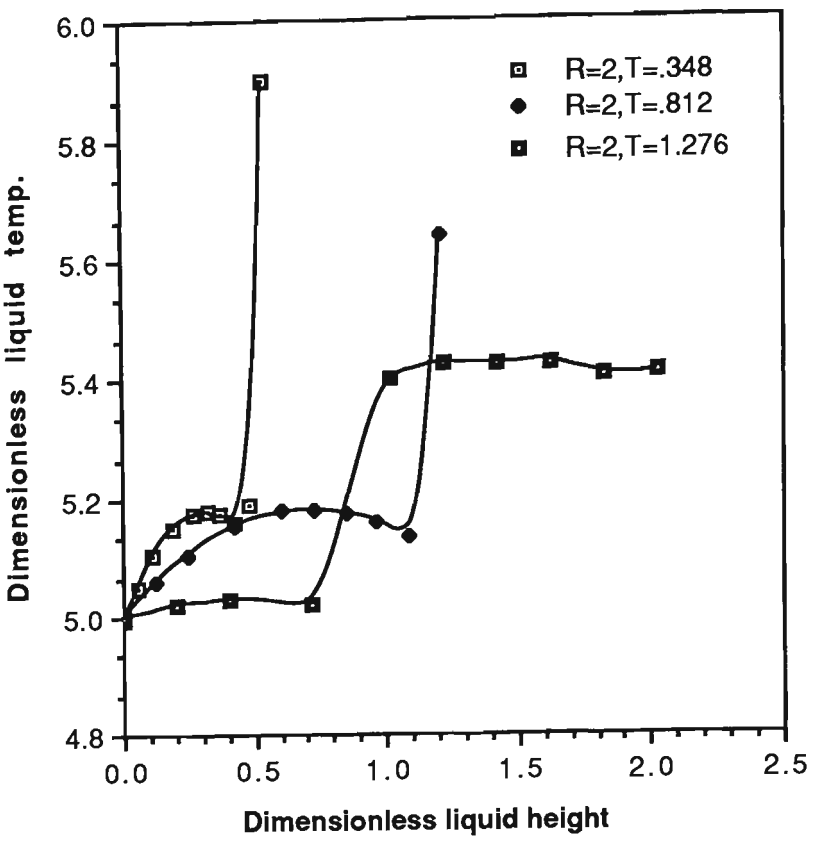

Fig. 5.7. Variation of liquid temperature in Z-direction.

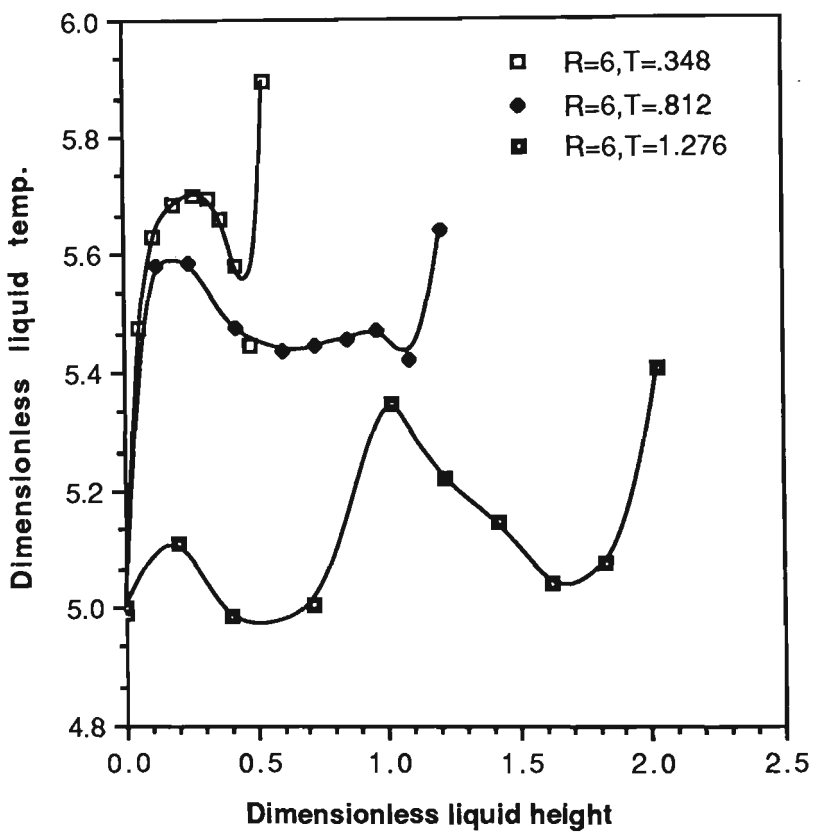

Fig. 5.8. Variation of liquid temperature in Z-direction.

the temperature in the radial direction (~30-200 C). It is interesting to note from these figures that, at the axis, the temperature is always lower than at the wall. The reason is that the heating due to energy dissipation, occurring in the first few skin depths of the induced current, causes the fluid to be less dense near the wall where the temperature is greatest. The light fluid near the wall rises in the upward z-direction and the cooler, more dense, liquid next to the centre falls under the action of gravity. There are small perturbations in a few curves in Figs 5.4 and 5.5 which we believe are due to different flow patterns of the liquid at different times (Figs. 5.1, 5.2 & 5.3) which gives different mixing patterns inside the liquid. From the careful inspection of Figs 5.4 to 5.6 near the wall, it is evident that a weak temperature gradient exists. This is because heat sources are localized near the wall where turbulence is decaying, and therefore, some inhomogeneity occurs. This temperature gradient is very useful to define the heat transfer coefficient in general practice.

The vertical liquid temperature profile shows a more or less similar trend, as seen in the radial liquid temperature profiles presented in Figs. 5.7 to 5.9. As evident from these figures, the temperature usually increases from the bottom of the crucible to the top of the liquid monotonically, except for a few perturbations. The temperature at the top of the liquid is usually higher than at the bottom, which is due to the top boundary condition of the liquid in which we have considered melting of the pellet, various reactions between gas, solid and liquid etc effect as discussed in previous Section 2D. The temperature at the bottom is always low because the thermal energy is lost by conduction to the bottom wall of the

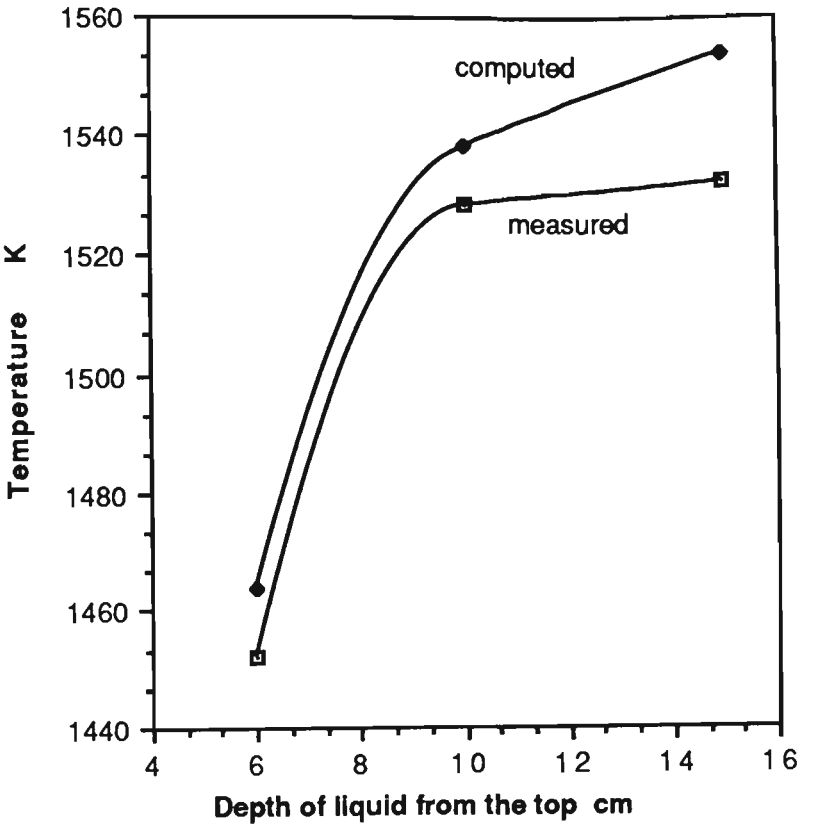

Fig. 5.11. Comparison between measured and predicted temperature at R=2 and constant time.

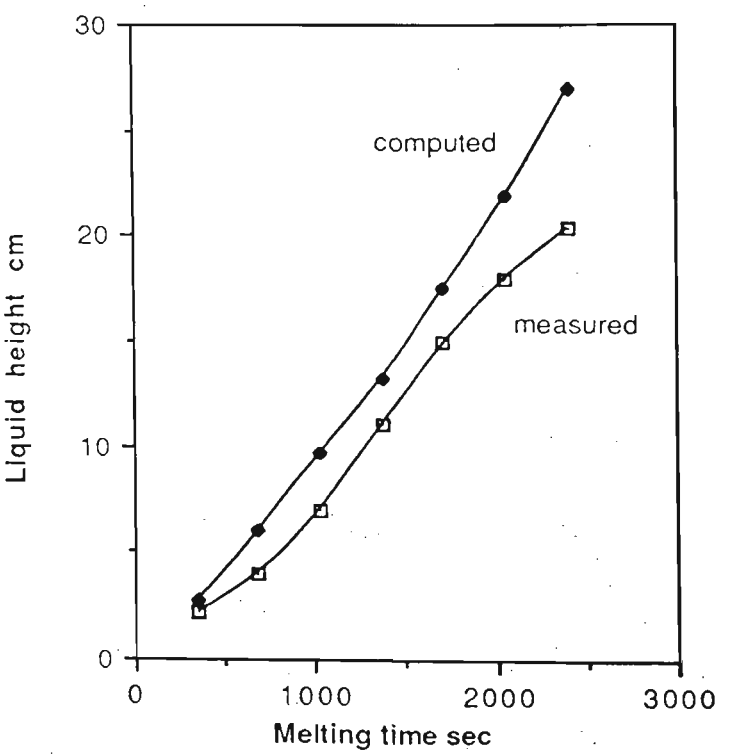

Fig. 5.12. Comparison between computed and measured liquid height with smelting time

crucible. The small perturbations in Figs. 5.7, 5.8 & 5.9 are due to the different flow patterns of the liquid at different times. Also flow patterns change from the centre of the crucible to the crucible wall. The shape of the curves in Fig. 5.9 can be justified on the basis of these flow patterns. For example curve in Fig. 5.9 at T=1.276 and R=14 shows a sinusoidal nature. If one compare this curve with the liquid flow pattern Fig. 5.3 then it explains the nature of the curve clearly. In the lower recirculating loop in Fig. 5.3 the fluid elements near the bottom of the crucible are travelling in a longer path, therefore loosing more energy hence becoming cooler. This fact is evident from the Fig. 5.9. As the vertical distance increases liquid get hotter and hotter till it crosses the lower portion of the upper recirculating loop. Again temperature started decreasing and can be explained in the same way as it is explained for the lower recirculating loop. In all these three figures the vertical temperature is normally increasing with liquid height at constant dimensionless time t=0.348. The reason may be that more electric heating is concentrates when the liquid pool is small, as is the case at t=0.348. Also there is only one circulation loop of the streamlines present at this stage as shown in Fig. 5.1. All these factors, we believe, give a different shape to these curves.

Figures 5.10 to 5.12 show a comparison between experimental and predicted results. In Fig. 5.10 results have been plotted for temperature (^{o}K) versus time(s) at constant value of R=6 and Z=8. Figs 5.11 and 5.12 are self explanatory. Results in Figs. 5.10 and 5.11 show a good agreement between experimentally obtained results and computed results with respect to the trend. The small

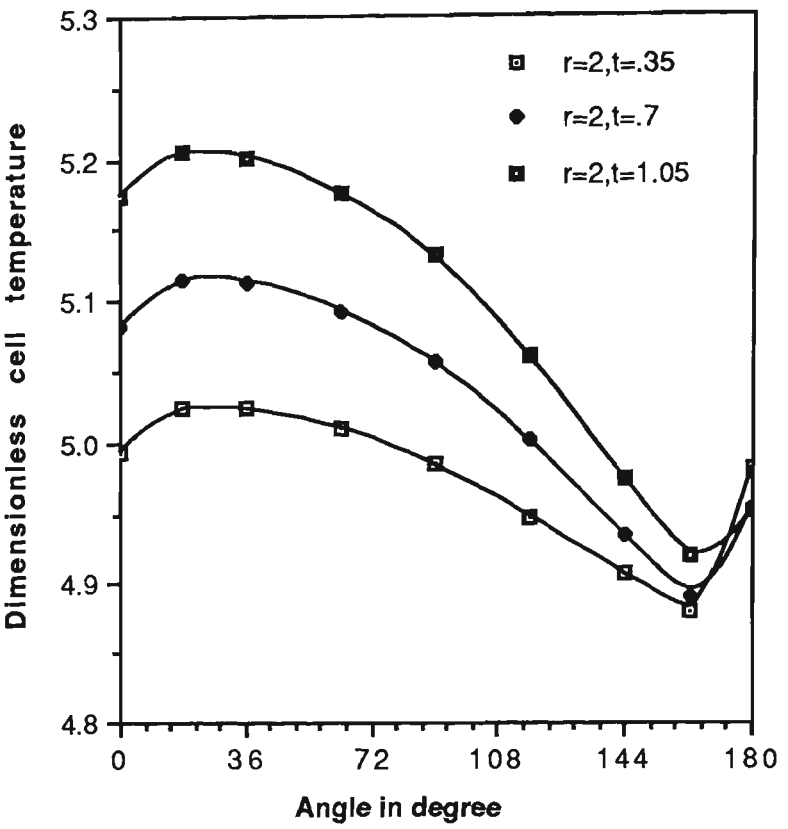

Fig. 5.13. Variation of cell temperature in Θ-direction.

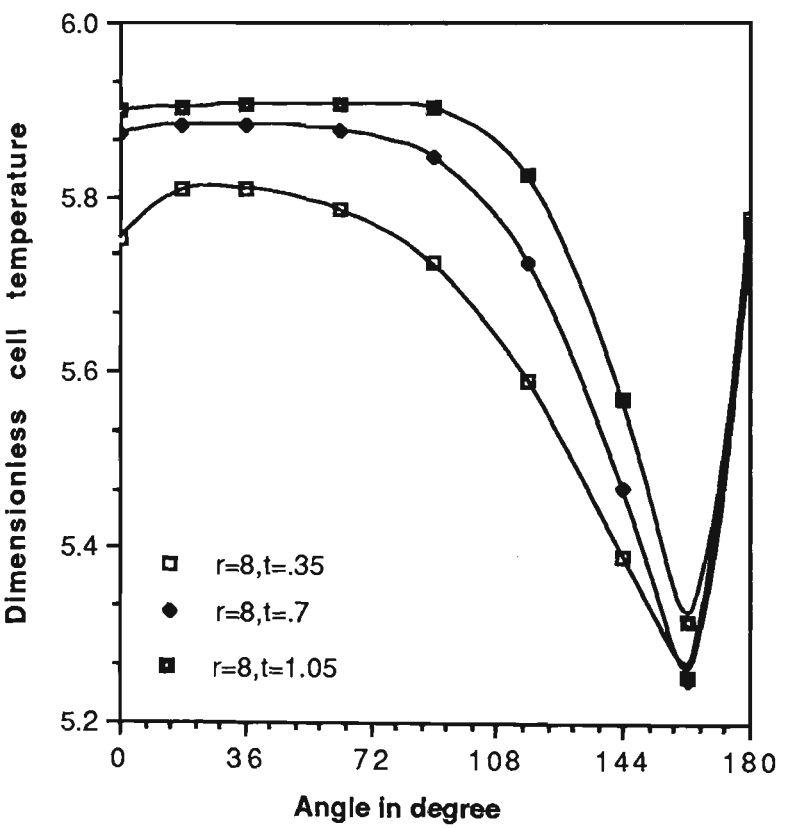

Fig. 5.14. Variation of cell temperature in Θ-direction.

difference in temperature is due to considering temperature independent properties of the liquid and specifying the constant temperature at the outside of the crucible walls. Here, one should note that measured temperatures during the experiment were not very reliable because a few temperatures obtained were very low, which cannot be expected when everything in the furnace is in the liquid state. Fig. 5.12 shows an excellent agreement between liquid height and smelting time obtained experimentally and theoretically. The small difference in liquid height at the end is due to the large splashing of slag from upper surface, probably due to carbon boil etc during experimentation. Also theoretically we have assumed all minor elements except carbon go with iron and slag which is not rigorously true in practice.

These results show a very good validity of the mathematical model developed for the Induction Smelting Process.

For the figures 5.13 to 5.23, results have been plotted at dimensionless time 0.35, 0.7 and 1.05 for the bed region which correspond to the different radius of pellets during the melting of one layer of pellets i.e. from starting (r_p = 1.0) to finish (r_p < 0.2).

Temperature profiles in the bed region along the selected radial values in θ–direction are given in Figs. 5.13 and 5.14. Monotonical decreasing of temperature is due to the endothermic chemical reaction occurring between FeO and C progressively in θ -direction. As the time increases, the reaction reaches its completion. Therefore, less endothermic effects are expected, which thus increase the temperature of the melt. As the time increases the

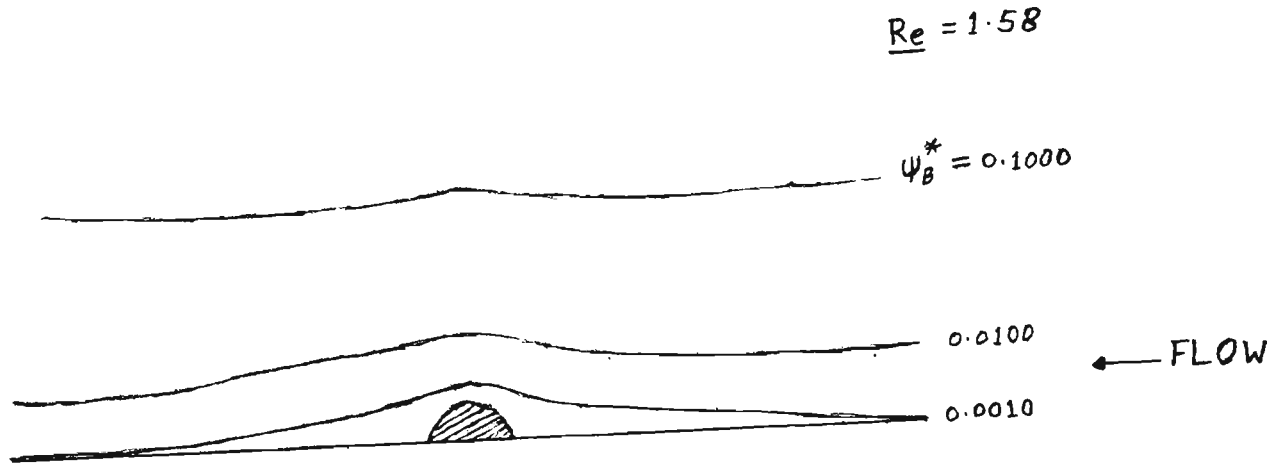

Fig. 5.18. STREAMLINES CONTOURS WITHIN THE CELL

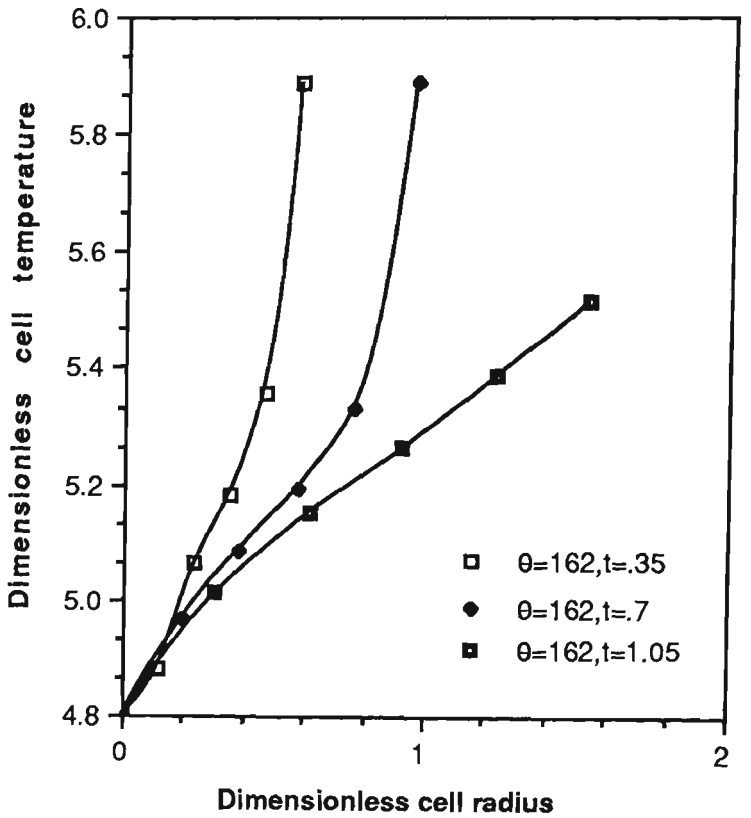

Fig. 5.17. Variation of cell temperature in r-direction.

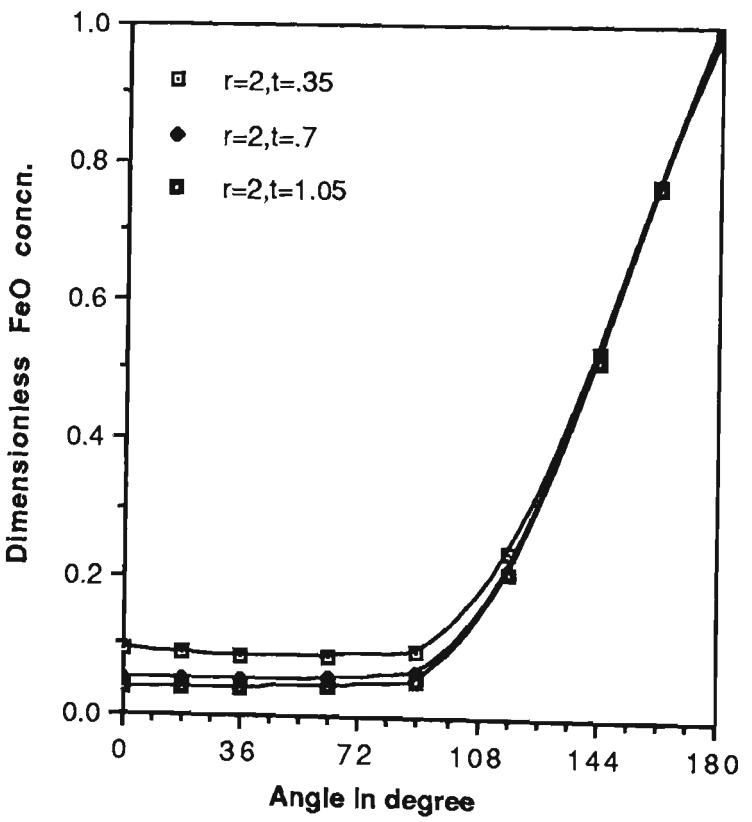

Fig. 5.19. Variation of FeO concentration within the cell in Θ-direction.

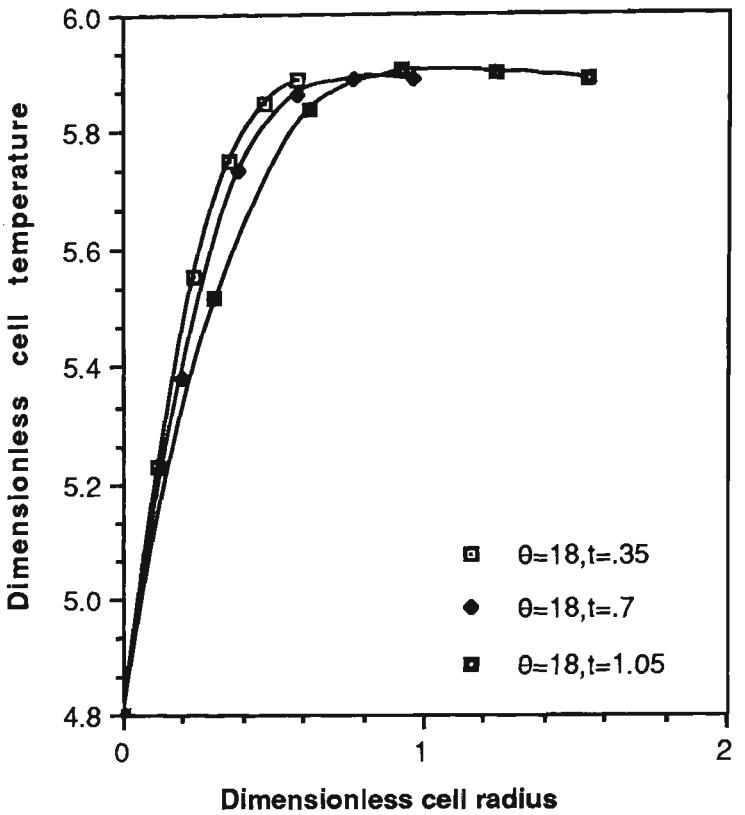

Fig. 5.15. Variation of cell temperature in r-direction.

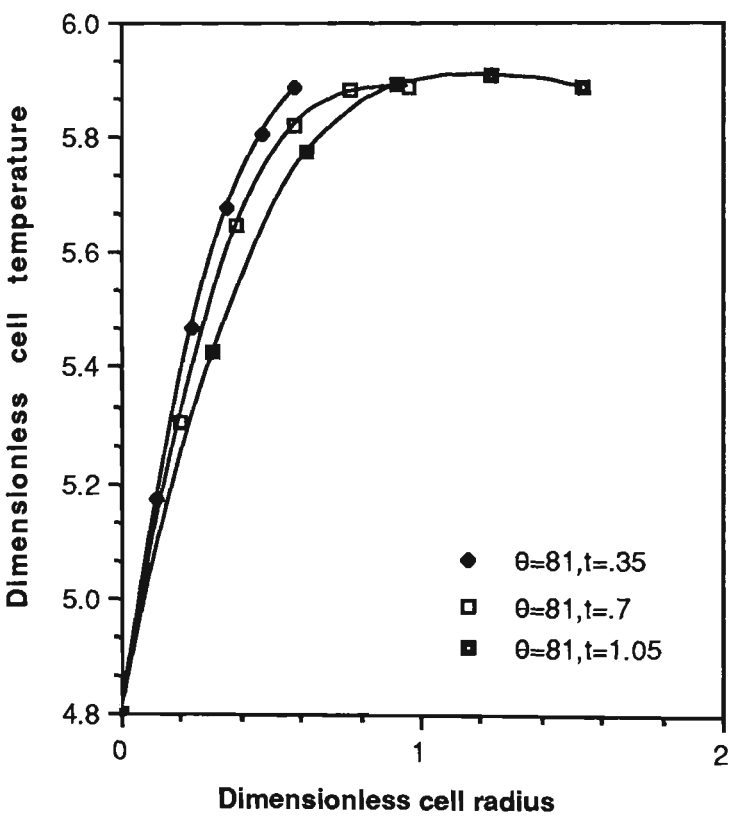

Fig. 5.16. Variation of cell temperature in r-direction.

radius of the pellet decreases and with it the Peclet number for heat transfer, which means less heat transfer occurred by bulk flow than by conduction. In this particular case the Peclet number varies from 37 to 25. For heat transfer, the Peclet number can be represented by the product of Reynolds number and Prandtl number. From Figures 5.13 and 5.14 it is evident that temperature the gradient near the front stagnation point of the pellet is largest and decreases with polar angle. Also it is clear from Figs. 5.13 and 5.14 that heat transfer increases at the rear of the pellet. This is due to fluid elements convected downstream forming a region of high temperature gradient. Furthermore, heat is transferred from the external stream to the rear of the pellet. Temperature in Fig. 5.14 is higher than in Fig. 5.13. This is because the temperature profiles in Fig. 5.14 are significantly closer to the external stream than the Fig. 5.13 profiles and thus heat transfer rate from the outer flow is much higher for Fig. 5.14 profiles.

Figures 5.15 to 5.17 show the temperature variation inside the cell in the radial direction at constant value of polar angle θ. As the radial distance increases, the temperature approaches the external stream temperature, which is obvious from these figures. Figure 5.17 looks slightly different but if one compares Figs. 5.13 and 5.14 with Fig. 5.17 then it is evident that this nature of the curve is due to the lowest temperature gradient at this angle (rear of the pellet) and its sudden increase due to heat transfer from the outer stream as explained earlier.

Figure 5.18 shows streamline contours calculated numerically at constant time i.e. steady flow. This steady flow past the pellet has

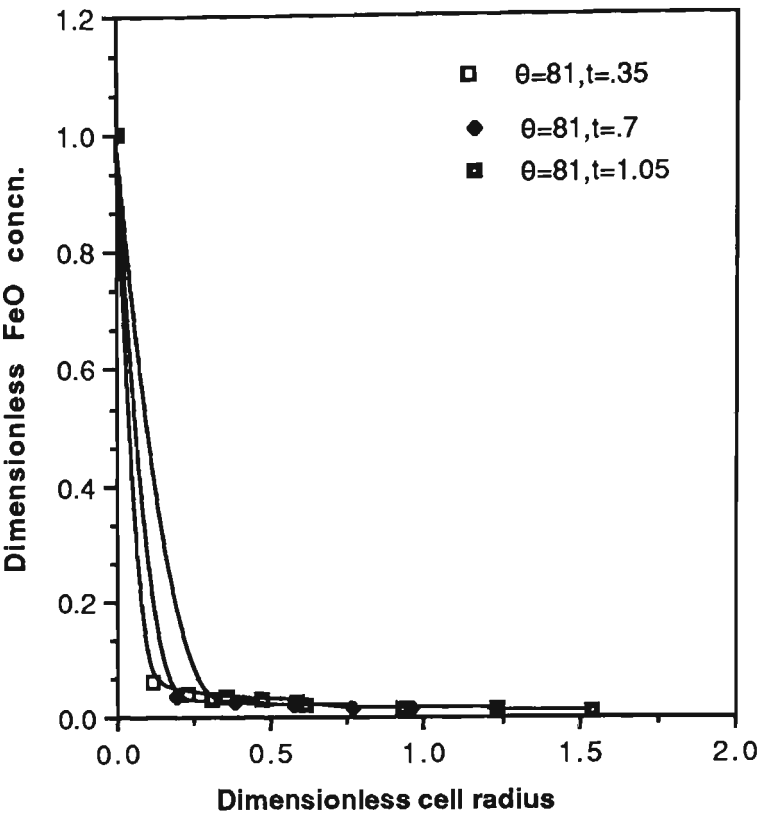

Fig. 5.22. Variation of FeO concentration in r-direction.

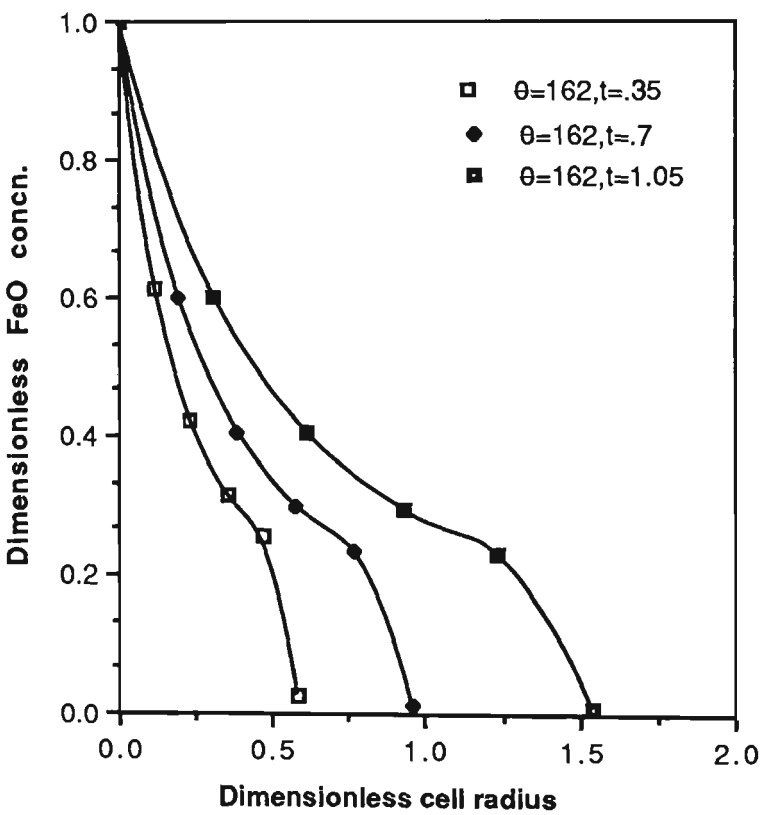

Fig. 5.23. Variation of FeO concentration in r-direction.

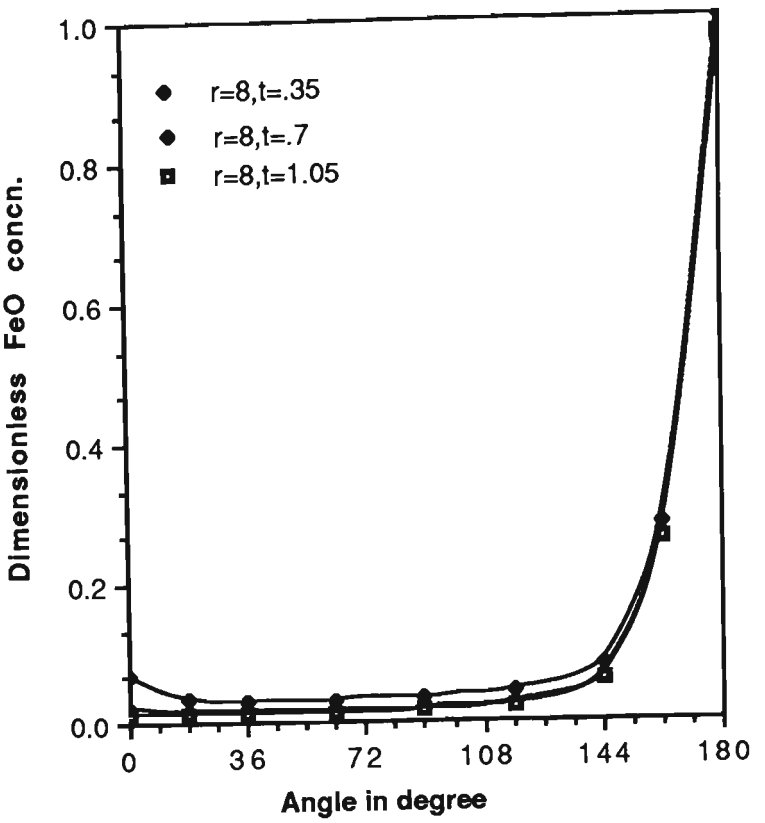

Fig. 5.20. Variation of FeO concentration within the cell in Θ-direction.

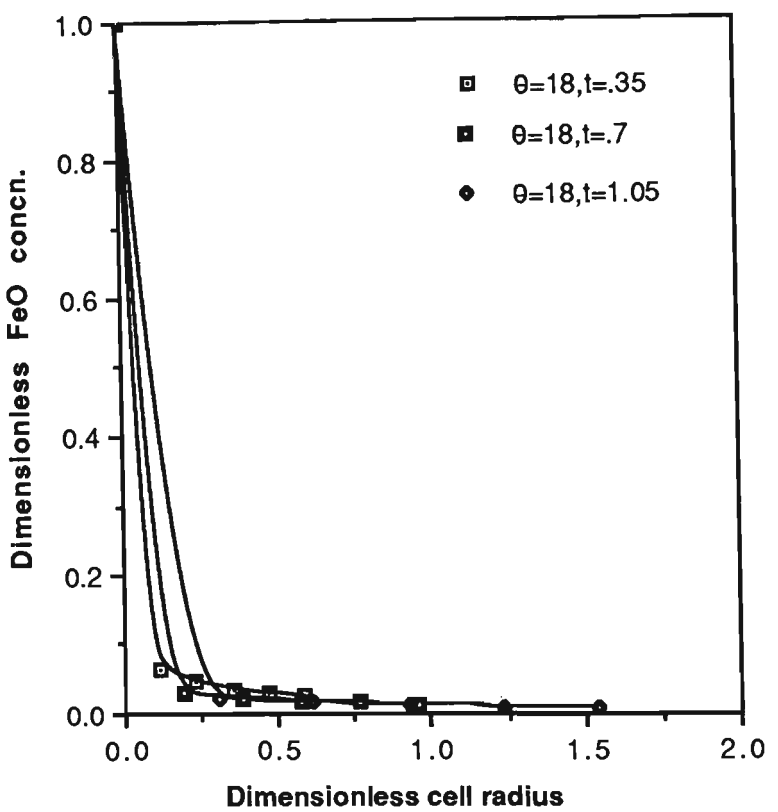

Fig. 5.21. Variation of FeO concentration in r-direction.

fore-and-aft symmetry for the Reynolds number 1.58 and it is unseparated flow. This finding is quite true at this Reynolds number[82]. Most of the Reynolds number values in this study fall into the creeping flow category and a few lie just above the creeping flow values i.e. in the intermediate Reynolds number range. In the present study, the Reynolds number belongs in the creeping flow region in which normally streamlines have fore-and-aft symmetry and show the same trend as shown in Fig. 5.18. Therefore, streamlines contours have not been shown here for other Reynolds numbers.

A typical set of FeO concentration profiles within the cell is given in Figs. 5.19 to 5.23. Since the dimensionless equation and boundary conditions, governing cell heat transfer and mass transfer are almost identical in nature, except for the source term and outer boundary conditions, the solutions to these equations in dimensionless form are expected to be same, which is evident from comparing concentrations figures with temperature figures. Concentration 1.0 shows the dimensionless FeO concentration at the pellet surface. The trend of these curves can be explained in the same way as it was done for the cell temperature.

From the curves it is clear that 3-4% FeO concentration is present in the outer stream of the flow. But Table VII shows the slag composition which contains approximately 7.5% FeO. This discrepancy in the computed and experiment results could be due to various factors like,

(i) In the rate equation for reaction (2B-13) the value of velocity constant has been taken constant (Kv= 0.41) which is not true as

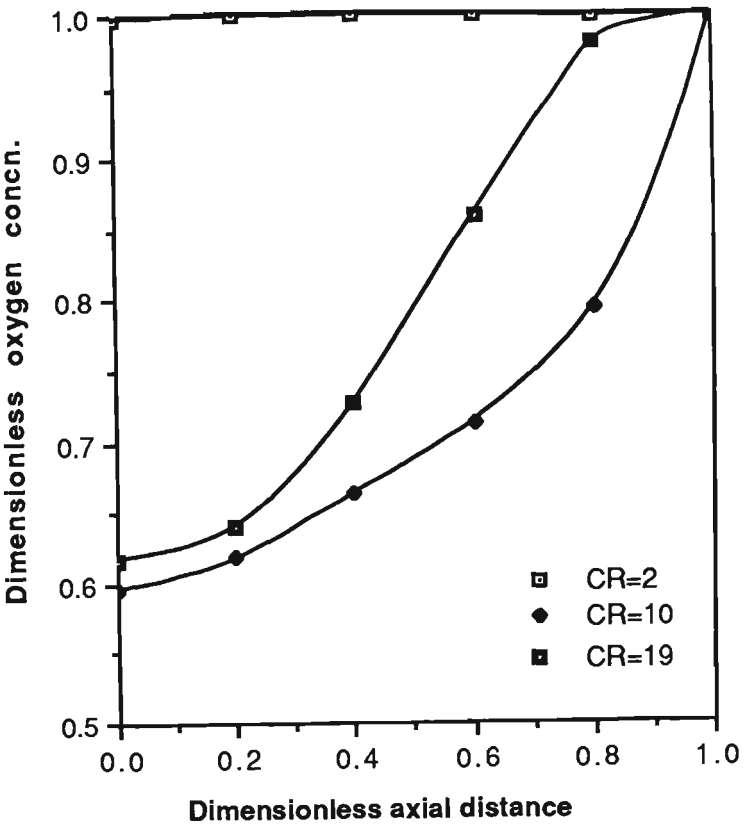

Fig. 5.26. Variation of oxygen concentration in z-direction.

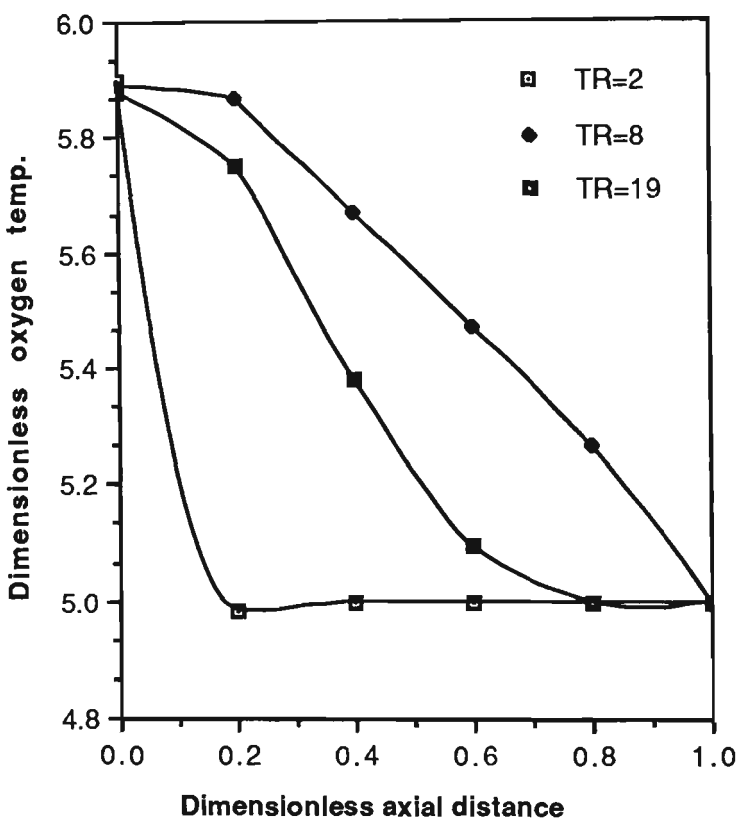

Fig. 5.27. Variation of oxygen temperature in z-direction.

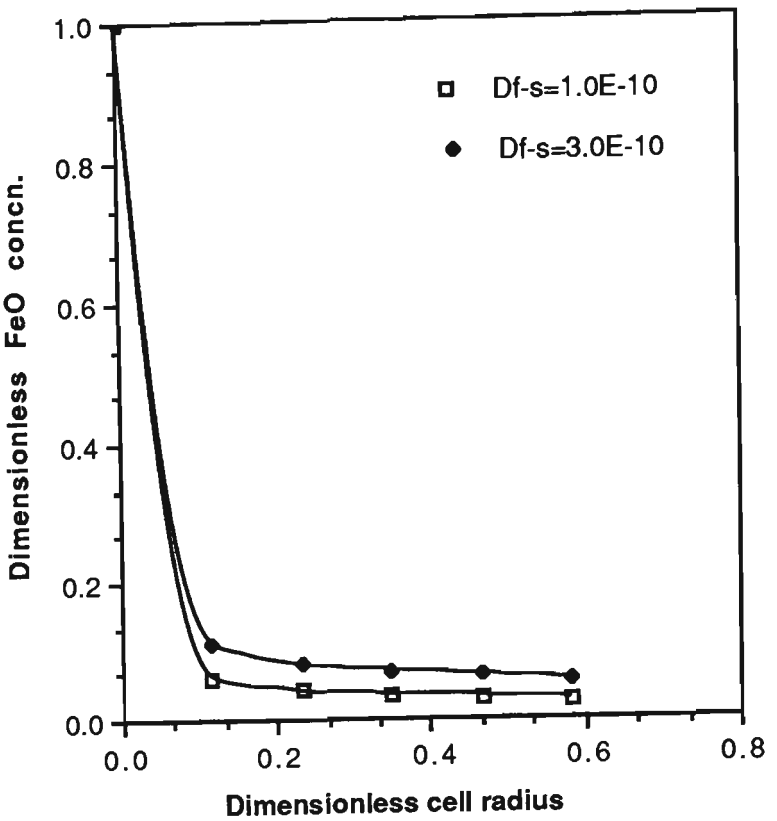

Fig. 5.24. Effect of diffusion coefficient on FeO concentration.

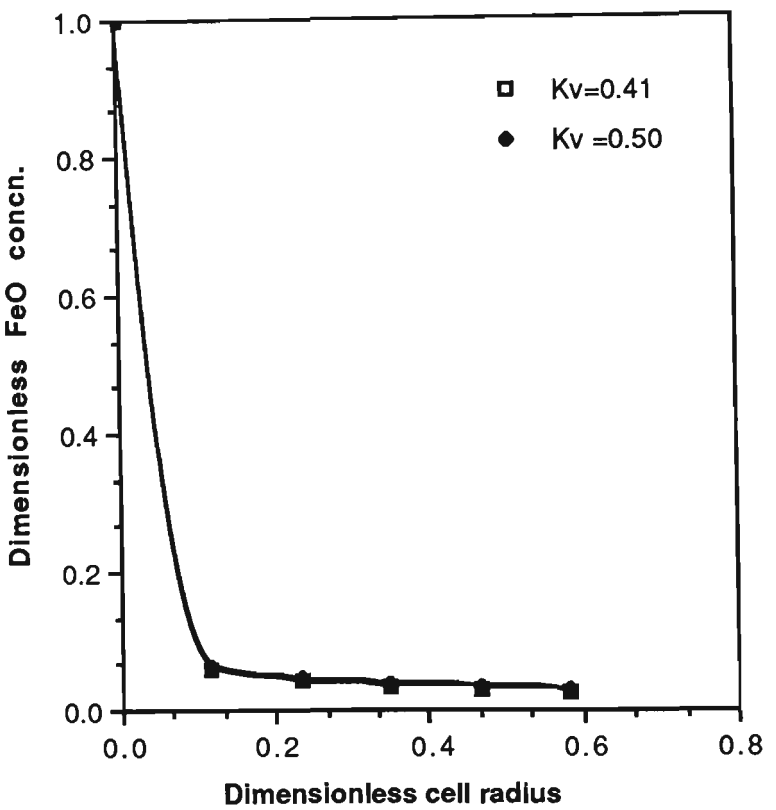

Fig. 5.25. Effect of velocity constant of the reaction on FeO concentration.

explained in Appendix B. The effect of the velocity constant is shown in Fig. 5.24, which shows that as the velocity constant increases slightly the FeO concentration also increases.

(ii) Kinetics of the reaction (2B-13) is itself very contradictory i.e. whether it is mass transfer controlled or chemically controlled. If it is chemically controlled then there is no need to solve the mass transfer equation for FeO and,

(iii) We have found great difficulty in ascertaining the data for the bed region especially for the diffusion coefficient for FeO-slag system. The effect of the diffusion coefficient on FeO concentration is shown in Fig. 5.25 which clearly shows the importance of this parameter. On a little increment in the diffusion coefficient, the FeO concentration in the outer stream almost doubles (6%).

Concentration and temperature profiles of the oxygen jet within the boundary layer are presented in Figs. 5.26 and 5.27 at constant values of radial distance. Results have been plotted at constant time in the z-direction. From Fig. 5.26 it is clear that at CR=2 the oxygen concentration is almost equal to the outerstream concentration which indicates that either the boundary layer has not developed properly or it is very-very thin which is true because the CR=2 point is next to the stagnation point. Therefore, the concentration values of oxygen will be the free stream concentration. Similar arguments apply for Fig. 5.27 to the case of the temperature profile, but here it seems a small thickness of the boundary layer has been developed.

Effect of Peclet numbers (for the liquid and bed regions) on the liquid and cell temperature are shown in Figs. 5.28 and 5.29 at

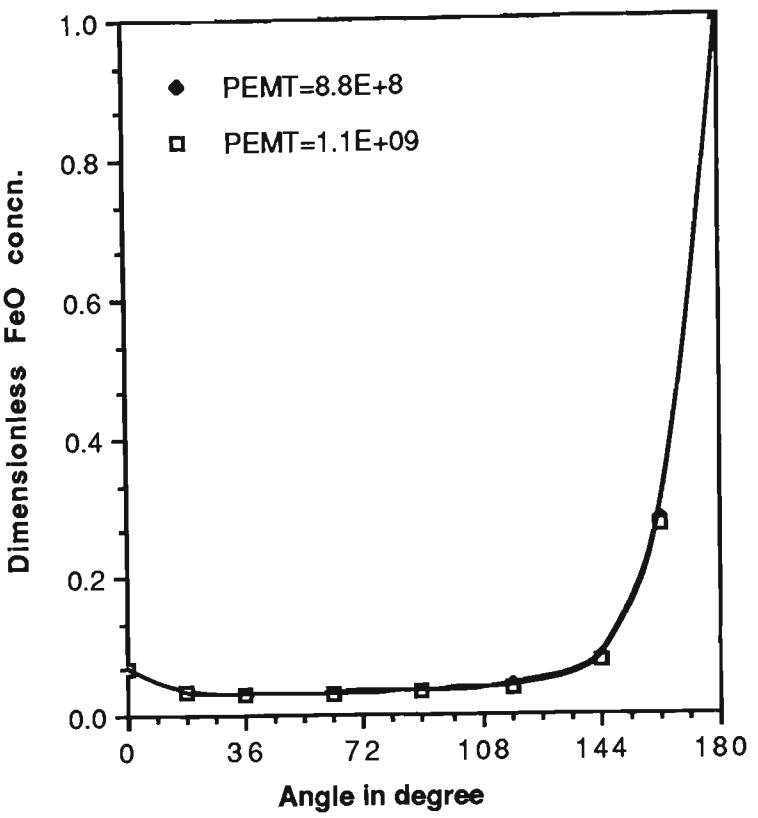

Fig. 5.30. Effect of Peclet number of mass transfer on FeO concentration.

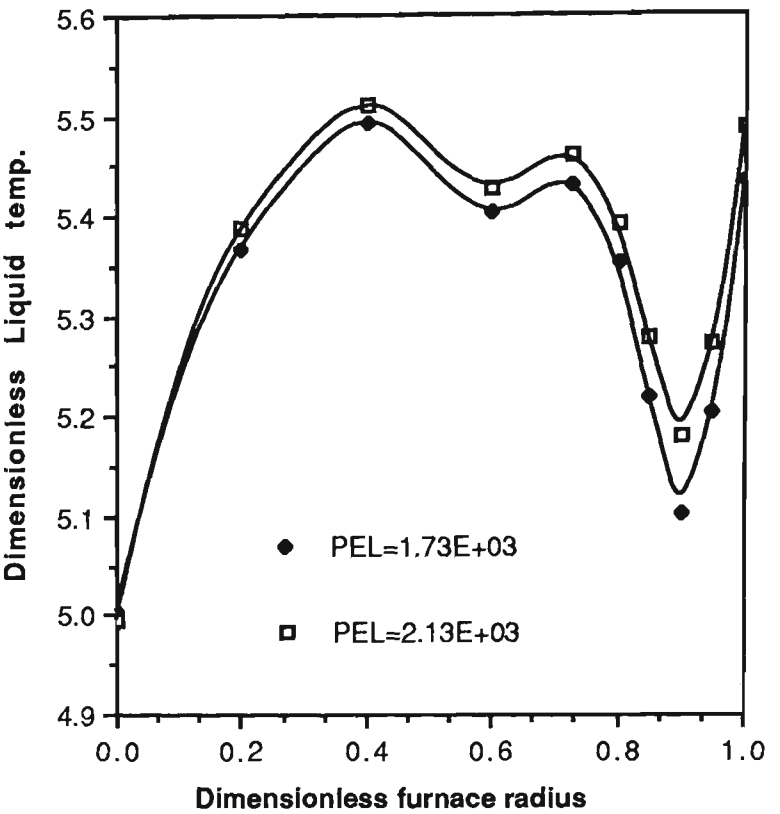

Fig. 5.28. Effect of liquid Peclet number on liquid temperature at const. time.

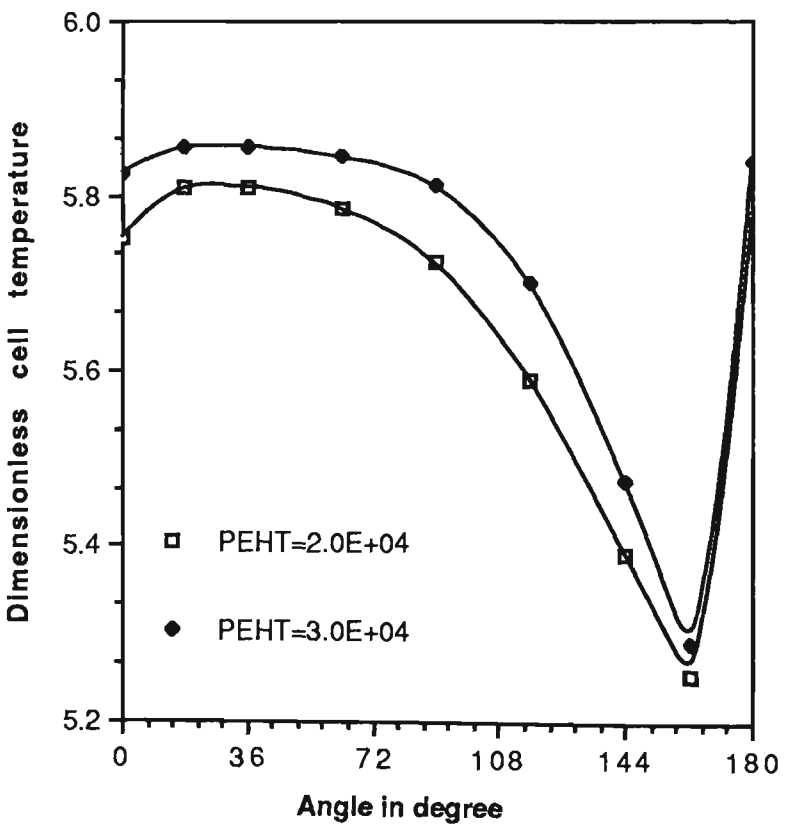

Fig. 5.29. Effect of Peclet number of heat transfer on cell temperature.

constant time. It is noticed that as the Peclet number increases or decreases, cell temperature also behaves in the same fashion. It is inferred from Fig. 5.29 that as the cell Peclet number increases, the temperature gradient at the front of the pellet also increases, as expected. In the liquid region, as the Peclet number increases the temperature also increases.

Figure 5.30 shows the effect of the Peclet number of mass transfer on FeO concentration. The actual data show that as the Peclet number increases the concentration decreases slightly, which is expected. The Peclet number of mass transfer plays the same role as it plays in heat transfer. Unfortunately, the effect of the Peclet number is not visible from Fig. 5.30 because the change in concentration is very low and is not possible to resolv on the scale which has been used in the figure. A figure drawn on amplified scale would show the difference.

The above results imply that the mathematical model is quite good in predicting the actual performance of the Induction Smelting Process which was the initial goal for developing this model. By including the variation in the liquid properties and further refinement to the temperature boundary conditions in the model it could be further improved. The other assumptions which have been made during the formulation seem quite reasonable. There are numerous variables in this process which are due to the highly complex nature of the problem. Most of these field variables are interdependent. Therefore, a careful analysis is required to select the proper parameters and to see their effect on the whole process in order to optimise the Smelting Process. From the model one can

see the effect of various parameters on the process performance like, bed and pellet void fractions, pellet size, gas jet velocity, induction heating i.e. energy consumption, FeO concentration present in the slag, design of the furnace etc.

5.1) POSSIBLE APPLICATION OF THE MODEL:

Although the computer code has been developed for the ISP it can nevertheless be used in parts to solve various other metallurgical operations. A few examples are given below.

The liquid region part can be used to predict flow behaviour and heat transfer in induction scrap melting and induction refining units. By employing this model one can discover the proper controlling parameters for the above mentioned applications and can optimise the process. These processes, especially refining of steel, producing high grade steel, making alloy steel etc are very sophisticated and can be controlled using the liquid region computer code. About the segregation and inclusion entrapment one wants to know the exact nature of the fluid velocities in order to control and reduce them to obtain high quality steel. For this purpose, a turbulent model should be used in conjunction with the present code. People have already started using mathematical modelling for induction stirring in continuous casting to produce high quality castings, which is a very promising field to which this model may be applied. One can also use this model for electromagnetic stirring in ladle metallurgy operations.

The bed region mathematical model can be successfully applied to many industrial processes like packed bed, fluidized bed, liquid - liquid extraction, solid leaching, floatation, fermentation etc. Minor modifications will be required to apply the model for these processes, depending upon the details of the process. The model can give an insight into flow, heat and mass behaviour for these processes. Models based on the cell approach are very good to understand the fluidized and packed bed behaviour. With the help of this model one can also make many fundamental studies in metallurgy, usually at high temperature which are very difficult to access by experiment, viz mechanism of heat and mass transfer through gas bubbles in slag - gas, gas - metal or gas - slag - metal systems. When applying this model for bubbles some major modifications may be required in the governing equations.

The jet region can be used as a whole for many other engineering applications, viz annealing of metal and plastic sheets, drying of textiles, papers, films etc, tempering of glass, cooling of microelectronics equipments etc. In these processes heat transfer, fluid velocity and mass transfer are quite important and one can use the present model in order to understand these processes and possibly improve the process after analysing the results and controlling the proper parameters.

The liquid region model in conjunction with the jet region model can be used to explore the kinetics of various gas liquid iron reactions such as the decarburization of liquid iron by oxidizing gas. Experimentally, researchers[140-142] have tried to measure the rate of reaction of gas - liquid iron in these conditions. In fact, A. K.

Kuchi et al.[143] have developed a mathematical model for this process in order to ascertain the kinetics of reaction and they found a good agreement between predicted and experimental results and predicted rate kinetics for few more gas - liquid reactions.

In summary, there are many possible application of parts of the present model, which can be used with some minor modifications depending upon the process. Other applications of the model will, no doubt, emerge in future.

CHAPTER 6

CONCLUSIONS AND SUGGESTIONS FOR FUTURE WORK

1) The proposed mathematical model appears to be predicting physically realistic profiles of liquid velocity, temperature, mixture velocity, temperature, concentration and oxygen temperature ,velocity and concentration in the Induction Smelting Process.

2) The analysis shows that results are sensitive to various parameters such as the diffusion coefficient, reaction velocity constant, Peclet numbers for heat and mass transfer, Reynolds number in various regions etc., and a proper prediction of the performance of Induction Smelting Process would require a careful consideration of these parameters.

3) The successful use of the cell model approach shows the possible use of this approach in materials processing operations.

4) The computer code has been developed for the ISP problem. However it can be used in part to simulate various other industrial problem. For example the liquid region model can be used for the induction melting and refining units in industries etc.

5) A mathematical model for prediction of composition of the melt (P, Si, S, Mn etc.) has also been developed in the present study, which may be incorporated in the model at a later stage.

6) A model with computer code has also been developed to predict the temperature profile inside the microwave heated composite pellets, which may be used with current computer code in order to see the effect of microwave treated pellets on the smelting process.

7) The velocity measurement device developed in the present study may be used successfully to measure the velocity of any fluid at high temperature taking the precautions against the possibility of the carbon rod reaction.

8) Proposed 2-dimensional model can be easily extended to 3-dimensional if required.

APPENDIX A

DERIVATION OF EQUATION OF MOTION FOR LIQUID REGION

From the equation (2A-1) we have:

$$\rho_L \frac{D\underline{u}}{Dt} = \nabla \underline{\tau} - \underline{\nabla} p + \rho_L \underline{F_b} \qquad (2A\text{-}1)$$

where D/Dt is known as the substantial derivative operator which can be expressed, by assuming the fluid density as a constant:

$$\frac{D\underline{u}}{Dt} = \frac{\partial}{\partial t} + \underline{u} \cdot \nabla \qquad (A\text{-}1)$$

where the first term, called the local derivative, represents changes at a fixed point in the fluid and the second term, the convective term, accounts for changes following the motion of the fluid.

$\underline{F_b}$ is the body force per unit volume. In the present case the body force may contain the Lorentz force and gravitational force.

$$\rho_L \underline{F_b} = \rho_g + \underline{J} \times \underline{B} \qquad (A\text{-}2a)$$

Here, we are neglecting the buoyancy forces.

After combining equation (2A-1) with the equation (A-2) and substituting the relationship of stress tensors into the equation of motion, assuming constant fluid viscosity, we obtain:

$$\rho_L \frac{D\underline{u}}{Dt} = \mu \nabla^2 \underline{u} + \rho \underline{g} + \underline{J} \times \underline{B} - \nabla p \qquad \text{(A-2)}$$

where

$\nabla^2 = \frac{\partial^2}{\partial x^2}( ) + \frac{\partial^2}{\partial y^2}( ) + \frac{\partial^2}{\partial z^2}( )$ is the Laplacean operator in cartesian co-ordinates.

Taking the curl of equation (A-2) and considering the steady state, and the gravitational field exerted only in the z-direction in cylindrical co-ordinate, yields:

$$\rho_L \nabla \times (\underline{u}. \nabla \underline{u}) = \mu \nabla \times (\nabla^2 \underline{u}) + \nabla \times (\underline{J} \times \underline{B}) - \nabla \times \{\nabla (p + \rho g z)\} \qquad \text{(A-3)}$$

After some manipulation it can be shown from the vector algebra (some important vector identities have been given in Appendix E)

$$\nabla \times (\underline{u}. \nabla \underline{u}) = - \nabla \times (\underline{u} \times \underline{\xi}) \qquad \text{(A-4)}$$

where

$$\nabla \times \underline{u} = \underline{\xi} \qquad \text{(A-5)}$$

On further simplification of the equation (A-4) we obtain:

$$\left\{ \frac{\partial}{\partial r} (u_r \xi) + \frac{\partial}{\partial z} (u_z \xi) \right\} \hat{e}_\theta = \nabla \times (\underline{u}. \nabla \underline{u}) \qquad \text{(A-6)}$$

The first term on the right side of the equation (A-3) can be manipulated from the vector algebra:

$$\nabla \times \nabla^2 \underline{u} = \nabla \times (- \nabla \times \xi) = \nabla^2 \xi \quad ; \text{because} \quad \nabla (\nabla . \xi) = 0 \qquad \text{(A-7)}$$

The velocity vector $\underline{u}$ in terms of the stream function, for axi-symmetric problem can be written:

$$\underline{u} = \underline{\nabla} \times \left(- \frac{\psi}{\partial} \hat{e}_\theta \right) \qquad \text{(A-8)}$$

which further gives:

$$u_r = \frac{1}{r} \frac{\partial \psi}{\partial z} \qquad \text{(A-9)}$$

$$u_z = - \frac{1}{r} \frac{\partial \psi}{\partial r} \qquad \text{(A-10)}$$

From the equations (A-5 & 8) it can be readily shown:

$$r \xi = \nabla^2 \psi \qquad \text{(A-11)}$$

where $\underline{\xi} = \xi \hat{e}_\theta$ i.e. the vorticity exists only in the θ-direction. Equation (A-7) in axi-symmetry form will result:

$$\nabla^2 \xi \hat{e}_\theta = \left\{ \frac{\partial}{\partial r} \left[\frac{1}{r} \frac{\partial}{\partial r} (r\xi) \right] + \frac{\partial}{\partial z} \left[\frac{1}{r} \frac{\partial}{\partial z} (r\xi) \right] \right\} \hat{e}_\theta \qquad \text{(A-12)}$$

After substituting equations (A-12), (A-9), (A-10) and (A-6), the equation (A-3) in terms of the vorticity and stream function becomes:

$$\left[\frac{\partial}{\partial z} \left\{ \frac{\xi}{r} \left(\frac{\partial \psi}{\partial r} \right) \right\} - \frac{\partial}{\partial r} \left\{ \frac{\xi}{r} \left(\frac{\partial \psi}{\partial z} \right) \right\} \right] \hat{e}_\theta +$$

$$\frac{\mu}{\rho_L} \left[\frac{\partial}{\partial r} \left\{ \frac{1}{r} \frac{\partial}{\partial r} (r\xi) \right\} + \frac{\partial}{\partial z} \left\{ \frac{1}{r} \frac{\partial}{\partial z} (r\xi) \right\} \right] \hat{e}_\theta +$$

$$\frac{1}{\rho_L} \left\{ \nabla \times (\underline{J} \times \underline{B}) \right\} = 0 \qquad \text{(A-13)}$$

where $\nabla \times \{ \nabla (p + \rho_L g z)\} = 0$ from the vector identity.

Equation (A-11) shows the relationship between the vorticity and stream function. After some manipulation it can be shown that:

$$\xi = \frac{\partial}{\partial z}\left(\frac{1}{r}\frac{\partial \psi}{\partial z}\right) + \frac{\partial}{\partial r}\left(\frac{1}{r}\frac{\partial \psi}{\partial r}\right) \qquad \text{(A-14)}$$

APPENDIX B

DERIVATION OF REACTION RATE EQUATION

1.) RATE EQUATION FOR FeO + C REACTION:

Countless research papers have been published on the reduction kinetics of the iron oxide and carbon in various conditions. No paper has yet appeared which gives a clear idea on the reduction kinetics of Fe_2O_3 and carbon in the iron-carbon melts, which is required in the present study. From the literature survey[22,23,144-158] no clear reduction kinetics is available for the Fe_2O_3 and carbon in the iron-carbon melts. But the literature reveals that usually Fe_2O_3 reduction occurs in the three steps (i) the reduction of hematite to magnetite,(ii) magnetite to wustite and,(iii) wustite to iron. It is very difficult to study the reduction kinetics of the first two steps, both very fast processes. Therefore, the major reaction has been considered between the wustite and carbon. Under these circumstances we are compelled to adopt step (iii) as a major reaction in the Induction Smelting Process. This is reasonable in the present study due to the very high operating temperature (1400 - 1600°C).

Several authors[144-146,22-23,155-156,158] have studied the reduction kinetics of FeO and C reaction in the liquid melts of various compositions. Results obtained by these authors are very contradictory. Many authors believe the reduction kinetics of FeO with C in the liquid melts is diffusion controlled, while some believe it is chemically controlled. After careful scrutiny of the

available papers on the reduction kinetics of FeO and C in the carbon saturated iron melts, the conclusion reached was that the FeO and C reaction is mass transfer controlled. Derivation of the rate equation for this reaction is based on the Dancy classical paper[144]. Dancy studied the reaction kinetics for the FeO reaction, which is

$$FeO + \underline{C} = Fe + CO \qquad (2B\text{-}13)$$

This reaction has been found to be of the first order for which the rate of reaction is given as

$$k_\upsilon = \frac{1}{t} \log_e \left(\frac{a}{a-x} \right) \qquad (B\text{–}1)$$

where k_υ is the velocity constant, a is the initial concentration of the reactant (FeO) and x is the amount of the reactant decomposed after time t. From equation (B-1),

$$k_\upsilon t = \log_e \left(\frac{a}{a-x} \right) \qquad (B\text{-}2)$$

or,

$$1 - f = e^{-k_\upsilon t} \qquad (B\text{-}3)$$

where f is the fraction of FeO reacted, which is

$$f = x/a \qquad (B\text{-}4)$$

On differentiating eqn. B-4, one has

$$\frac{df}{dt} = k_\upsilon \, e^{-k_\upsilon t} \qquad (B\text{-}5)$$

which is the desired rate equation for the FeO and C reaction. Here,

$$k_{\upsilon} = f(T)$$

which means the velocity constant depends on the temperature. The value of k_{υ} varies from 0.41 to 1.72 unevenly in the temperature range 1427 to 1577°C. From the available data it is difficult to establish a proper relationship between the velocity constant and temperature. In the present case, 0.41 has been taken as the constant value for k_{υ} .

2.) RATE EQUATION FOR C + O_2 REACTION:

In the smelting process, the oxygen jet is impinging on the surface of the pellets which contain carbon as a major constituent. Because the operating temperature is very high the only possible reaction between the carbon and oxygen which need be considered is

$$2\,C + O_2 = 2\,CO \qquad \text{(B-6)}$$

which indicates there is no CO_2 formation at this temperature. Moreover, it is an exothermic reaction; therefore, at the reacting surface the temperature is quite high which rules out any possibility of the forming of CO_2.

Now, the rate equation for the reaction B-6 can be written. The rate equation for this reaction has been taken from the ref. 159. For the brown coal char it is

$$r = A\,T^{N} \exp(-E/RT)\,P_{O2} \qquad \text{(B-7)}$$

where, for the brown coal char reaction,

$A = 0.132$ kg m^{-2} s^{-1}

$E/R = 16{,}400$ ^{o}K

and $N = 0$

Therefore, the desired rate equation for the reaction B-6 becomes

$$r = 0.132 \exp (-16{,}400/T) P_{O2} \qquad \text{(B-8)}$$

APPENDIX C

FINITE DIFFERENCE REPRESENTATION OF MODEL EQUATIONS.

In this appendix the discretized form of the equations (2E-50) and (2E-80) with their boundary conditions will be presented and the same procedure can be followed to discretize the rest of the equations with their boundary conditions, as given in Section 2E in their dimensionless form.

The governing differential equation of motion (2E-50) can be represented in its discretized form by using the finite difference and upwind scheme, as described in Chapter 3.

$$\frac{1}{R^*_i}\,\frac{\xi^*_{ij}-\xi_{ij\pm1}}{\Delta z^*}\,\frac{|\Delta\psi_i|}{2\Delta R^*}+\frac{1}{R^*_i}\,\frac{\xi^*_{i.j}-\xi_{i\pm1.j}}{\Delta R^*}\,\frac{|\Delta\psi_j|}{2\Delta z^*}+\frac{\xi^*_{i.j}}{R^{*2}_i}\,\frac{|\Delta\psi_j|}{2\Delta z^*}+\frac{1}{\eta}$$

$$\left[\frac{\xi^*_{i+1.j}-2\xi^*_{i.j}+\xi^*_{i-1.j}}{\Delta R^{*2}}+\frac{1}{R^*_i}\,\frac{\xi^*_{i+1.j}-\xi_{i-j}}{2\Delta R^*}-\frac{\xi^*_{i.j}}{R^{*2}_i}+\right.$$

$$\left.\frac{\xi^*_{i.j+1}-2\,\xi^*_{i.j}+\xi^*_{i.j-1}}{\Delta z^{*2}}\right]+\sin 2\kappa z^*_j \qquad DVAL = 0 \qquad \text{(C-1)}$$

where, $\Delta\psi_i = \psi^*_{i+1,j} - \psi^*_{i-1,j}$ (C-2)

and $\Delta\psi_j = \psi^*_{i,j+1} - \psi^*_{i,j-1}$ (C-3)

$$DVAL = \omega\kappa\mu_o\sigma R^2\,\frac{V_1aX_o-V_1bY_o-U_1bX_o-U_1aY_o}{2(a^2+b^2)(U_o^2+V_o^2)} \qquad \text{(C-3a)}$$

The upwind scheme has been used in the first two terms of the equation (C-1). Therefore, in order to get a numerically stable solution this equation must satisfy the following conditions.

In the first term of the equation (C-1) one should choose either the +ve sign or -ve sign, in $j\pm1$ term, depending upon the sign of $\Delta\psi_i$ in order to get stable solutions, therefore:

$$j-1 \quad \text{for} \quad \Delta\psi_i > 0 \tag{C-4}$$

and

$$j+1 \quad \text{for} \quad \Delta\psi_i < 0 \tag{C-5}$$

Similarly, the conditions for the second term of the equation (C-1) will be

$$i+1 \quad \text{for} \quad \Delta\psi_j > 0 \tag{C-6}$$

and

$$i-1 \quad \text{for} \quad \Delta\psi_j < 0 \tag{C-7}$$

Equation (C-1), for the condition, if $\Delta\psi_i > 0$ and $\Delta\psi_j > 0$, can be expressed, after some manipulation

$$\xi^*_{i,j}\left[|\Delta\psi_i|/2.\,R^*_i + |\Delta\psi_j|/2.\,R^*_i + |\Delta\psi_j|\Delta R^*/2.R_i^{*2} - 2.\Delta Z^*/\eta.\Delta R^* + \Delta R^*\,\Delta Z^*/R^*_i{}^2\eta - 2.\,\Delta R^*/\eta.\Delta Z^*\right] + \xi^*_{i+1,j}\left[-|\Delta\psi_j|/2.\,R^*_i + \Delta Z^*/\eta.\Delta R^* + \Delta Z^*/\eta.2.\,R_i^*\right] + \xi^*_{i-1,j}\left[\Delta Z^*/\eta.\Delta R^* - \Delta Z^*/2.R^*_i\,\eta\right] + \xi^*_{i,j+1}\left[\Delta R^*/\Delta Z^*\eta\right] + \xi^*_{i,j-1}\left[-|\Delta\psi_i|/2.R^*_i + \Delta R^*/\Delta Z^*.\eta\right] + \Delta R^*\,\Delta Z^*\sin 2\kappa z^*_j.\,DVAL = 0 \tag{C-8}$$

Similarly, the equation (C-1) can be expressed for the other three conditions.

The above mentioned equations are applicable for the grid points 1 to 7 in the R-direction, (Fig.17), with the grid spacing ΔR and for points 9 to 20 with the grid spacing ΔR_1. For point 8, one should use equations (3-16) and (3-17), as described in Section 3.2, to discretize the vorticity equation (2E-50), therefore,

$$\frac{1}{R_i^*}\,\frac{\xi^*_{i.j}-\xi^*_{i.j\pm1}}{\Delta Z^*}\,\frac{|\Delta\psi_i|_1}{\Delta R+\Delta R_1}+\frac{1}{R^*_i}\,\frac{\xi^*_{i.j}-\xi^*_{i\pm1.j}}{\Delta R^*}\,\frac{|\Delta\psi_j|}{2\Delta Z^*}+\frac{\xi^*_{i.j}}{R_i^{*2}}$$

$$\frac{|\Delta\psi_j|}{2\Delta Z^*}+\frac{1}{\eta}\left[\frac{2}{\Delta R^*+\Delta R^*_1}\left\{\frac{\xi^*_{i-1.j}-\xi^*_{i.j}}{\Delta R}+\frac{\xi^*_{i+1.j}-\xi^*_{i.j}}{\Delta R_1}\right\}+\frac{1}{R_i^*}\right.$$

$$\frac{1}{\Delta R^*+\Delta R_1^*}\left\{(\xi^*_{i+1.j}-\xi^*_{i.j})\,\frac{\Delta R^*}{\Delta R_1^*}-(\xi^*_{i-1.j}-\xi^*_{i.j})\,\frac{\Delta R^*_1}{\Delta R^*}\right\}-$$

$$\left.\frac{\xi^*_{i.j}}{Ri^{*2}}+\frac{\xi^*_{i.j+1}-2\xi^*_{i.j}+\xi^*_{i.j-1}}{\Delta Z^{*2}}\right]+\sin 2\kappa z^*_j\;.\;DVAL=0$$

(C-9)

where $$|\Delta\psi_i|_1=\left|(\psi^*_{i+1.j}-\psi^*_{i.j})\,\frac{\Delta R^*}{\Delta R^*_1}-(\psi^*_{i-1.j}-\psi^*_{i.j})\,\frac{\Delta R^*_1}{\Delta R^*}\right| \quad \text{(C-10)}$$

The conditions for the equation (C-10) are same as for the equation (C-1). Value of ΔR^* in the second term of the equation (C-10) depends upon the value of $\Delta\psi_j$ i.e.

$$\text{if } \Delta\psi_j > 0 \qquad \Delta R^* = \Delta R^*_1 \tag{C-11}$$

$$\text{if } \Delta\psi_j > 0 \qquad \Delta R^* = \Delta R^* \tag{C-12}$$

BOUNDARY CONDITIONS:

The boundary conditions for the equation (2E-50) can be expressed in the discretized form as follows:

$$\text{At} \quad R^* = 0 \quad \text{or} \quad i = 1 \qquad \xi^*_{i,j} = 0 \tag{C-13}$$

$$z^* = z^*_1 \quad \text{or} \quad j=M \qquad \xi^*_{i,M} = 0 \tag{C-16}$$

$$R^* = 1 \quad \text{or} \quad i=N \qquad \frac{2.\psi^*_{N-1,j}}{R^*_i \, \Delta R^{*2}_1} = \xi^*_{N,j} \tag{C-14}$$

$$\text{and} \quad z^* = 0 \quad \text{or} \quad j = 1 \qquad \frac{2.\psi^*_{i,2}}{R^*_i \, \Delta z^*} = \xi^*_{i,1} \tag{C-15}$$

The discretized form of all governing equations (2E-51,76,77,78 ect.) with their boundary conditions can be expressed in the same way as for the equation (C-1), for the point 8 and other points. The care of transient term can be taken by employing fully implicit method, described in Section 3.1.4, and shown below for the equation (2E-80).

Equation (2E-80) is a transient heat balance equation for the bed region in spherical co-ordinates, which can be discretized by adopting finite difference method, fully implicit method and upwind scheme. Therefore, equation (2E-80) written as

$$\frac{T^{*n+1}_{m\cdot i\cdot j} - T^{*n}_{m\cdot i\cdot j}}{\Delta t^{*}_{mHT}} + \frac{P_{eHT}}{R^{*2}_{m\cdot i}\sin\theta}\,\frac{|\Delta\psi_{B\cdot j}|}{2\Delta\theta}\,\frac{T^{*n+1}_{m\cdot i\cdot j} - T^{*n+1}_{m\cdot i+1\cdot j}}{\Delta R^{*}_{m}} +$$

$$\frac{P_{eHT}}{R^{*2}_{m\cdot i}\sin\theta}\,\frac{|\Delta\psi_{Bi}|}{2\Delta R^{*}_{m}}\,\frac{T^{*n+1}_{m\cdot i\cdot j} - T^{*n+1}_{m\cdot i\cdot j+1}}{\Delta\theta} = \frac{\alpha_{m\cdot i\cdot j}}{R^{*2}_{m\cdot i}}$$

$$\left[R^{*2}_{m\cdot i}\,\frac{T^{*n+1}_{m\cdot i+1\cdot j} - 2T^{*n+1}_{m\cdot i\cdot j} + T^{*n+1}_{m\cdot i-1\cdot j}}{\Delta R^{*2}_{m}} + R^{*}_{m\cdot i}\,\frac{T^{*n+1}_{m\cdot i+1\cdot j} - T^{*n+1}_{m\cdot i-1\cdot j}}{\Delta R^{*}_{m}} + \right.$$

$$\left. \frac{T^{*n+1}_{m\cdot i\cdot j+1} - 2T^{*n+1}_{m\cdot i\cdot j} + T^{*n+1}_{m\cdot i\cdot j-1}}{\Delta\theta^{2}} + \cot\theta\,\frac{T^{*n+1}_{m\cdot i\cdot j+1} - T^{*n+1}_{m\cdot i\cdot j-1}}{2\Delta\theta} \right] =$$

$$\Delta H^{*}/\rho^{*}_{m\cdot i\cdot j}\cdot C^{*}_{p\cdot m\cdot i\cdot j} \qquad \text{(C-17)}$$

where, $\Delta\psi_{Bi} = \psi B^{*}_{i+1.j} - \psi^{*}B_{\,i-1.j}$ (C-18)

and $\Delta\psi_{Bj} = \psi^{*}B_{i.j+1} - \psi B^{*}_{\,i.j-1}$ (C-19)

and the conditions for the equation (C-17) can be given by

$i-1$ for $\Delta\psi_{Bj} < 0$ (C-20)

$i+1$ for $\Delta\psi_{Bj} > 0$ (C-21)

$j+1$ for $\Delta\psi_{Bi} < 0$ (C-22)

$j-1$ for $\Delta\psi_{Bi} < 0$ (C-23)

These conditions (C-20) to (C-23) have been derived in the same way as they were derived for the equation (C-1). Here, the superscripts n and n+1 show the value of the variables at the current time step t_n and one time step advanced t_{n+1} respectively.

Equation (C-17), for the condition if $\Delta\psi_{Bi} < 0$ and $\Delta\psi_{Bj} < 0$ can be written as:

$$
{}^{n+1}T_{mi.j}\left[\frac{\Delta R^{*}_{m}\,\Delta\theta}{\Delta t^{*}_{mHT}}\;\frac{P_{eHT}}{R^{*2}_{m.i}\sin\theta_j}\;\frac{|\Delta\psi_{Bj}|}{2.}+\frac{P_{eHT}}{R^{*2}_{m.i}\sin\theta_j}\;\frac{|\Delta\psi_{Bi}|}{2}+\right.
$$

$$
\left.\frac{2.\,\alpha_{m.i.j}\Delta\theta}{\Delta R^{*}_{m}}+\frac{2.\alpha_{m.i.j}\,\Delta R^{*}_{m}}{R^{*2}_{m.i}\,\Delta\theta}\right]-{}^{n+1}T^{*}_{m\,i+1}\left[\frac{\alpha_{mi.j}\,\Delta\theta}{\Delta R^{*}_{m}}+\frac{\alpha_{m.i.j}\,\Delta\theta}{R^{*}_{m.i}}\right]-
$$

$$
{}^{n+1}T^{*}_{m\,i-1.j}\left[\frac{P_{eHT}}{R^{*2}_{m.i}\sin\theta_j}\;\frac{|\Delta\psi_{Bj}|}{2}+\alpha_{m.i.j}\,\Delta\theta\,\frac{\alpha_{m.i.j}\,\Delta\theta}{\Delta R^{*}_{m}}-\frac{\alpha_{m.i.j}\,\Delta\theta}{R^{*}_{m.i}}\right]-
$$

$$
{}^{n+1}T^{*}_{m.i.j+1}
$$

$$
\left[\frac{P_{eHT}}{R^{*2}_{m.i}\sin\theta_j}\;\frac{|\Delta\psi_{B.i}|}{2}+\frac{\alpha_{m.i.j}\,\Delta R^{*}_{m}}{R^{*2}_{m.i}\,\Delta\theta}+\frac{\alpha_{m.i.j}\,\Delta R^{*}_{m}}{2.\,R^{*2}_{m.i}}\cot\theta_j\right]-
$$

$$
{}^{n+1}T^{*}_{mi.j-1}\left[\frac{\alpha_{m.i.j}\,\Delta R^{*}_{m}}{R^{*2}_{m.i}\,\Delta\theta}-\frac{\alpha_{m.i.j}\,\Delta R^{*}_{m}}{2.R^{*2}_{m.i}}\cot\theta_j\right]=\;{}^{n}T^{*}_{mi.j}
$$

$$
\left[\frac{\Delta R^{*}_{m}\,\Delta\theta}{\Delta t^{*}_{MHT}}\right]+\frac{\Delta H^{*}\,\Delta R^{*}_{m}\,\Delta\theta}{\rho^{*}_{mi.j}\,C^{*}_{p.m.i.j}} \qquad \text{(C-24)}
$$

where i varies 2 to LNK1(10) and j varies 2 to LL1 (20).

In the same way equation (C-17) can be expressed for the other conditions.

BOUNDARY CONDITIONS:

The boundary conditions (2E-103,104,107 & 108), in the discretized form, for the equation (C-17), will be

At $i = 1$ or $R_m^* = 0$ $\quad T_m^*{}_{1,j} = T_m^*{}_{m.p.\ of\ pellet}$ (C-25)

$i = LNK$ or $R_m^* = 1$ $\quad T_m^*{}_{LNK\ j} = T_\infty^*$ (C-26)

For $\theta = 0$ or $j = 1$

$$\frac{T_{m+1}^{*\,n+1} - T_{m+1}^{*\,n+1}}{\Delta t_{mHT}} + \frac{P_{eHT}}{R_{m\cdot i}^{*2}\cos\theta}\,\frac{2|\Delta\psi_{B\cdot j}|}{\Delta\theta^2}\,\frac{T_{m+1}^{*\,n+1} - T_{m\cdot i\pm1\cdot j}^{*\,n+1}}{\Delta R_m^*} = \frac{\alpha_{m+j}}{R_{m\cdot i}^{*2}}$$

$$\left[R_{m\cdot i}^{*2}\,\frac{T_{m\cdot i+1\cdot1}^{*\,n+1} - 2T_{mi\cdot1}^{*\,n+1} + T_{m\cdot i-1\cdot1}^{*\,n+1}}{\Delta R_m^{*2}} + R_{m\cdot i}^{*}\,\frac{T_{m\cdot i+1\cdot1}^{*\,n+1} - T_{m\cdot i-1\cdot1}^{*\,n+1}}{\Delta R_m^{*}} + \right.$$

$$\left. \frac{2T_{m\cdot i\cdot2}^{*\,n+1} - T_{m\cdot i\cdot1}^{*\,n-1}}{\Delta\theta^2} + \cos^2\theta_1\,\frac{2T_{m\cdot i\cdot2}^{*\,n+1} - 2T_{m\cdot i\cdot1}^{*\,n-1}}{\Delta\theta^2} \right] + \frac{\Delta H^*}{\rho_{m\cdot i\cdot1}^{*}\,C_{p\cdot m\cdot i\cdot1}^{*}} \qquad \text{(C-27)}$$

Conditions for the above equation are

$i+1$ if $\Delta\psi_{Bj} > 0$ (C-28)

and $i-1$ if $\Delta\psi_{Bj} < 0$ (C-29)

Similarly,

For $\theta = \pi$ or $j = LL$

$$\frac{T^{*n+1}_{m,i,LL} - T^{*n+1}_{m,i,LL}}{\Delta t_{mHT}} + \frac{P_{eHT}}{R^{*2}_{m,i}\cos\theta}\,\frac{2|\Delta\psi_{B,j}|}{\Delta\theta^2}\,\frac{T^{*n+1}_{m,i,LL} - T^{*n+1}_{m,i\pm1,j}}{\Delta R^{*}_{m}} = \frac{\alpha_{m,i,j}}{R^{*2}_{m,i}}$$

$$\left[R^{*2}_{m,i}\,\frac{T^{*n+1}_{m,i+1,LL} - 2T^{*n+1}_{m,i,LL} + T^{*n+1}_{m,i-1,LL}}{\Delta R^{*2}_{m}} + R^{*}_{m,i}\,\frac{T^{*n+1}_{m,i+1,LL} - T^{*n+1}_{m,i-1,LL}}{\Delta R^{*}_{m}} + \right.$$

$$\left. \frac{2T^{*n+1}_{m,i,2} - T^{*n+1}_{m,i,LL}}{\Delta\theta^2} + \cos^2\theta_1 \frac{2T^{*n+1}_{m,i,2} - 2T^{*n+1}_{m,i,LL}}{\Delta\theta^2} \right] - \frac{\Delta H^{*}}{\rho^{*}_{m,i,LL} C^{*}_{p,m,i,LL}}$$

(C-30)

The conditions (C-28) and (C-29) are also applicable for the equation (C-30). The discretized form of the other transient equations can be obtained in the same way as mentioned for the equation (2E-80) in this appendix.

APPENDIX D

ESTIMATION OF PARAMETERS

The values of the density, thermal conductivity, viscosity etc. have been taken form the references 160-168. SI units have been used throughout this appendix.

Crucible dimensions:

Length of graphite crucible = 0.42 m

Radius of the crucible = 0.10 m

Pellet dimensions:

Average radius of pellet = 0.01 m

Jet dimensions:

Boundary layer thickness = 0.01 m

Distance between 0_2 lance and top layer of pellets = 0. 1 m

Step Sizes:

ΔR = R- direction step size (distance between two nodes) in Fig. 17, up to point 8.

$$= \frac{\text{Length up to point 8}}{\text{Total steps up to point 8}} = \frac{0.07}{7} \text{ m} = 0.01 \text{ m}$$

Similarly

$$\Delta R_1 = \frac{\text{Length from point 8 to 20}}{\text{Total steps from point 8 to 20}} = \frac{0.03}{12} \text{ m} = 0.0025 \text{m}$$

$$\Delta z = \frac{\text{Length from bottom of the crucible to the liquid surface}}{\text{Total steps up to Liquid surface in z-dimension}}$$

$$= \frac{0.20}{20} \text{ m} = 0.01 \text{ m}$$

Δz varies with time. For fixed steps.

$$\Delta z_g = \frac{\text{Boundary Layer thickness (Assumed)}}{\text{Total steps in B.L. in z-direction}} = \frac{0.01}{10} = 0.001 \text{ m}$$

$$R_m = \frac{\text{Radius of the cell-Radius of pellet}}{\text{Total steps in I-direction}} = \frac{0.0127-0.01}{10} = 2.7 \times 10^{-4} \text{ m}$$

ΔR_m is a function of time.

$$\Delta\theta = \frac{\text{Angle on axis of symmetry}}{\text{Total steps}} = \frac{180^\circ}{20} = 9^\circ = \frac{9^\circ \times \pi}{180^\circ} =$$

'0.12576796 radians

In dimensionless form

$$\Delta R^* = \frac{0.01}{\text{Radius of crucible(R)}} = \frac{0.01\text{m}}{0.1\text{m}} = 0.1$$

Similarly,

$$\Delta R^*_1 = \frac{0.0025\text{m}}{0.1\text{m}} = 0.025$$

$$\Delta z^* = \frac{0.01}{0.1} = 0.1$$

$$\Delta z_g^* = \frac{0.001}{0.1} = 0.01$$

$$\Delta R^*_m = \frac{2.7 \times 10^{-4}{}_m}{0.01_m \text{ (radius of pellet)}} = 0.027$$

and $\Delta\theta = 0.1576796$ radians

Wave Number k:

$$k = \frac{1}{\lambda} = \frac{1}{2 \times \text{spacing between induction coils}} = \frac{1}{2 \times 0.03}$$

$$= 16.6666 \ m^{-1}$$

Magnetic Field and Intensity:

From Section 4.6 we have

$$e = -N \frac{d\Phi}{dt} \qquad (4.3)$$

$$e_{rms} = 4.2V \text{ (measured)}$$

$$\left(\frac{d\Phi}{dt}\right) rms = \frac{4.2}{256}$$

But $\Phi = \Phi_{max} \text{ Sin } wt$

or $$\left(\frac{d\Phi}{dt}\right) rms = \Phi_{rms}\, 2\pi f$$

$$\therefore \Phi_{rms} = \frac{erms}{N.2\pi f}$$

magnetic flux intensity $B_{rms} = \frac{\Phi_{rms}}{\text{Coil Area}} = \frac{\Phi_{rms}}{\pi r_{coil}^2}$

or $$B = \frac{e_{rms}}{N 2\pi f \cdot \pi r_{coil}^2}\sqrt{2}$$

$$= \frac{(4.2) \times \sqrt{2}}{256\ 2 \times 2450 \times \times (3.68)^2 \times 10^{-6}} = 0.0354267\ Wb/m^2$$

$$Hz,O = \frac{B}{\mu o} = \frac{0.0354267}{1.257 \times 10^{-6}} = 2.81835 \times 10^4\ A/m$$

Where μ_o is the permeability of free space = 1.257×10^{-6} Henery

f = furnace frequency = 2450 Hz

$r_{coil} = 3.68 \times 10^{-3} m$

Characteristic Velocity of Liquid:

From Equation (2E- 5)

$$Uo = Hz.o \sqrt{\frac{\mu o}{\rho L}} = 2.81835 \times 10^4$$

$$\sqrt{\frac{1.257 \times 10^{-6}}{6900}} = 0.3803978\ m/s$$

where ρ is the liquid density = $6900 kg/m^3$

Calculation for η:

From equation (2E-4)

$$\eta = \frac{RH_{z\cdot o}\sqrt{\mu o \rho L}}{\mu} =$$

$$\frac{0.1 \times 2.818 \times 10^{4} \sqrt{1.256 \times 10^{-6} \times 6900 \cdot 0}}{6 \cdot 0 \times 10^{-3}} = 4.37457 \times 10^{4}$$

where μ is the viscosity of liquid iron = 6.0×10^{-3} kg/m-s

Liquid Peclet Number:

From equation (2E- 53)

$$P_{eL} = \frac{RU_{o}\rho_{L\cdot o}C_{p\cdot L\cdot o}}{k_{L\cdot o}}$$

$$= \frac{0.1 \times 0.3776709 \times 7600 \times 107.8}{18.0} = 1718.99$$

Electric Heat Generation Term:

From equation (2E-58)

$$CONSEH = \frac{\omega^{2}\mu_{o}^{2} R^{4} H_{z\cdot c}^{2} \sigma}{2k_{L\cdot o} T_{L\cdot c}}$$

$$= -\left(\frac{4\pi^{2} (2450)^{2} (1.257 \times 10^{-6})^{2} 10^{-4} (2.81835 \times 10^{4})^{2} 7.968 \times 10^{5}}{2.\ 18.0\ 300}\right)$$

$$= -2.1942098 \times 10^{3}$$

VSTRCO:

From Equation (2E-50)

$$= \frac{w\mu_o \sigma R^2 k}{2}$$

$$= \frac{2\pi.2450 \times 1.257\times10^{-6}. 10^{-2}. 16.667 \times 10^{-1}. 7.968 \times 10^{5}}{2}$$

$$= 128.50976$$

Resistivity (r_e) and Electrical Conductivity (σ):

By using the concept of integrated resistivity[1] γ_{int} one can write for linear material.

$$\gamma_{int} = \frac{\left(\sqrt{\gamma_2} + \sqrt{\gamma_1}\right)^2}{4}$$

Where γ_1, and γ_2 are the resistivities at the starting and finishing temperatures. This method of calculating integrated resistivity is fairly accurate even for non-linear materials like steel. From resistivity vs temperature curve[1] for carbon steel, which may have very little variation in resistivity for (saturated Iron, one gets $\gamma_1 \approx 1.21 \times 10^{-6}$ ohm-m at $\approx 1100°C$ and $\gamma_2 \approx 1.3 \times 10^{-6}$ at $\approx 1500°C$ therefore,

$$\gamma_{int} = r_e = \frac{\left(\sqrt{1.3} + \sqrt{1.21}\right)^2 \times 10^{-6}}{4} \approx 1.255 \times 10^{-6} \text{ohm-m}$$

Therefore, electrical conductivity $\sigma = \frac{1}{re}$.

or $$\sigma = \frac{1}{1.255 \times 10^{-6}} \text{ mho/m} \quad 7.968 \times 10^{5} \text{ mho/m}$$

Bed Reynolds Number:

From equation (2E- 72)

$$N_{Re} = \frac{2.\ U_{AV}\ r_p\ \rho_m}{\mu_m} = \frac{2. \times 4500.\ 0.38}{16 \times 10^{-1}}\ r_p\ (t)\ U^*_{AV}$$

$$= 1.8529835 \times 10^{3}\ r_p\ (t)\ U^*_{AV}$$

where $r_p(t)$ is in meters and is a function of time. U^*_{AV}, dimensionless velocity, is calculated at intermediate step within the computer program. Therefore, Reynolds number changes with time as smelting process begins but it is a constant for a particular time step.

Bed Peclet Number for Heat Transfer:

From equation (2E- 81)

$$P_{eHT} = \frac{U_{AV}\ r_p\ \rho_{p.o}\ C_{p.p.o}}{K_{p.o}} = \frac{0.3803978 \times 2230 \times 158}{2.4}\ U_{AV}^*\ r_p(t)$$

$$= 4.01224 \times 10^{4}\ U_{AV}^*\ r_p(t)$$

Bed Peclet Number for Mass Transfer:

From equation (2E-84)

$$Pe_{MT} = \frac{U_{AV}\, r_p}{D_{Feo\text{-}c}} = \frac{0.3803978}{1.\times 10^{-10}}\, U_{AV}^{*}\, r_p(t)$$

$$= 3.903978 \times 10^{9}\, U_{AV}^{*}\, r_{,}p(t)$$

Calculation for ΔR^{*}:

From equation (2E-85)

$$\Delta R^{*} = \bar{R}\, \frac{r_p^2}{D_{FeO\text{-}c}\, C_{FeO.i}}\, \frac{1000.\, \rho_m}{M_{FeO}}$$

$$= 0.41\ EXP\ (-0.41.\ (r_p^2)\ .1.4286 \times 10^{8}\ t^{*})$$

$$\frac{1000.\ 4500\ r_p^2}{72 \times 3.8188 \times 10^{5} \times 7.0 \times 10^{-9}}$$

$$= 9.09752 \times 10^{10}\, r_p^2\ EXP\ (-4.1 \times 10^{9}.\, r_p^2.\, t^{*})$$

Initial Molar Concentration of FeO ($C_{FeO.i}$):

By using Table V,

$$\text{Number of moles of } Fe_2O_3 = \frac{\text{mass of } Fe_2O_3}{\text{molecular wt of } Fe_2O_3}$$

$$= \frac{8.07 \times 1000}{160}\ \text{moles}$$

$$\text{Volume of mixture} = \frac{14.23}{3875}\ m^3$$

$$= 3.67225 \times 10^{-3}\ m^3$$

$$\therefore \text{ Initial concentration of } Fe_2O_3 = \frac{8.07 \times 1000}{160 \times 3.67225 \times 10^{-3}} \text{ mole/m}^3$$

$$= 1.3734737 \times 10^4$$

But if we consider following reaction

$$Fe_2C_3 + C \rightarrow 2FeO + CO$$

which indicates that each mole of Fe_2O_3 produces two moles of FeO, therefore

Initial concentration of FeO = 6.8673685×10^3 moles/m^3

Initial Molar Concentration of O_2 ($M_{02.\infty}$):

From the ideal gas equation $P_iV = n R_G T_i$

where n = number of moles

P_i = partial pressure of 0_2 = 1. Atm

V = volume of oxygen m^3

T_i = Room temperature = 300°K

$$\therefore \quad \frac{n}{v} = M_{02.\infty} = \frac{P_i}{R_{in}\, T_i} = \frac{1.0}{1.987 \times 300}$$

$$\frac{1.0332 \times 10^4}{0.4267} \frac{\text{mol - kgt}}{\text{m}^2\text{-kgf-m}} = 40.62023 \text{ moles/m}^3.$$

Gas Diffusion Coefficient $D_{O2\text{-}CO}$:

Diffusion coefficient between O_2-CO binary gas system can be given by:

$$D_{O2\text{-}CO} = \frac{0.0010\ T^{1.75} \sqrt{(1/M_{O2}) + (1/M_{CO})}}{P\ [\ (\Sigma v)_{O2}^{1/3} + (\Sigma v)_{CO}^{1/3}\ ]^2}$$

where v is the atomic diffusion volume of the molecule.

$$D_{O2\text{-}CO} = \frac{0.0010\ Tg^{1.75} \sqrt{(1/32) + (1/287)}}{1.0\ [(16.6)^{1/3} + (18.9)^{1/3}]^2}\ cm^2/sec$$

$$= 9.52 \times 10^{-10}\ Tg^{1.75}\ m^2/sec.$$

Gas Jet Velocity Wo:

During smelting process gas flow rate was between 20-25 liter/min and sometimes it was > 25 l/min. Therefore, flow velocity, considering average flow rate 22.5 l/min.

$$Wo = \frac{\text{flow rate}}{\text{Area of lance nozzle}} = \frac{22.5 l/min}{\pi r^2 lance}$$

$$Wo = \frac{22.5 \times 10\text{-}3 \times 106}{60 \times \pi \times 6.25}\ m/s = 19.1\ m/s$$

$Wo \approx 20$ m/s

where r_{lance} = radius of lance = 2.5 mm

Gas Peclet Number for Heat Transfer:

From equation (2E-114)

$$Peg_{HT} = \frac{Wo\ R\ \rho_{g.o}\ C_{p.g.o}}{K_{g.o}} = \frac{20 \times 0.1 \times 1.301 \times 7.0155}{6.36879 \times 10\text{-}3} \frac{103}{32}$$

$$= 8.9571325 \times 10^4$$

Gas Peclet Number for Mass Transfer:

From equation (2E-116)

$$Peg_{MT} = \frac{W_o R}{D_{02\text{-}co}}$$

$$= \frac{20\ .\ 0.1}{2.0587 \times 10^{-5}} = 9.71486 \times 10^4$$

Calculation of constants a,b,u_o, v_o, U1, V1, Xo and Yo:

From equations (2E- 40 & 41)

$a^2 - b^2 = k^2 R^2 = (16.67)\ (0.1)^2 = 2.778889 = c$ and,

$2ab = \omega\mu_o\sigma R^2 = 2\pi 2450.\ 1.257 \times 10^{-6}.\ 10^{-2}.\ 7.968 \times 10^5$

$= 154.181 = d$

where c and d are constant

$$a = \pm\sqrt{\frac{c \pm\sqrt{c^2 + d^2}}{2}}$$

$a = 8.8573147$

and

$$b = \frac{d}{2\left(\pm\sqrt{\frac{c \pm \sqrt{c^2 + d^2}}{2}}\right)}$$

$$= \quad 8.6990248$$

$$\rho_o = \sqrt{a2 + b2} \quad = \quad 12.414711$$

$$\phi = \tan\text{-}1\ \frac{b}{a} = 45.51657^o$$

Same value of a and b one wil get for other constants i.e. X_o, Y_o, U_1, V_1, u_o & v_o but value of ρ_o will be

$$\rho_o = 12.414711\ R^*_i$$

and value of Φ will be 45.51657

Heat of Reaction ΔHm:

Heat of reaction for reaction equation (2B-13) can be written in the following form, which depend upon the temperature only.

$$Hm = H^oT|_{Fe} + H^oT|_{CO} - H^oT|_{FeO} - H^oT|_C$$

$H^{o}_{T}|_{Fe} = -4310 + 10.3T$

$H^{o}_{T}|_{CO} = -25380 - 0.89T - 0.27 \times 10^{-3} T^{2} - 2.19 \times 10^{5} T^{-1}$

$H^{o}_{T}|_{FeO} = -59430 + 2.427 - 0.25 \times 10^{-3} T^{2} - 0.2 \times 10^{5} T^{-1}$

$H^{o}_{T}|_{C} = -1972 + 4.10T + 0.51 \times 10^{-3} T^{2} + 2.1 \times 10^{5} T^{-1}$

Substituting these values in the above equation one obtains

$\Delta Hm = 31712.0 + 2.89T - 0.53 \times 10^{-3} T^{2} - 4.09 \times 10^{5} T^{-1}$ cal/mole

In the same way one can calculate heat of reaction for reaction (B-5), which will be

$\Delta H_{1} = -22251.5 - 8.57T - 1.03 \times 10^{-3} T^{2} - 4.49 \times 10^{5} T^{-1}$ cal/mole

Dimensionless Heat of Reaction ΔH^{*}:

From equation (2E- 82)

$$\Delta H^{*} = \frac{df}{dt} \Delta H_{m} \rho_{m} \frac{rp^{2}}{T_{i} K_{p.o}} \times \frac{1000}{M_{mixt}} (1-\omega_{p})$$

$$= 0.41 \, Exp\left(-0.41 . r_{p}^{2} \frac{t^{*}}{9.259 \times 10^{-7}}\right) \frac{4500 \times 1000}{300 \times 2.0 \times 119} \Delta H_{m}$$

$\Delta H^{*} = 25.84 \, EXP \, (-4.42812 \times 10^{5} . r_{p}^{2} . t^{*}) \, (31712. + 2.89 \times T_{m} -$

$0.53 \times 10^{-3}. T_m^2 - 4.09 \times 10^5. T_m^{-1})$

Dimensionless Induced Power POWIND:

From equation (2E- 125)

$$POWIND = \frac{P_{init}}{\rho_{L.o}\, U_o\, \pi\, R^2\, C_{P.L.O}.\, T_i}$$

$$= \frac{50 \times 0.239 \times 54}{\pi \times 10^{-2} \times 0.3803978 \times 300. \times 7600 \times 5.822}$$

$$= 4.06786 \times 10^{-3}$$

Estimation of HEATBL, HITMEL, HFEPRO and ACUHIT:

From equation (2E-126)

$$HEATBL = \frac{1}{2C_{P.L.O}\, \rho_{L.O}.\, T_i\, U_o} =$$

$$\frac{1 \times 54}{2. \times 10^3 \times 5.822 \times 7600 \times 300 \times 0.3803978}$$

$$= 5.3471 \times 10^{-9}$$

From equation (2E-128)

$$HITMEL = \frac{(1-\omega p)\, NL1\, k_{p.O}\, rp}{R^2\, C_{P.L.O}\, \rho_{L.O}.\, U_o} =$$

$$\frac{165 \times 15000 \times 2.0 \times 54 \times r_p . (1-\omega p)}{10^{-2} \times 5.822 \times 7600 \times 0.381 \times 10^3}$$

$$= 7.90103 \times 10^2 \, r_p \, (1-\omega p)$$

From equation (2E-129)

$$HFEPRO = \frac{4}{3} \frac{D_{F-S} \; C_{FeO.i} \, N \, r_p}{R^2 \, C_{P.L.O} \, \rho_{L.O.} \, T_i \, U_o}$$

$$= \frac{4}{3} \frac{1 \times 10^{-10} \times 6.867 \times 103 \times 165 \times 54}{10^{-2} \times 5.822 \times 7600 \times 300 \times 0.381 \times 10^3}$$

$$= 1.61361 \times 10^{-10}$$

and from equation (2E-131)

$$ACUHIT = \frac{k_{L.O}}{\rho_{L.O.} \, C_{P.L.O.} \, U_o \, R} =$$

$$\frac{2.0 \times 54}{7600 \times 5.822 \times 0.381 \times 0.1 \times 10^3} = 6.4165262 \times 10^{-5}$$

Calculation for CFEOPR and COUTFL:

From eqution (2E- 133)

$$CFEOPR = \frac{M_{FeO} \; k_{p.o.} \, T_{p.i} \, x_{FeO} \, N4 \, r_p}{L_m \, M_{FeO} \, R \, C_{FeO.init} \, D_{F-S}}$$

$$\frac{72 \times 2.0 \times 300 \times 0.42 \times 165 \times rp \; (t) \; x}{26000 \times 72 \times 0.1 \times 6.86 \times 10^3 \times 1 \times 10^{-10} (1 - \omega p)}$$

$$= 2.3288 \times 10^7$$

From equation (2E-134)

$$COUTFL = \frac{R\,U_o}{D_{F-S}} = \frac{0.1 \times 0.381}{1. \times 10^{-10}} = 3.81 \times 10^{8}$$

Bed Void fraction:

Void fraction ω_B of the bed can be expressed as:

$$\omega_B = \frac{\text{Total Volume of bed - volume of all pellets}}{\text{Total Volume of Bed}}$$

$$= \frac{\pi R^2 H_B - \frac{4}{3}\pi r_p^3 . N}{\pi R^2 H_B}$$

where, H_B = Bed height and N = total number of pellets in bed = 165

$$= \frac{\pi \times 10^{-2} \times 0.045 - \frac{4}{3}\pi 1 \times 10^{-6} \times 165}{\pi \times 4.5 \times 10^{-4}}$$

$\omega_B = 0.5111$

Relation Between and $d\Phi/d\zeta$:

$y = d\Phi/d\zeta$ and $x = \sqrt{2}\,\zeta$

Relations	Value of x
$y = 0.77815\,x + 9.93 . 10^{-3}$	0 to 0.8

$y = 0.67513552\ x^{0.623344577}$	0.8 to 1.4
$y = 0.765416869\ x^{0.295065202}$	1.4 to 2.4
$y = 0.933135607\ x^{0.057749011}$	2.4 to 3.2
$y = 0.981417152\ x^{0.013897099}$	3.2 to 3.8
$y = 0.998025215\ x^{0.0012878478}$	3.8 to 4.6
$y = 1.0\ x^{0}$	4.6 to 10.1

Relation between and $d\Phi/d\zeta$:

$y = \Phi$ and $x = \sqrt{2}\,\zeta$	Value of x
$y = 0.278585691 x^{1.914735154}$	0 to 0.8
$y = 0.273729217\ x^{1.659996102}$	0.8 to 2.2
$y = 0.34383292\ x^{1.369405278}$	2.2 to 3.6
$y = 0.405733262\ x^{1.238435444}$	3.6 to 4.6
$y = 0.457765165\ x^{1.161625829}$	4.6 to 7.0
$y = 0.51115074\ x^{1.104852807}$	7.0 to 10.1

APPENDIX E

DIFFERENTIAL OPERATORS[169] AND VECTOR IDENTITIES

ψ = Scalar quantity; V = vector quantity

Rectangular coordinates (x, y, z)

$$\text{grad}_x \psi = \frac{\partial \psi}{\partial x}, \quad \text{grad}_y \psi = \frac{\partial \psi}{\partial y}, \quad \text{grad}_z \psi = \frac{\partial \psi}{\partial z}$$

$$\text{Div } \mathbf{V} = \frac{\partial V_x}{\partial x} + \frac{\partial V_y}{\partial y} + \frac{\partial V_z}{\partial z}$$

$$\nabla^2 \psi = \text{div grad } \psi = \frac{\partial^2 \psi}{\partial x^2} + \frac{\partial^2 \psi}{\partial y^2} + \frac{\partial^2 \psi}{\partial z^2}$$

$$\text{curl}_x \mathbf{V} = \frac{\partial V_z}{\partial y} - \frac{\partial V_y}{\partial z}, \quad \text{curl}_y \mathbf{V} = \frac{\partial V_x}{\partial z} - \frac{\partial V_z}{\partial x}, \quad \text{curl}_z \mathbf{V} = \frac{\partial V_y}{\partial x} - \frac{\partial V_x}{\partial y}$$

$$\frac{D}{Dt} = \frac{\partial}{\partial t} + V_x \frac{\partial}{\partial x} + V_y \frac{\partial}{\partial y} + V_z \frac{\partial}{\partial z}$$

Cylindrical coordinates (r, θ, z)

$$\text{grad}_r \psi = \frac{\partial \psi}{\partial r}, \quad \text{grad}_\theta \psi = \frac{1}{r} \frac{\partial \psi}{\partial \theta}, \quad \text{grad}_z \psi = \frac{\partial \psi}{\partial z}$$

$$\text{Div } \mathbf{V} = \frac{1}{r} \frac{\partial (r V_r)}{\partial r} + \frac{1}{r} \frac{\partial V_\theta}{\partial \theta} + \frac{\partial V_z}{\partial z}, \quad \nabla^2 \psi = \frac{\partial^2 \psi}{\partial r^2} + \frac{1}{r} \frac{\partial \psi}{\partial r} + \frac{1}{r^2} \frac{\partial^2 \psi}{\partial \theta^2} + \frac{\partial^2 \psi}{\partial z^2}$$

$$\text{curl}_r \mathbf{V} = \frac{1}{r} \frac{\partial V_z}{\partial \theta} - \frac{\partial V_\theta}{\partial z}, \quad \text{curl}_\theta \mathbf{V} = \frac{\partial V_r}{\partial z} - \frac{\partial V_z}{\partial r}, \quad \text{curl}_z \mathbf{V} = \frac{1}{r} \frac{\partial (r V_\theta)}{\partial r} - \frac{1}{r} \frac{\partial V_r}{\partial \theta}$$

$$\frac{D}{Dt} = \frac{\partial}{\partial t} + V_r \frac{\partial}{\partial r} + \frac{V_\theta}{r} \frac{\partial}{\partial \theta} + V_z \frac{\partial}{\partial z}$$

Spherical coordinates (r, θ, ϕ)

$$\text{grad}_r \psi = \frac{\partial \psi}{\partial r}, \quad \text{grad}_\theta \psi = \frac{1}{r}\frac{\partial \psi}{\partial \theta}, \quad \text{grad}_\phi \psi = \frac{1}{r \sin\theta}\frac{\partial \psi}{\partial \phi}$$

$$\text{Div } V = \frac{1}{r^2}\frac{\partial (r^2 V_r)}{\partial r} + \frac{1}{r \sin\theta}\frac{\partial (\sin\theta V_\theta)}{\partial \theta} + \frac{1}{r \sin\theta}\frac{\partial V_\phi}{\partial \phi}$$

$$\nabla^2 \psi = \frac{1}{r^2}\frac{\partial [r^2 (\partial \psi / \partial r)]}{\partial r} + \frac{1}{r^2 \sin\theta}\frac{\partial [\sin\theta (\partial \psi / \partial \theta)]}{\partial \theta} + \frac{1}{r^2 \sin^2\theta}\frac{\partial^2 \psi}{\partial \phi^2}$$

$$\text{curl}_r V = \frac{1}{r \sin\theta}\left[\frac{\partial (\sin\theta V_\phi)}{\partial \theta} - \frac{\partial V_\theta}{\partial \phi}\right], \quad \text{curl}_\theta V = \frac{1}{r}\frac{\partial (r V_\theta)}{\partial r} - \frac{1}{r}\frac{\partial V_r}{\partial \theta}$$

$$\text{curl}_\phi V = \frac{1}{r \sin\theta}\left[\frac{\partial V_r}{\partial \phi} - \sin\theta \frac{\partial (r V_\phi)}{\partial r}\right]$$

$$\frac{D}{Dt} = \frac{\partial}{\partial t} + V_r \frac{\partial}{\partial r} + \frac{V_\theta}{r}\frac{\partial}{\partial \theta} + \frac{V_\phi}{r \sin\theta}\frac{\partial}{\partial \phi}$$

$$\nabla \times \nabla \times A = \nabla (\nabla \cdot A) - \nabla^2 A$$

$$\nabla \cdot A \times B = B \cdot \nabla \times A - A \cdot \nabla \times B$$

$$A = \nabla \cdot (\nabla \times A) = 0 \quad ; \quad V = \nabla \times (\nabla V) = 0$$

$$V = \nabla \cdot (\nabla V) = \nabla^2 V$$

$$\nabla \times (A \times B) = A \nabla \cdot B - B \nabla \cdot A + (B \cdot \nabla) A - (A \cdot \nabla) B$$

APPENDIX F

FORTRAN Implementation

List of principal variables

All parameters are in dimensionless form unless stated.

Program Symbol	Definition
MAIN PROGRAM	
ITER	Number of iteration to be performed for the whole program.
ITERB	Number of iteration to be performed for bed and gas region subroutines
ITER1	Number of iteration to be performed for BEDSFVOR subroutine
ITERIN	Number of iteration to be performed for INDSTR subroutine
N	Total number of grid points in R - direction for liquid and jet regions
NN	The point in R - direction for LR and JR after which grid spacing changes
M	Total number of grid points in Z - direction in LR
NNN	Total number of grid points in r - direction for cell model in BR
LL	Total number of grid points in q - direction for cell model in BR
MP	Mid point of the furnace radius across which overall heat and mass balance have been done.
DR	Dimensionless step size before grid point NN in R - direction in LR and JR

DR1	Dimensionless step size after grid point NN in R - direction in LR and JR
ORIGZ, TOTZ	Total liquid height in meters
DZ	Step size in Z - direction in LR
DZG	Step size in Z - direction in JR
PAI	Value of π (=3.14...)
DRB	Step size in r - direction for cell model
DO	Step size in θ - direction for cell model
BEDH	Total bed height, m
RF	Radius of crucible, m
RP	Radius of pellet, m
DH	Bed height
DPOWER	Electric power
DAKP	Pellet thermal conductivity
AA,BB,U0 & V0	Constant used to evaluate Bessel function and defined in section 2A-1
ETA	A constant as defined in eqn. (2E-3)
PEL	Peclet number for heat transfer in LR
THKM	Themal condutivity of mixture, cal/m-s-^{o}K
DAKM	Thermal conductivity of mixture
PMW	Pellet molecular weight, g/mol.

AMWMIX	Molecular weight of mixture, g/mol
DLRP	Radius of pellet
ALHM	Total latent heat required to pellet to reach its melting point temperature, cal/mol
DLRCEL	Cell radius
ALHM1	Latent heat of melting for iron
DENP	Density of pellet, kg/m^3
DENMIX	Density of mixture, kg/m^3
COFSMR	Percentage of heat due to other minor reactions in BR
COFLAR	Percentage of heat due to major reaction between FeO + C in BR
ATMLOS	Atmospheric losses of heat
UCHAR	Characteristic velocity of liquid, m/s
TNP	Total number of pellets in BR
CONSEH	A constant used in energy balance eqn. in LR, defined in Appendix D
POWIND	Induced power term as defined by eqn. (2E-125)
HEATBL	Heat release term as defined by eqn. (2E-126), m^2-s/cal
HITMEL	Heat absorbed during melting of pellets, eqn. (2E-128)
HFEPRO	Heat absorbed term for iron production, eqn. (2E-129)
ACUHIT	Heat storage term, eqn. (2E-131)

CFEOPR	A constant defined by eqn. (2E-133)
COUTFL	A contant, defined by eqn. (2E-134)
VSTRCO	A constant used in equation of motion in LR, defined in Appendix D
TINIT	Room temperature, °K
RBLV	Oxygen jet velocity in JR, m/s
PEGHT	Peclet number for gas heat transfer
PEGMT	Peclet number for gas mass transfer
VFP	Void fraction for pellet
VFB	Void fraction for packed bed
DELT	Time step used in energy balance equation in LR
DELTB	Time step used in heat balance equation in BR
DELTB1	Time step used in mass balance equation in BR
DELTGH	Time step used in gas heat transfer equation
DELTGM	Time step used in gas mass transfer equation
UVF,OSF,UFE,	Under-relaxation parameters used for LR vorticity
UFG,UFW	Stream function, BR vorticity, G function and stream function, respectively.
RYN	Reynolds number in BR
PEHT	Peclet number for heat transfer in BR
PEMT	Peclet number for mass transfer in BR

BEDSFVOR	Subroutine to calculate bed stream function & vorticity
BEDHTMT	Subroutine to calculate bed temp. and FeO concn.
JETREG	Subroutine to calculate gas velocity, temp. & concn.
INDSTR	Subroutine to calculate liquid stream function & vorticity
INDTMP	Subroutine to calculate liquid temperature
TAU	Time required for melting (a variable)
TD	Calculate temp. flux over the pellet surface
AVTD	Average of TD
AVRM	Average rate of melting of the pellet
VOID	Total volume of the voids in BR
VOIDPP	Void volume per cell in BR
TCELV	Total volume of cell, m
RCEL	Cell radius, m
TRM	Total rate of melting (variable), kg/s
TOTM	Total melting rate of pellet, kg/s
VOLOFM	Volume of melt obtained from melting of pellet, m^3
HINCRE	Increment in the height of the liquid in Z-direction, m
XX,YY,UU,VV	Variable, as defined in Section 2A-1.
RHOL,RHOM,	Variable densities for liquid, mixture & gas,

RHOG	respectively.
CPL,CPM,CPG	Variable specific heats for liquid, mixture and gas, respectively.
AKL,AKM,AKG	Variable thermal conductivities for liquid, mixture and gas, respectively
W, WB	Variable stream functions for LR & BR
E, EB	Variable vorticities for LR & BR, respectively
TL, TM, TG	Variable temperature for LR, BR and JR, respectively
Z	Variable liquid height
R	Variable furnace radius
AR	Variable cell radius
G, F	Intermediate variables, used in BR, to calculate SF and vorticity and are defined in section 2B
CFEO, CMO2	Variable concn. for FeO and Oxygen, respectively
DOA, DOABL	Variable diffusion coefficient for FeO-slag and O2-CO, respectively
TMAV	Average temperature of mixture inside the cell
ARM	Rate of melting of pellets
TLAV	Average liquid temperature in BR
UINF	Liquid velocity in BR, given by eqn. (2D-2)
TINF	Liquid temperature in BR
TURAV	Average radial velocity of liquid in BR

A, B, C, D	Coefficient arrays of the tridiagonal matrix and the right hand side (COMMON IN ALL SUBROUTINES)
I, J, K, II, JJ, KK, JJJ, KKK, LNK, KLM, LNK etc.	Are variables used in main program and its subroutines

Subroutine TRIDAG

BETA, GAMMA	Vectors of intermediate coefficients
IF, L	Corresponds to first and last equations to be solved
V	Vector containing the computed solution

Subroutine AVRG

PUT, POUR	Arrays for averaging temperature, velocity in BR
OAV, GAV	Arrays to average LR temperature and velocity in BR

Subroutine TINFAVIT

DOWN, VIN	Arrays for calculating temparature
UP	Arrays for calculating rate of melting of pellet

Subroutine PTEMPAV

STM	Arrays for averaging cell temp.

Subroutine INDSTR

SF	Arrays for current values of stream function in LR
VCR	Arrays for current values of vorticity in LR

DVAL	Intermediate coefficient used in calculation of right hand side arrays in tridiagonal matrix
DELWI, DELWJ	Intermediate variables used in calculating the SF difference in I and J directions
ABSWI, ABSWJ	Absolute values of the above mentioned variables
UR, UZ	Arrays of liquid velocities in R and Z directions in LR

Subroutinr INDTMP

BH	Intermediate coefficient used in calculation of right hand side arrays in tridiagonal matrix
ABSUR, ABSUZ	Absolute values of radial and axial velocities in LR
GASHIT	A parameter used to calculate heat generation due to gas boundary layer, defined by eqn. (2E-127), $cal/m^2\text{-}s$
BCPART	Parameter used to calculate heat absorbed for iron production as defined in eqn. (2E-130)
BVAL	Intermediate coefficient used in calculation of diagonal arrays in tridiagonal matrix for transition grid point (8)
DVAL	Intermediate coefficient used in calculation of right hand side arrays in tridiagonal matrix for transition grid point (8) only
ABSUR,ABSUZ	Absolute values of liquid radial and axial velocities

Subroutine BEDSFVOR

ABSUIN	Absolute value of liquid velocity U_∞ in BR
CRYN	Actual Reynolds number value used in calculation in BR
DELWI,DELWJ	Intermediate variable used for calculating the SF and vorticity in BR

ABSWI,ABSWJ	Absolute values of the above mentioned variables

Subroutine BEDHTMT

CPEHT	Actual Peclet number value of heat transfer used in BR
CPEMT	Actual Peclet number value of mass transfer used in BR
DELWI,DELWJ, ABSWI,ABSWJ	Same as defined in subroutine BEDSFVOR
AVAL,BVAL,CVAL DVAL,AAVAL, BBVAL,CCVAL, FFVAL,EEVAL	Intermediate coefficient used in calculation of leftand right hand side arrays in tridiagonal matrix
ALF	Arrays of thermal diffusivity used in Bed temp. calculation

Subroutine JETREG

U2ZETA,PHI,	Variables used to calculate oxygen velocities in JR,
DFIDZ	Defined in eqn. (2C-7)
VR,VZ	Arrays of gas velocities in R and Z direction

APPENDIX G

COMPUTER CODE FOR MODEL PROBLEM

```
C*****************************************************************
C              INDUCTION SMELTING PROCESS
C*****************************************************************
C    FULL COMPUTER CODE FOR SMELTING OF COMPOSITE PELLETS
C     IN AN INDUCTION FURNACE
C
$INITWARN
$CALLWARN
$ALIGNWARN
      COMMON/AREA1/LL,LL1,LNK,LNK1,DRB,D0,D0R,RYN,PEMT,PEHT,
     1VFB,DELTB,DELTB1,TIMEB,TIMEB1,RP,RF,TNP,PAI,ITERB,ITER1,UFG,
     2MP,UFW,UFE,THKM,DENP,BEDH,TOTZ,DLRP,ALHM,VFP,DAKP,
     3DAKM,UCHAR,COFSMR,COFLAR,ATMLOS,PMW,AMWMIX,DENMIX,
     3DLRCEL,CONSEH,POWIND,HEATBL,HITMEL,HFEPRO,ACUHIT,
     4CFEOPR,COUTFL,VSTRCO,TINIT,ALHM1
      COMMON/AREA2/DOA(21,21),RHOM(21,21),CPM(21,21),AKM(21,21),
     1F(21,21),G(21,21),ALF(21,21)
      COMMON/AREA3/WB(21,21),EB(21,21),TM(21,21),CFEO(21,21),
     1TL(21,21),W(21,21),E(21,21),TG(31,31),CMO2(31,31),UR(21,21),
     2UZ(21,21),VR(31,31),VZ(31,31)
      COMMON/AREA4/THETA(21),AR(21)
      COMMON/AREA5/A(31),B(31),C(31),D(31),TT(31)
      COMMON/AREA6/MM,MM1,DZG,PEGHT,PEGMT,RBLV,DELTGH,
     1TIMEG,DELTGM
      COMMON/AREA7/U2ZETA(31),PHI(31),DFIDZ(31),AZ(31)
      COMMON/AREA8/CPG(31,31),AKG(31,31),RHOG(31,31),DOABL(31,31)
      COMMON/AREA9/N,M,NN,N1,M1,DZ,DR,DR1,DTLR,PEL,DPOWER,
     1ITERIN,DELT,NNN1,TIME,ETA,ADR,DDR,UVF,OSF,AA,BB,U0,V0,
     2NNN,ORIGZ,DH
      COMMON/AREA10/R(22),Z(22),UU(22),VV(22),XX(22),YY(22)
      COMMON/AREA11/RHOL(22,22),CPL(22,22),AKL(22,22)
      DIMENSION TRM(0:20)
      OPEN(UNIT=21,FILE='for21')
      OPEN(UNIT=31,FILE='for31')
C     OPEN(UNIT=32,FILE='for32')
      OPEN(UNIT=33,FILE='for33')
      OPEN(UNIT=34,FILE='for34')
      OPEN(UNIT=35,FILE='for35')
      OPEN(UNIT=36,FILE='for36')
      OPEN(UNIT=37,FILE='for37')
      OPEN(UNIT=38,FILE='for38')
      OPEN(UNIT=39,FILE='for39')
      OPEN(UNIT=40,FILE='for40')
      OPEN(UNIT=41,FILE='for41')
      OPEN(UNIT=42,FILE='for42')
      OPEN(UNIT=43,FILE='for43')
      OPEN(UNIT=44,FILE='for44')
      OPEN(UNIT=45,FILE='for45')
      OPEN(UNIT=46,FILE='for46')
      ITER=14
      ITERB=15
      ITER1=150
      ITERIN=100
      N=20
      NN=8
      M=21
      MM=31
      MM1=MM-1
      N1=N-1
      M1=M-1
      NNN=11
      NNN1=NNN-1
      LL=21
      LL1=LL-1
      LNK=11
      LNK1=LNK-1
      MP=6
      DR=0.1
      DR1=0.025
      ADR=DR+DR1
      DDR=DR/DR1
      ORIGZ=0.04
      TOTZ=0.4
      DZ=0.02
      DZG=0.01
      PAI=3.1415926
```

```
      DRB=0.027
      D0=PAI/LL1
      D0R=D0/DRB
      BEDH=0.045
      RF=0.1
      RP=0.01
      DH=BEDH/RF
      DPOWER=1.0
      DAKP=1.0
      AA=8.8573147
      BB=8.6990248
      U0=-474.19780012
      V0=566.41766419
      ETA=4.37457E+04
      PEL=1.7313E+03
      DTLR=DR/DZ
      THKM=0.8
      DAKM=1.0
      PMW=119.0
      AMWMIX=63.
      DLRP=1.0
      ALHM=26000.0
      ALHM1=7500.0
      DLRCEL=1.27
      DENP=3875.0
      DENMIX=4500.
      COFSMR=0.02
      COFLAR=0.98
      ATMLOS=1.0
      UCHAR=0.3803978
      TNP=165.0
      CONSEH=2.194207E+03
      POWIND=4.06786E-03
      HEATBL=5.3471E-09
      HITMEL=1.8523607E+02
      HFEPRO=6.50868E-09
      ACUHIT=6.4165262E-05
      CFEOPR=2.2110791E+07
      COUTFL=5.43425E+08
      VSTRCO=1.2848664E+02
      TINIT=300.0
      RBLV=20.0
      PEGHT=8.9571325E+04
      PEGMT=1.71486E+05
      VFP=0.423
      VFB=0.511
      UFE=0.7
      DELTB1=4.6E-05
      TIMEB1=0.0
      DELTB=0.35
      TIMEB=0.5
      DELTGH=0.15
      DELTGM=0.14
      TIMEG=0.0
      UFG=0.5
      UFW=0.4
      DELT=0.116
      TIME=0.0
      UVF=0.5
      OSF=0.8
C     INITIALISATION.....
      DO 3 J=1,N
       READ(21,1101) XX(J),YY(J),UU(J),VV(J)
1101  FORMAT(2X,4F16.8/)
3     CONTINUE
      DO 8 I=1,N
      DO 7 J=1,M
      RHOL(I,J)=1.0
      CPL(I,J)=1.0
      AKL(I,J)=1.0
      AKM(I,J)=1.0
7     CONTINUE
8     CONTINUE
      DO 15 I=1,N
      E(I,M)=0.0
      W(I,M)=0.0
```

```
      TM(I,M+1)=5.8
      W(I,M1)=0.001
      TL(I,M)=6.0
      TL(I,1)=6.2
      W(I,1)=0.0
15    CONTINUE
      R(1)=0.0
      Z(1)=0.0
      DO 14 J=1,M1
      Z(J+1)=Z(J)+DZ
      E(1,J)=0.0
14    CONTINUE
      DO 6 I=1,N1
      IF(I.GT.7) DR=DR1
      R(I+1)=R(I)+DR
6     CONTINUE
      DR=0.1
      DO 31 I=1,N
      DO 32 J=1,M1
      TL(I,J+1)=TL(I,J)-0.02
      W(I,J+1)=W(I,J)+0.0001
32    CONTINUE
31    CONTINUE
      DO 33 I=2,N
      DO 34 J=1,M1
      E(I,J+1)=E(I-1,J)+0.001
34    CONTINUE
33    CONTINUE
C     INITIALISATION.....
      DO 10 J=1,LL
      WB(1,J)=0.1E-05
      G(1,J)=0.2E-05
      F(1,J)=0.2E-05
      TM(1,J)=5.1
      CFEO(1,J)=0.05
10    CONTINUE
      DO 20 I=1,LNK1
      DO 25 J=1,LL
      WB(I+1,J)=WB(I,J)+0.2E-05
      G(I+1,J)=G(I,J)+2.E-05
      F(I+1,J)=F(I,J)+2.E-05
      TM(I+1,J)=TM(I,J)+0.04
      CFEO(I+1,J)=CFEO(I,J)+0.04
25    CONTINUE
20    CONTINUE
      DO 320 I=1,LNK
      DO 325 J=1,LL
      DOA(I,J)=1.0
      RHOM(I,J)=1.161
      CPM(I,J)=1.519
      AKM(I,J)=0.5
325   CONTINUE
320   CONTINUE
      THETA(1)=0.0
      AR(1)=1.0
      DO 5 J=1,LL1
5     THETA(J+1)=THETA(J)+D0
      DO 9 I=1,LNK1
      AR(I+1)=AR(I)+DRB
9     CONTINUE
C     INITIALISATION FOR JET-REGION.....
      DO 1107 I=1,N
      DO 1108 J=M,MM
      AKG(I,J)=1.0
      RHOG(I,J)=1.0
      CPG(I,J)=1.0
      DOABL(I,J)=1.0
1108  CONTINUE
      TG(I,M)=6.0
      CMO2(I,M)=0.6
1107  CONTINUE
      DO 1109 J=M,MM1
      DO 1110 I=1,N
      TG(I,J+1)=TG(I,J)-0.1
      CMO2(I,J+1)=CMO2(I,J)+0.02
1110  CONTINUE
```

```
1109 CONTINUE
      TMAV=0.0
      TLAV=0.0
      UINF=0.0
      TINF=0.0
      TURAV=0.0
     CPEHT=0.0
     CPEMT=0.0
     DR=0.1
C    MAIN PROGRAMME.....
     DO 990 KL=1,ITER
     TIME=TIME+DELT
     DTLR=DR/DZ
     DO 1202 J=1,M1
     Z(J+1)=Z(J)+DZ
1202 CONTINUE
     CALL INDSTR
     CALL INDTMP
     DO 1136 KKKK=1,ITER
     IF(KL.EQ.KKKK*2) GO TO 1139
1136 CONTINUE
     DO 1181 I=1,N
     TG(I,M)=6.0
     CMO2(I,M)=0.6
1181 CONTINUE
     DO 1182 J=M,MM
     DO 1183 I=1,N
     TG(I,J+1)=TG(I,J)-0.1
     CMO2(I,J+1)=CMO2(I,J)+0.02
1183 CONTINUE
1182 CONTINUE
     DO 1175 J=1,LL
     TM(1,J)=5.1
     CFEO(1,J)=0.05
1175 CONTINUE
     DO 1173 I=1,LNK1
     DO 1174 J=1,LL
     TM(I+1,J)=TM(I,J)+0.04
     CFEO(I+1,J)=CFEO(I,J)+0.04
1174 CONTINUE
1173 CONTINUE
     JJJ=1
     RP=0.01
     DRB=0.027
     TIMEB=0.0
     TIMEB1=0.0
1139 TAU=0.0
     DO 991 KKL=JJJ,ITERB
     TAU=TAU+DELTB
     TIMEB=TIMEB+DELTB
     TIMEB1=TIMEB1+DELTB1
     D0R=D0/DRB
     RYN=(0.852983E+03)*RP
     PEHT=(2.01224E+04)*RP
     PEMT=(5.9039E+09)*RP
     AR(1)=1.0
     DO 1102 I=1,LNK1
     AR(I+1)=AR(I)+DRB
1102 CONTINUE
     IF(KKL.EQ.ITERB) GO TO 1219
     CALL BEDSFVOR
     CALL BEDHTMT
     CALL JETREC
     TD=0.0
     DO 1105 J=1,LL
     TD=DAKM*(TM(2,J)-TM(1,J))/(DRB)+TD
1105 CONTINUE
     AVTD=TD/LL
       AVRM=AVTD*(1.-VFP)*(4.*PAI*THKM*TINIT*AMWMIX*RP)/
    1(ALHM*1000.)
      RP=RP-AVRM*DELTB*120./(DENMIX*4.*PAI*(RP**2))
      VOID=PAI*((RP**2)*BEDH-(4./3.)*(RP**3)*TNP)
     VOIDPP=VOID/TNP
     TCELV=(4./3.)*(RP**3)*PAI+VOIDPP
     RCEL=(3.*TCELV/(4.*PAI))**(1./3.)
     DLRCEL=RCEL/RP
```

```
      DRB=(DLRCEL-DLRP)/LNK1
      TRM(0)=0.0
       TRM(KKL)=AVRM+TRM(KKL-1)
      print*,KKL
       WRITE(42,1147) DRB,RCEL,AVRM,TD
1147 FORMAT(1X,'VALUE OF DRB = ',F12.6,2X,'RCEL = ',F12.6,2X,
     1'AVRM = ',F12.6,2X,'TD = ',F16.3/)
       WRITE(42,1018) KKL,TIMEB,RP
1018  FORMAT(1X,'AFTER',I4,'TH ITERATION OR',F9.6,'SEC.(RADIUS OF
     1 PELLET=',F9.6,') THE FIRST 11 VALUES OF BED TEMP. ARE:',/)
       WRITE(42,1019) ((TM(I,J),I=1,LNK),J=1,LL)
1019 FORMAT(2X,11F11.5/)
       WRITE(41,1022) KKL
1022 FORMAT(1X,'AFTER',I4,'TH ITERATION THE FIRST 11 VALUES OF
     1BED CONCENTRATION  ARE:',/)
       WRITE(41,1023) ((CFEO(I,J),I=1,LNK),J=1,LL)
1023 FORMAT(2X,11F11.5/)
       WRITE(43,1121) TIMEG
1121 FORMAT(1X,'AFTER',F10.4,'TIME THE GAS CONCN. ARE:',/)
       WRITE(43,1122) ((CMO2(I,J),J=M,MM),I=1,N)
1122 FORMAT(2X,11F11.5/)
       WRITE(44,1123) TIMEG
1123 FORMAT(1X,'AFTER',F10.4,'TIME THE GAS TEMP. ARE:',/)
      WRITE(44,1124) ((TG(I,J),J=M,MM),I=1,N)
1124 FORMAT(2X,11F11.5/)
      IF(RP.LT.0.0025) GO TO 1140
      DO 1148 MMMM=1,ITER
      IF(KL.EQ.MMMM*2) GO TO 991
1148 CONTINUE
      IF(RP.LT.0.006) GO TO 1135
991  CONTINUE
      GO TO 1140
1135 JJJ=KKL+1
       TOTM=TRM(KKL)
      GO TO 1141
1140 TOTM=TRM(KKL)
1141  VOLOFM=((TOTM*TAU*120.*TNP)/DENMIX+(1.-VFP)*(4./3.)*PAI*
     1(RP**3)*TNP)*0.42
       THINCRE=VOLOFM/(PAI*(RF**2))
      ORIGZ=ORIGZ+THINCRE
      TOTZ=ORIGZ/RF
      DZ=TOTZ/M1
      TRM(KKL)=0.0
      print*, kl,dz,drb,rcel,origz
       WRITE(31,1146) DZ,ORIGZ,TOTM,TOTZ,TMAV,TLAV,UINF,TINF
1146 FORMAT(1X,'VALUES OF DZ = ',F12.6,2X,'ORIGZ = ',F12.6,2X,
     1'TOTM = ',F12.6,2X,'TOTZ = ',F12.6,2X,'TMAV = ',F12.6,2X,
     2'TLAV = ',F12.6,2X,'UINF = ',F12.6,2X,'TINF = ',F12.6/)
      WRITE(31,810) TIME
810  FORMAT(1X,'AFTER',F10.4,'TIME THE FIRST 10 VALUES OF LIQUID
     1TEMP. ARE:',/)
      WRITE(31,820) ((TL(I,J),I=1,NNN1),J=1,M)
820  FORMAT(2X,10F11.5/)
      WRITE(31,811) TIME
811  FORMAT(1X,'AFTER',F10.4,'TIME THE LAST 11 VALUES OF THE
     1LIQUID TEMP. IN RADIAL DIRECTION ARE:',/)
      WRITE(31,812) ((TL(I,J),I=NNN,N),J=1,M)
812  FORMAT(2X,10F11.5/)
      WRITE(35,831) KL
831  FORMAT(1X,'AFTER',I4,'TH ITERN. THE LIQUID  RADIALVEL. ARE:',/)
      WRITE(35,832) ((UR(I,J),I=1,N),J=1,M)
832  FORMAT(2X,10F11.5/)
      WRITE(36,833) KL
833  FORMAT(1X,'AFTER',I4,'TH ITERATION THE LIQ. AXIAL VEL. ARE:',/)
      WRITE(36,834) ((UZ(I,J),I=1,N),J=1,M)
834  FORMAT(2X,10F11.5/)
      WRITE(45,1125) KL
1125 FORMAT(1X,'AFTER',I4,'TH ITERATION THE GAS RAD. VEL. ARE:',/)
      WRITE(45,1126) ((VR(I,J),J=M,MM),I=1,N)
1126 FORMAT(2X,11F11.5/)
      WRITE(46,1127) KL
1127 FORMAT(1X,'AFTER',I4,'TH ITERAT. THE GAS AXIAL VEL. ARE:',/)
      WRITE(46,1128) ((VZ(I,J),J=M,MM),I=1,N)
1128 FORMAT(2X,11F11.5/)
990  CONTINUE
1219 END
```

```
C
C          ***************************************************
C
C     SUBROUTINE TRIDAG
C
C          ***************************************************
C
      SUBROUTINE TRIDAG (IF,L,A,B,C,D,V)
      SAVE
      DIMENSION A(31),B(31),C(31),D(31),V(31),BETA(31),GAMMA(31)
      BETA(IF)=B(IF)
      GAMMA(IF)=D(IF)/BETA(IF)
      IFP1=IF+1
      DO 1 I=IFP1,L
      BETA(I)=B(I)-A(I)*C(I-1)/BETA(I-1)
    1 GAMMA(I)=(D(I)-A(I)*GAMMA(I-1))/BETA(I)
      V(L)=GAMMA(L)
      LAST=L-IF
      DO 2 K=1,LAST
      I=L-K
    2 V(I)=GAMMA(I)-C(I)*V(I+1)/BETA(I)
      RETURN
      END
C
C          ***************************************************
C     SUBROUTINE FOR Uinfinity AND AVRAGE INDUCTION TEMP.
C          ***************************************************
C
      SUBROUTINE AVRG (PUT,POUR,M,DZ,MP,OAV,GAV,TURAV)
      SAVE
      DIMENSION PUT(21,21),POUR(21,21)
      IF(DZ.GT.0.19) KMK=2
      IF((DZ.LE.0.19).AND.(DZ.GT.0.13)) KMK=3
      IF((DZ.LE.0.13).AND.(DZ.GE.0.1)) KMK=4
      IF((DZ.GT.0.06).AND.(DZ.LT.0.1)) KMK=6
      IF(DZ.LE.0.06) KMK=8
      KLM=M-KMK
      U=0.0
      TLT=0.0
      TLUR=0.0
      DO 767 JJ=KLM,M
      U=PUT(MP,JJ)+U
      TLT=POUR(MP,JJ)+TLT
      TLUR=PUT(MP,JJ)*POUR(MP,JJ)+TLUR
  767 CONTINUE
      OAV=U/(KMK+1)
      GAV=TLT/(KMK+1)
      TURAV=TLUR/(KMK+1)
      RETURN
      END
C
C          ***************************************************
C     SUBROUTINE FOT Tinfinity AND AVERAGE RATE OF MELTING
C          ***************************************************
C
      SUBROUTINE TINFAVIT (DOWN,VIN,LL,N,M,DAKP,DRB,TINF,UP)
      SAVE
      DIMENSION DOWN(21,21),VIN(21,21)
      YZ=0.0
      XY=0.0
      DO 2 II=1,N
      XY=VIN(II,M)+XY
    2 CONTINUE
      DO 4 III=1,LL
      YZ=DAKP*(DOWN(2,III)-DOWN(1,III))/DRB+YZ
    4 CONTINUE
      TINF=XY/N
      UP=YZ/LL
      RETURN
      END
C
C
C
C          ***************************************************
C     SUBROUTINE FOR AVRAGE CELL TEMPERATURE
C          ***************************************************
```

```
C
      SUBROUTINE PTEMPAV (STM,LL,LNK,TMAV)
      SAVE
      DIMENSION STM(21,21),EEE(21)
      FFF=0.0
      DO 1201 IJ=1,LNK
      DDD=0.0
      DO 1202 JI=1,LL
      DDD=STM(IJ,JI)+DDD
1202  CONTINUE
      EEE(IJ)=DDD/LL
      FFF=EEE(IJ)+FFF
1201  CONTINUE
      TMAV=FFF/LNK
      RETURN
      END
C
C              ***************************************************
C
C       SUBROUTINE FOR STREAM FUNCTION AND VORTICITY  IN
C       INDUCTION REGION
C
C              ***************************************************
C
      SUBROUTINE INDSTR
      SAVE
       COMMON/AREA1/LL,LL1,LNK,LNK1,DRB,D0,D0R,RYN,PEMT,PEHT,
       1VFB,DELTB,DELTB1,TIMEB,TIMEB1,RP,RF,TNP,PAI,ITERB,ITER1,UFG,
       2MP,UFW,UFE,THKM,DENP,BEDH,TOTZ,DLRP,ALHM,VFP,DAKP,
       3DAKM,UCHAR,COFSMR,COFLAR,ATMLOS,PMW,AMWMIX,DENMIX,
      3DLRCEL,CONSEH,POWIND,HEATBL,HITMEL,HFEPRO,ACUHIT,
      4CFEOPR,COUTFL,VSTRCO,TINIT,ALHM1
       COMMON/AREA3/WB(21,21),EB(21,21),TM(21,21),CFEO(21,21),
      1TL(21,21),W(21,21),E(21,21),TG(31,31),CMO2(31,31),UR(21,21),
      2UZ(21,21),VR(31,31),VZ(31,31)
       COMMON/AREA5/A(31),B(31),C(31),D(31),TT(31)
        COMMON/AREA9/N,M,NN,N1,M1,DZ,DR,DR1,DTLR,PEL,DPOWER,
        1ITERIN,DELT,NNN1,TIME,ETA,ADR,DDR,UVF,OSF,AA,BB,U0,V0,
      2NNN,ORIGZ,DH
       COMMON/AREA10/R(22),Z(22),UU(22),VV(22),XX(22),YY(22)
      COMMON/AREA11/RHOL(22,22),CPL(22,22),AKL(22,22)
       DIMENSION SF(21,21),VOR(21,21)
C      CALCULATION FOR STREAM FUNCTION.....
      DO 1111 MKK=1,ITERIN
       PRINT*,MKK
C     J-DIRECTION.....
      DO 21 I=1,N
      DO 22 J=1,M
      SF(I,J)=W(I,J)
22    CONTINUE
21    CONTINUE
      DO 25 I=1,N
      DO 30 J=1,M
      DR=0.1
      DTLR=DR/DZ
C     IF(J.GT.M) GO TO 25
      IF(I.EQ.NN) GO TO 31
      IF(I.GT.NN) GO TO 32
      GO TO 33
32    DR=DR1
      DTLR=DR/DZ
33    IF(I.EQ.1) GO TO 35
      IF(I.EQ.N) GO TO 40
      IF(J.EQ.1) GO TO 45
      IF(J.EQ.M) GO TO 50
       A(J)=R(I)*(DTLR**2)
        B(J)=-(2.*R(I)+2.*R(I)*(DTLR**2))
       C(J)=R(I)*(DTLR**2)
       D(J)=-SF(I-1,J)*(R(I)+DR/2.)-SF(I+1,J)*(R(I)-DR/2.)+E(I,J)*
      1R(I)*R(I)*DR*DR
      GO TO 30
31    IF(J.EQ.1) GO TO 45
      IF(J.EQ.M) GO TO 50
      A(J)=R(I)/(DZ*DZ)
       B(J)=-(2.*R(I)/(DZ*DZ)+2.*R(I)/(ADR*DR)+2.*R(I)/(ADR*DR1)-
     1DDR/ADR+1./(ADR*DDR))
```

```
      C(J)=R(I)/(DZ*DZ)
        D(J)=-SF(I-1,J)*(2.*R(I)/(ADR*DR)+1./(ADR*DDR))-SF(I+1,J)*
     1(2.*R(I)/(ADR*DR1)-DDR/ADR)+E(I,J)*R(I)*R(I)
      GO TO 30
35    A(J)=0.0
      B(J)=1.0
      C(J)=0.0
      D(J)=0.0
      GO TO 30
40    A(J)=0.0
      B(J)=1.0
      C(J)=0.0
      D(J)=0.0
      GO TO 30
45    A(1)=0.0
      B(1)=1.0
      C(1)=0.0
      D(1)=0.0
      GO TO 30
50    A(M)=0.0
      B(M)=1.0
      C(M)=0.0
      D(M)=0.0
30    CONTINUE
      CALL TRIDAG (1,M,A,B,C,D,TT)
      DO 55 J=1,M
      SF(I,J)=TT(J)
55    CONTINUE
25    CONTINUE
C     I-DIRECTION.....
      DO 60 J=1,M
      DO 65 I=1,N
      DR=0.1
      DTLR=DR/DZ
      IF(I.EQ.NN) GO TO 61
      IF(I.GT.NN) GO TO 62
      GO TO 63
62     DR=DR1
       DTLR=DR/DZ
63    IF(I.EQ.1) GO TO 75
      IF(I.EQ.N) GO TO 85
      IF(J.EQ.1) GO TO 70
      IF(J.EQ.M) GO TO 72
      A(I)=R(I)+DR/2.
       B(I)=-(2.*R(I)+2.*R(I)*(DTLR**2))
      C(I)=R(I)-DR/2.
       D(I)=-SF(I,J-1)*(R(I)*(DTLR**2))-SF(I,J+1)*(R(I)*(DTLR**2))+
      1E(I,J)*R(I)*R(I)*DR*DR
C     print *,DR,DTLR
      GO TO 65
61    IF(J.EQ.1) GO TO 70
      IF(J.EQ.M) GO TO 72
       A(I)=2.*R(I)/(ADR*DR)+1./(ADR*DDR)
       B(I)=-(2.*R(I)/(DZ*DZ)+2.*R(I)/(ADR*DR)+2.*R(I)/(ADR*DR1)-
      1DDR/ADR+1./(ADR*DDR))
       C(I)=2.*R(I)/(ADR*DR1)-DDR/ADR
       D(I)=-SF(I,J+1)*(R(I)/(DZ*DZ))-SF(I,J-1)*(R(I)/(DZ*DZ))+
      1E(I,J)*R(I)*R(I)
      GO TO 65
70    A(I)=0.0
      B(I)=1.0
      C(I)=0.0
      D(I)=0.0
      GO TO 65
72    A(I)=0.0
      B(I)=1.0
      C(I)=0.0
      D(I)=0.0
      GO TO 65
75    A(1)=0.0
      B(1)=1.0
      C(1)=0.0
      D(1)=0.0
      GO TO 65
85    A(N)=0.0
      B(N)=1.0
```

```
      C(N)=0.0
      D(N)=0.0
   65 CONTINUE
      CALL TRIDAG (1,N,A,B,C,D,TT)
      DO 90 I=1,N
   90 SF(I,J)=TT(I)
   60 CONTINUE
      DO 91 I=1,N
      DO 92 J=1,M
       W(I,J)=OSF*SF(I,J)+(1.-OSF)*W(I,J)
   92 CONTINUE
   91 CONTINUE
C     CALCULATION FOR VORTICITY.....
C     J-DIRECTION.....
      DO 111 I=1,N
      DO 112 J=1,M
      VOR(I,J)=E(I,J)
  112 CONTINUE
  111 CONTINUE
      DO 110 I=2,N1
      DO 115 J=2,M1
      DR=0.1
      DTLR=DR/DZ
        DVAL=VSTRCO*(SIN(3.3334*Z(J)))*((VV(I)*AA*XX(I)-VV(I)*BB*
       1YY(I)-UU(I)*BB*XX(I)-UU(I)*AA*YY(I))/((AA*AA+BB*BB)*(U0*
      2U0+V0*V0)))
C     RHOL(I,J)=(8102.2-0.7170S*(TL(I,J)*300.))/7600.
C     RHOL(I,J)=1.0
       IF(I.EQ.NN) GO TO 116
       IF(I.GT.NN) GO TO 117
       GO TO 113
  117  DR=DR1
       DTLR=DR/DZ
  113  DELWJ=W(I,J+1)-W(I,J-1)
       DELWI=W(I+1,J)-W(I-1,J)
       ABSWJ=ABS(DELWJ)
       ABSWI=ABS(DELWI)
C      print *,DR,DTLR
       IF((DELWJ.LT.0.0).AND.(DELWI.LT.0.0)) GO TO 301
       IF((DELWJ.GE.0.0).AND.(DELWI.GE.0.0)) GO TO 302
       IF((DELWJ.LT.0.0).AND.(DELWI.GE.0.0)) GO TO 303
       IF((DELWJ.GE.0.0).AND.(DELWI.LT.0.0)) GO TO 304
  301  A(J)=DTLR/(ETA*RHOL(I,J))
        B(J)=(ABSWI/(2.0*R(I))+ABSWJ/(2.*R(I))+ABSWJ*DR/(R(I)*
       1R(I)*2.)-2./(DTLR*ETA*RHOL(I,J))-DR*DZ/(R(I)*R(I)*ETA*RHOL(I,J))-
      2(2.*DTLR/(ETA*RHOL(I,J)))
       C(J)=-(ABSWI/(2.*R(I))-DTLR/(ETA*RHOL(I,J)))
       D(J)=-E(I+1,J)*(1./(DTLR*ETA*RHOL(I,J))+DZ/(2.*R(I)*ETA*
       1RHOL(I,J)))-E(I-1,J)*(-ABSWJ/(2.*R(I))+DZ/(DR*ETA*RHOL(I,J))-
       2DZ/(ETA*RHOL(I,J)*2.*R(I)))-DVAL*DR*DZ/RHOL(I,J)
       GO TO 115
  302  A(J)=-(ABSWI/(2.*R(I))-DTLR/(ETA*RHOL(I,J)))
        B(J)=(ABSWI/(2.0*R(I))+ABSWJ/(2.*R(I))+ABSWJ*DR/(R(I)*
       1R(I)*2.)-2./(DTLR*ETA*RHOL(I,J))-DR*DZ/(R(I)*R(I)*ETA*RHOL(I,J))-
      2(2.*DTLR/(ETA*RHOL(I,J)))
       C(J)=DTLR/(ETA*RHOL(I,J))
        D(J)=-E(I+1,J)*(-ABSWJ/(2.*R(I))+1./(DTLR*ETA*RHOL(I,J))+
       1DZ/(2.*R(I)*ETA*RHOL(I,J)))-E(I-1,J)*(1./(DTLR*ETA*RHOL(I,J))-
       2DZ/(2.*R(I)*ETA*RHOL(I,J)))-DVAL*DR*DZ/RHOL(I,J)
       GO TO 115
  303  A(J)=-(ABSWI/(2.*R(I))-DTLR/(ETA*RHOL(I,J)))
        B(J)=(ABSWI/(2.0*R(I))+ABSWJ/(2.*R(I))+ABSWJ*DR/(R(I)*
       1R(I)*2.)-2./(DTLR*ETA*RHOL(I,J))-DR*DZ/(R(I)*R(I)*ETA*RHOL(I,J))-
      2(2.*DTLR/(ETA*RHOL(I,J)))
       C(J)=DTLR/(ETA*RHOL(I,J))
        D(J)=-E(I+1,J)*(1./(DTLR*ETA*RHOL(I,J))+DZ/(2.*R(I)*ETA*
       1RHOL(I,J)))-E(I-1,J)*(-ABSWJ/(2.*R(I))+DZ/(DR*ETA*RHOL(I,J))-
       2DZ/(ETA*RHOL(I,J)*2.*R(I)))-DVAL*DR*DZ/RHOL(I,J)
       GO TO 115
  304  A(J)=DTLR/(ETA*RHOL(I,J))
        B(J)=(ABSWI/(2.0*R(I))+ABSWJ/(2.*R(I))+ABSWJ*DR/(R(I)*
       1R(I)*2.)-2./(DTLR*ETA*RHOL(I,J))-DR*DZ/(R(I)*R(I)*ETA*RHOL(I,J))-
      2(2.*DTLR/(ETA*RHOL(I,J)))
       C(J)=-(ABSWI/(2.*R(I))-DTLR/(ETA*RHOL(I,J)))
        D(J)=-E(I+1,J)*(-ABSWJ/(2.*R(I))+1./(DTLR*ETA*RHOL(I,J)))+
       1DZ/(2.*R(I)*ETA*RHOL(I,J)))-E(I-1,J)*(1./(DTLR*ETA*RHOL(I,J))-
```

```
     2DZ/(2.*R(I)*ETA*RHOL(I,J)))-DVAL*DR*DZ/RHOL(I,J)
     GO TO 115
 116 DELWI=(W(I+1,J)-W(I,J))*DDR-(W(I-1,J)-W(I,J))*(1./DDR)
     DELWJ=W(I,J+1)-W(I,J-1)
     ABSWI=ABS(DELWI)
     ABSWJ=ABS(DELWJ)
      BVAL=ABSWI+ABSWJ*ADR/(2.*R(I))-2.*R(I)*DZ/(ETA*RHOL(I,J)*DR)
     1-2.*R(I)*DZ/(ETA*RHOL(I,J)*DR1)-DZ*DDR/(ETA*RHOL(I,J))+DZ/(DDR*
     2ETA*RHOL(I,J))-ADR*DZ/(R(I)*ETA*RHOL(I,J))-2.*R(I)*ADR/(DZ*ETA*
     3RHOL(I,J))
     IF((DELWJ.LT.0.0).AND.(DELWI.LT.0.0)) GO TO 306
     IF((DELWJ.GE.0.0).AND.(DELWI.GE.0.0)) GO TO 307
     IF((DELWJ.LT.0.0).AND.(DELWI.GE.0.0)) GO TO 308
     IF((DELWJ.GE.0.0).AND.(DELWI.LT.0.0)) GO TO 309
 306 A(J)=R(I)*ADR/(DZ*ETA*RHOL(I,J))
      B(J)=ABSWJ*ADR/(2.*DR)+BVAL
      C(J)=-(ABSWI-R(I)*ADR/(DZ*ETA*RHOL(I,J)))
      D(J)=-E(I+1,J)*(2.*R(I)*DZ/(ETA*RHOL(I,J)*DR1)+DZ*DDR/(ETA*
     1RHOL(I,J)))+E(I-1,J)*(ABSWJ*ADR/(2.*DR)-2.*R(I)*DZ/(ETA*DR*
     2RHOL(I,J)))+DZ/(DDR*ETA*RHOL(I,J)))-DVAL*R(I)*ADR*DZ/RHOL(I,J)
     GO TO 115
 307 A(J)=-(ABSWI-R(I)*ADR/(DZ*ETA*RHOL(I,J)))
      B(J)=ABSWJ*ADR/(2.*DR1)+BVAL
      C(J)=R(I)*ADR/(DZ*ETA*RHOL(I,J))
      D(J)=E(I+1,J)*(ABSWJ*ADR/(2.*DR1)-2.*R(I)*DZ/(DR1*ETA*RHOL(I,J)))-
     1DZ*DDR/(ETA*RHOL(I,J)))-E(I-1,J)*(2.*R(I)*DZ/(ETA*RHOL(I,J)*DR)-
     2DZ/(DDR*ETA*RHOL(I,J)))-DVAL*R(I)*ADR*DZ/RHOL(I,J)
     GO TO 115
 308 A(J)=-(ABSWI-R(I)*ADR/(DZ*ETA*RHOL(I,J)))
      B(J)=ABSWJ*ADR/(2.*DR)+BVAL
      C(J)=R(I)*ADR/(DZ*ETA*RHOL(I,J))
      D(J)=-E(I+1,J)*(2.*R(I)*DZ/(ETA*RHOL(I,J)*DR1)+DZ*DDR/(ETA*
     1RHOL(I,J)))+E(I-1,J)*(ABSWJ*ADR/(2.*DR)-2.*R(I)*DZ/(ETA*DR*
     2RHOL(I,J)))+DZ/(DDR*ETA*RHOL(I,J)))-DVAL*R(I)*ADR*DZ/RHOL(I,J)
     GO TO 115
 309 A(J)=R(I)*ADR/(DZ*ETA*RHOL(I,J))
      B(J)=ABSWJ*ADR/(2.*DR1)+BVAL
      C(J)=-(ABSWI-R(I)*ADR/(DZ*ETA*RHOL(I,J)))
      D(J)=E(I+1,J)*(ABSWJ*ADR/(2.*DR1)-2.*R(I)*DZ/(DR1*ETA*RHOL(I,J)))-
     1DZ*DDR/(ETA*RHOL(I,J)))-E(I-1,J)*(2.*R(I)*DZ/(ETA*RHOL(I,J)*DR)-
     2DZ/(DDR*ETA*RHOL(I,J)))-DVAL*R(I)*ADR*DZ/RHOL(I,J)
 115 CONTINUE
     CALL TRIDAG (2,M1,A,B,C,D,TT)
     DO 120 J=2,M1
 120 VOR(I,J)=TT(J)
 110 CONTINUE
     DO 125 J=1,M
     VOR(1,J)=0.0
      VOR(N,J)=2.*W(N-1,J)/(R(N)*DR1*DR1)
 125 CONTINUE
     DO 140 I=2,N
     VOR(I,M)=0.0
      VOR(I,1)=2.*W(I,2)/(R(I)*DZ*DZ)
 140 CONTINUE
 C    I-DIRECTION.....
     DO 145 J=2,M1
     DO 150 I=2,N1
     DR=0.1
     DTLR=DR/DZ
       DVAL=VSTRCO*(SIN(3.3334*Z(J)))*((VV(I)*AA*XX(I)-VV(I)*BB*
      1YY(I)-UU(I)*BB*XX(I)-UU(I)*AA*YY(I))/((AA*AA+BB*BB)*(U0*
     2U0+V0*V0)))
 C    RHOL(I,J)=(8102.2-0.7170S*(TL(I,J)*300.))/7600.
 C    RHOL(I,J)=1.0
     IF(I.EQ.NN) GO TO 141
     IF(I.GT.NN) GO TO 142
     GO TO 143
 142 DR=DR1
     DTLR=DR/DZ
 143 DELWJ=W(I,J+1)-W(I,J-1)
      DELWI=W(I+1,J)-W(I-1,J)
      ABSWJ=ABS(DELWJ)
      ABSWI=ABS(DELWI)
     IF((DELWJ.LT.0.0).AND.(DELWI.LT.0.0)) GO TO 311
     IF((DELWJ.GE.0.0).AND.(DELWI.GE.0.0)) GO TO 312
     IF((DELWJ.LT.0.0).AND.(DELWI.GE.0.0)) GO TO 313
```

```
      IF((DELWJ.GE.0.0).AND.(DELWI.LT.0.0)) GO TO 314
  311 A(I)=-ABSWJ/(2.*R(I))+1./(DTLR*ETA*RHOL(I,J))-DZ/(2.*R(I)*ETA*
     1RHOL(I,J))
        B(I)=(ABSWI/(2.*R(I))+ABSWJ/(2.*R(I))+ABSWJ*DR/(R(I)*
     1R(I)*2.)-2./(DTLR*ETA*RHOL(I,J))-DR*DZ/(R(I)*R(I)*ETA*RHOL(I,J))-
     2(2.*DTLR/(ETA*RHOL(I,J))))
        C(I)=(1./(DTLR*ETA*RHOL(I,J))+DZ/(2.*R(I)*ETA*RHOL(I,J)))
        D(I)=E(I,J+1)*(ABSWI/(2.*R(I))-DTLR/(ETA*RHOL(I,J)))-E(I,J-1)*
     1(DTLR/(ETA*RHOL(I,J)))-DVAL*DR*DZ/RHOL(I,J)
      GO TO 150
  312 A(I)=(1./(DTLR*ETA*RHOL(I,J))-DZ/(2.*R(I)*ETA*RHOL(I,J)))
        B(I)=(ABSWI/(2.*R(I))+ABSWJ/(2.*R(I))+ABSWJ*DR/(R(I)*
     1R(I)*2.)-2./(DTLR*ETA*RHOL(I,J))-DR*DZ/(R(I)*R(I)*ETA*RHOL(I,J))-
     2(2.*DTLR/(ETA*RHOL(I,J))))
        C(I)=-ABSWJ/(2.*R(I))+1./(DTLR*ETA*RHOL(I,J))+DZ/(2.*R(I)*ETA*
     1RHOL(I,J))
        D(I)=-E(I,J+1)*(DTLR/(ETA*RHOL(I,J)))+E(I,J-1)*(ABSWI/(2.*R(I))-
     1DTLR/(ETA*RHOL(I,J)))-DVAL*DR*DZ/RHOL(I,J)
      GO TO 150
  313 A(I)=-ABSWJ/(2.*R(I))+1./(DTLR*ETA*RHOL(I,J))-DZ/(2.*R(I)*ETA*
     1RHOL(I,J))
        B(I)=(ABSWI/(2.*R(I))+ABSWJ/(2.*R(I))+ABSWJ*DR/(R(I)*
     1R(I)*2.)-2./(DTLR*ETA*RHOL(I,J))-DR*DZ/(R(I)*R(I)*ETA*RHOL(I,J))-
     2(2.*DTLR/(ETA*RHOL(I,J))))
        C(I)=(1./(DTLR*ETA*RHOL(I,J))+DZ/(2.*R(I)*ETA*RHOL(I,J)))
        D(I)=-E(I,J+1)*(DTLR/(ETA*RHOL(I,J)))+E(I,J-1)*(ABSWI/(2.*R(I))-
     1DTLR/(ETA*RHOL(I,J)))-DVAL*DR*DZ/RHOL(I,J)
      GO TO 150
  314 A(I)=(1./(DTLR*ETA*RHOL(I,J))-DZ/(2.*R(I)*ETA*RHOL(I,J)))
        B(I)=(ABSWI/(2.*R(I))+ABSWJ/(2.*R(I))+ABSWJ*DR/(R(I)*
     1R(I)*2.)-2./(DTLR*ETA*RHOL(I,J))-DR*DZ/(R(I)*R(I)*ETA*RHOL(I,J))-
     2(2.*DTLR/(ETA*RHOL(I,J))))
        C(I)=-ABSWJ/(2.*R(I))+1./(DTLR*ETA*RHOL(I,J))+DZ/(2.*R(I)*ETA*
     1RHOL(I,J))
        D(I)=E(I,J+1)*(ABSWI/(2.*R(I))-DTLR/(ETA*RHOL(I,J)))-E(I,J-1)*
     1(DTLR/(ETA*RHOL(I,J)))-DVAL*DR*DZ/RHOL(I,J)
      GO TO 150
  141 DELWI=(W(I+1,J)-W(I,J))*DDR-(W(I-1,J)-W(I,J))*(1./DDR)
      DELWJ=W(I,J+1)-W(I,J-1)
      ABSWI=ABS(DELWI)
      ABSWJ=ABS(DELWJ)
       BVAL=ABSWI+ABSWJ*ADR/(2.*R(I))-2.*R(I)*DZ/(ETA*RHOL(I,J)*DDR)
     1-2.*R(I)*DZ/(ETA*RHOL(I,J)*DR1)-DZ*DDR/(ETA*RHOL(I,J))+DZ*
     2(DDR*ETA*RHOL(I,J))-ADR*DZ/(R(I)*ETA*RHOL(I,J))-2.*R(I)*ADR/
     3(DZ*ETA*RHOL(I,J))
       AVAL=(ABSWJ*ADR/(2.*DR)-2.*R(I)*DZ/(ETA*RHOL(I,J)*DR)+
     1DZ/(DDR*ETA*RHOL(I,J)))
      CVAL=2.*R(I)*DZ/(ETA*RHOL(I,J)*DR1)+DZ*DDR/(ETA*RHOL(I,J))
      IF((DELWJ.LT.0.0).AND.(DELWI.LT.0.0)) GO TO 221
      IF((DELWJ.GE.0.0).AND.(DELWI.GE.0.0)) GO TO 222
      IF((DELWJ.LT.0.0).AND.(DELWI.GE.0.0)) GO TO 223
      IF((DELWJ.GE.0.0).AND.(DELWI.LT.0.0)) GO TO 224
  221 A(I)=-AVAL
       B(I)=ABSWJ*ADR/(2.*DR)+BVAL
      C(I)=CVAL
       D(I)=E(I,J+1)*(ABSWI-R(I)*ADR/(DZ*ETA*RHOL(I,J)))-E(I,J-1)*(R(I)*
     1ADR/(DZ*ETA*RHOL(I,J)))-DVAL*R(I)*ADR*DZ/RHOL(I,J)
      GO TO 150
  222 A(I)=2.*R(I)*DZ/(ETA*RHOL(I,J)*DR)-DZ/(DDR*ETA*RHOL(I,J))
       B(I)=ABSWJ*ADR/(2.*DR1)+BVAL
       C(I)=-(ABSWJ*ADR/(2.*DR1)-2.*R(I)*DZ/(DR1*ETA*RHOL(I,J)))-
     1DZ*DDR/(ETA*RHOL(I,J))
       D(I)=-E(I,J+1)*(R(I)*ADR/(DZ*ETA*RHOL(I,J)))+E(I,J-1)*(ABSWI-R(I)*
     1ADR/(DZ*ETA*RHOL(I,J)))-DVAL*R(I)*ADR*DZ/RHOL(I,J)
      GO TO 150
  223 A(I)=-AVAL
       B(I)=ABSWJ*ADR/(2.*DR)+BVAL
      C(I)=CVAL
       D(I)=-E(I,J+1)*(R(I)*ADR/(DZ*ETA*RHOL(I,J)))+E(I,J-1)*(ABSWI-R(I)*
     1ADR/(DZ*ETA*RHOL(I,J)))-DVAL*R(I)*ADR*DZ/RHOL(I,J)
      GO TO 150
  224 A(I)=2.*R(I)*DZ/(ETA*RHOL(I,J)*DR)-DZ/(DDR*ETA*RHOL(I,J))
       B(I)=ABSWJ*ADR/(2.*DR1)+BVAL
       C(I)=-(ABSWJ*ADR/(2.*DR1)-2.*R(I)*DZ/(DR1*ETA*RHOL(I,J)))-
     1DZ*DDR/(ETA*RHOL(I,J)))
       D(I)=E(I,J+1)*(ABSWI-R(I)*ADR/(DZ*ETA*RHOL(I,J)))-E(I,J-1)*(R(I)*
```

```
     1ADR/(DZ*ETA*RHOL(I,J)))-DVAL*R(I)*ADR*DZ/RHOL(I,J)
150 CONTINUE
    CALL TRIDAG (2,N1,A,B,C,D,TT)
    DO 155 I=2,N1
155 VOR(I,J)=TT(I)
145 CONTINUE
    DO 160 I=2,N
    VOR(I,M)=0.0
    VOR(I,1)=2.*W(I,2)/(R(I)*DZ*DZ)
160 CONTINUE
    DO 165 J=1,M
    VOR(1,J)=0.0
     VOR(N,J)=2.*W(N-1,J)/(R(N)*DR1*DR1)
165 CONTINUE
    DO 166 I=1,N
    DO 167 J=1,M
     E(I,J)=UVF*VOR(I,J)+(1.-UVF)*E(I,J)
167 CONTINUE
166 CONTINUE
C   IF(MKK.EQ.ITERIN-1) GO TO 1131
    IF(MKK.EQ.ITERIN) GO TO 1131
    GO TO 1111
1131 WRITE(33,900) MKK
900  FORMAT(1X,'AFTER',I4,'TH ITERATION THE FIRST 10 VALUES OF
     1INDUCTION STREAM FUNCTION IN RADIAL DIRECTION ARE:',/)
      WRITE(33,910) ((W(I,J),I=1,NNN1),J=1,M)
910  FORMAT(2X,10F11.5/)
     WRITE(33,911) MKK
911   FORMAT(1X,'AFTER',I4,'TH ITERATION THE LAST 11 VALUES OF
    1INDUCTION STREAM FUNCTION IN RADIAL DIRECTION ARE:',/)
     WRITE(33,912) ((W(I,J),I=NNN,N),J=1,M)
912  FORMAT(2X,10F11.5/)
     WRITE(34,901) MKK
901  FORMAT(1X,'AFTER',I4,'TH ITERATION THE FIRST 10 VALUES OF
    1INDUCTION VORTICITY IN RADIAL DIRECTION ARE:',/)
    WRITE(34,902) ((E(I,J),I=1,NNN1),J=1,M)
902  FORMAT(2X,10F12.4/)
     WRITE(34,904) MKK
```

```
904   FORMAT(1X,'AFTER',I4,'TH ITERATION THE LAST 11 VALUES OF
     1INDUCTION VORTICITY IN RADIAL DIRECTION ARE:',/)
      WRITE(34,905) ((E(I,J),I=NNN,N),J=1,M)
905   FORMAT(2X,10F12.4/)
1111  CONTINUE
     DR=0.1
     DO 97 I=2,N1
     DO 98 J=2,M1
C     print *,DR,DTLR
     IF(I.EQ.8) GO TO 93
     IF(I.GT.8) GO TO 99
     GO TO 96
99   DR=DR1
96    UR(I,J)=(W(I,J+1)-W(I,J-1))/(R(I)*2.*DZ)
      UZ(I,J)=-((W(I+1,J)-W(I-1,J))/(R(I)*2.*DR))
     GO TO 98
93    UZ(I,J)=-(1./ADR*R(I))*((W(I+1,J)-W(I,J))*DDR-(W(I-1,J)-W(I,J))*
    1(1./DDR))
      UR(I,J)=(W(I,J+1)-W(I,J-1))/(R(I)*2.*DZ)
98   CONTINUE
97   CONTINUE
     DO 101 I=2,N1
     IF(I.GT.8) GO TO 231
     GO TO 232
231  DR=DR1
232  UZ(I,1)=-((W(I+1,1)-W(I-1,1))/(2.*R(I)*DR))
      UZ(I,M)=-((W(I+1,M)-W(I-1,M))/(2.*R(I)*DR))
      UR(I,1)=(W(I,2)-W(I,1))/(R(I)*DZ)
      UR(I,M)=(W(I,M)-W(I,M1))/(R(I)*DZ)
101  CONTINUE
     DR=0.1
     DO 102 J=2,M1
      UZ(1,J)=-(2.*(W(2,J)-W(1,J)))/(DR*DR)
      UZ(N,J)=-((W(N,J)-W(N1,J))/(R(N)*DR1))
     UR(1,J)=0.0
      UR(N,J)=(W(N,J+1)-W(N,J-1))/(2.*R(N)*DZ)
102  CONTINUE
     UR(1,1)=0.0
```

```
      UR(I,M)=0.0
       UZ(1,1)=-(2.*(W(2,1)-W(1,1)))/(DR*DR)
       UZ(N,1)=-((W(N,1)-W(N1,1))/(R(N)*DR1))
       UR(N,1)=(W(N,2)-W(N,1))/(R(N)*DZ)
       UR(N,M)=(W(N,M)-W(N,M1))/(R(N)*DZ)
       UZ(1,M)=-(2.*(W(2,M)-W(1,M)))/(DR*DR)
       UZ(N,M)=-(W(N,M)-W(N1,M))/(R(N)*DR1)
      DR=0.1
      DTLR=DR/DZ
       RETURN
      END
C
C     ****************************************************
C
C      SUBROUTINE FOR LIQUID TEMP. IN INDUCTION REGION
C
C     ****************************************************
C
       SUBROUTINE INDTMP
       SAVE
        COMMON/AREA1/LL,LL1,LNK,LNK1,DRB,D0,D0R,RYN,PEMT,PEHT,
       1VFB,DELTB,DELTB1,TIMEB,TIMEB1,RP,RF,TNP,PAI,ITERB,ITER1,UFG,
       2MP,UFW,UFE,THKM,DENP,BEDH,TOTZ,DLRP,ALHM,VFP,DAKP,
       3DAKM,UCHAR,COFSMR,COFLAR,ATMLOS,PMW,AMWMIX,DENMIX,
      3DLRCEL,CONSEH,POWIND,HEATBL,HITMEL,HFEPRO,ACUHIT,
      4CFEOPR,COUTFL,VSTRCO,TINIT,ALHM1
       COMMON/AREA3/WB(21,21),EB(21,21),TM(21,21),CFEO(21,21),
      1TL(21,21),W(21,21),E(21,21),TG(31,31),CMO2(31,31),UR(21,21),
      2UZ(21,21),VR(31,31),VZ(31,31)
       COMMON/AREA5/A(31),B(31),C(31),D(31),TT(31)
       COMMON/AREA6/MM,MM1,DZG,PEGHT,PEGMT,RBLV,DELTGH,
      1TIMEG,DELTGM
       COMMON/AREA8/CPG(31,31),AKG(31,31),RHOG(31,31),DOABL(31,31)
        COMMON/AREA9/N,M,NN,N1,M1,DZ,DR,DR1,DTLR,PEL,DPOWER,
        1ITERIN,DELT,NNN1,TIME,ETA,ADR,DDR,UVF,OSF,AA,BB,U0,V0,
      2NNN,ORIGZ,DH
       COMMON/AREA10/R(22),Z(22),UU(22),VV(22),XX(22),YY(22)
      COMMON/AREA11/RHOL(22,22),CPL(22,22),AKL(22,22)
        UINF=0.0
        TMAV=0.0
        TLAV=0.0
        TINF=0.0
        ARM=0.0
        TURAV=0.0
        CALL PTEMPAV (TM,LL,LNK,TMAV)
        CALL AVRG (UR,TL,M,DZ,MP,UINF,TLAV,TURAV)
        CALL TINFAVIT (TM,TL,LL,N,M,DAKP,DRB,TINF,ARM)
        ABSUIN=ABS(UINF)
        ABSTUR=ABS(TURAV)
C      J-DIRECTION.....
       DO 30 I=1,N
       DO 35 J=1,M
       DR=0.1
       DTLR=DR/DZ
          EH=(CONSEH*((SIN(1.6667*Z(J)))**2)*((4.*UU(I)*VV(I)*U0*V0*
          1(AA**2-BB*2)+4.*UU(I)*VV(I)*AA*BB*(U0**2-V0**2)-4.*U0*V0*
         2AA*BB*((UU(I))**2-(VV(I))**2)+(AA**2-BB**2)*((UU(I))**2-
         3(VV(I))**2)*(U0**2-V0**2))/(((AA**2+BB**2)**2)*((U0**2+
       4V0**2)**2))))
C      RHOL(I,J)=(8102.2-0.71708*(TL(I,J)*300.))/7600.
       RHOL(I,J)=1.0
       IF(TL(I,J).LE.5.8) GO TO 501
       CPL(I,J)=(10.052+4.08E-05*(TL(I,J)*300.)-8.4E+03/
      1((TL(I,J)*300.)**2))/5.82157
       GO TO 499
  501  CPL(I,J)=(4.82+2.92E-03*(TL(I,J)*300.)-8.4E+03/
      1((TL(I,J)*300.)**2))/5.82157
C      PRINT *,EH
  499  ABSUR=ABS(UR(I,J))
       ABSUZ=ABS(UZ(I,J))
       IF(I.EQ.NN) GO TO 500
       IF(I.GT.NN) GO TO 502
       GO TO 503
  502  DR=DR1
       DTLR=DR/DZ
  503  IF((I.EQ.1).AND.(J.EQ.1)) GO TO 51
```

```
      IF((I.EQ.N).AND.(J.EQ.1)) GO TO 52
      IF(J.EQ.1) GO TO 40
      IF(J.EQ.M) GO TO 45
      IF(I.EQ.1) GO TO 31
      IF(I.EQ.N) GO TO 32
      IF((UR(I,J).GE.0.0).AND.(UZ(I,J).GE.0.0)) GO TO 41
      IF((UR(I,J).LT.0.0).AND.(UZ(I,J).LT.0.0)) GO TO 42
      IF((UR(I,J).LT.0.0).AND.(UZ(I,J).GE.0.0)) GO TO 43
      IF((UR(I,J).GE.0.0).AND.(UZ(I,J).LT.0.0)) GO TO 44
   41 A(J)=-(PEL*RHOL(I,J)*CPL(I,J)*ABSUZ*DR*DR/DZ+AKL(I,J)*DR*
     1DR/(DZ*DZ))
      B(J)=RHOL(I,J)*CPL(I,J)*DR*DR/DELT+PEL*RHOL(I,J)*CPL(I,J)*
      1ABSUR*DR+PEL*RHOL(I,J)*CPL(I,J)*ABSUZ*DR*DR/DZ+2.*AKL(I,J)+2.*
     2AKL(I,J)*DR*DR/(DZ*DZ)
      C(J)=-AKL(I,J)*DR*DR/(DZ*DZ)
      D(J)=TL(I-1,J)*(PEL*RHOL(I,J)*CPL(I,J)*ABSUR*DR+AKL(I,J)-
      1AKL(I,J)*DR/(2.*R(I)))+TL(I+1,J)*(AKL(I,J)+AKL(I,J)*DR/(2.*
      2R(I)))+EH*DR*DR+TL(I,J)*(RHOL(I,J)*CPL(I,J)*DR*DR/DELT)
      GO TO 35
   42 A(J)=-AKL(I,J)*DR*DR/(DZ*DZ)
      B(J)=RHOL(I,J)*CPL(I,J)*DR*DR/DELT+PEL*RHOL(I,J)*CPL(I,J)*
      1ABSUR*DR+PEL*RHOL(I,J)*CPL(I,J)*ABSUZ*DR*DR/DZ+2.*AKL(I,J)+2.*
     2AKL(I,J)*DR*DR/(DZ*DZ)
      C(J)=-(PEL*RHOL(I,J)*CPL(I,J)*ABSUZ*DR*DR/DZ+AKL(I,J)*DR*
     1DR/(DZ*DZ))
      D(J)=TL(I-1,J)*(AKL(I,J)-AKL(I,J)*DR/(2.*R(I)))+TL(I+1,J)*
      1(PEL*RHOL(I,J)*CPL(I,J)*ABSUR*DR+AKL(I,J)*DR/(2.*R(I))+
      2AKL(I,J))+EH*DR*DR+TL(I,J)*(RHOL(I,J)*CPL(I,J)*DR*DR/DELT)
      GO TO 35
   43 A(J)=-(PEL*RHOL(I,J)*CPL(I,J)*ABSUZ*DR*DR/DZ+AKL(I,J)*DR*
     1DR/(DZ*DZ))
      B(J)=RHOL(I,J)*CPL(I,J)*DR*DR/DELT+PEL*RHOL(I,J)*CPL(I,J)*
      1ABSUR*DR+PEL*RHOL(I,J)*CPL(I,J)*ABSUZ*DR*DR/DZ+2.*AKL(I,J)+2.*
     2AKL(I,J)*DR*DR/(DZ*DZ)
      C(J)=-AKL(I,J)*DR*DR/(DZ*DZ)
      D(J)=TL(I-1,J)*(AKL(I,J)-AKL(I,J)*DR/(2.*R(I)))+TL(I+1,J)*
      1(PEL*RHOL(I,J)*CPL(I,J)*ABSUR*DR+AKL(I,J)*DR/(2.*R(I))+
      2AKL(I,J))+EH*DR*DR+TL(I,J)*(RHOL(I,J)*CPL(I,J)*DR*DR/DELT)
      GO TO 35
   44 A(J)=-AKL(I,J)*DR*DR/(DZ*DZ)
      B(J)=RHOL(I,J)*CPL(I,J)*DR*DR/DELT+PEL*RHOL(I,J)*CPL(I,J)*
      1ABSUR*DR+PEL*RHOL(I,J)*CPL(I,J)*ABSUZ*DR*DR/DZ+2.*AKL(I,J)+2.*
     2AKL(I,J)*DR*DR/(DZ*DZ)
      C(J)=-(PEL*RHOL(I,J)*CPL(I,J)*ABSUZ*DR*DR/DZ+AKL(I,J)*DR*
     1DR/(DZ*DZ))
      D(J)=TL(I-1,J)*(PEL*RHOL(I,J)*CPL(I,J)*ABSUR*DR+AKL(I,J)-
      1AKL(I,J)*DR/(2.*R(I)))+TL(I+1,J)*(AKL(I,J)+AKL(I,J)*DR/
      2(2.*R(I)))+EH*DR*DR+TL(I,J)*(RHOL(I,J)*CPL(I,J)*DR*DR/DELT)
      GO TO 35
   31 IF(UZ(I,J).GE.0.0) GO TO 46
      A(J)=-AKL(I,J)*DR*DR/(DZ*DZ)
      B(J)=RHOL(I,J)*CPL(I,J)*DR*DR/DELT+PEL*RHOL(I,J)*CPL(I,J)*
      1ABSUZ*DR*DR/DZ+4.*AKL(I,J)+2.*AKL(I,J)*DR*DR/(DZ*DZ)
      C(J)=-(PEL*RHOL(I,J)*CPL(I,J)*ABSUZ*DR*DR/DZ+AKL(I,J)*DR*
     1DR/(DZ*DZ))
      D(J)=EH*DR*DR+TL(I,J)*(RHOL(I,J)*CPL(I,J)*DR*DR/DELT)+
     1TL(I+1,J)*(4.*AKL(I,J))
      GO TO 35
   46 A(J)=-(PEL*RHOL(I,J)*CPL(I,J)*ABSUZ*DR*DR/DZ+AKL(I,J)*DR*
     1DR/(DZ*DZ))
      B(J)=RHOL(I,J)*CPL(I,J)*DR*DR/DELT+PEL*RHOL(I,J)*CPL(I,J)*
      1ABSUZ*DR*DR/DZ+4.*AKL(I,J)+2.*AKL(I,J)*DR*DR/(DZ*DZ)
      C(J)=-AKL(I,J)*DR*DR/(DZ*DZ)
      D(J)=EH*DR*DR+TL(I,J)*(RHOL(I,J)*CPL(I,J)*DR*DR/DELT)+
     1TL(I+1,J)*(4.*AKL(I,J))
      GO TO 35
   32 A(J)=AKL(I,J)/DR
      B(J)=-(AKL(I,J)/DR+0.327222/(-0.1823215))
      C(J)=0.0
      D(J)=-4.0*0.3272222/(-0.1823215)
      GO TO 35
C
C
C
C
C
```

```
     1DR/(DZ*DZ))
C    B(J)=RHOL(I,J)*CPL(I,J)*DR*DR/DELT+PEL*RHOL(I,J)*CPL(I,J)*
C    1ABSUZ*DR*DR/DZ+2.*AKL(I,J)+2.*AKL(I,J)*DR*DR/(DZ*DZ)
C    C(J)=-AKL(I,J)*DR*DR/(DZ*DZ)
C    D(J)=EH*DR*DR+TL(I,J)*(RHOL(I,J)*CPL(I,J)*DR*DR/DELT)+
C    1TL(I-1,J)*(2.*AKL(I,J))
C    GO TO 35
40       A(J)=0.0
         B(J)=((TTIM**(1./2.))/DZ-35.0
         C(J)=-((TTIM**(1./2.))/DZ)
         D(J)=-2.0*35.0
         GO TO 35
C

C    A(J)=0.0
C    B(J)=RHOL(I,J)*CPL(I,J)*DR*DR/DELT+PEL*RHOL(I,J)*CPL(I,J)*
C    1ABSUR*DR+2.*AKL(I,J)+2.*AKL(I,J)*DR*DR/(DZ*DZ)
C    C(J)=-(2.*AKL(I,J)*DR*DR/(DZ*DZ))
C    D(J)=EH*DR*DR+TL(I,J)*(RHOL(I,J)*CPL(I,J)*DR*DR/DELT)+
C    1TL(I+1,J)*(AKL(I,J)+AKL(I,J)*DR/(2.*R(I)))+TL(I-1,J)*(PEL*
C    2RHOL(I,J)*CPL(I,J)*ABSUR*DR+AKL(I,J)-AKL(I,J)*DR/(2.*R(I)))
C    GO TO 35
45   GASHIT=((1.17965E+01)*(1.-VFP)*(EXP(-54.667/TINF))*
     1(-22251.5-8.57*300.*TINF-(1.03E+03)*((300.*TINF)**2)-
     2(4.49E+05)/(300.*TINF))-19.10637*AKG(I,M)*((TG(I,M+1)-
     3TG(I,M))/DZG))*R(I)*R(I)
     BCPART=(5.85714E+03)*(EXP((-5.85714E+03)*TIMEB))*((DLRCEL**3)-
     1(DLRP**3))*(31712.+2.89*300.*TMAV-(0.53E-03)*((300.*TMAV)**2)-
     2(4.09E+05)/(300.*TMAV))
     A(J)=0.0
     B(J)=1.0
     C(J)=0.0
     D(J)=(RHOL(I,J)*CPL(I,J)*R(N)*DH*ABSTUR+POWIND*(DH*DPOWER/
     1TOTZ)+HEATBL*GASHIT-HITMEL*(1.-VFP)*RP*(-ARM*(DLRP**2)/
     2ALHM1*HFEPRO*RP*BCPART+ACUHIT*(R(N)**2)*DH*RHOL(I,J))*
     3CPL(I,J)*TL(I,M)/DELT)/(RHOL(I,J)*CPL(I,J)*R(N)*DH*ABSUIN+
     4(ACUHIT*(R(N)**2)*DH*RHOL(I,J)*CPL(I,J))/DELT)
     GO TO 35

51       A(J)=0.0
         B(J)=1.0
         C(J)=0.0
         D(J)=4.9
         GO TO 65
52       A(J)=0.0
         B(J)=1.0
         C(J)=0.0
         D(J)=4.9

     GO TO 35
500  BVAL=RHOL(I,J)*CPL(I,J)*ADR/DELT+ABSUZ*PEL*RHOL(I,J)*
     1CPL(I,J)*ADR/DZ+2.*AKL(I,J)/DR+2.*AKL(I,J)/DR1+AKL(I,J)*
     2DDR/R(I)-AKL(I,J)/(R(I)*DDR)+2.*AKL(I,J)*ADR/(DZ*DZ)
     DVAL=EH*ADR+TL(I,J)*(RHOL(I,J)*CPL(I,J)*ADR/DELT)
     IF(J.EQ.1) GO TO 506
     IF(J.EQ.M) GO TO 45
     IF((UR(I,J).LT.0.0).AND.(UZ(I,J).LT.0.0)) GO TO 511
     IF((UR(I,J).GE.0.0).AND.(UZ(I,J).GE.0.0)) GO TO 512
     IF((UR(I,J).GE.0.0).AND.(UZ(I,J).LT.0.0)) GO TO 513
     IF((UR(I,J).LT.0.0).AND.(UZ(I,J).GE.0.0)) GO TO 514
511  A(J)=-(AKL(I,J)*ADR/(DZ*DZ))
       B(J)=PEL*RHOL(I,J)*CPL(I,J)*ABSUR*ADR/DR1+BVAL
       C(J)=-(PEL*RHOL(I,J)*CPL(I,J)*ABSUZ*ADR/DZ+AKL(I,J)*
     1ADR/(DZ*DZ))
       D(J)=TL(I+1,J)*(PEL*RHOL(I,J)*CPL(I,J)*ABSUR*ADR/DR1+2.*
     1AKL(I,J)/DR1+AKL(I,J)*DDR/R(I))+TL(I-1,J)*(2.*AKL(I,J)/DR-
     2AKL(I,J)/(R(I)*DDR))+DVAL
     GO TO 35
512  A(J)=-(PEL*RHOL(I,J)*CPL(I,J)*ABSUZ*ADR/DZ+AKL(I,J)*
     1ADR/(DZ*DZ))
       B(J)=PEL*RHOL(I,J)*CPL(I,J)*ABSUR*ADR/DR+BVAL
     C(J)=-(AKL(I,J)*ADR/(DZ*DZ))
```

```
     D(J)=TL(I+1,J)*(2.*AKL(I,J)/DR1+AKL(I,J)*DDR/R(I))+TL(I-1,J)*
     1(PEL*RHOL(I,J)*CPL(I,J)*ABSUR*ADR/DR+2.*AKL(I,J)/DR-
     2AKL(I,J)/(R(I)*DDR))+DVAL
     GO TO 35
513  A(J)=-(AKL(I,J)*ADR/(DZ*DZ))
      B(J)=PEL*RHOL(I,J)*CPL(I,J)*ABSUR*ADR/DR+BVAL
      C(J)=-(PEL*RHOL(I,J)*CPL(I,J)*ABSUZ*ADR/DZ+AKL(I,J)*ADR/(DZ*DZ))
      D(J)=TL(I+1,J)*(2.*AKL(I,J)/DR1+AKL(I,J)*DDR/R(I))+TL(I-1,J)*
     1(PEL*RHOL(I,J)*CPL(I,J)*ABSUR*ADR/DR+2.*AKL(I,J)/DR-
     2AKL(I,J)/(R(I)*DDR))+DVAL
     GO TO 35
514  A(J)=-(PEL*RHOL(I,J)*CPL(I,J)*ABSUZ*ADR/DZ+AKL(I,J)*
    1ADR/(DZ*DZ))
      B(J)=PEL*RHOL(I,J)*CPL(I,J)*ABSUR*ADR/DR1+BVAL
     C(J)=-(AKL(I,J)*ADR/(DZ*DZ))
      D(J)=TL(I+1,J)*(PEL*RHOL(I,J)*CPL(I,J)*ABSUR*ADR/DR1+2.*
     1AKL(I,J)/DR1+AKL(I,J)*DDR/R(I))+TL(I-1,J)*(2.*AKL(I,J)/DR-
     2AKL(I,J)/(R(I)*DDR))+DVAL
     GO TO 35
506  IF(UR(I,J).GE.0.0) GO TO 507
     A(J)=0.0
     B(J)=RHOL(I,J)*CPL(I,J)*ADR/DELT+PEL*RHOL(I,J)*CPL(I,J)*
     1ABSUR*ADR/DR1+2.*AKL(I,J)/DR+2.*AKL(I,J)/DR1+AKL(I,J)*
     2DDR/R(I)-AKL(I,J)/(R(I)*DDR)+2.*AKL(I,J)*ADR/(DZ*DZ)
     C(J)=-(2.*AKL(I,J)*ADR/(DZ*DZ))
      D(J)=TL(I+1,J)*(PEL*RHOL(I,J)*CPL(I,J)*ABSUR*ADR/DR1+2.*
     1AKL(I,J)/DR1+AKL(I,J)*DDR/R(I))+TL(I-1,J)*(2.*AKL(I,J)/DR-
     2AKL(I,J)/(R(I)*DDR))+DVAL
     GO TO 35
507  A(J)=0.0
     B(J)=RHOL(I,J)*CPL(I,J)*ADR/DELT+PEL*RHOL(I,J)*CPL(I,J)*
     1ABSUR*ADR/DR+2.*AKL(I,J)/DR+2.*AKL(I,J)/DR1+AKL(I,J)*
     2DDR/R(I)-AKL(I,J)/(R(I)*DDR)+2.*AKL(I,J)*ADR/(DZ*DZ)
     C(J)=-(2.*AKL(I,J)*ADR/(DZ*DZ))
      D(J)=TL(I+1,J)*(2.*AKL(I,J)/DR1+AKL(I,J)*DDR/R(I))+TL(I-1,J)*
     1(PEL*RHOL(I,J)*CPL(I,J)*ABSUR*ADR/DR+2.*AKL(I,J)/DR-
     2AKL(I,J)/(R(I)*DDR))+DVAL
 35  CONTINUE
     CALL TRIDAG (1,M,A,B,C,D,TT)
     DO 50 J=1,M
 50  TL(I,J)=TT(J)
 30  CONTINUE
C    I-DIRECTION.....
     DO 60 J=1,M
     DO 65 I=1,N
     DR=0.1
     DTLR=DR/DZ
       ETT=(CONSET*((SIN(1.6667*Z(J)))**2)*((4.*UU(I)*VV(I)*U0*V0*
       1(AA**2-BB**2)+4.*UU(I)*VV(I)*AA*BB*(U0**2-V0**2)-4.*U0*V0*
       2AA*BB*(UU(I)**2-VV(I)**2)+(AA**2-BB**2)*(UU(I)**2-
       3VV(I)**2)*(U0**2-V0**2))/(((AA**2+BB**2)**2)*((U0**2+
     4V0**2)**2))))
C    RHOL(I,J)=(8102.2-0.7170S*(TL(I,J)*300.))/7600.
     RHOL(I,J)=1.0
     IF(TL(I,J).LE.5.8) GO TO 549
     CPL(I,J)=(10.052+4.08E-05*(TL(I,J)*300.)-8.4E+03/
     1((TL(I,J)*300.)**2))/5.82157
     GO TO 548
549  CPL(I,J)=(4.82+2.92E-03*(TL(I,J)*300.)-8.4E+03/
     1((TL(I,J)*300.)**2))/5.82157
548  ABSUR=ABS(UR(I,J))
     ABSUZ=ABS(UZ(I,J))
     IF(I.EQ.NN) GO TO 551
     IF(I.GT.NN) GO TO 552
     GO TO 553
552  DR=DR1
     DTLR=DR/DZ
553  IF(I.EQ.1).AND.(J.EQ.1)) GO TO 81
     IF((I.EQ.N).AND.(J.EQ.1)) GO TO 82
     IF(J.EQ.1) GO TO 66
     IF(J.EQ.M) GO TO 67
     IF(I.EQ.1) GO TO 70
     IF(I.EQ.N) GO TO 75
     IF((UR(I,J).GE.0.0).AND.(UZ(I,J).GE.0.0)) GO TO 71
     IF((UR(I,J).LT.0.0).AND.(UZ(I,J).LT.0.0)) GO TO 72
     IF((UR(I,J).LT.0.0).AND.(UZ(I,J).GE.0.0)) GO TO 73
```

```
      IF((UR(I,J).GE.0.0).AND.(UZ(I,J).LT.0.0)) GO TO 74
   71  A(I)=-(PEL*RHOL(I,J)*CPL(I,J)*ABSUR*DR+AKL(I,J)-AKL(I,J)*
     1DR/(2.*R(I)))
      B(I)=RHOL(I,J)*CPL(I,J)*DR*DR/DELT+PEL*RHOL(I,J)*CPL(I,J)*
      1ABSUR*DR+PEL*RHOL(I,J)*CPL(I,J)*ABSUZ*DR*DR/DZ+2.*AKL(I,J)+2.*
     2AKL(I,J)*DR*DR/(DZ*DZ)
      C(I)=-(AKL(I,J)+AKL(I,J)*DR/(2.*R(I)))
      D(I)=TL(I,J-1)*(PEL*RHOL(I,J)*CPL(I,J)*ABSUZ*DR*DR/DZ+AKL(I,J)*
      1DR*DR/(DZ*DZ))+TL(I,J+1)*(AKL(I,J)*DR*DR/(DZ*DZ))+EH*DR*DR+
     2TL(I,J)*(RHOL(I,J)*CPL(I,J)*DR*DR/DELT)
      GO TO 65
   72  A(I)=-(AKL(I,J)-AKL(I,J)*DR/(2.*R(I)))
      B(I)=RHOL(I,J)*CPL(I,J)*DR*DR/DELT+PEL*RHOL(I,J)*CPL(I,J)*
      1ABSUR*DR+PEL*RHOL(I,J)*CPL(I,J)*ABSUZ*DR*DR/DZ+2.*AKL(I,J)+2.*
     2AKL(I,J)*DR*DR/(DZ*DZ)
      C(I)=-(PEL*RHOL(I,J)*CPL(I,J)*ABSUR*DR+AKL(I,J)+AKL(I,J)*
     1DR/(2.*R(I)))
      D(I)=TL(I,J+1)*(PEL*RHOL(I,J)*CPL(I,J)*ABSUZ*DR*DR/DZ+AKL(I,J)*
      1DR*DR/(DZ*DZ))+TL(I,J-1)*(AKL(I,J)*DR*DR/(DZ*DZ))+EH*DR*DR+
     2TL(I,J)*(RHOL(I,J)*CPL(I,J)*DR*DR/DELT)
      GO TO 65
   73  A(I)=-(AKL(I,J)-AKL(I,J)*DR/(2.*R(I)))
      B(I)=RHOL(I,J)*CPL(I,J)*DR*DR/DELT+PEL*RHOL(I,J)*CPL(I,J)*
      1ABSUR*DR+PEL*RHOL(I,J)*CPL(I,J)*ABSUZ*DR*DR/DZ+2.*AKL(I,J)+2.*
     2AKL(I,J)*DR*DR/(DZ*DZ)
      C(I)=-(PEL*RHOL(I,J)*CPL(I,J)*ABSUR*DR+AKL(I,J)+AKL(I,J)*
     1DR/(2.*R(I)))
      D(I)=TL(I,J-1)*(PEL*RHOL(I,J)*CPL(I,J)*ABSUZ*DR*DR/DZ+AKL(I,J)*
      1DR*DR/(DZ*DZ))+TL(I,J+1)*(AKL(I,J)*DR*DR/(DZ*DZ))+EH*DR*DR+
     2TL(I,J)*(RHOL(I,J)*CPL(I,J)*DR*DR/DELT)
      GO TO 65
   74  A(I)=-(PEL*RHOL(I,J)*CPL(I,J)*ABSUR*DR+AKL(I,J)-AKL(I,J)*
     1DR/(2.*R(I)))
      B(I)=RHOL(I,J)*CPL(I,J)*DR*DR/DELT+PEL*RHOL(I,J)*CPL(I,J)*
      1ABSUR*DR+PEL*RHOL(I,J)*CPL(I,J)*ABSUZ*DR*DR/DZ+2.*AKL(I,J)+2.*
     2AKL(I,J)*DR*DR/(DZ*DZ)
      C(I)=-(AKL(I,J)+AKL(I,J)*DR/(2.*R(I)))
      D(I)=TL(I,J+1)*(PEL*RHOL(I,J)*CPL(I,J)*ABSUZ*DR*DR/DZ+AKL(I,J)*
      1DR*DR/(DZ*DZ))+TL(I,J-1)*(AKL(I,J)*DR*DR/(DZ*DZ))+EH*DR*DR+
     2TL(I,J)*(RHOL(I,J)*CPL(I,J)*DR*DR/DELT)
      GO TO 65
   66  A(I)=0.0
      B(I)=((TTIM**(1./2.))/DZ-35.0
      C(I)=-((TTIM**(1./2.))/DZ)
      D(I)=-2.0*35.0
      GO TO 65
C     D(I)=TL(I,J)*(RHOL(I,J)*CPL(I,J)*DR*DR/DELT)+EH*DR*DR+
C    1TL(I,J+1)*(2.*AKL(I,J)*DR*DR/(DZ*DZ))
C     GO TO 65
C     A(I)=-(PEL*RHOL(I,J)*CPL(I,J)*ABSUR*DR+AKL(I,J)-AKL(I,J)*
C    1DR/(2.*R(I)))
C     B(I)=RHOL(I,J)*CPL(I,J)*DR*DR/DELT+PEL*RHOL(I,J)*CPL(I,J)*
C     1ABSUR*DR+2.*AKL(I,J)+2.*AKL(I,J)*DR*DR/(DZ*DZ)
C     C(I)=-(AKL(I,J)+AKL(I,J)*DR/(2.*R(I)))
C     D(I)=TL(I,J)*(RHOL(I,J)*CPL(I,J)*DR*DR/DELT)+EH*DR*DR+
C    1TL(I,J+1)*(2.*AKL(I,J)*DR*DR/(DZ*DZ))
C     GO TO 65
   67  GASHIT=((1.17965E+01)*(1.-VFP)*(EXP(-54.667/TINF))*
      1(-22251.5-8.57*300.*TINF-(1.03E+03)*((300.*TINF)**2)-
      2(4.49E+05)/(300.*TINF))-19.10637*AKG(I,M)*((TG(I,M+1)-
      3TG(I,M))/DZG))*R(I)*R(I)
      BCPART=(5.85714E+03)*(EXP((-5.8571HE+03)*TIMEB))*((DLRCEL**3)-
      1(DLRP**3))*(31712.+2.89*300.*TMAV-(0.53E-03)*((300.*TMAV)**2)-
      2(4.09E+05)/(300.*TMAV))
      A(I)=0.0
      B(I)=1.0
      C(I)=0.0
      D(I)=(RHOL(I,J)*CPL(I,J)*R(N)*DH*ABSTUR+POWIND*(DH*DPOWER/
      1TOTZ)+HEATBL*GASHIT-HITMEL*(1.-VFP)*RP*(-ARM*(DLRP**2)/
      2ALHMT*HEEPRO*RP*BCPART+ACUHIT*(R(N)**2)*DH*RHOL(I,J)*
      3CPL(I,J)*TL(I,M)/DELT)/(RHOL(I,J)*CPL(I,J)*R(N)*DH*ABSUIN+
      4(ACUHIT*(R(N)**2)*DH*RHOL(I,J)*CPL(I,J))/DELT)
      GO TO 65
   70  IF(UZ(I,J).GE.0.0) GO TO 77
      A(I)=0.0
```

```
      B(I)=RHOL(I,J)*CPL(I,J)*DR*DR/DELT+PEL*RHOL(I,J)*CPL(I,J)*
     1ABSUZ*DR*DR/DZ+4.*AKL(I,J)+2.*AKL(I,J)*DR*DR/(DZ*DZ)
      C(I)=-4.*AKL(I,J)
       D(I)=TL(I,J-1)*(AKL(I,J)*DR*DR/(DZ*DZ))+TL(I,J+1)*(PEL*RHOL(I,J)*
     1CPL(I,J)*ABSUZ*DR*DR/DZ+AKL(I,J)*DR*DR/(DZ*DZ))+EH*DR*DR+
     2TL(I,J)*(RHOL(I,J)*CPL(I,J)*DR*DR/DELT)
      GO TO 65
   77 A(I)=0.0
      B(I)=RHOL(I,J)*CPL(I,J)*DR*DR/DELT+PEL*RHOL(I,J)*CPL(I,J)*
     1ABSUZ*DR*DR/DZ+4.*AKL(I,J)+2.*AKL(I,J)*DR*DR/(DZ*DZ)
      C(I)=-4.*AKL(I,J)
       D(I)=TL(I,J+1)*(AKL(I,J)*DR*DR/(DZ*DZ))+TL(I,J-1)*(PEL*RHOL(I,J)*
     1CPL(I,J)*ABSUZ*DR*DR/DZ+AKL(I,J)*DR*DR/(DZ*DZ))+EH*DR*DR+
     2TL(I,J)*(RHOL(I,J)*CPL(I,J)*DR*DR/DELT)
      GO TO 65
   75   A(I)=AKL(I,J)/DR
        B(I)=-(AKL(I,J)/DR+0.327222/(-0.1823215))
        C(I)=0.0
        D(I)=-4.0*0.3272222/(-0.1823215)
        GO TO 65
```

```
C     1ABSUZ*DR*DR/DZ+2.*AKL(I,J)+2.*AKL(I,J)*DR*DR/(DZ*DZ)
C     C(I)=0.0
C      D(I)=TL(I,J+1)*(AKL(I,J)*DR*DR/(DZ*DZ))+TL(I,J-1)*(AKL(I,J)*DR*
C     1DR/(DZ*DZ)+PEL*RHOL(I,J)*CPL(I,J)*ABSUZ*DR*DR/DZ)+TL(I,J)*
C     2(RHOL(I,J)*CPL(I,J)*DR*DR/DELT)+EH*DR*DR
C     GO TO 65
   81   A(I)=0.0
        B(I)=1.0
        C(I)=0.0
        D(I)=4.9
        GO TO 65
```

```
   82   A(I)=0.0
        B(I)=1.0
        C(I)=0.0
        D(I)=4.9
        GO TO 35
```

```
      BVAL=RHOL(I,J)*CPL(I,J)*ADR/DELT+ABSUZ*PEL*RHOL(I,J)*
     1CPL(I,J)*ADR/DZ+2.*AKL(I,J)/DR+2.*AKL(I,J)/DR1+AKL(I,J)*
     2DDR/R(I)-AKL(I,J)/(R(I)*DDR)+2.*AKL(I,J)*ADR/(DZ*DZ)
       DVAL=EH*ADR+TL(I,J)*(RHOL(I,J)*CPL(I,J)*ADR/DELT)
      IF(J.EQ.1) GO TO 554
      IF(J.EQ.M) GO TO 67
      IF((UR(I,J).LT.0.0).AND.(UZ(I,J).LT.0.0)) GO TO 555
      IF((UR(I,J).GE.0.0).AND.(UZ(I,J).GE.0.0)) GO TO 556
      IF((UR(I,J).GE.0.0).AND.(UZ(I,J).LT.0.0)) GO TO 557
      IF((UR(I,J).LT.0.0).AND.(UZ(I,J).GE.0.0)) GO TO 558
  555 A(I)=-(2.*AKL(I,J)/DR-AKL(I,J)/(R(I)*DDR))
       B(I)=PEL*RHOL(I,J)*CPL(I,J)*ABSUR*ADR/DR1+BVAL
       C(I)=-(PEL*RHOL(I,J)*CPL(I,J)*ABSUR*ADR/DR1+2.*AKL(I,J)/DR1+
     1AKL(I,J)*DDR/R(I))
       D(I)=TL(I,J+1)*(PEL*RHOL(I,J)*CPL(I,J)*ABSUZ*ADR/DZ+AKL(I,J)*
     1ADR/(DZ*DZ))+TL(I,J-1)*(AKL(I,J)*ADR/(DZ*DZ))+DVAL
      GO TO 65
  556 A(I)=-(PEL*RHOL(I,J)*CPL(I,J)*ABSUR*ADR/DR+2.*AKL(I,J)/DR-
     1AKL(I,J)/(R(I)*DDR))
       B(I)=PEL*RHOL(I,J)*CPL(I,J)*ABSUR*ADR/DR+BVAL
       C(I)=-(2.*AKL(I,J)/DR1+AKL(I,J)*DDR/R(I))
       D(I)=TL(I,J+1)*(AKL(I,J)*ADR/(DZ*DZ))+TL(I,J-1)*(PEL*
     1RHOL(I,J)*CPL(I,J)*ABSUZ*ADR/DZ+AKL(I,J)*ADR/(DZ*DZ))+DVAL
      GO TO 65
  557 A(I)=-(PEL*RHOL(I,J)*CPL(I,J)*ABSUR*ADR/DR+2.*AKL(I,J)/DR-
     1AKL(I,J)/(R(I)*DDR))
       B(I)=PEL*RHOL(I,J)*CPL(I,J)*ABSUR*ADR/DR+BVAL
       C(I)=-(2.*AKL(I,J)/DR1+AKL(I,J)*DDR/R(I))
       D(I)=TL(I,J+1)*(PEL*RHOL(I,J)*CPL(I,J)*ABSUZ*ADR/DZ+AKL(I,J)*
     1ADR/(DZ*DZ))+TL(I,J-1)*(AKL(I,J)*ADR/(DZ*DZ))+DVAL
```

```
      GO TO 65
  558 A(I)=-(2.*AKL(I,J)/DR-AKL(I,J)/(R(I)*DDR))
       B(I)=PEL*RHOL(I,J)*CPL(I,J)*ABSUR*ADR/DR1+BVAL
       C(I)=-(PEL*RHOL(I,J)*CPL(I,J)*ABSUR*ADR/DR1+2.*AKL(I,J)/DR1+
      1AKL(I,J)*DDR/R(I))
       D(I)=TL(I,J+1)*(AKL(I,J)*ADR/(DZ*DZ))+TL(I,J-1)*(PEL*
      1RHOL(I,J)*CPL(I,J)*ABSUZ*ADR/DZ+AKL(I,J)*ADR/(DZ*DZ))+DVAL
      GO TO 65
  551 IF(UR(I,J).GE.0.0) GO TO 559
       A(I)=-(2.*AKL(I,J)/DR-AKL(I,J)/(R(I)*DDR))
       B(I)=RHOL(I,J)*CPL(I,J)*ADR/DELT+PEL*RHOL(I,J)*CPL(I,J)*
      1ABSUR*ADR/DR1+2.*AKL(I,J)/DR+2.*AKL(I,J)/DR1+AKL(I,J)*
      2DDR/R(I)-AKL(I,J)/(R(I)*DDR)+2.*AKL(I,J)*ADR/(DZ*DZ)
       C(I)=-(PEL*RHOL(I,J)*CPL(I,J)*ABSUR*ADR/DR1+2.*AKL(I,J)/DR1+
      1AKL(I,J)*DDR/R(I))
       D(I)=TL(I,J+1)*(2.*AKL(I,J)*ADR/(DZ*DZ))+DVAL
      GO TO 65
  559 A(I)=-(PEL*RHOL(I,J)*CPL(I,J)*ABSUR*ADR/DR+2.*AKL(I,J)/DR-
      1AKL(I,J)/(R(I)*DDR))
       B(I)=RHOL(I,J)*CPL(I,J)*ADR/DELT+PEL*RHOL(I,J)*CPL(I,J)*
      1ABSUR*ADR/DR+2.*AKL(I,J)/DR+2.*AKL(I,J)/DR1+AKL(I,J)*
      2DDR/R(I)-AKL(I,J)/(R(I)*DDR)+2.*AKL(I,J)*ADR/(DZ*DZ)
       C(I)=-(2.*AKL(I,J)/DR1+AKL(I,J)*DDR/R(I))
       D(I)=TL(I,J+1)*(2.*AKL(I,J)*ADR/(DZ*DZ))+DVAL
   65 CONTINUE
      CALL TRIDAG (1,N,A,B,C,D,TT)
      DO 569 I=1,N
  569 TL(I,J)=TT(I)
   60 CONTINUE
      DR=0.1
      DTLR=DR/DZ
      RETURN
      END
C
C     ****************************************************
C
C     SUBROUTINE FOR BED STREAM FUNCTION AND VORTICITY.....
C
C     ****************************************************
      SUBROUTINE BEDSFVOR
      SAVE
      COMMON/AREA1/LL,LL1,LNK,LNK1,DRB,D0,D0R,RYN,PEMT,PEHT,
     1VFB,DELTB,DELTB1,TIMEB,TIMEB1,RP,RF,TNP,PAI,ITERB,ITER1,UFG,
     2MP,UFW,UFE,THKM,DENP,BEDH,TOTZ,DLRP,ALHM,VFP,DAKP,
     3DAKM,UCHAR,COFSMR,COFLAR,ATMLOS,PMW,AMWMIX,DENMIX,
     5DLRCEL,CONSEH,POWIND,HEATBL,HTMEL,HFEPRO,ACUHT,
     4CFEOPR,COUTFL,VSTRCO,TINIT,ALHM1
      COMMON/AREA2/DOA(21,21),RHOM(21,21),CPM(21,21),AKM(21,21),
     1F(21,21),G(21,21),ALF(21,21)
      COMMON/AREA3/WB(21,21),EB(21,21),TM(21,21),CFEO(21,21),
     1TL(21,21),W(21,21),E(21,21),TG(31,31),CMO2(31,31),UR(21,21),
     2UZ(21,21),VR(31,31),VZ(31,31)
      COMMON/AREA4/THETA(21),AR(21)
      COMMON/AREA5/A(31),B(31),C(31),D(31),TT(31)
      COMMON/AREA9/N,M,NN,N1,M1,DZ,DR,DR1,DTLR,PEL,DPOWER,
     1ITERIN,DELT,NNN1,TIME,ETA,ADR,DDR,UVF,OSF,AA,BB,U0,V0,
     2NNN,ORIGZ,DII
      UINF=0.0
      TLAV=0.0
      TURAV=0.0
      CALL AVRG (UR,TL,M,DZ,MP,UINF,TLAV,TURAV)
      ABSUIN=ABS(UINF)
      CRYN=RYN*ABSUIN
C     POINT-BY-POINT METHOD.....
      DO 1170 J=1,LL
      WB(1,J)=0.1E-05
      G(1,J)=0.2E-05
      F(1,J)=0.2E-05
 1170 CONTINUE
      DO 1171 I=1,LNK1
      DO 1172 J=1,LL
      WB(I+1,J)=WB(I,J)+0.2E-05
      G(I+1,J)=G(I,J)+2.E-05
      F(I+1,J)=F(I,J)+2.E-05
 1172 CONTINUE
 1171 CONTINUE
```

```
      DO 31 KNK=1,ITER1
       print*,KNK
      DO 40 I=2,LNK1
      DO 45 J=2,LL1
         WB(I,J)=(WB(I+1,J)*(D0R**2)+WB(I-1,J)*(D0R**2)+WB(I,J+1)*
     1(1./(AR(I)**2)-D0*(COS(THETA(J))/SIN(THETA(J))))/(2.*
     2(AR(I)**2)))+WB(I,J-1)*(1./(AR(I)**2)+D0*(COS(THETA(J))/
     3SIN(THETA(J))))/(2.*(AR(I)**2)))-G(I,J)*(D0*D0))/(2.*
     4(D0R**2)+2./(AR(I)**2))
45    CONTINUE
40    CONTINUE
      DO 50 I=1,LNK
      WB(I,1)=0.0
      WB(I,LL)=0.0
50    CONTINUE
      DO 55 J=2,LL1
      WB(1,J)=0.0
        WB(LNK,J)=UFW*(((AR(LNK)**2)*(SIN(THETA(J)))**2)/2.)+
     1(1.-UFW)*WB(LL,J)
55    CONTINUE
C     POINT-BY-POINT METHOD.....
      DO 100 I=2,LNK1
      DO 105 J=2,LL1
       DELWI=WB(I+1,J)-WB(I-1,J)
       DELWJ=WB(I,J+1)-WB(I,J-1)
       ABSWI=ABS(DELWI)
       ABSWJ=ABS(DELWJ)
      IF((DELWJ.GE.0.0).AND.(DELWI.GE.0.0)) GO TO 110
      IF((DELWJ.LT.0.0).AND.(DELWI.LT.0.0)) GO TO 115
      IF((DELWJ.GE.0.0).AND.(DELWI.LT.0.0)) GO TO 120
      IF((DELWJ.LT.0.0).AND.(DELWI.GE.0.0)) GO TO 125
110   G(I,J)=(G(I+1,J)*D0R+G(I-1,J)*D0R+G(I,J+1)*(DRB/((AR(I)**2)*
     1D0)-DRB*(COS(THETA(J))/SIN(THETA(J))))/(2.*(AR(I)**2)))+
     2G(I,J-1)*(DRB/((AR(I)**2)*D0)+DRB*(COS(THETA(J)))/
     3SIN(THETA(J))))/((AR(I)**2)*2.))-((CRYN*SIN(THETA(J))))/4.)*
     4(ABSWI*(F(I,J)-F(I,J-1))+ABSWJ*(F(I,J)-F(I+1,J)))))/(2.*
     5D0R+2.*DRB/((AR(I)**2)*D0))
      GO TO 105
115   G(I,J)=(G(I+1,J)*D0R+G(I-1,J)*D0R+G(I,J+1)*(DRB/((AR(I)**2)*
     1D0)-DRB*(COS(THETA(J))/SIN(THETA(J))))/(2.*(AR(I)**2)))+
     2G(I,J-1)*(DRB/((AR(I)**2)*D0)+DRB*(COS(THETA(J)))/
     3SIN(THETA(J))))/((AR(I)**2)*2.))-((CRYN*SIN(THETA(J))))/4.)*
     4(ABSWI*(F(I,J)-F(I,J+1))+ABSWJ*(F(I,J)-F(I-1,J)))))/(2.*
     5D0R+2.*DRB/((AR(I)**2)*D0))
      GO TO 105
120   G(I,J)=(G(I+1,J)*D0R+G(I-1,J)*D0R+G(I,J+1)*(DRB/((AR(I)**2)*
     1D0)-DRB*(COS(THETA(J))/SIN(THETA(J))))/(2.*(AR(I)**2)))+
     2G(I,J-1)*(DRB/((AR(I)**2)*D0)+DRB*(COS(THETA(J)))/
     3SIN(THETA(J))))/((AR(I)**2)*2.))-((CRYN*SIN(THETA(J))))/4.)*
     4(ABSWI*(F(I,J)-F(I,J+1))+ABSWJ*(F(I,J)-F(I+1,J)))))/(2.*
     5D0R+2.*DRB/((AR(I)**2)*D0))
      GO TO 105
125   G(I,J)=(G(I+1,J)*D0R+G(I-1,J)*D0R+G(I,J+1)*(DRB/((AR(I)**2)*
     1D0)-DRB*(COS(THETA(J))/SIN(THETA(J))))/(2.*(AR(I)**2)))+
     2G(I,J-1)*(DRB/((AR(I)**2)*D0)+DRB*(COS(THETA(J)))/
     3SIN(THETA(J))))/((AR(I)**2)*2.))-((CRYN*SIN(THETA(J))))/4.)*
     4(ABSWI*(F(I,J)-F(I,J-1))+ABSWJ*(F(I,J)-F(I-1,J)))))/(2.*
     5D0R+2.*DRB/((AR(I)**2)*D0))
105   CONTINUE
100   CONTINUE
      DO 135 I=1,LNK
      G(I,1)=0.0
      G(I,LL)=0.0
135   CONTINUE
      DO 140 J=2,LL1
      G(LNK,J)=0.0
       G(1,J)=UFG*((2.*ABS(WB(2,J))/(DRB*DRB)))+(1.-UFG)*G(1,J)
140   CONTINUE
      DO 180 I=2,LNK1
      DO 185 J=2,LL1
       F(I,J)=G(I,J)/((AR(I)**2)*((SIN(THETA(J)))**2))
185   CONTINUE
180   CONTINUE
      DO 190 I=1,LNK
      F(I,1)=G(I,2)/((AR(I)**2)*D0*D0)
      F(I,LL)=(G(I,LL1)/((AR(I)**2)*D0*D0))
```

```
190 CONTINUE
    DO 195 J=2,LL1
    F(LNK,J)=0.0
     F(1,J)=G(1,J)/((AR(1)**2)*((SIN(THETA(J)))**2))
195 CONTINUE
    DO 200 I=1,LNK
    DO 205 J=1,LL
     EB(I,J)=F(I,J)*AR(I)*SIN(THETA(J))
205 CONTINUE
200 CONTINUE
C    IF(KNK.EQ.(ITER1-1)) GO TO 210
    IF(KNK.EQ.ITER1) GO TO 210
C    DO 215 KKK=1,ITER1/50
C    IF(KNK.EQ.(50*KKK)) GO TO 210
C15   CONTINUE
    GO TO 31
C10   IF(KNK.EQ.50) GO TO 31
C    IF(KNK.EQ.100) GO TO 31
C    IF(KNK.EQ.150) GO TO 31
C    IF(KNK.EQ.200) GO TO 31
C    IF(KNK.EQ.250) GO TO 31
210   WRITE(37,1000) ITERB,CRYN
1000 FORMAT(1X,'AFTER',I4,'TH ITERATION AND REYNOLDS NO.',F12.6,
     1'THE 11 VALUES OF THE STREAM FUNCTION ARE:',/)
      WRITE(37,1001) ((WB(I,J),I=1,LNK),J=1,LL)
1001 FORMAT(2X,11F11.5/)
      WRITE(38,1004) ITERB
1004 FORMAT(1X,'AFTER',I4,'TH ITERATION THE FIRST 11 VALUES OF
     1VORTICITY ARE:',/)
      WRITE(38,1005) ((EB(I,J),I=1,LNK),J=1,LL)
1005 FORMAT(2X,11F11.5/)
       WRITE(40,1014) ITERB
1014 FORMAT(1X,'AFTER',I4,'TH ITERATION THE FIRST 11 VALUES OF
     1F FUNCTION ARE:',/)
      WRITE(40,1015) ((F(I,J),I=1,LNK),J=1,LL)
1015 FORMAT(2X,11F11.5/)
      WRITE(39,1008) ITERB
1008 FORMAT(1X,'AFTER',I4,'TH ITERATION THE FIRST 11 VALUES OF
     1G FUNCTION ARE:',/)
      WRITE(39,1009) ((G(I,J),I=1,LNK),J=1,LL)
1009 FORMAT(2X,11F11.5/)
31    CONTINUE
      RETURN
      END
C     ****************************************************
C
C     SUBROUTINE FOR BED HEAT AND MASS TRANSFER
C     CALCULATION
C
C     ****************************************************
      SUBROUTINE BEDHTMT
      SAVE
       COMMON/AREA1/LL,LL1,LNK,LNK1,DRB,D0,D0R,RYN,PEMT,PEHT,
      1VFB,DELTB,DELTB1,TIMEB,TIMEB1,RP,RF,TNP,PAI,ITERB,ITER1,UFG,
      2MP,UFW,UFE,THKM,DENP,BEDH,TOTZ,DLRP,ALHM,VFP,DAKP,
      3DAKM,UCHAR,COFSMR,COFLAR,ATMLOS,PMW,AMWMIX,DENMIX,
     3DLRCEL,CONSEH,POWIND,HEATBL,HITMEL,HFEPRO,ACUHT,
     4CFEOPR,COUTFL,VSTRCO,TINIT,ALHM1
     COMMON/AREA2/DOA(21,21),RHOM(21,21),CPM(21,21),AKM(21,21),
     1F(21,21),G(21,21),ALF(21,21)
      COMMON/AREA3/WB(21,21),EB(21,21),TM(21,21),CFEO(21,21),
     1TL(21,21),W(21,21),E(21,21),TG(31,31),CMO2(31,31),UR(21,21),
     2UZ(21,21),VR(31,31),VZ(31,31)
      COMMON/AREA4/THETA(21),AR(21)
     COMMON/AREA5/A(31),B(31),C(31),D(31),TT(31)
      COMMON/AREA9/N,M,NN,N1,ML,DZ,DR,DR1,DTER,PFL,DPOWER,
      ITERIN,DELT,NNN1,TIME,ETA,ADR,DDR,UVF,OSF,AA,BB,U0,V0,
     2NNN,ORIGZ,DIT
     COMMON/AREA10/R(22),Z(22),UU(22),VV(22),XX(23),YY(22)
     TINF=0.0
     ARM=0.0
     UINF=0.0
     TLAV=0.0
     TURAV=0.0
    CPEHT=0.0
    CPEMT=0.0
```

```
      CALL TINFAVIT (TM,TL,LL,N,M,DAKP,DRB,TINF,ARM)
      CALL AVRG (UR,TL,M,DZ,MP,UINF,TLAV,TURAV)
      ABSUIN=ABS(UINF)
     CPEHT=PEHT*ABSUIN
      CPEMT=PEMT*ABSUIN
C    LINE-BY-LINE METHOD.....
C    J-DIRECTION.....
     DO 350 I=1,LNK
     DO 355 J=2,LL1
     IF(I.EQ.1) GO TO 356
     IF(I.EQ.LNK) GO TO 356
      DELWI=WB(I+1,J)-WB(I-1,J)
      DELWJ=WB(I,J+1)-WB(I,J-1)
      ABSWI=ABS(DELWI)
      ABSWJ=ABS(DELWJ)
       BVAL=(DRB*D0/DELTB1+CPEMT*ABSWJ/((AR(I)**2)*2.*SIN(THETA(J)))
      1+CPEMT*ABSWI/((AR(I)**2)*2.*SIN(THETA(J)))+2.*DOA(I,J)*D0/
      2DRB+2.*DOA(I,J)*DRB/((AR(I)**2)*D0))
       AAVAL=CPEMT*ABSWI/((AR(I)**2)*2.*SIN(THETA(J)))+DOA(I,J)*
      1DRB/((AR(I)**2)*D0)-(COS(THETA(J))/SIN(THETA(J)))*DOA(I,J)*
      2DRB/((AR(I)**2)*2.)
       CVAL=CPEMT*ABSWJ/((AR(I)**2)*2.*SIN(THETA(J)))+DOA(I,J)*D0/
      1DRB+DOA(I,J)*D0/AR(I)
       CCVAL=DOA(I,J)*DRB/((AR(I)**2)*D0)+DOA(I,J)*DRB*
      1(COS(THETA(J))/SIN(THETA(J)))/((AR(I)**2)*2.)
       FFVAL=DOA(I,J)*DRB/((AR(I)**2)*D0)-DOA(I,J)*DRB*
      1(COS(THETA(J))/SIN(THETA(J)))/((AR(I)**2)*2.)
  356 AVAL=DOA(I,J)*D0/DRB-DOA(I,J)*D0/AR(I)
      DVAL=CFEO(I,J)*(DRB*D0/DELTB1)+((9.58603E+07)*(RP**2)*
      1(EXP((-5.85726E+07)*(RP**2)*TIMEB1)))*DRB*D0
      EEVAL=DOA(I,J)*D0/DRB+DOA(I,J)*D0/AR(I)
      IF(I.EQ.1) GO TO 360
      IF(I.EQ.LNK) GO TO 365
      IF((DELWJ.GE.0.0).AND.(DELWI.GE.0.0)) GO TO 390
      IF((DELWJ.LT.0.0).AND.(DELWI.LT.0.0)) GO TO 395
      IF((DELWJ.GE.0.0).AND.(DELWI.LT.0.0)) GO TO 400
      IF((DELWJ.LT.0.0).AND.(DELWI.GE.0.0)) GO TO 405
  390 A(J)=-AAVAL
       B(J)=BVAL
       C(J)=-CCVAL
       D(J)=CFEO(I,J)*CVAL+CFEO(I-1,J)*AVAL+DVAL
      GO TO 355
  395 A(J)=-FFVAL
       B(J)=BVAL
       C(J)=-(CPEMT*ABSWI/((AR(I)**2)*2.*SIN(THETA(J)))+CCVAL)
       D(J)=CFEO(I+1,J)*EEVAL+CFEO(I-1,J)*(CPEMT*ABSWJ/(2.*
       1(AR(I)**2)*SIN(THETA(J)))+AVAL)+DVAL
      GO TO 355
  400 A(J)=-FFVAL
       B(J)=BVAL
       C(J)=-(CPEMT*ABSWI/((AR(I)**2)*2.*SIN(THETA(J)))+CCVAL)
       D(J)=CFEO(I+1,J)*CVAL+CFEO(I-1,J)*AVAL+DVAL
      GO TO 355
  405 A(J)=-(CPEMT*ABSWI/((AR(I)**2)*2.*SIN(THETA(J)))+FFVAL)
       B(J)=BVAL
       C(J)=-CCVAL
       D(J)=CFEO(I+1,J)*EEVAL+CFEO(I-1,J)*(CPEMT*ABSWJ/(2.*
       1(AR(I)**2)*SIN(THETA(J)))+AVAL)+DVAL
      GO TO 355
  360 A(J)=0.0
       B(J)=1.0
       C(J)=0.0
       D(J)=1.0
      GO TO 355
  365 A(J)=0.0
       B(J)=1.0
       C(J)=0.0
        D(J)=((CFEOPR*(1.-VFP)*RP/((R(N)**2)*DH*(1.-VFB)))*(-ARM*
       1(DLRP**2))+(5.85714E+07)*(RP**2)*(EXP((-5.85714E+07)*(RP**2)*
      2TIMEB1))+CFEO(I,J)/DELTB1)/((1./DELTB1)+COUTFL*ABSUIN/(R(N)*
      3(1.-VFB)))
      GO TO 355
  355 CONTINUE
      CALL TRIDAG (2,LL1,A,B,C,D,TT)
      DO 410 J=2,LL1
  410 CFEO(I,J)=TT(J)
```

```
350 CONTINUE
C    I-DIRECTION.....
     DO 415 J=1,LL
     DO 420 I=1,LNK
     IF(I.EQ.1) GO TO 422
     IF(I.EQ.LNK) GO TO 422
     IF(J.EQ.1) GO TO 422
     IF(J.EQ.LL) GO TO 422
      DELWI=WB(I+1,J)-WB(I-1,J)
      DELWJ=WB(I,J+1)-WB(I,J-1)
      ABSWI=ABS(DELWI)
      ABSWJ=ABS(DELWJ)
       BVAL=(DRB*D0/DELTB1+CPEMT*ABSWJ/((AR(I)**2)*2.*SIN(THETA(J)))
     1+CPEMT*ABSWI/((AR(I)**2)*2.*SIN(THETA(J)))+2.*DOA(I,J)*D0/
     2DRB+2.*DOA(I,J)*DRB/((AR(I)**2)*D0))
       AAVAL=CPEMT*ABSWI/((AR(I)**2)*2.*SIN(THETA(J)))+DOA(I,J)*
     1DRB/((AR(I)**2)*D0)-(COS(THETA(J))/SIN(THETA(J)))*DOA(I,J)*
     2DRB/((AR(I)**2)*2.)
       CVAL=CPEMT*ABSWJ/((AR(I)**2)*2.*SIN(THETA(J)))+DOA(I,J)*D0/
     1DRB+DOA(I,J)*D0/AR(I)
      CCVAL=DOA(I,J)*DRB/((AR(I)**2)*D0)+DOA(I,J)*DRB*
     1(COS(THETA(J))/SIN(THETA(J)))/((AR(I)**2)*2.)
      FFVAL=DOA(I,J)*DRB/((AR(I)**2)*D0)-DOA(I,J)*DRB*
     1(COS(THETA(J))/SIN(THETA(J)))/((AR(I)**2)*2.)
422  AVAL=DOA(I,J)*D0/DRB-DOA(I,J)*D0/AR(I)
      DVAL=CFEO(I,J)*(DRB*D0/DELTB1)+((9.58603E+07)*(RP**2)*
     1(EXP((-5.85726E+07)*(RP**2)*TIMEB1)))*DRB*D0
     EEVAL=DOA(I,J)*D0/DRB+DOA(I,J)*D0/AR(I)
     IF(I.EQ.1) GO TO 425
     IF(I.EQ.LNK) GO TO 430
     IF(J.EQ.1) GO TO 435
     IF(J.EQ.LL) GO TO 440
     IF((DELWJ.GE.0.0).AND.(DELWI.GE.0.0)) GO TO 445
     IF((DELWJ.LT.0.0).AND.(DELWI.LT.0.0)) GO TO 450
     IF((DELWJ.GE.0.0).AND.(DELWI.LT.0.0)) GO TO 455
     IF((DELWJ.LT.0.0).AND.(DELWI.GE.0.0)) GO TO 460
445  A(I)=-AVAL
     B(I)=BVAL
     C(I)=-CVAL
      D(I)=CFEO(I,J+1)*CCVAL+CFEO(I,J-1)*AAVAL+DVAL
     GO TO 420
450  A(I)=-(CPEMT*ABSWJ/((AR(I)**2)*2.*SIN(THETA(J)))+AVAL)
     B(I)=BVAL
     C(I)=-EEVAL
      D(I)=CFEO(I,J+1)*(CPEMT*ABSWI/((AR(I)**2)*2.*SIN(THETA(J)))+
     1CCVAL)+CFEO(I,J-1)*FFVAL+DVAL
     GO TO 420
455  A(I)=-AVAL
     B(I)=BVAL
     C(I)=-CVAL
      D(I)=CFEO(I,J+1)*(CPEMT*ABSWI/((AR(I)**2)*2.*SIN(THETA(J)))+
     1CCVAL)+CFEO(I,J-1)*FFVAL+DVAL
     GO TO 420
460  A(I)=-(CPEMT*ABSWJ/((AR(I)**2)*2.*SIN(THETA(J)))+AVAL)
     B(I)=BVAL
     C(I)=-EEVAL
      D(I)=CFEO(I,J+1)*CCVAL+CFEO(I,J-1)*AAVAL+DVAL
     GO TO 420
425  A(I)=0.0
     B(I)=1.0
     C(I)=0.0
     D(I)=1.0
     GO TO 420
430  A(I)=0.0
     B(I)=1.0
     C(I)=0.0
      D(I)=((CFEOPR*(1.-VFP)*RP/((R(N)**2)*DH*(1.-VFB)))*(-ARM*
     1(DLRP**2))+(5.85714E+07)*(RP**2)*(EXP((-5.85714E+07)*(RP**2)*
     2TIMEB1))+CFEO(I,J)/DELTB1)/((1./DELTB1)+COUTFL*ABSUIN/(R(N)*
     3(1.-VFB)))
     GO TO 420
435  DELWJ=WB(I,J+1)-WB(I,J)
      ABSWJ=ABS(DELWJ)
       BBVAL=DRB*D0/DELTB1+CPEMT*2.*ABSWJ/((AR(I)**2)*D0*
     1COS(THETA(J)))+2.*DOA(I,J)*D0/DRB+2.*DOA(I,J)*DRB/((AR(I)**2)*
     2D0)+2.*DOA(I,J)*(COS(THETA(J))**2)*DRB/((AR(I)**2)*D0)
```

```
      IF(DELWJ.LT.0.0) GO TO 436
      A(I)=-AVAL
      B(I)=BBVAL
       C(I)=-(EEVAL+CPEMT*2.*ABSWJ/((AR(I)**2)*COS(THETA(J))*D0))
      D(I)=CFEO(I,J+1)*(2.*DOA(I,J)/((AR(I)**2)*D0R)+2.*DOA(I,J)*
     1(COS(THETA(J)))**2)/((AR(I)**2)*D0R))+DVAL
      GO TO 420
  436 A(I)=-(AVAL+CPEMT*2.*ABSWJ/((AR(I)**2)*COS(THETA(J))*D0))
      B(I)=BBVAL
      C(I)=-EEVAL
       D(I)=CFEO(I,J+1)*(2.*DOA(I,J)/((AR(I)**2)*D0R)+2.*DOA(I,J)*
      1(COS(THETA(J)))**2)/((AR(I)**2)*D0R))+DVAL
C     TYPE *,A,B,C,D
      GO TO 420
  440 DELWJ=WB(I,J-1)-WB(I,J)
       ABSWJ=ABS(DELWJ)
        BBVAL=DRB*D0/DELTB1+CPEMT*2.*ABSWJ/((AR(I)**2)*D0*
      1COS(THETA(J)))+2.*DOA(I,J)*D0/DRB+2.*DOA(I,J)*DRB/((AR(I)**2)*
      2D0)+2.*DOA(I,J)*(COS(THETA(J)))**2)*DRB/((AR(I)**2)*D0)
      IF(DELWJ.LT.0.0) GO TO 441
      GO TO 442
  441 A(I)=-AVAL
      B(I)=BBVAL
       C(I)=-(EEVAL+CPEMT*2.*ABSWJ/((AR(I)**2)*COS(THETA(J))*D0))
       D(I)=CFEO(I,LL1)*(2.*DOA(I,J)/((AR(I)**2)*D0R)+2.*DOA(I,J)*
       1(COS(THETA(J)))**2)/((AR(I)**2)*D0R))+DVAL
      GO TO 420
  442 A(I)=-(AVAL+CPEMT*2.*ABSWJ/((AR(I)**2)*COS(THETA(J))*D0))
      B(I)=BBVAL
      C(I)=-EEVAL
       D(I)=CFEO(I,LL1)*(2.*DOA(I,J)/((AR(I)**2)*D0R)+2.*DOA(I,J)*
       1(COS(THETA(J)))**2)/((AR(I)**2)*D0R)+DVAL
  420  CONTINUE
      CALL TRIDAG (1,LNK,A,B,C,D,TT)
      DO 465 I=1,LNK
  465 CFEO(I,J)=TT(I)
  415 CONTINUE
C
C     HEAT TRANSFER CALCULATION.....
C
C    J-DIRECTION.....
      DO 550 I=1,LNK
      DO 555 J=1,LL
       ALF(I,J)=AKM(I,J)/(RHOM(I,J)*CPM(I,J))
      IF(I.EQ.1) GO TO 556
      IF(I.EQ.LNK) GO TO 556
      IF(J.EQ.1) GO TO 556
      IF(J.EQ.LL) GO TO 556
       DELWI=WB(I+1,J)-WB(I-1,J)
       DELWJ=WB(I,J+1)-WB(I,J-1)
       ABSWI=ABS(DELWI)
       ABSWJ=ABS(DELWJ)
        BVAL=(DRB*D0/DELTB+CPEHT*ABSWJ/((AR(I)**2)*2.*SIN(THETA(J)))+
       1CPEHT*ABSWI/((AR(I)**2)*2.*SIN(THETA(J)))+2.*ALF(I,J)*D0/
      2DRB+2.*ALF(I,J)*DRB/((AR(I)**2)*D0))
        AAVAL=CPEHT*ABSWI/((AR(I)**2)*2.*SIN(THETA(J)))+ALF(I,J)*
      1DRB/((AR(I)**2)*D0)-(COS(THETA(J))/SIN(THETA(J)))*ALF(I,J)*
      2DRB/((AR(I)**2)*2.)
       CVAL=CPEHT*ABSWJ/((AR(I)**2)*2.*SIN(THETA(J)))+ALF(I,J)*D0/
      1DRB+ALF(I,J)*D0/AR(I)
       FFVAL=ALF(I,J)*DRB/((AR(I)**2)*D0)-ALF(I,J)*DRB*
      1(COS(THETA(J))/SIN(THETA(J)))/((AR(I)**2)*2.)
       CCVAL=ALF(I,J)*DRB/((AR(I)**2)*D0)+ALF(I,J)*DRB*
      1(COS(THETA(J))/SIN(THETA(J)))/((AR(I)**2)*2.)
  556 AVAL=ALF(I,J)*D0/DRB-ALF(I,J)*D0/AR(I)
       DVAL=(((EXP((-4.42064E+05)*(RP**2)*TIMEB))*25.8356763*
      1(RP**2)*((COFLAR*(31712.+2.89*300.*TM(I,J)-(0.53E-03)*
      2((TM(I,J)*300.)**2)-(4.09E+05)/(TM(I,J)*300.))+
      3COFSMR*(-117825.))*ATMLOS))*DRB*D0)/(RHOM(I,J)*CPM(I,J))+
      4TM(I,J))*(DRB*D0/DELTB)
  552 EEVAL=ALF(I,J)*D0/DRB+ALF(I,J)*D0/AR(I)
      IF(I.EQ.1) GO TO 560
      IF(I.EQ.LNK) GO TO 565
      IF(J.EQ.1) GO TO 570
      IF(J.EQ.LL) GO TO 575
      IF((DELWJ.GE.0.0).AND.(DELWI.GE.0.0)) GO TO 590
```

```
      IF((DELWJ.LT.0.0).AND.(DELWI.LT.0.0)) GO TO 595
      IF((DELWJ.GE.0.0).AND.(DELWI.LT.0.0)) GO TO 600
      IF((DELWJ.LT.0.0).AND.(DELWI.GE.0.0)) GO TO 605
  590 A(J)=-AAVAL
      B(J)=BVAL
      C(J)=-CCVAL
       D(J)=TM(I+1,J)*CVAL+TM(I-1,J)*AVAL+DVAL
      GO TO 555
  595 A(J)=-FFVAL
      B(J)=BVAL
       C(J)=-(CPEHT*ABSWI/((AR(I)**2)*2.*SIN(THETA(J)))+CCVAL)
       D(J)=TM(I+1,J)*EEVAL+TM(I-1,J)*(CPEHT*ABSWJ/(2.*
      1(AR(I)**2)*SIN(THETA(J)))+AVAL)+DVAL
      GO TO 555
  600 A(J)=-FFVAL
      B(J)=BVAL
       C(J)=-(CPEHT*ABSWI/((AR(I)**2)*2.*SIN(THETA(J)))+CCVAL)
       D(J)=TM(I+1,J)*CVAL+TM(I-1,J)*AVAL+DVAL
      GO TO 555
  605 A(J)=-(CPEHT*ABSWI/((AR(I)**2)*2.*SIN(THETA(J)))+FFVAL)
      B(J)=BVAL
      C(J)=-CCVAL
       D(J)=TM(I+1,J)*EEVAL+TM(I-1,J)*(CPEHT*ABSWJ/(2.*
      1(AR(I)**2)*SIN(THETA(J)))+AVAL)+DVAL
      GO TO 555
  560 A(J)=0.0
      B(J)=1.0
      C(J)=0.0
      D(J)=4.9
      GO TO 555
  565 A(J)=0.0
      B(J)=1.0
      C(J)=0.0
      D(J)=TINF
      GO TO 555
  570 DELWJ=WB(I,J+1)-WB(I,J)
       ABSWJ=ABS(DELWJ)
       BBVAL=DRB*D0/DELTB+CPEHT*2.*ABSWJ/((AR(I)**2)*D0*
      1COS(THETA(J)))+2.*ALF(I,J)*D0/DRB+2.*ALF(I,J)*DRB/((AR(I)**2)*
      2D0)+2.*ALF(I,J)*(COS(THETA(J))**2)*DRB/((AR(I)**2)*D0)
      IF(DELWJ.LT.0.0) GO TO 571
      A(J)=0.0
      B(J)=BBVAL
       C(J)=-(2.*ALF(I,J)*(COS(THETA(J))**2)/((AR(I)**2)*D0R)+2.*
      1ALF(I,J)/(D0R*(AR(I)**2)))
       D(J)=DVAL+TM(I+1,J)*(CPEHT*2.*ABSWJ/((AR(I)**2)*D0*
      1COS(THETA(J)))+EEVAL)+TM(I-1,J)*AVAL
      GO TO 555
  571 A(J)=0.0
      B(J)=BBVAL
       C(J)=-(2.*ALF(I,J)*(COS(THETA(J))**2)/((AR(I)**2)*D0R)+2.*
      1ALF(I,J)/(D0R*(AR(I)**2)))
       D(J)=DVAL+TM(I+1,J)*EEVAL+TM(I-1,J)*(CPEHT*2.*ABSWJ/((AR(I)**2)*
      1COS(THETA(J)))*D0)+AVAL)
      GO TO 555
  575 DELWJ=WB(I,J-1)-WB(I,J)
       ABSWJ=ABS(DELWJ)
       BBVAL=DRB*D0/DELTB+CPEHT*2.*ABSWJ/((AR(I)**2)*D0*
      1COS(THETA(J)))+2.*ALF(I,J)*D0/DRB+2.*ALF(I,J)*DRB/((AR(I)**2)*
      2D0)+2.*ALF(I,J)*(COS(THETA(J))**2)*DRB/((AR(I)**2)*D0)
      IF(DELWJ.LT.0.0) GO TO 576
      GO TO 577
  576 A(J)=-(2.*ALF(I,J)*(COS(THETA(J))**2)/((AR(I)**2)*D0R)+2.*
      1ALF(I,J)/(D0R*(AR(I)**2)))
      B(J)=BBVAL
      C(J)=0.0
       D(J)=DVAL+TM(I+1,J)*(CPEHT*2.*ABSWJ/((AR(I)**2)*D0*
      1COS(THETA(J)))+EEVAL)+TM(I-1,J)*AVAL
      GO TO 555
  577 A(J)=-(2.*ALF(I,J)*(COS(THETA(J))**2)/((AR(I)**2)*D0R)+2.*
      1ALF(I,J)/(D0R*(AR(I)**2)))
      B(J)=BBVAL
      C(J)=0.0
       D(J)=DVAL+TM(I+1,J)*EEVAL+TM(I-1,J)*(CPEHT*2.*ABSWJ/((AR(I)**2)*
      1COS(THETA(J)))*D0)+AVAL)
  555 CONTINUE
```

```
      CALL TRIDAG (1,LL,A,B,C,D,TT)
      DO 610 J=1,LL
  610 TM(I,J)=TT(J)
  550 CONTINUE
C     I-DIRECTION.....
      DO 615 J=1,LL
      DO 620 I=1,LNK
       ALF(I,J)=AKM(I,J)/(RHOM(I,J)*CPM(I,J))
      IF(I.EQ.1) GO TO 621
      IF(I.EQ.LNK) GO TO 621
      IF(J.EQ.1) GO TO 621
      IF(J.EQ.LL) GO TO 621
       DELWI=WB(I+1,J)-WB(I-1,J)
       DELWJ=WB(I,J+1)-WB(I,J-1)
       ABSWI=ABS(DELWI)
       ABSWJ=ABS(DELWJ)
        BVAL=(DRB*D0/DELTB+CPEHT*ABSWJ/((AR(I)**2)*2.*SIN(THETA(J)))+
       1CPEHT*ABSWI/((AR(I)**2)*2.*SIN(THETA(J)))+2.*ALF(I,J)*D0/
       2DRB+2.*ALF(I,J)*DRB/((AR(I)**2)*D0))
         AAVAL=CPEHT*ABSWI/((AR(I)**2)*2.*SIN(THETA(J)))+ALF(I,J)*
       1DRB/((AR(I)**2)*D0)-(COS(THETA(J))/SIN(THETA(J)))*ALF(I,J)*
       2DRB/((AR(I)**2)*2.)
        CVAL=CPEHT*ABSWJ/((AR(I)**2)*2.*SIN(THETA(J)))+ALF(I,J)*D0/
       1DRB+ALF(I,J)*D0/AR(I)
        FFVAL=ALF(I,J)*DRB/((AR(I)**2)*D0)-ALF(I,J)*DRB*
       1(COS(THETA(J))/SIN(THETA(J)))/((AR(I)**2)*2.)
        CCVAL=ALF(I,J)*DRB/((AR(I)**2)*D0)+ALF(I,J)*DRB*
       1(COS(THETA(J))/SIN(THETA(J)))/((AR(I)**2)*2.)
  621 AVAL=ALF(I,J)*D0/DRB-ALF(I,J)*D0/AR(I)
       DVAL=(((EXP((-4.42064E+05)*(RP**2)*TIMEB))*25.856763*
       1(RP**2)*((COFLAR*(31712.+2.89*300.*TM(I,J)-(0.53E-03)*
       2((TM(I,J)*300.)**2)-(4.09E+05)/(TM(I,J)*300.))+
       3COFSMR*(-117825.))*ATMLOS))*DRB*D0)/(RHOM(I,J)*CPM(I,J))+
       4TM(I,J)*(DRB*D0/DELTB)
  617 EEVAL=ALF(I,J)*D0/DRB+ALF(I,J)*D0/AR(I)
      IF(I.EQ.1) GO TO 625
      IF(I.EQ.LNK) GO TO 630
      IF(J.EQ.1) GO TO 635
      IF(J.EQ.LL) GO TO 640
      IF((DELWJ.GE.0.0).AND.(DELWI.GE.0.0)) GO TO 645
      IF((DELWJ.LT.0.0).AND.(DELWI.LT.0.0)) GO TO 650
      IF((DELWJ.GE.0.0).AND.(DELWI.LT.0.0)) GO TO 655
      IF((DELWJ.LT.0.0).AND.(DELWI.GE.0.0)) GO TO 660
  645 A(I)=-AVAL
      B(I)=BVAL
      C(I)=-CVAL
       D(I)=TM(I,J+1)*CCVAL+TM(I,J-1)*AAVAL+DVAL
      GO TO 620
  650 A(I)=-(CPEHT*ABSWJ/((AR(I)**2)*2.*SIN(THETA(J)))+AVAL)
      B(I)=BVAL
      C(I)=-EEVAL
       D(I)=TM(I,J+1)*(CPEHT*ABSWI/((AR(I)**2)*2.*SIN(THETA(J)))+
      1CCVAL)+TM(I,J-1)*FFVAL+DVAL
      GO TO 620
  655 A(I)=-AVAL
      B(I)=BVAL
      C(I)=-CVAL
       D(I)=TM(I,J+1)*(CPEHT*ABSWI/((AR(I)**2)*2.*SIN(THETA(J)))+
      1CCVAL)+TM(I,J-1)*FFVAL+DVAL
      GO TO 620
  660 A(I)=-(CPEHT*ABSWJ/((AR(I)**2)*2.*SIN(THETA(J)))+AVAL)
      B(I)=BVAL
      C(I)=-EEVAL
       D(I)=TM(I,J+1)*CCVAL+TM(I,J-1)*AAVAL+DVAL
      GO TO 620
  625 A(I)=0.0
      B(I)=1.0
      C(I)=0.0
      D(I)=4.9
      GO TO 620
  630 A(I)=0.0
      B(I)=1.0
      C(I)=0.0
      D(I)=TINT
      GO TO 620
  635 DELWJ=WB(I,J+1)-WB(I,J)
```

```
      ABSWJ=ABS(DELWJ)
       BBVAL=DRB*D0/DELTB+CPEHT*2.*ABSWJ/((AR(I)**2)*D0*
     1COS(THETA(J)))+2.*ALF(I,J)*D0/DRB+2.*ALF(I,J)*DRB/((AR(I)**2)*
     2D0)+2.*ALF(I,J)*(COS(THETA(J))**2)*DRB/((AR(I)**2)*D0)
      IF(DELWJ.LT.0.0) GO TO 636
      A(I)=-AVAL
      B(I)=BBVAL
       C(I)=-(EEVAL+CPEHT*2.*ABSWJ/((AR(I)**2)*COS(THETA(J)))*D0))
       D(I)=TM(I,J+1)*(2.*ALF(I,J)/((AR(I)**2)*D0R)+2.*ALF(I,J)*
     1(COS(THETA(J))**2)/((AR(I)**2)*D0R))+DVAL
      GO TO 620
  636 A(I)=-(AVAL+CPEHT*2.*ABSWJ/((AR(I)**2)*COS(THETA(J)))*D0))
      B(I)=BBVAL
      C(I)=-EEVAL
       D(I)=TM(I,J+1)*(2.*ALF(I,J)/((AR(I)**2)*D0R)+2.*ALF(I,J)*
     1(COS(THETA(J))**2)/((AR(I)**2)*D0R))+DVAL
      GO TO 620
  640 DELWJ=WB(I,J-1)-WB(I,J)
      ABSWJ=ABS(DELWJ)
       BBVAL=DRB*D0/DELTB+CPEHT*2.*ABSWJ/((AR(I)**2)*D0*
     1COS(THETA(J)))+2.*ALF(I,J)*D0/DRB+2.*ALF(I,J)*DRB/((AR(I)**2)*
     2D0)+2.*ALF(I,J)*(COS(THETA(J))**2)*DRB/((AR(I)**2)*D0)
      IF(DELWJ.LT.0.0) GO TO 641
      GO TO 642
  641 A(I)=-AVAL
      B(I)=BBVAL
       C(I)=-(EEVAL+CPEHT*2.*ABSWJ/((AR(I)**2)*COS(THETA(J)))*D0))
       D(I)=TM(I,LL1)*(2.*ALF(I,J)/((AR(I)**2)*D0R)+2.*ALF(I,J)*
     1(COS(THETA(J))**2)/((AR(I)**2)*D0R))+DVAL
      GO TO 620
  642 A(I)=-(AVAL+CPEHT*2.*ABSWJ/((AR(I)**2)*COS(THETA(J)))*D0))
      B(I)=BBVAL
      C(I)=-EEVAL
       D(I)=TM(I,LL1)*(2.*ALF(I,J)/((AR(I)**2)*D0R)+2.*ALF(I,J)*
     1(COS(THETA(J))**2)/((AR(I)**2)*D0R))+DVAL
  620 CONTINUE
      CALL TRIDAG (1,LNK,A,B,C,D,TT)
      DO 665 I=1,LNK
  665 TM(I,J)=TT(I)
  615 CONTINUE
       WRITE(42,1222) CPEHT,UINF,TINF,TMAV,CPEMT
 1222 FORMAT(1X,'VALUE OF CPEHT = ',F12.6,2X,'VALUE OF UINF= ',
     1F12.6,2X,'VALUE OF TINF= ',F12.6,2X,'VALUE OF TMAV= ',F12.6
     2,2X,'AND THE VALUE OF CPEMT= ',E16.12/)
      RETURN
      END
C
C
C     ****************************************************************
C
C     SUBROUTINE JET-REGION
C
C     ****************************************************************
C
      SUBROUTINE JETREG
      SAVE
      COMMON/AREA3/WB(21,21),EB(21,21),TM(21,21),CFEO(21,21),
     1TL(21,21),W(21,21),E(21,21),TG(31,31),CMO2(31,31),UR(21,21),
     2UZ(21,21),VR(31,31),VZ(31,31)
       COMMON/AREA1/LL,LL1,LNK,LNK1,DRB,D0,D0R,RYN,PEMT,PEHT,
     1VFB,DELTB,DELTB1,TIMEB,TIMEB1,RP,RF,TNP,PAI,ITERB,ITER1,UFG,
     2MP,UFW,UFE,THKM,DENP,BEDH,TOTZ,DLRP,ALHM,VFP,DAKP,
     3DAKM,UCHAR,COFSMR,COFLAR,ATMLOS,PMW,AMWMIX,DENMIX,
     3DLRCEL,CONSELL,POWIND,HEATBL,THTMEL,HFEPRO,ACUHT,
     4CFEOPR,COUTFL,VSTRCO,TINIT,ALHM1
      COMMON/AREA5/A(31),B(31),C(31),D(31),TT(31)
       COMMON/AREA6/MM,MM1,DZG,PEGHT,PEGMT,RBLV,DELTGH,
     1TIMEG,DELTGM
       COMMON/AREA7/U2ZETA(31),PHI(31),DHDZ(31),AZ(31)
      COMMON/AREA8/CPG(31,31),AKG(31,31),RHOG(31,31),DOABL(31,31)
       COMMON/AREA9/N,M,NN,N1,M1,DZ,DR,DR1,DTLR,PEL,DPOWER,
       1ITERIN,DELT,NNN1,TIME,ETA,ADR,DDR,UVF,OSF,AA,BB,U0,V0,
     2NNN,ORIGZ,DH
      COMMON/AREA10/R(22),Z(22),UU(22),VV(22),XX(22),YY(22)
     DR=0.1
     AZ(M)=0.0
```

```
      DO 25 J=M,MM
      IF(J.EQ.MM) GO TO 26
      AZ(J+1)=AZ(J)+DZG*0.1
   26 U2ZETA(J)=AZ(J)*1000.375
      IF((U2ZETA(J).GE.0.0).AND.(U2ZETA(J).LT.0.8)) DFIDZ(J)=0.7782*
     1U2ZETA(J)+9.93E-03
      IF((U2ZETA(J).GE.0.0).AND.(U2ZETA(J).LT.0.9)) PHI(J)=0.278586*
     1(U2ZETA(J)**1.914735)
      IF((U2ZETA(J).GE.0.8).AND.(U2ZETA(J).LT.1.5)) DFIDZ(J)=0.675136*
     1(U2ZETA(J)**0.623345)
      IF((U2ZETA(J).GE.0.9).AND.(U2ZETA(J).LT.2.3)) PHI(J)=0.2737292*
     1(U2ZETA(J)**1.659996)
      IF((U2ZETA(J).GE.1.5).AND.(U2ZETA(J).LT.2.6)) DFIDZ(J)=0.765417*
     1(U2ZETA(J)**0.2950652)
      IF((U2ZETA(J).GE.2.6).AND.(U2ZETA(J).LT.3.2)) DFIDZ(J)=0.933136*
     1(U2ZETA(J)**0.057749)
      IF((U2ZETA(J).GE.2.3).AND.(U2ZETA(J).LT.3.7)) PHI(J)=0.3438329*
     1(U2ZETA(J)**1.3694053)
      IF((U2ZETA(J).GE.3.2).AND.(U2ZETA(J).LT.3.8)) DFIDZ(J)=0.981417*
     1(U2ZETA(J)**0.0138971)
      IF((U2ZETA(J).GE.3.8).AND.(U2ZETA(J).LT.4.6)) DFIDZ(J)=0.998025*
     1(U2ZETA(J)**0.00128785)
      IF((U2ZETA(J).GE.3.7).AND.(U2ZETA(J).LT.4.6)) PHI(J)=0.4057333*
     1(U2ZETA(J)**1.2384354)
      IF((U2ZETA(J).GE.4.6).AND.(U2ZETA(J).LT.10.1)) DFIDZ(J)=1.0*
     1(U2ZETA(J)**0.0)
      IF((U2ZETA(J).GE.4.6).AND.(U2ZETA(J).LT.7.1)) PHI(J)=0.4577653*
     1(U2ZETA(J)**1.161625S)
      IF((U2ZETA(J).GE.7.1).AND.(U2ZETA(J).LT.10.1)) PHI(J)=0.51115*
     1(U2ZETA(J)**1.1048528)
      DO 35 I=1,N
      VZ(I,J)=-(PHI(J)*0.2827366)/RBLV
      VR(I,J)=(DFIDZ(J)*R(I)*10.0)/RBLV
   35 CONTINUE
   25 CONTINUE
      print*,rblv,dr
C     J-DIRECTION.....
      DO 70 I=1,N
      DO 80 J=M,MM
      RHOG(I,J)=((3.91870E+05)*((TG(I,J)*300.)**(-1.0007)))/1.30103E+03
      CPG(I,J)=(7.16+(1.0E-03)*(TG(I,J)*300.)-
     1(0.4E+05)/((TG(I,J)*300.)**2))/7.0155
      DR=0.1
      IF(J.EQ.MM) GO TO 76
      IF(J.EQ.M) GO TO 74
      IF(I.EQ.NN) GO TO 71
      IF(I.GT.NN) GO TO 73
      GO TO 77
   73 DR=DR1
   77 IF(I.EQ.1) GO TO 72
      A(J)=-(PEGHT*RHOG(I,J)*CPG(I,J)*VZ(I,J)/2.+AKG(I,J)/DZG)
      B(J)=RHOG(I,J)*CPG(I,J)*DZG/DELTGH+PEGHT*RHOG(I,J)*CPG(I,J)*
     1VR(I,J)*(DZG/DR)+2.*AKG(I,J)/DZG
      C(J)=PEGHT*RHOG(I,J)*CPG(I,J)*VZ(I,J)/2.-AKG(I,J)/DZG
      D(J)=TG(I,J)*RHOG(I,J)*CPG(I,J)*(DZG/DELTGH)+TG(I-1,J)*PEGHT*
     1RHOG(I,J)*CPG(I,J)*VR(I,J)*(DZG/DR)
      GO TO 80
   71 A(J)=-(RHOG(I,J)*CPG(I,J)*PEGHT*VZ(I,J)/2.+AKG(I,J)/DZG)
      B(J)=RHOG(I,J)*CPG(I,J)*DZG/DELTGH-RHOG(I,J)*CPG(I,J)*PEGHT*
     1VR(I,J)*DZG*DDR/ADR+RHOG(I,J)*CPG(I,J)*VR(I,J)*PEGHT*
     2DZG/(ADR*DDR)+2.*AKG(I,J)/DZG
      C(J)=RHOG(I,J)*CPG(I,J)*PEGHT*VZ(I,J)/2.-AKG(I,J)/DZG
      D(J)=-TG(I+1,J)*(DZG*PEGHT*VR(I,J)*DDR*RHOG(I,J)*CPG(I,J)/ADR)+
     1TG(I-1,J)*(PEGHT*VR(I,J)*DZG*RHOG(I,J)*CPG(I,J)/(ADR*DDR))+
     2TG(I,J)*(RHOG(I,J)*CPG(I,J)*DZG/DELTGH)
      GO TO 80
   72 A(J)=-(PEGHT*RHOG(I,J)*CPG(I,J)*VZ(I,J)/2.+AKG(I,J)/DZG)
      B(J)=RHOG(I,J)*CPG(I,J)*(DZG/DELTGH)+2.*AKG(I,J)/DZG
      C(J)=PEGHT*RHOG(I,J)*CPG(I,J)*VZ(I,J)/2.-AKG(I,J)/DZG
      D(J)=TG(I,J)*RHOG(I,J)*CPG(I,J)*(DZG/DELTGH)
      GO TO 80
   74 A(M)=0.0
      B(M)=1.0
      C(M)=0.0
      D(M)=TL(I,J)
      GO TO 80
```

```
76  A(MM)=0.0
    B(MM)=1.0
    C(MM)=0.0
    D(MM)=1.2
80  CONTINUE
    CALL TRIDAG (M,MM,A,B,C,D,TT)
    DO 82 J=M,MM
82  TG(I,J)=TT(J)
70  CONTINUE
    print*,peght,dzg
C   J-DIRECTION.....
    DO 41 I=1,N
    DO 30 J=M,MM
    DOABL(I,J)=((9.52E-10)*((TG(I,J)*300.)**1.75))/(2.0587E-05)
    DR=0.1
    IF(J.EQ.MM) GO TO 40
    IF(J.EQ.M) GO TO 42
    IF(I.EQ.NN) GO TO 83
    IF(I.GT.NN) GO TO 84
    GO TO 86
84  DR=DR1
86  IF(I.EQ.1) GO TO 45
    A(J)=-((PEGMT*VZ(I,J))/2.+DOABL(I,J)/DZG)
    B(J)=DZG/DELTGM+PEGMT*VR(I,J)*(DZG/DR)+2.*DOABL(I,J)/DZG
    C(J)=PEGMT*VZ(I,J)/2.-DOABL(I,J)/DZG
    D(J)=CMO2(I-1,J)*PEGMT*VR(I,J)*(DZG/DR)+CMO2(I,J)*DZG/DELTGM
    GO TO 30
83  A(J)=-(PEGMT*VZ(I,J)/2.+DOABL(I,J)/DZG)
    B(J)=(DZG/DELTGM-PEGMT*VR(I,J)*DZG*DDR/ADR+PEGMT*VR(I,J)*
   1DZG/(ADR*DDR)+DOABL(I,J)*2./DZG)
    C(J)=PEGMT*VZ(I,J)/2.-DOABL(I,J)/DZG
    D(J)=CMO2(I-1,J)*(PEGMT*VR(I,J)*DZG/(ADR*DDR))-CMO2(I+1,J)*
   1(DZG*PEGMT*VR(I,J)*DDR/ADR)+CMO2(I,J)*(DZG/DELTGM)
    GO TO 30
42  A(M)=0.0
    B(M)=1.0
    C(M)=-1.0
    D(M)=-(DZG*(1.-VFP)*(4.9981292E+04)*
   1EXP(-54.667/(TG(I,J)))/DOABL(I,J))
    GO TO 30
40  A(MM)=0.0
    B(MM)=1.0
    C(MM)=0.0
    D(MM)=1.0
    GO TO 30
45  A(J)=-((PEGMT*VZ(I,J))/2.+DOABL(I,J)/DZG)
    B(J)=DZG/DELTGM+DOABL(I,J)*2./DZG
    C(J)=PEGMT*VZ(I,J)/2.-DOABL(I,J)/DZG
    D(J)=CMO2(I,J)*(DZG/DELTGM)
30  CONTINUE
    CALL TRIDAG (M,MM,A,B,C,D,TT)
    DO 50 J=M,MM
50  CMO2(I,J)=TT(J)
41  CONTINUE
    print*,pegmt,dr,ddr
    DR=0.1
    DTLR=DR/DZ
    RETURN
    END
C
C
C
C
```

```
C   PROGRAM FOR BESSEL EQUATION
C
      IMPLICIT REAL*8(A-H,O-Z)
     DOUBLE PRECISION SUM1,SUM2,LL,I2,I3,KK
C    INTEGER SUM1,SUM2
      DIMENSION XX(22),YY(22),UU(22),VV(22)
      OPEN(UNIT=91,FILE='for91')
     NMAX=10
      N=20
      R=0.0
      DR=0.1
      DR1=0.025
     KMM=0
      XX(1)=0.0
      YY(1)=0.0
      UU(1)=0.0
       VV(1)=0.0
        PI=3.1415926
          PHI=45.51657*PI/180.0
     SUM1=0
     SUM2=0
     DO 55 J=2,N
     IF(J.GT.8) DR=DR1
     GO TO 56
56   R=R+DR
       print*,R
      RHO=12.414711*R
     SUMR0=0.0
     SUMR1=0.0
      SUMI0=0.0
      SUMI1=0.0
     DO 5 I=KMM,NMAX
     IF(I.EQ.0) GO TO 10
      SUM1=SUM1*I*I
       SUM2=SUM2*I*(I+1)
     GO TO 15
10    SUM1=1
     SUM2=1
15      I2=2*I
       I3=2*I+1
      RHO2=RHO**I2
      RHO3=RHO**I3
        LL=2**I2
        KK=2**I3
      SUMR0=RHO2*COS(PHI*I2)/(SUM1*LL)+SUMR0
       SUMI0=RHO2*SIN(PHI*I2)/(SUM1*LL)+SUMI0
       SUMR1=RHO3*COS(PHI*I3)/(SUM2*KK)+SUMR1
        SUMI1=RHO3*SIN(PHI*I3)/(SUM2*KK)+SUMI1
5    CONTINUE
     XX(J)=SUMR0
     YY(J)=SUMI0
     UU(J)=SUMR1
      VV(J)=SUMI1
55   CONTINUE
     DO 3 J=1,N
      WRITE(91,102) XX(J),YY(J),UU(J),VV(J)
102  FORMAT(2X,4F16.8/)
3    CONTINUE
C     STOP
     END
C
```

APPENDIX H

FEW PHOTOGRAPHS OF AN INDUCTION SMELTING PROCESS

Photograph 1. Pellet charging during induction smelting process.

Photograph 2. Induction smelting process in full operation.

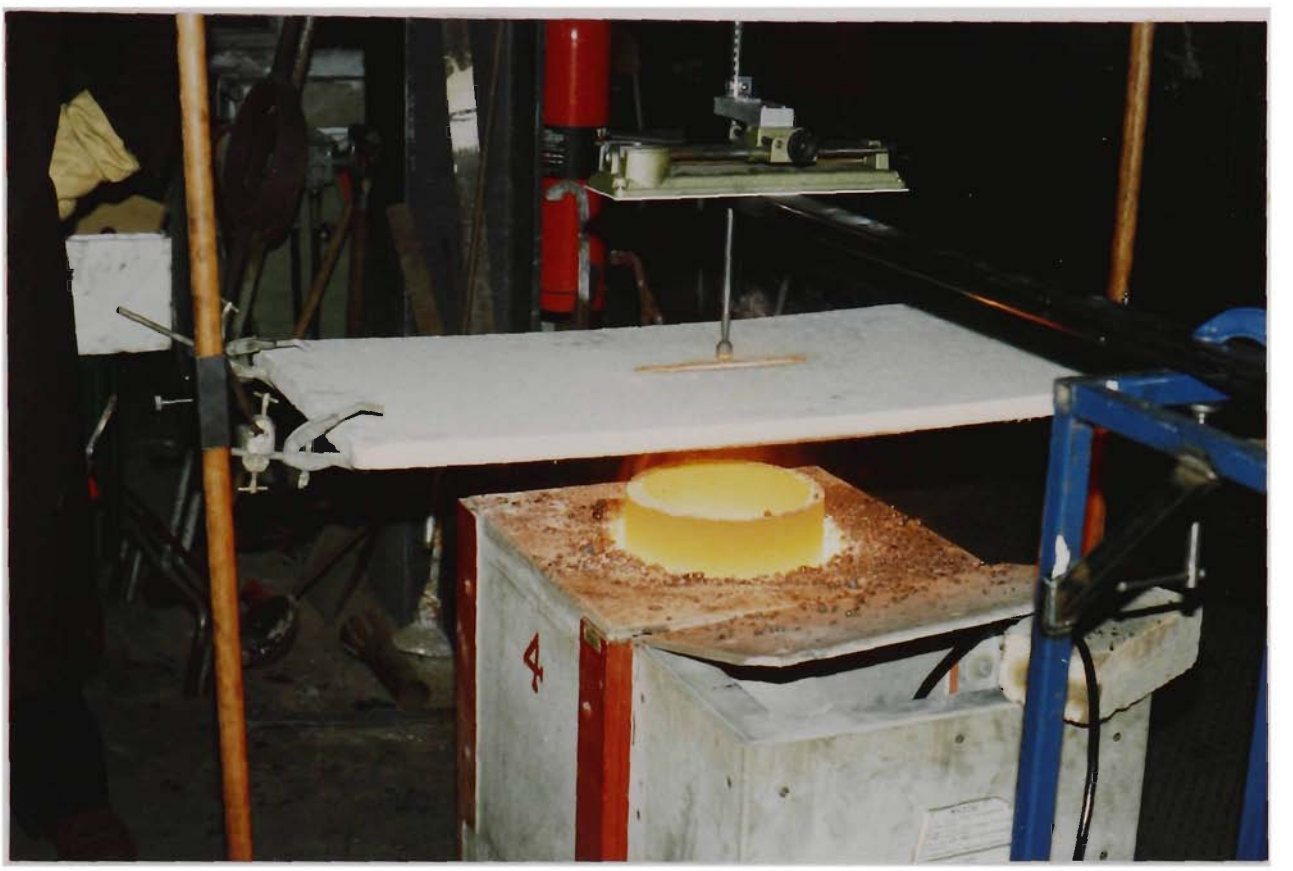

Photograph 3. Liquid iron velocity measurement during smelting process.

REFERENCES

1. J. Davis and P. Simpson: Induction Heating Handbook; McGraw Hill, London, 1979.
2. J.O. Stephenson and R.M. Smailer: Direct Reduced Iron-Technology and Econimics of Production and Use; Iron & Steel Society, P.A., U.S.A., 1980.
3. C.G. Davis, J.F. McFarlin and H.R. Pratt: Direct-reduction technology and economics; **Ironmaking Steelmaking, vol. 9, no. 3**,1982, p93-129.
4. J.G. Sibakin: **Iron Steelmaker, vol. 7**, Jan. 1980, p16-22.
5. R.B. Smith and M.J. Corbett: Coal bades iron making; **Ironmaking Steelmaking, vol. 14,** 1987, p49
6. F. Oeters and G. Gorl: Develpoment tendencies of chemical metallurgy in Europe; **Steel Research, vol. 61, no. 9,** 1990, p285-400.
7. R.B. Smith and M.J. Corbett: Process technology conference; **ISS-AIME, vol. 7,** 1988, p147-178.
8. J.A. Innes et. al., **ibid,** p225-231.
9. R.J. Fruehan, K. Ito and B. Ozfurk: Analysis of both smelting processes for producing iron; p673-698 in proc. Metallurgical Processes for the Year 2000, Eds. H.Y. Sohn and E.S. Geskin, TMS, PA, U.S.A., 1988.
10. K. Koch, U. Harter and R. Bruckhaus: Smelting reduction of liquid iron oxides with different means of reduction; **Steel Research, vol. 61, no. 1,** 1990, p14.
11. K.Sadrnezhaad: Direct reduction iron: An advantageous charge material for induction furnace; **ibid,** p761.

12. U. Harter and K. Koch: Investigation on smelting reduction with top blowing of carbon monoxide onto iron-oxides melts; **Steel Research, vol. 61, no. 2**, 1990, p47.

13. U. Harter, R. Bruckhaus and K. Koch: Investigation on smelting reduction of iron oxide melts by injecting or bottom blown carbon monoxide or solid carbon; **ibid,** p53.

14. J.O. Edstrom and J. Ma: Influence of the type of coal on energy consumption in shaft furnace smelting reduction processes; **Scandinavian J. of Metallurgy, vol. 18,** 1989, p105-112.

15. K. Brotzmann: New concepts and methods for iron and steel production; Steelmaking Proceedings, **ISS-AIME, vol. 70**, 1987, p3.

16. M. Tokuda: Conceptual and fundamental problwms of smelting reduction process for iron making; **Trans. ISIJ, vol. 26,** 1986, pB192.

17. S. Orsten and F Oeters: Dissolution of carbon in liquid iron; PTD Proc., **ISS-AIME, vol. 6**, 1986, p143.

18. E. Aukrust: The AISI program for direct steelmaking; p637-346 (in ref. 9).

19. Y. Fukuzawa et.al.: Reaction in the continuous melting and smelting reduction furnace; **ISIJ, vol. 29, no. 10,** 1989, p836-842.

20. R. Nagabayashi, M. Hino and S. Ban-ya: Mathematical expression of phosphorous distribution in steelmaking process byquadratic formalism; **ISIJ, vol. 29, no. 2,** 1989, p140-147.

21. E.T. Turkdogan: Reaction of liquid steel with slag during furnace tapping; **Ironmaking Steelmaking, vol. 15, no. 6,** 1988, p311-18.

22. A. Sato et.al.: Melting rate of iron oxide pellets into iron melt, **Trans. ISIJ, vol. 21**, 1981, p879-886.

23. I.D. Sommerville, P. Grieveson and J. Tayler: Kinetics of reduction of iron oxide in slag by carbon in iron, part 1, **Ironmaking Steelmaking, no. 1**, 1980, p25-31.

24. R.J. Pomfret and P. Grieveson: The kinetics of slag-metal reactions; **Canadian Met. Quart., vol. 22, no. 3,** 1983, p287-99.

25. K. Mori et. al.: Rate of transfer of phosphorus between metal and slag; **Trans ISIJ, vol. 18,** 1978, p261-68.

26. G. Derge, W.O. Philbrook and K. Goldman: The mechanism of sulpher transfer between carbon-saturated iron and CaO-SiO_2-Al_2O_3 slags; **J. of Metal, vol. 188,** Sep. 1950, p1111-19.

27. B. Deo and P. Grieveson: Kinetics of desulphurisation of molten pig iron; **Steel Research, vol. 57, no. 10**, 1986, p514-19.

28. K. Ogawa and T. Onoue: Mixing and mass transfer in ladle refining process; **ISIJ, vol. 29, no. 2,** 1989, p148-53.

29. R.J. Pomfret and P. Grieveson: Kinetics of fast initials stage of reduction of MnO from silicate slags by carbon in molten iron; **Ironmaking Steelmaking, no. 5,** 1978, p191-97.

30. K.M. Goldman, G. Derge and W.O. Philbrook: Effect of SI, Mn, P, C, Ni and Cu on the mechanism of sulphur transfer across a slag-metal interface; **J. of Metal, May** 1954, p534-540.

31. N. Tsuchiya et. al.: The transfer of silicon from the gas phase to molten iron inthe blast furnace; **Met. Trans., vol. 7B,** Sep. 1976, p315-20.

32. C. Yamagata et.al.: Desiliconization reaction of pig iron with high FeO containing blast furnace slag under pressurized and

cokj-coexisting condition; **ISIJ, vol. 30, no. 9**, 1990, p740-47.

33. Y. Kim and R.D. Pehlke: Mass transfer during dissolution of solid into liquid in the iron carbon system; **Met. Trans., vol. 5, no. 12,** 1974, p2527-32.
34. J. Szekely and Y.K. Chang: Melting and dissolution of low-carbon steel in Fe-C melts; **Met. Trans., no. 3**, 1973, p2825.
35. G.D. McAdam, A. McNabb and E. Bradford: Experimental support for a coupled diffusion model of iron oxide reduction; **Ironmaking Steelmaking, vol. 15, no. 5**, 1988.
36. P.G. Sismanis and S.A. Argyropoulos: Modelling of exothermic dissolution; **Can. Met. Quart., vol. 27, no. 2**, 1988, p123-33.
37. D.G.C. Robertson, B. Deo and S. Ohguchi: Multicomponent mixed-transport-control theory for kinetics of coupled slag/metal and slag/metal/gas reactions: application to desulphurization of molten iron; **Ironmaking Steelmaking, vol. 11, no. 1**, 1984, p41-55.
38. T. Debroy, N.H. El-Kaddah and D.G.C. Robertson: Mixed transport control in gas-liquid metal reactions; **Met. Trans., vol. 8B**, June 1977, p271-277.
39. B. Deo, P. Ranjan and A. Kumar: Mathematical model for computer simulation and control of steelmaking; **Steel Research, vol. 58, no. 9,** 1987, p427-31.
40. N.H. El-Kaddah and J. Szekely: Mathematical model for desulphurization kinetics in argon-stirred ladles; **Ironmaking Steelmaking, no. 6,** 1981, p269-278.
41. N. Standish, H.K. Worner and G.S. Gupta: Temperature distribution in microwave heated iron ore-carbon composites;

J. Microwave Power Electromagnetic Energy, vol. 25, n0. 2, 1990, p75-80.

42. H.K. Worner: Some pioneering pyrometallurgy, **Aust. IMM Bulletin and Proc., vol. 293, no. 8**, p36-43.

43. J. Szekely and C.W. Chang: Turbulent electromagnetically driven flow in metals processing part I & II, **Ironmaking and Steelmaking, No. 3**, 1977, p190-204.

44. J. Szekely and S. Asai: A general mathematical statement of turbulent recirculating flows, **Trans. ISIJ, vol. 15**, 1975, p270-275.

45. N. El-Kaddah and J. Szekely: The turbulent recirculating flow field in a coreless induction furnace, a comparison of theoretical predictions with measurements, **J. Fluid Mech., vol. 133**, 1983, p37-46.

46. D.J. Moore and J.C.R. Hunt: Flow, turbulence and unsteadiness in coreless induction furnaces, p93-107 in Proc. Metallurgical Applications of Magnetohydrodynamics, Eds. H.K. Moffatt and M.R.E. Proctor, The Metal Society, London, 1984.

47. S. Koanda and Y.R. Fautrelle: Modelling of coreless induction furnaces; some theoretical and experimental results, p120-128, (in ref. 6).

48. J.D. Lavers and P.P. Biringer: The influence of system geometry on the electromgnetic stirring forces in crucible induction melting furnaces, p62-77, (in ref. 6).

49. E.D. Tarapore and J.W. Evans: Fluid velocities in induction melting furnaces part I & II, **Met. Trans. B, vol. 7B**, 1976, p343-357, and part II, **Met. Trans. B, vol. 8B**, 1977, p179-184.

50. W.F. Hughes and F.J. Young: The Electromagnetodynamics of Fluids, John Wiley, N.Y., 1966.

51. O.J. Ilegbusi and D.B. Spalding: Prediction of fluid flow and heat transfer characteristics of turbulent shear flows with a two-fluid model of turbulence, **Int. J. Heat Mass Transfer, vol. 32, no. 4,** 1989, p767-774.

52. N.J. Damaskos, F.J. Young and W.F. Hughes: The magnetohydrodynamics of the coreless induction furnace, **Proc. I.E.E., vol. 110, no. 6**, 1963, p1089-1095.

53. N.J. Damaskos and F.J. Young: The stability of thermally induced flow in the coreless induction furnaces, **Int. J. Heat Mass Transfer, vol. 8**, 1965, p721-728.

54. O.J. Ilegbusi and J. Szekely: Mathematical midelling of electromagnetic stirring of molten metal-solid suspension; **Trans. ISIJ, vol. 28,** 1988, p97-103.

55. O.J. Ilegbusi and J. Szekely: Melt stratification in ladles; **Trans ISIJ, vol. 27,** 1987, p563-69.

56. O.J. Ilegbusi and J. Szekely: Three-dimensional velocity fields for Newtonian and Non-Newtonian melts produced by rotating magnetic field; **Trans. ISIJ, vol. 29, no. 6,** p462-68.

57. J. Szekely and K. Nakanishi: Stirring its effects on Aluminium deoxidation in the ASEA-SKF furnace: part II mathematical representation of the turbulent flow field and of tracer dispersion; **Met. Trans. B, vol. 6B,** 1975, p245-56.

58. Y. Sundberg: Mechanical stirring power in molten metal in ladles obtained by induction stirring and gas blowing; **Scand. J. Met., vol 7,** 1978, p81-87.

59. P. Badar: Pressure and thermal effects in liquid metal due to collapse of external magnetic field; **Int. J. Heat Mass Transfer, vol. 32, n0. 6,** 1989, p1053-61.

60. V.K. Reichert: A numerical method to calculate induction heating installations; **Elektrowarme Int., vol. 26, no. 4,** 1968, p113-23.

61. A. Moros and J.C.R. Hunt: Recirculating flows in the cross-section of a channel induction furnace; **Int. J. Heat Mass Transfer, vol. 31, n0. 7,** 1988, p1497-1515.

62. Xi Chen: Heat transfer and flow in a radio frequency plasma torch- a new modelling approach; **Int. J. Heat Mass Transfer, vol. 33, n0. 5,** 1990, p815-26.

63. Y. Kishida et.al.: Anisotropic effect of magnetohydrodynamics on metal solidification; **Trans. ISIJ, vol. 30, no. 1,** 1990, p34-46.

64. H. Iwata et.al.: Electromagnetic stirring of molten core in continuous casting of high carbon steel; **Trans ISIJ, vol. 16,** 1976, p374-81.

65. Ch. Vives and R. Ricou: Fluid flow phenomena in a single phase coreless induction furnace; **Met. Trans. B, vol. 16B,** 1985, p227-35.

66. A.D. Sneyd: Stability of fluid layers carrying a normal electric current; **J. Fluid Mech., vol. 156,** 1985, p223-36.

67. V.K. Reichert: Die numerische berechung der elektromagnetisch verursachten stromung in induktionstiegelofen; **Scientia Electrica, vol. 1b, no. 4,** 1970, p126-46.

68. A.D. Sneyd: Fluid flow induced by a rapidly alternating or ratating magnetic field; **J. Fluid Mech., vol. 92, part I,** 1979, p35-51.

69. A.J. Mestel: On the flow in a channel induction furnace; **J. Fluid Mech., vol. 147,** 1984, p431-47.

70. W.R. Hodgkins: Mathematical calculations on electromagnetic stirring; Elect. Council Res. Centre, Job no. 481, U.K., 1972.

71. K.H. Lie, D.N. Riahi and J.S. Walker: Buoyancy and surface tension driven flows in float zone crystal growth with a strong axial magnetic field; **Int. J. Heat Mass Transfer, vol. 32, no. 12,** 1989, p2409-20.

72. H. Tse-Chiang, T. Lehner and B. Kjelberg: Fluid flow in ladles - experimantal results; **Scand. J. Met., vol. 9,** 1980, p105-10.

73. I.J.D. Craig and A.D. Sneyd: A dynamic relaxation technique for determining the structure and stability of coronal magnetic field; **Astrophysical J., vol. 311,** 1986, p451-59.

74. A.H. Dilawari et.al.: Fluid flow and heat transfer in plasma reactors- II. A critical comparison of experimentally measured and theoretical predicted temperature profiles in plasma jets in the absence and presence of side stream injection; **Int. J. Heat Mass Transfer, vol. 32, no. 6,** 1989, p35-46.

75. P.E. King: Magntohydrodynamics in electric arc furnace steelmaking; Int. Bu. mines, PA29213, 1990, p1-13.

76. T. Watanabe et.al.: The flow, temperature and concentration fields in a radio frequency argon-helium plasma; **J. Chem. Eng. Japan, vol. 23, no. 4,** 1990, p389-95.

77. A. Serizawa et.al.: MHD effect on NaK-Nitrogen two-phase flow and heat transfer in a vertical round tube; **Int. J. Multiphase Flow, vol. 16, no. 5,** 1990, p761-88.

78. J. Szekely: Fluid flow phenomena in metals processing; Academic Press Inc, N.Y., 1979.

79. V. Stanek and J. Szekely: The effect of non-uniform porosity in causing flow maldistribution in isothermal packed beds, **Can. J. Chem. Eng., vol. 50**, 1972, p9-14.

80. V. Stanek and Szekely: Flow maldistribution in two dimensional packed bed part II-the behaviour of non-isothermal systems, **Can. J. Chem. Eng., vol. 51**, 1973, p22-30.

81. V. Stanek and J. Szekely: Three dimensional flow of fluids through non-uniform packed beds, **AIChE, vol. 20, no. 5,** 1974, p 974-980.

82. R. Clift, J.R. Grace and M.E. Weber: Bubbles, Drops and Particles, Academic Press, N.Y., 1978.

83. B.P. LeClair: Viscous flow in multiparticle systems at intermediate Reynolds number, Ph.D. Thesis, 1970, McMaster Univ.,Canada.

84. G.R. Rigby and C.E.Capes: Bed expansion and bubble wakes in three-phase fluidization, **Can. J. Chem. Eng., vol. 48,** 1970, p343-348.

85. J.H. Masliyah and N. Epstein: Numerical solution of heat and mass transfer from spheroids in steady axy-symmetric flow; **Prog. Heat Mass Transfer, vol. 6,** 1972, p613-632.

86. C. Narasimhan and W.H. Gauvin: Heat and mass transfer to spheres in high temperature surroundings, **Can. J. Chem. Eng., vol. 45**, 1967, p181-188.

87. P. Sykes and A. Gomezplata: Particle liquid mass transfer in stirred tanks, **Can. J. Chem. Eng., vol. 45,** 1967, p189.

88. P.S.B. Stewart and J.F. Davidson: Three phase fluidization, water, particles and air, **Chem. Eng. Sci., vol. 19,** 1964, p319-322.

89. E. Achenbach: The effects of surface roughness and tunnel blockage on the flow past spheres, **J. Fluid. Mech., vol. 65, part 1,** 1974, p113-125.

90. S.C.R. Dennis, J.D.A. Walker and J.D. Hudson: Heat transfer from a sphere at low Reynolds numbers, **J. Fluid Mech. vol. 60, part2,** 1973, p273-283.

91. B.P. LeClair, A.E. Hamielec and H.R. Pruppacher: A numerical study of the drag on a sphere at low and intermediate Reynolds numbers, **J. Atmosph. Sci., vol. 27,** 1970, p308-315.

92. D.L.R. Oliver and J.N. Chung: Unsteady conjugate heat transfer from a translating fluid sphere at moderate Reynolds numbers; **Int. J. Heat Mass Transfer, vol. 33, no. 1,** 1990, p401-08.

93. B.M. Abramzon and I. Borde: Conjugate unsteady state heat transfer from a droplet in creeping flow; **A.I.Ch.E.J., vol. 26,** 1980, p991-93.

94. L.E. Scriven: Dynamics of a fluid interface-equation of motion for Newtonian surface fluids; **Chem. Eng. Sci., vol. 12,** 1960, p98-108.

95. J.F. Davidson: On the liquidlike behavior of fluidized beds; **Ann. Rev. Fluid Mech., vol. 9,** 1977, p55-86.

96. J.F. Harper: The motion of bubbles and drops through liquids; **Adv. in App. Mech., vol. 12,** 1972, p59-125.

97. D.L.R. Oliver and J.N. Chung: Flow about a fluid sphere at low to moderate Reynolds numbers; **J. Fluid Mech., vol. 177,** 1987, p1-18.

98. J.S. McNown and J.T. Newlin: Drag of spheres within cylinderical boundaries; US National Congress of App. Mech., 1st Proc., 1951, p801-06.

99. G.G. Stokes: On the effect of internal friction of fluid on the motion of pendulums; **Cambridge Phil. Society Trans., vol. 9, Part II,** 1851, P8-106.

100. F. Cooper: Heat transfer from a sphere to an infinite medium; **Int. J. Heat Mass Transfer, vol. 20,** 1976, p991-93.

101. S.C.R. Dennid, J.D.A. Walker and J.D. Hudson: Heat transfer from a sphere at low Reynolds number; **J. Fluid Mech., vol. 60,** 1973, p273-83.

102. H. Schlichting: Boundary Layer Theory, McGraw Hill, N.Y., 1979.

103. H. Miyazaki and E. Silberman: Flow and heat transfer on a flate plate normal to a two-dimensional laminar jet issuing from a nozzle of finite height, **Int. J. Heat Mass Transfer, vol 15,** 1972, p2097-2107.

104. R. Gardon and J.C. Akfirat: Heat transfer characteristics of impinging two-dimensional air jets, **J. Heat Transfer, vol. 88(1),** 1966. p101-108.

105. A.R.P. van Heiningen, A.S. Mujumdar and W.J.M. Douglas: Numerical prediction of the flow field and impinging heat transfer caused by laminar slot jet, **J. Heat Transfer, vol. 98,** 1976, p654-658.

106. X.S. Wang, Z. Dagan and L.M. Jiji: Heat transfer between a circular free impinging jet and solid surface with non-uniform

wall temperature or wall heat flux - Part 1&2, **Int. J. Heat Mass Transfer, vol. 32, no. 7,** 1989, p1351-1371.

107. T.D. Yuan, J.A. Liburdy and T. Wang: Buoyancy effects on laminar impinging jets, Int. **J. Heat Mass Transfer, vol. 31, no. 10**, 1988, p2137-45.

108. O.J. Ilegbusi: Turbulent boundary layer on a porous flate plate with severe injection at various angles to the surface; **Int. J. Heat Mass Transfer, vol. 32, no. 4,** 1989, p761-65.

109. H. Yoshida, K. Suenaga and R. Echigo: Turbulence structure and heat transfer of a two-dimensional impinging jet with gas-solid suspensions; **Int. J. Heat Mass Transfer, vol. 33, no. 5,** 1990, p859-67.

110. X.S. Wang, Z. Dagan and L.M. Jiji: Heat transfer between a circular free impinging jet and a solid surface with non-uniform wall temperature or wall heat flux-1. Solution for the stagnation region; **Int. J. Heat Mass Transfer, vol. 32, no. 7,** 1989, p1351-60.

111. R.S.R. Gorla: The final approach to steady state in a non-steady axisymmetric stagnation point heat transfer; **Warme-und Staffubertr, vol. 22, 1/2,** 1988, p37.

112. R. Krishnaswamy and G. Nath: Unsteady compressible axisymmetric stagnation-point boundary-layer flow with a magnetic field; **Revue Roum. Sci. Tech. Ser. Mec. Appliquee, vol. 32, no. 4,** 1987, p365.

113. Y.B. Lebedev: Anomalous effect of surface temperature on stability of a laminar gas boundary layer; **J. Appl. Mech. Tech. Phys., vol. 29, n0. 2,** 1988, p185.

114. K.N. Lakshmisha, S. Venkateswaran and G. Nath: Three-dimensional unsteady flow with heat and mass transfer over

a continuous stretching surface; **J. Heat Transfer, vol. 110, no. 3,** 1988, p590.

115. T. Wang: Heat transfer to an underlying fluid due to the axisymmetric spreading of material on the surface; **Appl. Scient. Res., vol. 45, no. 4,** 1988, p367.
116. L.E. Kalikhman: Element of Magnetogasdynamics, 1967, W. B. Saunders, Philadelphia,PA, U.S.A.
117. Shih-I Pai: Magnetogasdynamics and Plasma dynamics, 2nd edition, 1963, Springer-Verlag, Vienna.
118. M. Salavdeon and R.I.L. Guthrie, **Met. Trans. B, vol. 9B,** 1978, p673-680.
119. V.G. Jenson, Proc. R. Soc. Ser. A249, 1959, p346-366.
120. G.E. Myers: Analytical Methods in Conduction Heat Transfer, 1971, McGraw Hill, N.Y.
121. L.J. Briggs and A.N. Lowan: Table of Bessel Functions $J_0(Z)$ and $J_1(Z)$ For Complex Arguments, 1943, Columbia University Press, N.Y.
122. A.E. Hamielec, T.W. Hoffman and L.L. Ross: Numerical solution of the Navier-Stokes equation for flow past spheres, Part I & II, **A.I.Ch.E., vol. 13, no. 2**, 1967, p212-224.
123. G.S. Gupta: Computer Simulation of a Multiple Hearth Roaster, M. Tech. Thesis, I.I.T. Kanpur, India, 1987.
124. F.J. Bayley, J.M. Owen and A.B. Turner: Heat Transfer, 1972, Thomas Nelson, London.
125. B. Carnahan, H.A. Luther and J.O. Wilkes: Applied Numerical Methods, 1969, John Wiley, N.Y.
126. T.M. Shih: Numerical Heat Transfer, 1976, Hemisphere, Washington.

127. T. Sundararajan: Course on Computer Applications in Metallurgical Engineering, 1985, I.I.T. Kanpur, India, p219-261.

128. G.S. Gupta, N. Chakraborti and T. Sundararajan: Development of a mathematical model for Multiplehearth Roasters, **Met. Trans. B, vol. 20B,** 1989, p925-935.

129. T. Sundararajan: Ph.D. Thesis, 1983, University of Pennsylvania, Philadelphia, PA, U.S.A.

130. S.V. Patankar: Numerical Heat Transfer and Fluid Flow, Hemisphere, Washington, D.C., 1980.

131. T. Sundararajan and P.S. Ayyaswamy: Hydrodynamics and heat transfer associated with condensation on a moving drop - solution for intermediate Reynolds number, **J. Fluid Mech., vol. 149**, 1984, p33-58.

132. G.E. Myers: Analytical Methods in Conduction Heat Transfer, McGraw Hill, N.Y., 1971.

133. T. Sundararajan, I.I.T. Kanpur, India, private communication.

134. T.M. Shih: Numerical Properties and Methodologies in Heat Transfer, Hemisphere, Washington, 1983.

135. J. Szekely, C.W. Chang and R.E. Ryan: The measurement and prediction of the melt velocities in a turbulent, electromagnetically driven recirculating low melting alloy system, **Met. Trans. B, vol. 8B,** 1977, p333-338.

136. R. Ricou and C. Vives: Local velocity and mass transfer measurements in molten metals using an incorporated magnet probe, **Int. J. Heat Mass Transfer, vol. 25, n0. 10**, 1982, p1579-1588.

137. T.C. Hsiao: Experimental measurement of flow velocities in gas stirred ladles, **MEFOS Report, MF79063E/2.**

138. D.C. Lillicrap: A technique for velocity measurement in coreless induction furnace, p46-56, in Proc.: Metallurgical Applications of Magnetohydrodynamics, 1982, Cambridge, The Metals Society, Eds. H.K. Moffatt and M.R.E. Proctor.

139. D. Moore, and J. Hunt: Liquid -Metal Flows and Magnetohydrodynamics, American Inst. of Aeronautics and Astronautics, New York, N.Y., 1983, vol. 84, p359-373.

140. R.D. Pehlke and J.F. Elliott: Solubility of nitrogen in liquid iron alloy II, kinetics, **Trans. Met. Soc. AIME, vol. 227**, 1963, p844-855.

141. L.A. Baker and R.G. Ward, Reaction of an iron - carbon droplet during free fall through oxygen, **JISI, vol. 205, part 9,** 1967, p714-717.

142. J.H. Swishzer and E.T. Turkdogan: Decarburization of the iron-carbon melts in CO_2-CO atmospheres; kinetics of gas-metal surface reactions, **Trans. Met. Soc. AIME, vol. 239,** 1967, p602-610.

143. A. K uchi et.al.: Fluid flow and mass transfer in the gas-liquid iron system with a laboratory-scale induction furnace, p79-92 (in ref. 6).

144. T.E. Dancy: The kinetics of the reduction of iron oxide above 1400°C, **J. Iron Steel Inst., vol. 169**, 1951, p17-24.

145. Y. Sasaki and T. Soma: Reduction mechanism of molten iron oxide by solid carbon, **Met. Trans. B, vol. 8B**, 1977, p189-190

146. W.O. Philbrook and L.D. Kirkbride: Rate of FeO reduction from a $CaO\text{-}SiO_2\text{-}Al_2O_3$ slag by carbon saturated iron, **Trans AIME, March 1956**, p351-356.

147. D.I. Ryzhonkov et.al.: **Chernaya Met., no. 4**, 1960, p19-22.

148. V.V. Kondakov et.al.: **ibid, no. 4**, 1960, p23-28.

149. P. Grieveson and E.T. Turkdogan: Kinetics of oxidation and reduction of molten iron oxide, **Trans. Met. Soc. AIME, vol. 230**, 1964, p1609-1614.

150. D.R. MacRae: Kinetics and Mechanism of the reduction of solid iron oxide in iron-carbon melts, **J. of Metals, 17**, 1965, p1391.

151. G.W. Lloyd, D.R. Young and L.A. Baker: Reaction of iron oxide with iron-carbon melts, **Ironmaking Steelmaking, no. 1**, 1975, p49-55.

152. A. Sato and R. Nakagawa: Melting rate of directly reduced iron pellets into iron melt, **Trans. ISIJ, vol. 19, no.2**, 1979, p112-118.

153. M. Sugata: Reduction of iron oxide contained in molten slags with solid carbon, **Trans. ISIJ, vol.14, no. 2**, 1974,p88-95.

154. T. Soma et.al.: Reduction of molten iron with solid carbon, **Tetsu-To-Hagane, vol. 61, no. 11**, 1975, p2525-2530.

155. A. Sato et.al.: Reduction rate iron oxide in molten slag by carbon in molten iron, **Trans. ISIJ, vol. 23, no. 9**, 1983.

156. W.O. Philbrook and L.D. Kirkbride: **J. of Metals, vol. 8**, 1965, p351.

157. S.V. Shabrin and I. Vuzov: **Chernaya Met., no. 5**, 1964, p7.

158. S.K. Torby and W.O. Philbrook: The rate and mechanism of the reduction of FeO and MnO from silicate and aluminate slags by carbon-saturated iron, **Trans. AIME, vol. 239**, 1967, p1005.

159. L.D. Smoot and P.J. Smith: Coal Combustion and Gasification, 1985, Plenum, N.Y.

160. H.A. Fine and G.H. Geiger: Handbook on Material and Energy Balance Calculations in Metallurgical Processes, TMS AIME, Warrendale, PA, 1979.

161. M.L.J. Young: Heat Transfer in Metallurgical Ores, M. Eng. Thesis, 1976, Univ. of Witwatersrand, South Africa.

162. W. Gerlach: Heat Exchange in the Cohesive Zone of a Blast Furnace, Ph.D. Thesis, 1989, Univ. Aachen, W. Germany.

163. R.H. Perry et.al.: Chemical Engineering Handbook, 5th edition, 1973, McGraw Hill, N.Y.

164. J.F. Elliott, M. Gleiser and K. Ramakrishna: Thermochemistry for Steelmaking vol. I & II, Addison-Wesley, Massachusetts, 1960.

165. W.T. Lankford et.al.: The Making Shaping and Treating of Steel, 10th edition, 1985, US Steel, Assoc. Iron Steel Eng., PA.

166. G.W.G. Kaye and T.H. Laby: Tables of Physical and Chemical Constants, 14th edition, 1973, Longman, London.

167. R.E. Bolz and G.L. Tuve: CRC Handbook of Tables for Applied Engineering Science, 2nd edition, 1976, CRC Press, Florida.

168. E.A. Brandes: Smithells Metals Reference Book, 6th edition, 1983, Butterworth, London.

169. K.R. Cramer and S. Pai: Magnetofluid-dynamics for Engineers and Applied Physicists, 1973, Scripta Publishing, Washington, D.C., U.S.A.

170. J.A. Shercliff: A Textbook of Magnetohydrodynamics, 1965, Pergman, Oxford.